



University of HUDDERSFIELD

University of Huddersfield Repository

Daraz, Alsadak Aboubaker Salem

CONDITION MONITORING OF CENTRIFUGAL MACHINERY BASED ON ADVANCED DATA ANALYTIC TECHNIQUES AND MULTIPLE DATA SOURCES

Original Citation

Daraz, Alsadak Aboubaker Salem (2021) CONDITION MONITORING OF CENTRIFUGAL MACHINERY BASED ON ADVANCED DATA ANALYTIC TECHNIQUES AND MULTIPLE DATA SOURCES. Doctoral thesis, University of Huddersfield.

This version is available at <http://eprints.hud.ac.uk/id/eprint/35693/>

The University Repository is a digital collection of the research output of the University, available on Open Access. Copyright and Moral Rights for the items on this site are retained by the individual author and/or other copyright owners. Users may access full items free of charge; copies of full text items generally can be reproduced, displayed or performed and given to third parties in any format or medium for personal research or study, educational or not-for-profit purposes without prior permission or charge, provided:

- The authors, title and full bibliographic details is credited in any copy;
- A hyperlink and/or URL is included for the original metadata page; and
- The content is not changed in any way.

For more information, including our policy and submission procedure, please contact the Repository Team at: E.mailbox@hud.ac.uk.

<http://eprints.hud.ac.uk/>

**CONDITION MONITORING OF CENTRIFUGAL
MACHINERY BASED ON ADVANCED DATA ANALYTIC
TECHNIQUES AND MULTIPLE DATA SOURCES**

A THESIS SUBMITTED IN PARTIAL FULFILMENT OF THE REQUIREMENT FOR
THE DEGREE OF DOCTOR OF PHILOSOPHY AT THE UNIVERSITY OF
HUDDERSFIELD

By

ALSADAK ABOUBAKER SALEM DARAZ

School of Computing and Engineering

University of Huddersfield

UK

April 2021

ABSTRACT

The centrifugal pump is a primary agent in process manufacturing. The condition of any one of its component parts can affect its operations, and effective condition monitoring (CM) is necessary to avoid unpredicted failure, minimize disruption costs and improve machine accessibility.

The primary purpose of this research is to develop effective CM tools for centrifugal pumps, which can be easily deployed in practice. To this end two measurements: surface vibration and airborne acoustics are selected as data sources due to their being information-rich in the dynamics of pump operations, especially the acoustic signal which can be obtained remotely with minimal disturbance of production lines. These information-rich datasets are adversely affected by noise contamination, so effective data processing tools need to be used. A gap found in present applications is the use of the modulation signal bispectrum (MSB) to improve fault detection due to its capability of suppressing random noise while retaining phase information, enhancing its ability to detect nonlinear components. A second gap was the lack of a structured comparison of the detection of faults in a centrifugal pump using its acoustic and vibration signals.

An analytic study has revealed that both vibration and acoustic data contain non-linear interactions between deterministic excitations such as impeller rotation, bearing defects and random hydraulic flow and system resonances. As a result, the data can be modelled as the modulations between these mechanisms, and demodulation tools such as MSB can usefully be used to diagnose characteristic features, based on experimental studies. Using MSB and comparing it with more traditional methods such as envelope analysis, and the power spectrum showed both airborne acoustic signals, and pump surface vibrations could be used to correctly detect and diagnose bearing faults, mechanical seal defects, and impeller blade wear seeded into the test pump.

It is demonstrated that both acoustic and vibration signals are capable of providing sufficient information to detect seeded bearing defects when using MSB analysis to remove random noise and improve modulation component detection. It was confirmed that remotely measured airborne acoustic signals are effective tools for monitoring pump health and detecting and distinguishing between inner and outer race faults and that the acoustic signals could provide better differentiation between healthy and defective cases

than vibration signals when investigating inner race faults. However, in the case of the outer race fault, the vibration signal provided greater separation of baseline and fault states.

Both the airborne sound and vibration signals generated by a seeded mechanical seal defect contained sufficient information to detect the presence of the fault. For fault detection, MSB and power spectrum analysis-based methods were used separately. The results show that harmonics of the shaft drive frequency (48.3 Hz) in the acoustic signal allowed for easier fault detection than the spectrum. The MSB of the airborne sound provided good separation between baseline and fault harmonics over a wide range of flow rates.

The MSB and power spectrum were also used to detect the seeded impeller faults at different flow rates. The experimental results show good separation of blade pass frequency between healthy and faulty cases for both the MSB analysis and the power spectrum of the acoustic signal. However, the harmonics of the shaft frequency (48.3 Hz) in the acoustic signals obtained using MSB provided a greater distinction between healthy and faulty cases for all harmonics than the power spectrum, suggesting that averaging MSB peaks in the low-frequency range which contains the shaft drive frequency should allow strong differentiation of impeller wear defects. Moreover, the vane passing frequency (338.3 Hz) for the baseline and seeded impeller faults showed clear separation of the acoustic peak magnitudes between baseline and both wear faults for MSB plots and the power spectrum. The experimental results show that the acoustic signal, whether analysed using MSB or power spectrum, outperformed vibration analysis.

ACKNOWLEDGEMENTS

First, I want to express my sincere thanks to my academic supervisors, Professors Andrew Ball and Fengshou Gu, for their constant support, guidance, inspiration, and advice, and providing me with so many invaluable experiences during this project.

Second, I would like to express my heartfelt gratitude to my friends and colleagues in the Centre for Efficiency and Performance Engineering research group for their ongoing support and the memorable moments we shared over the last four years.

Finally, I thank my beautiful family, particularly my wife, for their continuing support, encouragement, and love. My mum, my father's spirit, and all of my brothers and sisters deserve special thanks for their high expectations and inspiration. Also, I am eternally thankful to my mother for her love and patience with me.

COPYRIGHT

- i. The author of this thesis (including any appendices and/or schedules to this thesis) owns any copyright in it (the “Copyright”) and s/he has given The University of Huddersfield the right to use such copyright for any administrative, promotional, educational and/or teaching purposes.
- ii. Copies of this thesis, either in full or in extracts, may be made only in accordance with the regulations of the University Library. Details of these regulations may be obtained from the Librarian. This page must form part of any such copies made.
- iii. The ownership of any patents, designs, trademarks and any and all other intellectual property rights except for the Copyright (the “Intellectual Property Rights”) and any reproductions of copyright works, for example graphs and tables (“Reproductions”), which may be described in this thesis, may not be owned by the author and may be owned by third parties. Such Intellectual Property Rights and Reproductions cannot and must not be made available for use without the prior written permission of the owner(s) of the relevant Intellectual Property Rights and/or Reproductions.

STATEMENT OF ORIGINALITY

I hereby certify that all of the work described in this thesis is the author's original work. None of the work outlined in this study has been used to endorse an application for another degree or certificate at this or any other university.

Alsadak Daraz

LIST OF PUBLICATIONS

Conference Papers

1. Osama Hamomd, Samir Alabied, Yuandong Xu, **Alsadak Daraz**, Fengshou Gu and Andrew D. Ball. (2017). Vibration based centrifugal pump fault diagnosis based on modulation signal bispectrum analysis. Proc. 23rd Int. Conf. on Automation & Computing, Huddersfield, UK.
2. Samir Alabied, Osama Hamomd, **Alsadak Daraz**, Fengshou Gu, and Andrew D Ball. (2017). Fault Diagnosis of Centrifugal Pumps based on the Intrinsic Time-scale Decomposition of Motor Current Signals. Proc. 23rd Int. Conf. on Automation & Computing, Huddersfield, UK.
3. **Alsadak Daraz**, Samir Alabied, Ann Smith, Fengshou Gu and Andrew D Ball. (2018). Detection and Diagnosis of Centrifugal Pump Bearing Faults Based on the Envelope Analysis of Airborne Sound Signals. Proc. 24th Int. Conf. on Automation & Computing, University Newcastle upon Tyne, UK.
4. Samir Alabied, Usama Haba, **Alsadak Daraz**, Fengshou Gu and Andrew D Ball. (2018). Empirical Mode Decomposition of Motor Current Signatures for Centrifugal Pump Diagnostics. Proc. 24th Int. Conf. on Automation & Computing, University, Newcastle upon Tyne, UK.
5. **Alsadak Daraz**, Samir Alabied, Fengshou Gu and Andrew D. Ball. (2019). Modulation Signal Bispectrum Analysis of Acoustic Signals for the Impeller Wear Detection of Centrifugal Pumps. Proc. 25th Int. Conf. on Automation & Computing, Lancaster, UK.
6. **Alsadak Daraz**, Samir Alabied, Dong Zhen, Fengshou Gu and Andrew D. Ball. (2019). Detection and Diagnosis of Mechanical Seal Faults in Centrifugal Pumps Based on Acoustic Measurement. Int. Congress and Exhibition on Condition Monitoring and Diagnostic Engineering Management, Huddersfield, UK.
7. Weili Tang, Fengshou Gu, Hanling Mao, Andrew D. Ball, **Alsadak Daraz**. (2019). Rotor Dynamics in a Pump System with Magneto-electrical, Fluid and Mechanical

Effects using ANSYS. 16th Int. Conf. on Condition Monitoring and Asset Management. British Institute of Non-Destructive Testing.

8. Samir Alabied, **Alsadak Daraz**, Khalid Rabeyee, Ibrahim Alqatawneh, Fengshou Gu and Andrew D. Ball. (2019). Motor Current Signal Analysis Based on Machine Learning for Centrifugal Pump Fault Diagnosis. Proc. 25th Int. Conf. on Automation & Computing, Lancaster, UK.
9. **Alsadak Daraz**, Samir Alabied, Fengshou Gu and Andrew D. Ball. (2020). A comparative study of acoustic and vibration signals for bearing fault detection and diagnosis based on MSB analysis. 5th Int. Conf. on Maintenance Engineering (IncoME-V) & The Efficiency and Performance Engineering Network (TEPEN) (2020) Oct 23rd-24th, Zhuhai, China.

TABLE OF CONTENTS

ABSTRACT	I
ACKNOWLEDGEMENTS	III
COPYRIGHT	IV
STATEMENT OF ORIGINALITY	V
LIST OF PUBLICATIONS	VI
TABLE OF CONTENTS	VIII
LIST OF TABLES	XX
LIST OF ABBREVIATIONS	XXI
LIST OF NOMENCLATURE	XXIII
CHAPTER 1: Introduction and Review of Condition Monitoring of Centrifugal Pumps ...	1
1.1 Introduction	2
1.2 Condition Monitoring of Centrifugal Pumps	3
1.2.1 Condition Monitoring using Visual Inspection	4
1.2.2 Condition Monitoring using AE signals	5
1.2.3 Condition Monitoring using Temperature Measurement	6
1.2.4 Condition Monitoring using the Motor-Current	6
1.2.5 Condition Monitoring using Vibration Signal	7
1.2.6 Condition Monitoring using Acoustic Signals	9
1.3 Previous Studies into the Detection of Centrifugal Pump Faults	10
1.3.1 Bearing faults	10
1.3.2 Mechanical seal faults	12
1.3.3 Impeller fault	13
1.4 Research Motivation	14
1.5 Research Aims and Objectives	15
1.6 Research Objectives	15

1.7 Thesis Organization.....	16
CHAPTER 2: Structure, Operation and Vibro-acoustic Sources in Centrifugal Pumps....	20
2.1 Introduction	21
2.2 The Centrifugal Pump	21
2.3 The Centrifugal Pump in Industry	22
2.4 Structure of a Centrifugal Pump.....	23
2.4.1 The Impeller	24
2.4.2 The Casing.....	26
2.4.3 The Bearings and Bearing Housing.....	27
2.4.4 Mechanical Seal.....	27
2.5 Operation of the Centrifugal Pump	29
2.5.1 Pump Head, Theoretical	30
2.5.2 Pump Capacity.....	32
2.6 Centrifugal Pump Characteristic and Performance Parameters	33
2.7 Sources of Vibration In Hydraulic Systems	34
2.7.1 Hydraulic Induced Vibration in Centrifugal Pump Systems.....	35
2.7.2 Cavitation	36
2.8 Key Findings	38
CHAPTER 3: Common Mechanical Faults in Centrifugal Pumps and Vibro-acoustic Measurement	39
3.1 Introduction to Centrifugal Pump Failures.....	40
3.2 Mechanical Seals	40
3.2.1 Basic Design and Sliding Contact	41
• Dry Friction.....	44
• Fluid Friction	44
• Boundary Friction	44

• Mixed Friction	45
3.2.2 General Failure Modes of Seals	45
3.3 Bearings	46
3.3.1 Characteristic Bearing Fault Frequencies.....	48
3.4 Impellers	49
3.4.1 Blade Passing Frequency	51
3.5 Pump Vibration Overview.....	51
3.6 Airborne Sound Radiation from Vibration Surface.....	53
3.6.1 Background of Airborne Acoustic: Propagation and Reverberation.....	53
3.6.2 Sound Wave Propagation	54
3.6.3 Reverberation and Diffusion	55
3.7 Key Findings	56
CHAPTER 4: Processing of Vibro-acoustic Signal from Centrifugal Pumps Techniques	57
4.1 Introduction	58
4.2 Time-Domain Analysis	58
4.2.1 Root Mean Square (RMS).....	59
4.2.2 Peak Value.....	59
4.2.3 Crest Factor (CF).....	59
4.2.4 Kurtosis.....	60
4.3 Frequency Domain Analysis	60
4.3.1 Envelope Analysis	61
4.4 Higher Order Spectra.....	63
4.4.1 Power Spectrum (PS)	63
4.4.2 Traditional Bispectrum	64
4.4.3 Modulation Signal Bispectrum.....	65
4.4.4 The Performance of Bispectrum.....	66

4.5 Key Findings	67
<i>CHAPTER 5: Experimental Test Rig Facility and Fault Simulation</i>	68
5.1 Introduction	69
5.2 Test-Rig Facility and Description	69
5.3 Measurement System.....	71
5.3.1 The Speed Controller.....	72
5.3.2 Vibration Sensor-Accelerometer	73
5.3.3 Acoustic Microphone	74
5.3.4 Flow Rate Transducers	76
5.3.5 Shaft Encoder	77
5.3.6 Data Acquisition System	78
5.3.7 Intel Pressure Transducer and Discharge Sensors.....	79
5.4 The Centrifugal Pump	81
5.4.1 The Relation Between Pump Flow Rate and Pump Head	82
5.5 Fault Simulation	82
5.5.1 Bearing Faults.....	82
5.5.2 Mechanical Seal Fault Simulation.....	83
5.5.3 Impeller Wear Inlet Vane Fault Simulation	84
5.6 Test Procedures	84
5.7 Key Findings	86
<i>CHAPTER 6: Detection and Diagnosis of Bearing Faults Using Envelope Analysis of Vibro-acoustic Signals</i>	87
6.1 Introduction	88
6.2 Generation of Surface Vibration and Sounds	88
6.3 Bearing Fault Frequency Calculations	89
6.4 Impact of Bearing Defects on Pump Performance Curve	90

6.5 Time Domain of Acoustic Signals.....	91
6.6 Spectrum Analysis of Vibro-Acoustic Signals.....	93
6.7 Envelope Spectrum of Vibro-acoustic Signals.....	95
6.8 Comparison of Fault Diagnoses	97
6.8.1 Envelope Spectrums at Different Flow Rates.....	97
6.8.2 Statistical Parameters for Envelope Signals	99
6.9 Key Findings	101
CHAPTER 7: Acoustic and Vibration Signal Based Detections of Bearing Faults using Modulation Signal Bispectrum Analysis.....	102
7.1 Introduction	103
7.2 The Flow Chart for Bearing Fault Detection.....	103
7.3 Test Rig and Experimental Procedure	104
7.4 Bearing Fault Detection and Diagnosis Using MSB Analysis.....	105
7.5 Comparison of detection results based on MSB peaks.....	108
7.6 Key Findings	111
CHAPTER 8: Detection of Fault Modes of Mechanical Seals of a Centrifugal Pump Using Vibro-Acoustic Measurements	112
8.1 Introduction	113
8.2 Flow Chart for Mechanical Seal Fault Detection	113
8.3 Performance Curve of Pump with Defective Seal.....	114
8.4 Time and Frequency Domains of the Vibration Signal.....	115
8.5 Time and Frequency Domains of the Acoustic Signals	117
8.6 Comparison of Statistical Parameters: Acoustic and Vibration Signals.....	119
8.7 Fault Detection by MSB Analysis	120
8.7.1 MSB Analysis of the vibration signals.....	120
8.7.2 MSB Analysis of the Acoustic Signal	124

8.8 Key Finding	129
CHAPTER 9: Detection of Impeller Wear in Centrifugal Pumps Using Modulation Signal Bispectrum Analysis of Vibro-acoustic Signals	130
9.1 Introduction	131
9.2 Fault Simulation	131
9.3 Framework of Impeller Fault Detection	132
9.4 Impact of Impeller Wear on Pump Performance Curves	132
9.5 Time Domain Analysis of Vibration and Acoustic Signals	133
9.6 Statistical Parameter Comparison of Acoustic and Vibration Signals	134
9.7 Impeller Fault Vibration and Acoustic Signal Spectrum Analysis.....	136
9.8 MSB Analysis Based Detection	137
9.8.1 Impeller Wear Fault Detection by MSB of Vibration Signals	137
9.8.2 Comparison of Detection of Impeller Wear Faults Based on the Power Spectrum and MSB Analysis of the Vibration Signals.....	140
9.8.3 Impeller Wear Fault Detection by MSB of Acoustic Signal	142
9.8.4 Comparison of Detection of Impeller Wear Faults Based on the Power Spectrum and MSB Analysis of the Acoustic Signals.....	145
9.9 Key Findings	148
CHAPTER 10: Conclusions and Proposals for Future Work	149
10.1 Aim, Objectives and Achievements	150
10.2 Conclusions	153
10.3 Contributions to Knowledge.....	155
10.4 Recommendations for Future Work	156
References:	157
Appendix A	167

LIST OF FIGURES

Figure 1-1: Schematic of condition monitoring [3].....	3
Figure 1-2 Flowchart of research work	19
Figure 2-1 Pump classification [90]	22
Figure 2-2 Investment in different pump applications[99].....	23
Figure 2-3 Centrifugal pump structure [100]	24
Figure 2-4 Open impeller [104].....	25
Figure 2-5 Semi-open impeller [105]	25
Figure 2-6 Closed impeller.....	26
Figure 2-7 Pump casing [106]	26
Figure 2-8 Bearings of a centrifugal pump.....	27
Figure 2-9 Mechanical seal [56].....	29
Figure 2-10 The cross-section of the impeller [3]	30
Figure 2-11 Diagram of inlet and exit velocities of the pump impeller [3].....	31
Figure 2-12 Pump performance and characteristics [116].....	33
Figure 2-13 Double and single volute [107].....	36
Figure 2-14 Components of axial thrust [107]	36
Figure 2-15 Effects of cavitation on pump volute [131]	37
Figure 3-1 (a) Causes of pump failure (b) Pump repair costs [134].....	40
Figure 3-2 Common causes of failure in mechanical seals [134].....	41
Figure 3-3 Mechanical seal component [135]	42
Figure 3-4 (a) Mechanical seal running with different lubrication films (b) Hydrodynamic groove in the surface of a sliding face [138]	43
Figure 3-5 Friction conditions between seal faces [71].....	44
Figure 3-6 Damage type of bearing	47
Figure 3-7 Diagrammatic representation of a reverberant sound field in a closed space [169]	55

Figure 4-1 Data processing methods [106]	58
Figure 4-2 Specimen acoustic time domain signals of bearing inner race, bearing outer race and baseline, see Chapter 6.....	59
Figure 4-3 Specimen vibration frequency domain signals of bearing inner race, bearing outer race and baseline, see Chapter 6.....	61
Figure 4-4 Steps in the process of envelope implementation	62
Figure 4-5 Example of envelope spectrums for two bearing faults. (a, b, c) Impulses at equal time intervals with no random noise. (d, e, f) original signal with 0.75% random fluctuations imposed [184].....	63
Figure 5-1 The Test-Rig, showing Pedrollo pump and transducers	70
Figure 5-2 Test rig schematic.....	70
Figure 5-3 Omron 3G3MV inverter-type speed controller	73
Figure 5-4 Accelerometer and location of accelerometer	74
Figure 5-5 Acoustic microphone and position close to the pump	75
Figure 5-6 Rotor Flow Meter	76
Figure 5-7 Hengstler Model-RI 32 shaft encoder.....	77
Figure 5-8 Data Acquisition system Sinocera YE6232B	78
Figure 5-9 Pressure transducer Sinocera CY-YB-0-5 in suction line	79
Figure 5-10 Sinocera Y084602 pressure sensor in outlet line.....	80
Figure 5-11 Centrifugal pump Pedrollo F32/200AH	81
Figure 5-12 The baseline curve of pump flow rate against pump head	82
Figure 5-13 Bearings faults (a) Inner-race, and (b) Outer-race.....	83
Figure 5-14 Seal fault simulation	84
Figure 5-15 Wear fault in inlet vane of impeller	84
Figure 6-1 Bearing structure.....	89
Figure 6-2 Impact of bearing defect on the performance curve	91
Figure 6-3 Samples of time-domain acoustic signal for baseline, inner and outer races ...	92

Figure 6-4 RMS of time domain acoustic signals for baseline, inner and outer races	92
Figure 6-5 Acoustic spectrum for three flow rates Acoustic spectrum for bearings with and without faults for three flow rates (f_i and f_o are inner and outer race characteristic frequencies, respectively)	94
Figure 6-6 Vibration spectrum for bearings with and without faults for three flow rates (f_i and f_o are inner and outer race characteristic frequencies, respectively, and v_{pf} is vane passing frequency).....	94
Figure 6-6 Envelope spectrums of acoustic signals for maximum flow rate 431 l/min (f_i and f_o are inner and outer race characteristic frequencies, respectively).....	95
Figure 6-7 Envelope spectra of vibration signals for maximum flow rate 431 l/min (f_i and f_o are inner and outer race characteristic frequencies, respectively).....	96
Figure 6-8 Envelope spectrum of vibration signals (f_i and f_o are inner and outer race characteristic frequencies, respectively).....	98
Figure 6-9 Envelope spectra of acoustic signals (f_i and f_o are inner and outer race characteristic frequencies, respectively).....	98
Figure 6-10 Envelope signal RMS of vibration signals for baseline, inner and outer race faults	99
Figure 6-11 Envelope RMS values of acoustic signals for baseline, inner and outer race faults	99
Figure 7-1 Framework of the process for bearing fault detection and diagnosis.	104
Figure 7-2 MSB magnitudes and coherences for the acoustic signal for flow rate around 450l/m for bearings with and without seeded faults.....	106
Figure 7-3 MSB magnitudes and coherences for the acoustic signal for flow rate around 250 l/m for bearings with and without seeded faults.....	106
Figure 7-4 MSB magnitudes and coherences of vibration signal for flow rate around 450 l/m for bearings with and without seeded faults.....	107
Figure 7-5 MSB magnitudes and coherences of vibration signal for flow rate around 250 l/m for bearings with and without seeded faults.....	107

Figure 7-6 Averaged MSB peaks for 1st and 2nd harmonics of outer race fault and baseline for (a) Vibration signals, and (b) Acoustic signals.....	108
Figure 7-7 Combined averaged of MSB peaks for 1st and 2nd harmonics of outer race fault and baseline (a) Vibration signals and (b) Acoustic signals.....	109
Figure 7-8 Average MSB peaks of 1st and 2nd harmonics of inner race fault (a) Vibration signals, and (b) Acoustic signals.	109
Figure 7-9 Combined average of MSB peaks at 1st and 2nd harmonics of inner race fault (a) Vibration signals, and (b) Acoustic signals.....	110
Figure 8-1 Framework of the process for pump mechanical seal fault detection and diagnosis	114
Figure 8-2 Impact of seal fault on performance curve	115
Figure 8-3 Vibration signal in the time domain with and without faulty seal for three flow rates.....	116
Figure 8-4 Frequency domain of vibration signal with and without faulty seal	117
Figure 8-5 Acoustic signal in the time domain with and without faulty seal for three flow rates.....	118
Figure 8-6 Spectrum of the acoustic signal with and without faulty seal.....	119
Figure 8-7 RMS of vibration signals in the time domain	120
Figure 8-8 RMS of acoustic Signals in the time domain.....	120
Figure 8-9 The MSB magnitude and coherence of vibration signal at around 430 l/m with and without faulty seal.....	121
Figure 8-10 The MSB magnitude and coherence of vibration signal at around 300 l/m with and without faulty seal.....	121
Figure 8-11 The MSB magnitude and coherence of vibration signal at around 100 l/m with and without faulty seal.....	122
Figure 8-12 Magnitude of vibration peaks at the first five harmonics of shaft drive frequency (48.3 Hz), with and without faulty seal	123
Figure 8-13 Averaged MSB peak for vibration signal, first five harmonics of shaft drive frequency (48.3 Hz) with and without faulty seal	124

Figure 8-14 The MSB magnitude and coherences of acoustic signal at around 430 l/m flow rate with and without faulty seal.....	125
Figure 8-15 The MSB magnitude and coherences of acoustic signal at around 300 l/m flow rate with and without faulty seal.....	125
Figure 8-16 The MSB magnitude and coherences of acoustic signal at around 100 l/m flow rate with and without faulty seal.....	126
Figure 8-17 Magnitude of MSB acoustic spectral harmonics for shaft drive frequency (48.3 Hz), with and without faulty seal.....	127
Figure 8-18 Amplitude of first five harmonics of shaft drive frequency (48.3 Hz) in the acoustic power spectrum with and without faulty seal.....	128
Figure 9-1 Initial fault simulation of impeller wear	132
Figure 9-2 Framework of impeller wear fault analysis	132
Figure 9-3 Performance curve of centrifugal pump with and without impeller wear faults	133
Figure 9-4 Acoustic and vibration signals in the time domain for healthy impeller and impeller with “small” and “large” faults	134
Figure 9-5 Statistical parameters (RMS, Peak, Peak Factor and Kurtosis) for vibration and acoustic signals in the time domain with and without impeller faults.....	135
Figure 9-6 Spectrum analysis of vibration signal with and without impeller faults for three flow rates	136
Figure 9-7 Spectrum analysis of acoustic signal with and without impeller faults for three flow rates	137
Figure 9-8 MSB Magnitude and coherence of vibration signals for impeller with and without faults at flow around 430 l/min.....	138
Figure 9-9 MSB Magnitude and coherence of vibration signals for impeller with and without faults at flow around 300 l/min.....	139
Figure 9-10 MSB Magnitude and coherence of vibration signals for impeller with and without faults at flow around 150 l/min	139

Figure 9-11 Magnitude of the vibration power spectrum plots of the first five harmonics of 48.3 Hz with flow rate.	140
Figure 9-12 Magnitude of the MSB vibration plots of the first five harmonics of 48.3 Hz with flow rate.....	141
Figure 9-13 Comparison of (a) power spectrum plots and (b) plots obtained using MSB for the vane passing frequency (338.3 Hz) of the vibration signal.	142
Figure 9-14 MSB Magnitude and coherence of acoustic signals for impeller with and without faults at flow around 430 l/min	143
Figure 9-15 MSB Magnitude and coherence of acoustic signals for impeller with and without at flow around 300 l/min	144
Figure 9-16 MSB Magnitude and coherence of acoustic signals for impeller with and without at flow around 150 l/min	144
Figure 9-17 Magnitude of the acoustic power spectrum plots for the first five harmonics of 48.3 Hz with flow rate	145
Figure 9-18 Magnitude of the MSB plots for the first five harmonics of 48.3 Hz in the acoustic signals with flow rate.....	146
Figure 9-19 Comparison of (a) Power spectrum plot and (b) Plot obtained using MSB for the vane passing frequency (338.3 Hz) of the acoustic signal.....	147

LIST OF TABLES

Table 3-1 Bearing fault frequencies	48
Table 5-1 Test-rig components.....	71
Table 5-2 Piping system components.....	71
Table 5-3 Characteristics of the Omron 3G3MV inverter-type speed controller.....	73
Table 5-4 Characteristics of the vibration sensor	74
Table 5-5 Acoustic microphone characteristics.....	75
Table 5-6 Flow meter characteristics	76
Table 5-7 Characteristics of Hengstler Model-RI 32 shaft encoder	77
Table 5-8 Connection Order for Channels	78
Table 5-9 Characteristics of Sinocera data acquisition system	79
Table 5-10 Characteristics of transducer in inlet line.....	80
Table 5-11 Characteristics of Sinocera Y084602 pressure transducer in outlet line.....	80
Table 5-12 Characteristics of the centrifugal pump Bedrollo F32/200AH.	81
Table 5-13 The bearing characteristics.....	83
Table 6-1 Bearing fault frequencies	89
Table 6-2 Specification of FAG TYPE 6307 ball bearing	90

LIST OF ABBREVIATIONS

CM	Condition Monitoring
AE	Acoustic Emission
EMD	Empirical Mode Decomposition
MCSA	Motor Current Signature Analysis
HOS	Higher-Order Spectral
RMS	Root Mean Square
PDF	Probability Density Function
SD	Standard Deviation
MSB	Modulation Signal Bispectrum
BEP	Best Efficiency Point
Q	Pump capacity
IEEE	Institution of Electrical & Electronics Engineers
EPRI	Electric Power Research Institute
NPSHa	Net Positive Suction Head Available
NPSHr	Net Positive Suction Head Required
ISO	International Organization for Standardization
MDM	Multiple-Domain Manifold
SVD	Singular Value Decomposition
DC	Direct Current
SVM	Support Vector Machine
ANN	Artificial Neural Network
PDF	Probability Density Function
PkF	peak factor
CF	Crest Factor

FFT	Fast Fourier Transform
HT	Hilbert Transform
PS	Power Spectrum
QPC	Quadratic Phase Coupling
CEPE	Centre for Efficiency and Performance Engineering
DAS	Data Acquisition System
A.C	Alternating Current
RFO	Rotor Flow
EA	Envelope Analysis
PS	Power Spectrum
DFT	Discrete Fourier Transform
DAS	Data Acquisition System
PC	Personal computer
BL	Baseline
IRF	Inner Race Fault
ORF	Outer Race Fault
vpf	Vane Pass Frequency
fo	Fundamental Frequency
BPO	ball pass outer race
BPI	ball pass inner race

LIST OF NOMENCLATURE

H	Velocity head (m)
P	Pressure head produced by the pump (Pa)
ρ	Density of working fluid (kg.m-3)
g	9.8 ms-2
T	Torque acting on working fluid (N.m)
Q	Volume flow rate of pump (m ³ /s)
ρ	Density of working fluid (kg.m ⁻³)
r_1	Inner diameter of impeller (m)
r_2	Outlet diameter of impeller (m)
V_{t1}	Absolute tangential velocity at inlet (m/s)
V_{t2}	Absolute tangential velocity at exit (m/s)
ω	Angular velocity of pump shaft (rad/s)
H_{th}	Pump head (m)
u_1	The rotational velocity at the inlet (m/s)
u_2	The rotational velocity at the outlet (m/s)
b_1	Width of inlet blade (m)
P_o	Power supplied to the working fluid (kW)
BHP	Motor power (kW)
V_{n1}	Radial component of velocity (m/s).
σ	Radiation ratio of the surface
ρc	Acoustic impedance of the liquid
S	Area of the vibrating surface
\bar{v}^2	Mean square surface-averaged velocity of that surface
S_0	Reference surface zone
v_0	Reference means square speed
f_{vp}	Impeller mesh frequency
f_r	Rotational frequency
N_{vp}	Number of vanes in the impeller
N	Number of samples
x_i	Sampled time signal

$x(t)$	Random signal
σ	Standard deviation
μ	Mean of the signal
x_{in}	Input signal
x_a	Analytic signal
X_a	FFT of analytic signal
X_{env}	Envelope spectrum
x_{env}	Analysed envelope signal
$P(f)$	power spectrum
$X(n)$	Calculated according
(f)	Fourier transform
$X^*(f)$	Complex conjugate of $X(f)$
$E(.)$	Mathematical operators
$B(f_1, f_2)$	bi-frequency
n	Number of balls
Bd	Ball diameter
PD	Pitch diameter
Φ	Contact angle
f_i	Inner-Race
f_o	Outer-Race
f_{cage}	Cage
f_{ball}	Rolling Element or Ball

CHAPTER 1:

Introduction and Review of Condition Monitoring of Centrifugal Pumps

This literature review explains fault detection and condition monitoring methods that are investigated and applied to centrifugal pumps. The chapter presents a brief literature review of previous work in this field as a basis for identifying gaps in relevant knowledge and defining the research aim and associated objectives.

1.1 Introduction

Most manufacturing firms are looking to improve productivity by preventing machine failure and increasing machine working life. The purpose of condition monitoring (CM) of machinery is to recognise or warn, at the earliest stage possible, of any malfunction or defect which occurs during its operation. To assist in the diagnosis of the condition of any machine, CM is crucial to obtain the necessary data to protect the integrity of both mechanical and electrical machinery [1-3]. Different parameters can be applied to measure and investigate a machine's condition, such as noise and vibration signals, acoustic emission (AE), oil pressure and temperature, and current conductivity. Simulation models of machinery have been created to predict likely trends for these parameters [3]. The featured parameters, vibration, etc., change according to the machine's condition, and these variations can be used by either maintenance technologists or automatically to improve the performance and maintenance of the machine.

For a CM system to operate effectively, it must be able to obtain sufficient accurate information to monitor a running machine and detect any defect at the earliest possible moment. This enables improving the machine's performance and delaying severe deterioration of the system, including breakdown or failure. Therefore, the CM system must have the ability to locate and identify faults clearly, as well as providing detailed expectations of the machine's remaining operational life.

CM of machinery is a critical measure in industrial-based maintenance; it is also an essential element in an efficient maintenance plan in any industry. If a machine is continuously operated at maximum capacity, breakdowns may occur which can sometimes be catastrophic. The consequences can have a significant effect on both safety and productivity. Preventive maintenance should be the first step in keeping the machine in a healthy condition [4].

In order to perform high-quality machine maintenance, different techniques can be used for extracting information about the condition of the machine, for instance, vibration and acoustic analysis [4]. The operation of a centrifugal pump, for example, requires the consumption of energy to power the mechanical performance and move the working fluid. The operating mechanism is generally rotary or reciprocating, and the pump can

be powered in many ways by manual operation, electricity, wind power or a combustion engine of some type [5, 6].

1.2 Condition Monitoring of Centrifugal Pumps

An essential part of many industrial operations is the centrifugal pump. Centrifugal pumps are widely used in situations requiring a high flow rate but low-pressure head, and the financial output of a factory can be significantly improved by adopting a system for monitoring and maintaining the health of such pumps. However, factors such as liquid contamination, including solid particles and chemically reactive substances, can lead to damage of pump components such as impellers, bearings, and mechanical seals. There are two common methods for checking a centrifugal pump, monitoring its performance and/or its condition [2, 7].

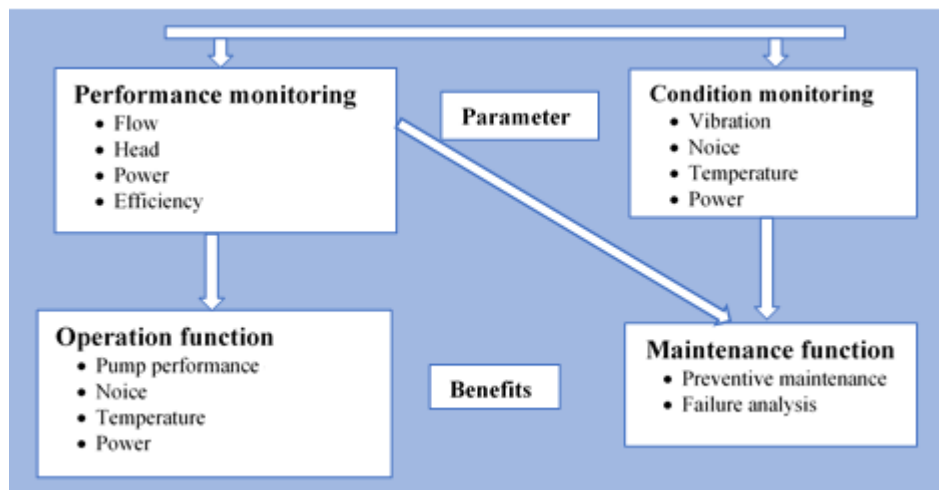


Figure 1-1: Schematic of condition monitoring [3]

Depending on the variables monitored, the benefits of CM will be obtained by following one or other of the routes shown in Figure 1-1 [3]. However, it is not a case of choosing either one or the other because often, both performance and condition monitoring can be realised simultaneously, as the two methods are complementary.

Al Thobiani, et al. [8] utilised spectral entropy of an acoustic signal as well as surface vibration to monitor cavitation in a centrifugal pump. The proposed method was sufficient for detection of cavitation. Similarly, Nasiri, et al. [9] analysed the vibration signal from a centrifugal pump to detect the onset of cavitation. They identified particular features as the input parameters for a neural network system to diagnose faults automatically. Yunlong and Peng [10] applied an advanced signal processing approach

known as Empirical Mode Decomposition (EMD) to the analysis of the vibration of the surface of a centrifugal pump to identify a misalignment. The EMD, which is considered a data-driven technique, extracted nonlinear features from the signal to identify the defect, after which a Least Square Support Vector Machine categorised the fault. It was found that the method was extremely efficient.

CM of electrical machinery typically uses the parameters of motor current and voltage. However, vibration analysis is also widely used because the cyclic excitation forces resulting from wear, failure or imbalance have their own distinct vibration signatures [11]. Other techniques include the monitoring and analysis of motor oil, vibration and acoustic signals, AE, and instantaneous angular speed. Although vibration analysis is popular and can accurately identify most faults in a motor, the approach has one major disadvantage, which is the cost of the vibration sensors required to monitor the machine. However, these mechanical sensors can be replaced by analysis of variations of the motor current or acoustic signals produced by changes in machine condition.

1.2.1 Condition Monitoring using Visual Inspection

Historically, visual inspection was the most important CM process, and is broadly defined as using any of the human the senses (or any non-specialised equipment) to inspect and provide an initial assessment of a machine's condition [7]. It is a wide-ranging approach utilising hearing, sight, smell and touch for facilities maintenance [12]. Visual investigation of the machine, usually by an experienced individual, can distinguish and identify defects via a noticeable change in the running condition of the machine. To help investigators examine parts which are not clearly visible, the investigators might utilise a hand-held videoscope to get reliable and precise pictures [13]. Furthermore, the visual observations can assess the condition of an entire machine before real deterioration happens, and may be part of the routine tasks of a machine operator. Moreover, it is known for its ability to detect potential issues early, for instance, leakage, cracks, and corrosion.

Although it gives immediate details of machine condition, subjective assessment has a significant limitation, investigators may provide different assessments of the same machine depending on their individual skills, background, experience and knowledge. Also, while this subjective approach may give a precise assessment of the system health, each individual may obtain the same diagnosis by different methods [14]. It has been

demonstrated that alternative, technologically advanced approaches, will give not just more accurate predictions but also earlier warning of machine faults [15].

Fault detection and diagnosis has been continuously and considerably improved using AE, temperature, motor current, vibration, and acoustic measurements, all of which are briefly reviewed below. These parameters are inherent in the movement of a pump, are rich sources of information on the condition of the pump and offer numerous opportunities for non-intrusive assessment of pump condition. The great leaps in computational power over the past decades have also greatly enhanced advanced signal processing, assisting analysis of the measurements obtained [16].

1.2.2 Condition Monitoring using AE signals

AE monitoring is employed to detect and measure transitory elastic waves produced by the fast release of the energy generated by a material undergoing deformation or surface damage. The energy is propagated as broadband waves through the structure and the properties of the AE signal make it a delicate tool for early fault detection [17]. In this technique, the most common signal parameters for analysis are events, amplitude, energy, RMS, and kurtosis, all of which are measures of the AE signals generated by rotating machinery due to such effects as friction, impact, leakage, cavitation, cyclic fatigue, and material loss [18].

The frequency range of AE is between 100 kHz to 1 MHz; thus, it is less likely to be affected by signals of frequencies under 1 kHz produced by resonances excited in the structure and/or structure-borne background noise. The high sensitivity of the AE signals makes this a sensitive technique for early-stage fault detection [19]. However, a drawback of AE, restricting its usefulness in monitoring a wide range of rotary component is that the amplitude of the signal decays very rapidly, so the sensor must be located near to the source. Hence, there is a challenge to be overcome in obtaining and analysing AE data produce an accurate description of any machine fault. [20, 21] Sharma & Parey [22] claim to have used AE for monitoring the health of bearings and gears and to successfully detect and diagnose faults. These authors showed experimentally how operational parameters, including speed and load, affected the AE signal and presented a theoretical model to describe how the operating parameters impacted on the AE signal generated. The model was based on the existence of surface asperities and their interactions, assuming Hertzian contact. The model was extended to include defects on

inner and outer races and the rolling element, and the authors claim “satisfactory” agreement between experimental and predicted results.

1.2.3 Condition Monitoring using Temperature Measurement

Maintaining observation of the operational temperature and component surface temperature is known as temperature monitoring and can be used for performance monitoring and fault detection. The significance of temperature monitoring lies in the fact that the temperature of the components can be directly correlated to the wear in the machine elements, especially in places prone to insufficient lubrication such as journal bearings. Many techniques have been developed for accurate and efficient temperature monitoring of machine parts, these include thermocouples, optical pyrometers, resistance thermometers and thermography [23].

To measure the temperature at a point with, say, a thermocouple, is often simple to do and can provide significant useful data. However, a limitation in terms of monitoring temperature using a thermo-vision camera, for example, is that extraneous heat sources including environmental temperature may change and affect accuracy and reliability, more serious is that local hot points may merge and the signal will represent an overall body measurement[24].

1.2.4 Condition Monitoring using the Motor-Current

For condition monitoring of mechanical equipment driven by electric motors, such as compressors, pumps, motorised valves, and other processing machinery, the diagnostic process known as motor current signature analysis (MCSA) is a possible option. A primary use of MCSA is CM of mechanical components and the identification, characterisation and trend analyses of instantaneous load variations that help diagnose changes in pump running condition. This tracks immediate variations in the electric current, i.e., tracks the electrical noise content, thereby monitoring current flow through power leads to the electric motor that drives the mechanical load. This process uses the motor as a transducer, sensing load variations and then converting them to corresponding variation in the current generated within the windings of the motor. The variations in current within the motor windings are sensed, amplified and processed to allow inspection of temporal and spectral characteristics [23]. Accessing the motor current

signals provides promptly accessible and significant data from the inner working of the rotating machine.

Kia, et al., [25] utilised wavelet analysis for monitoring the well-being of a gearbox using the stator current signature of the driving induction motor to compare in detail a healthy motor and a faulty one, into which a defect had been seeded and to detect the presence of the fault.

Because MCSA utilises an electric motor parameter it decreases implementation difficulties and has numerous other positive features, such as much lower transducer costs as no extra sensors are required. In addition, these signals are ordinarily promptly accessible; however, there is a need for advanced processes for analysing such complex signals [26].

Mohantly, et al., utilised MCSA by building a self-diagnostic capability structure for fault diagnosis of the impeller of a centrifugal pump. Healthy and a faulty impellers have been analysed using time and frequency domains, and considerable differences were observed enabling this approach to be developed as strategy for fault prediction [27].

More recently Irfan et al., [28] have successfully detected and diagnosed impeller faults in a centrifugal pump using this method, and claim that their use of statistical relations extracted from the phase relations between the current signals provided a novel and superior method of fault detection compared to previously published MCSA methods for diagnosis of faults in centrifugal pumps.

1.2.5 Condition Monitoring using Vibration Signal

Many different approaches have been developed for centrifugal pump monitoring and fault detection [29, 30]. The most commonly used for detection and diagnosis of faults is vibration signature analysis [29, 31]. Vibration monitoring is categorised as a non-destructive test. A sensor is used to detect degradation or damage by analysing system behaviour, diagnosing changes in characteristic vibration frequencies during operation. Vibration monitoring is one of the most popular techniques used to detect faults. In simple terms, it works by gathering vibration signals produced by the machine and then analysing them to detect any defects or changes that occur [32].

Each machine produces a vibration from mechanical or other sources, and every rotating element generates a specific vibration signal at a particular frequency, a factor that is

highly significant to machine condition monitoring [33]. A significant change in vibration signals may happen due to particular defects in the machine when contrasted with a predetermined baseline signal. Analysts have utilised this characteristic for initial stage fault detection and diagnosis in rotating machines prior to system failure. One of the most common CM techniques is vibration monitoring which is considered as a basis for programs for predictive maintenance. Different components in centrifugal pumps generate specific vibration signals, and by appropriate signal processing the faulty component can be detected, for instance, bearing or impeller.

The best method for online diagnosis of rotating components and avoiding failure is to apply strategies dependent on machine vibration, measuring the the vibration signals of the components during operation [34-36] utilising the dynamics of the measuring signals to monitor a machine's condition, with the accelerometer the sensor most commonly utilised to gather vibration information. Then different signal processing approaches are used for analysing the data, including the statistical parameters such as RMS and crest factor, while in the frequency domain, higher-order spectral analyses (HOS) can be used [37].

The generated vibration signal and the structure of the accelerometer are coupled, and the frequency response of the accelerometer has to be matched to the frequency content of the signal to be measured. The sources of the vibration signals may be non-linear and non-stationary, but in addition the signal from every source might be influenced by its transmission path and the medium through which it is passing. However, the application of vibration monitoring sensors can cause significant changes to feature such as mass and rigidity, and therefore its implementation may face challenges. Thus, vibration monitoring may not be a sufficient system for all CM [38]. The main challenge is how to determine precise vibration measurements in different environments from a limited number of locations on the machine during operation [39].

Any defect will usually be a local phenomenon, and in rotating machinery may have less significant influence on lower-frequency responses generated from a component. Rehab, et al., [40] examined the condition of increasing radial clearance in the inner and outer races of a roller bearing using the higher order bispectrum to analyse the vibration signal. The results showed the fault frequency amplitude changed with changes in radial clearance and change in load zone angle. Therefore, considering the previously mentioned disadvantages, plainly the vibration monitoring system may not always give

an exact answer to CM issues. The limits in the use of the vibration bispectrum in early fault detection and identification is a gap in present technical knowledge that needs to be addressed.

1.2.6 Condition Monitoring using Acoustic Signals

Airborne acoustic sound signal analysis is another non-destructive approach utilised for machine CM. Compared with vibration, the measurement of airborne sound signals can be described as non-intrusive and enables the possibility of collecting superimposed signals that appear as a single signal. This offers the possibility of better detection of faults, but background noise from nearby devices can easily influence airborne sound signals [41].

This technique focuses on the noise or acoustic waveforms generated by the operation or process. These sounds are generally attributed to the surface vibration of components and propagated through the air from a solid object. In this monitoring technique, the acoustic or sound signal generated from components is acquired using microphones appropriate for higher frequency response ranges [42].

The measurement of airborne sound can be a strategy for maintaining rotating machinery. The vibration will generate acoustic sound while the machine is working, and a suitable microphone can be used to pick up the airborne signals, and appropriate signal processing methods can be used to provide useful data for machine CM. The acoustic method is considered as non-intrusive and uses reasonably priced receivers which do not need to be directly mounted on the machine. The main limitation of the acoustic approach to CM is that the signal is easily contaminated by background noise, in particular, the noise produced from moving parts such as motor drive, cooling fan and other machines nearby [43]. Thus, analysis of the airborne signal from a machine must make some allowance for background noise and sources [38].

Lee, et al., [44] studied the interactions of unstable flow through axial-flow pumps with unsteady pressure reaction on the rotor blades, and concluded that the acoustic signal from the pump could be directly related to the efficiency of the pump and provided a means by which to monitor pump performance. The results confirmed conclusions previously published that the detection and diagnosis of various defect in rotary machines can be achieved utilising acoustic techniques; that the airborne sound signal

can identify different deficiencies in centrifugal pumps [45, 46]. For example, Al-Hashmi, et al., [3] had used the acoustic signal to detect and diagnose centrifugal cavitation. Al-Hashmi, et al., [47] presented approaches for identifying cavitation in centrifugal pumps by analysing the acoustic signal in terms of its probability density function (PDF) and standard deviation (SD). Baydar, [48] was an earlier successful application of the wavelet transform for detecting gear faults using its acoustic signals. This line of enquiry has been productively applied to centrifugal pumps by, amongst others, Al Thobiani, et al., [8] and Rapur & Tiwari [49].

However, what is clear from the review of the literature is that there is a gap in formal comparison of acoustic and vibration methods for the detection of faults/flaws in centrifugal pumps. Here we introduce three common faults each of two magnitudes into a pump and then use both acoustic and vibration methods to detect the presence of the seeded faults. It is considered that the detection of faults seeded onto bearing races, pump impeller and mechanical seals using both airborne sound and surface vibration obtained from the test-rig via MSB analysis has not been done before and as such fills a gap in present knowledge. Such an investigation will provide a comparative appreciation of the detection efficiency of the measured surface vibration and airborne sound signals using MSB, envelope and power spectrum analysis.

1.3 Previous Studies into the Detection of Centrifugal Pump Faults

1.3.1 Bearing faults

Condition monitoring plays an important role in the early warning and early activation of rotating part maintenance plans, especially bearings and gears. From preventive to predictive maintenance, early detection of defects will improve the maintenance strategy, achieving reduced costs and earlier notice of breakdowns [50].

Various quantities have been used to classify bearing defects based on vibration, noise, temperature and the presence of certain chemicals. [32, 51]. Many papers on bearing fault identification and diagnosis using vibration-based monitoring have been published in the literature [50]. For stationary machine conditions, characteristic statistical parameters such as kurtosis, and spectral domain characteristics such as envelope analysis are usually used. But for non-stationary systems, time-frequency domain analysis using, for example, the Wigner-Ville distribution, Hilbert-Huang, or wavelet

transforms are more appropriate. Some techniques are data-driven, which is another tool used to describe the physical relationship between the bearing geometry, the particular fault frequencies of the bearing, shaft rotational speed and the impulsive actions generated by bearing faults [52-54].

Gan & Wang [4] diagnosed system faults by representative feature extraction based on such methods as Multiple-Domain Manifold (MDM), Singular Value Decomposition (SVD) and machine learning. For the identification of bearing defects in piston pumps the measurement was based on a novel symmetric cross-value neutrosophic cross-entropy. Kumar et al., [55] defined a newly developed symmetric measure of fuzzy cross-entropy. Li, et al., [56] introduced a vibration signal method using statistical feature learning for diagnosis of failure in rotating machines. Lara et al., [57] suggested an approach using the acoustic quality of the airborne sound produced during the pulse width modulation of the three stages of the current induction motor feed.

Jena & Panigrahi [58] developed an approach focused on vibration and acoustic signals for gear and bearing fault localization, using time-frequency analysis, after which a robust peak detection technique was applied. For selected classifiers for early fault diagnosis in DC engines, Głowacz [59] proposed a method of feature extraction using the Shortened Frequency Selection Method. For fault detection and size estimation of roller bearings, Hemmati, et al., [60] used wavelet packet transformation of acoustic signals. He, et al., [61] proposed a novel method, using acoustic emission for diagnosing bearing faults. Predictive maintenance has been investigated by Scheffer and Girdhar [62], which enabled appropriate action to improve cost-effectiveness by reducing the time spent due to unforeseen system downtimes.

To identify the bearing fault of a centrifugal pump, Mendel, et al., [63] used pattern recognition based on envelope analysis of the vibration signals. Automatic detection of bearing faults based on adaptive artificial intelligence was also proposed by Kumar & Kumar [64]. By applying the empirical wavelet transform, Wang, et al., [65] were able to successfully diagnose bearing faults. Bandt and Pompe [66] suggested studying complex and irregular vibration signals based on permutation entropy. A permutation entropy approach was also applied by Tian, et al., [67] to decompose non-linear and non-stationary vibration signals based on a self-adaptive diagnosis of bearing faults. Glowacz & Glowacz [68] proposed focusing on main component analysis and Bayesian sensor

fusion analysis for the diagnosis and identification of bearing faults in an induction motor. Hamomd, et al., [69] suggested an MSB-based approach using vibration signals for fault diagnosis of a centrifugal pump. Mondal, et al., [70] used the modulation bispectrum of the acoustic signature for diagnosis of faults in reciprocating compressors.

1.3.2 Mechanical seal faults

Mechanical seal CM and fault diagnosis has been widely studied because some 95% of rotating equipment used in chemical processing use mechanical seals to stop leakages between the power drive shaft and cover [71, 72]. The gas and oil industry spends millions of dollars a year repairing and replacing failed mechanical seals. A crucial factor with such failures is predicting failure in real operating situations by data analysis to enable timely repairs [73, 74]. The two main components of a mechanical seal are a dynamic portion and a stationary ring sufficiently closely spaced so as to avoid the incidence of unnecessary leakage, see Figure 3-3. Friction between the stationary and spinning portions, scratching, wear, and the resulting generation of heat will result in poor contact and leakage [75]. CM can provide an early warning of such events, and, by measuring and evaluating the data gathered, can predict the remaining useful life of the seal.

Numerous methods have been used to reliably recognize mechanical seal faults in order to maintain seal efficiency, including acoustic emission and temperature measurements. Much of the earlier research concentrated on using acoustic emission for the identification of mechanical seal faults. Li, et al., proposed contact state monitoring based on acoustic emission detection for seal end faces whose usage depended on an autoregression genetic particulate filter and hypersphere SVM [76]. Jianjun, et al., presented a numerical study of a mechanical seal on a new hydrodynamic pump where the leakage rate and opening force was found to increase with increase in diameter of the channel, fluid pressure and spiral angle [77]. The use of acoustic emission was investigated by Zhang, et al., to track the condition of the seal-end faces in the presence of friction using empirical mode decomposition, the Laplace wavelet and coherence coefficient to monitoring the state of the seal [71].

A further research paper by [78] on increasing the speed of fault detection used the wavelet packet, radial base function and an artificial neural network (ANN). Fan, et al., provided multiple signal classification using HOS to extract critical characteristics from

noisy AE signals from the mechanical seal of a pump [79]. It was also noted that transient AE signals were observed during the operation of mechanical seals while the drive shaft was rotating, and that even when AE bursts were not detected, an acoustic signal from the mechanical seal was modulated by the shaft frequency. A model of mechanical seals predicting AE signals useful for CM and fault detection has been developed by Towsyfyan, et al., [72].

Hence, detecting and diagnosing failing mechanical seals in a centrifugal pump using vibration and airborne acoustic signals via MSB analysis has not yet been achieved. Thus, the information extracts remotely monitoring from the surface vibrations and airborne sound signals. In practice, the focus is on the measured signals generated from friction between seal faces, which links noise contamination to fluid turbulence, component vibrations and noise in industrial environments.

1.3.3 Impeller fault

The stability of a centrifugal pump can be influenced by numerous variables including imbalance of the mechanical rotating elements which will affect the hydraulic flow and invariably increase the vibration induced [80] and can lead to material surface corrosion and even impeller failure [81].

Many researchers have established different approaches to centrifugal pump fault detection [29, 30]. Vibration signature analysis for identification and diagnosis of faults in machine components is the most common and widely used method for condition monitoring [29, 32] but other parameters such as the emitted acoustic signal, temperature, wear, pressure and torque characteristics are used. Vibration and acoustic measurements offer numerous opportunities for non-intrusive signal measurement to provide data rich in information and, combined with the high computational power and advanced signal processing techniques available today have made huge strides forward.

The probability density function (PDF) and standard deviation (SD) values based on the acoustic signal were proposed by Al-Hashmi [47] for the detection of cavitation in a centrifugal pump but these statistical parameters alone, while providing an overview of the state of the pump did not reveal specific faults. The same process has been repeated more recently by Al-Obaidi [82] using the vibration signals. The interaction of unstable

flows inside axial pumps due to the large unstable pressure response on the rotor blades was investigated by Lee, et al., [44].

Liao, et al., [83] suggested a system based on the multi-scale hybrid hidden Markov model for tracking instrument wear by analysing cutting force signals. However, the conclusion to be drawn from most publications relating to fault identification and diagnosis using acoustic signals from rotating machines is that the acoustic signal should be capable of detecting wear defects in a centrifugal pump [45, 46].

Naturally, some wear will occur where the impeller and the pump casing come closest to being in contact, and this is due to the liquid being squeezed through a limited clearance. In addition, tiny particles invisible to the human eye can wear and erode the impeller. Larger solid particles, including those produced by boiler scale or rust can produce similar faults, though industrial effluent and well water can also cause erosion. Erosion can affect many of the pump's components, not only the impeller, including casing wear rings, mechanical seal faces, and shaft sleeves[84, 85].

Wear can be exacerbated by corrosion, where the surface of a material is subject to chemical or electrochemical attack. Corrosion increases with temperature and oxygen content of the fluid in contact with the surface or with increased fluid velocity. Wear will also increase when the pump uses a small impeller operating at a high speed, when the impeller tip can suffer rapid wear. Bachus & Custodio claim that in 95% of cases the high speed of the working fluid is the cause of excessive wear in pump components.

This research aims to extending current knowledge of how to detect a pump's condition in terms of impeller erosion by using both acoustic and vibration signals and MSB analysis to eliminate background noise, enhance the modulating components and increase the effectiveness of impeller wear monitoring. The power spectrum, a traditional form of analysis will be used for comparative tests.

1.4 Research Motivation

The earlier faults are detected in any system, the longer its working life and the greater its efficiency. Thus, the drive to detect faults at an ever earlier stage in their development is an ongoing process of which this research programme is part. To improve current CM methods and develop an effective method for detecting and diagnosing of pump faults in its early stages, preferably at low cost, is an ongoing challenge. This work uses

acoustic signals and surface vibration combined with MSB advanced signal analysis to investigate the effects of specific mechanical faults on the vibro-acoustic signals from a centrifugal pump. These effects are then used for pump fault detection and diagnosis.

With rotating machinery, it can be a challenge to instal accelerometers. However, the great advantage of the airborne sound signal is that it can be measured remotely and at less cost. Thus, this research focuses on the characteristics of the measured airborne sound for detecting and diagnosing centrifugal pump faults and to explore the effect of different defects on the measured acoustic signals. These measurements are implemented using a microphone situated near the pump housing to measure the sound signals and then suitable HOS analysis to extract the most useful features for early-stage fault detection.

The main purpose of the research is to improve CM and fault detection techniques for centrifugal pumps based on dynamic measurements: surface vibration and airborne sound, which allow for non-intrusive inspections CM system deployment.

1.5 Research Aims and Objectives

The primary aim of this research is to develop a potential approach for the detection and diagnosis of developing faults (bearing faults, failing mechanical seals, and impeller wear) in a centrifugal pump using surface vibration and airborne acoustic signals based on the advanced signal analysis MSB. To investigate the effective analytics of using advanced signal processing methods based on airborne sound and vibration signals, for the purpose of condition monitoring of centrifugal pumps. The secondary aim is to test in a structured and organised manner a comparison of the ease of detecting the seeded faults using the acoustic and the vibration signals separately.

1.6 Research Objectives

Objective 1- To describe operational functionalities of condition monitoring systems and identify the mechanical components of centrifugal pumps.

Objective 2-To clarify the requirements of the pump test rig test and facilities to be used to perform experiments, seeding different faults, and gaining experimental data. To study the use of advanced methods, including data analytics of pumps, the monitoring and detecting defects using multiple data sources (surface vibration, airborne acoustic) and identifying the main research gaps.

Objective 3- To simulate different mechanical faults: inner and outer race bearing faults, mechanical seal, and impeller wear, and to investigate how these faults influence pump performance under different flow rates.

Objective 4- To explore the dynamic interactions between mechanical and hydraulic sources of centrifugal pump and the critical behaviour of these sources, and when faults occur.

Objective 5- To examine the traditional methods (e.g., time and frequency domain analysis) for pump CM and detection of mechanical defects. To improve detection of the modulation components in both the vibration and acoustic signals and enhance them by implementing advanced signal process techniques such as the modulation signal bispectrum and envelope analysis, and then compare these results with conventional methods to ascertain how to obtain a more accurate identification and quantification of the faults.

Objective 6- To examine vibration and acoustic measurements and compare the effectiveness of these techniques for healthy and faulty cases.

Objective 7- To examine the capacity of vibro-acoustic signals to extract weak and noise-contaminated fault signals from the centrifugal pump for detection and diagnosis of pump faults with a high degree of accuracy.

Objective 8- To provide recommendations and guidelines for future research in pump condition monitoring.

1.7 Thesis Organization

The thesis is structured as 10 chapters:

Chapter 1 - provides an introduction and general background into CM techniques for fault detection and diagnosis applied to centrifugal pumps. It also contains an overview of the relevant literature and identifies gaps in knowledge appropriate to this research project. The chapter also provides the research aims and associated objectives based on the gaps identified in the literature. The chapter ends by describing the organisation of the thesis.

Chapter 2 - reviews the relevant literature on the fundamentals of the centrifugal pump, its structure, and various applications. It also reviews the characteristics of the pump and pump parameters, and then common faults are explored in association with their causes and contributions to pump failure.

Chapter 3-provides an overview of the introduction to pump failures, and it describes the main pump components and their functions and explains the main reasons for failure in mechanical seals, bearings, and impellers and can act as sources of vibration and sound. Moreover, these are the three most prevalent mechanical faults. The mechanisms that cause such wear, as well as the anticipated effects, are outlined. Faults are displayed and explained that will be seeded into the pump to demonstrate early detection of such common defects. Finally, the chapter discusses vibro-acoustic measurements in real, reverberant environments.

Chapter 4- presents different CM approaches for detection and diagnosis of faults in a centrifugal pump. Starting with time-domain analysis, then statistical parameters obtained, then envelope analysis. It also reviews HOS methods including the power spectrum, traditional bispectrum and finally the MSB.

Chapter 5- begins by detailing the test-rig and experimental facilities required for detection and diagnosis of centrifugal pump faults. Moreover, it presents the details of measuring equipment, data acquisition devices linked to the application system, sensors, and control systems. It also provides a description of the faults seeded into the centrifugal pump and test procedures.

Chapter 6- reports an examination of the detection and diagnosis of pump bearing faults using vibro-acoustic signals and envelope analysis. This chapter presents the impact of the bearing defect on pump performance, then the time domain and spectral analyses of the acoustic signals. It then introduces the envelope spectrum of the acoustic and vibration signals and compares them. Finally, statistical parameters obtained from the envelope analysis of both the acoustic and vibration signals are compared.

Chapter 7- examines the enhancement of detection and diagnosis of a bearing fault in a centrifugal pump, beginning with presenting the initial means for finding the fault via time and frequency domain analyses. Because of its capability to substantially reduce random noise and detect nonlinear components, the MSB was used for bearing fault detection using vibro-acoustic measurements. Finally, a comparison was made of the result obtained from the acoustic and vibration signals for detecting and diagnosing faults in the inner and outer races of the pump bearings.

Chapter 8- explains how to detect the failure modes of mechanical seals in centrifugal pumps based on vibro-acoustic mechanisms. This chapter presents the impact of a fault in the mechanical seal on pump performance, followed by using time and frequency domain analyses to detect and diagnose the fault. In addition, statistical parameters obtained from the surface vibration and acoustic signals are compared. Finally, MSB analysis is applied to both acoustic and vibration signals, and the results compared.

Chapter 9- examines an impeller fault caused by wear, applying MSB analysis to the vibro-acoustic signals for detection and diagnosis. The impact of small and large wear of the impeller inlet on centrifugal pump performance are explained, then the vibration and acoustic signals are analysed in the time and frequency domains. Finally, the chapter presents impeller wear fault detection using MSB analysis, and compares the results obtained with spectral analysis for both acoustic and vibration signals.

Chapter 10- provides the conclusions of the research and gives an evaluation of the primary achievements. It also presents the novelty of the research, and finally offers suggestions for future work on the condition monitoring of centrifugal pump operations, and additional enhancements of certain aspects of this work.

Figure 1-2 General schematic of the research work plan.

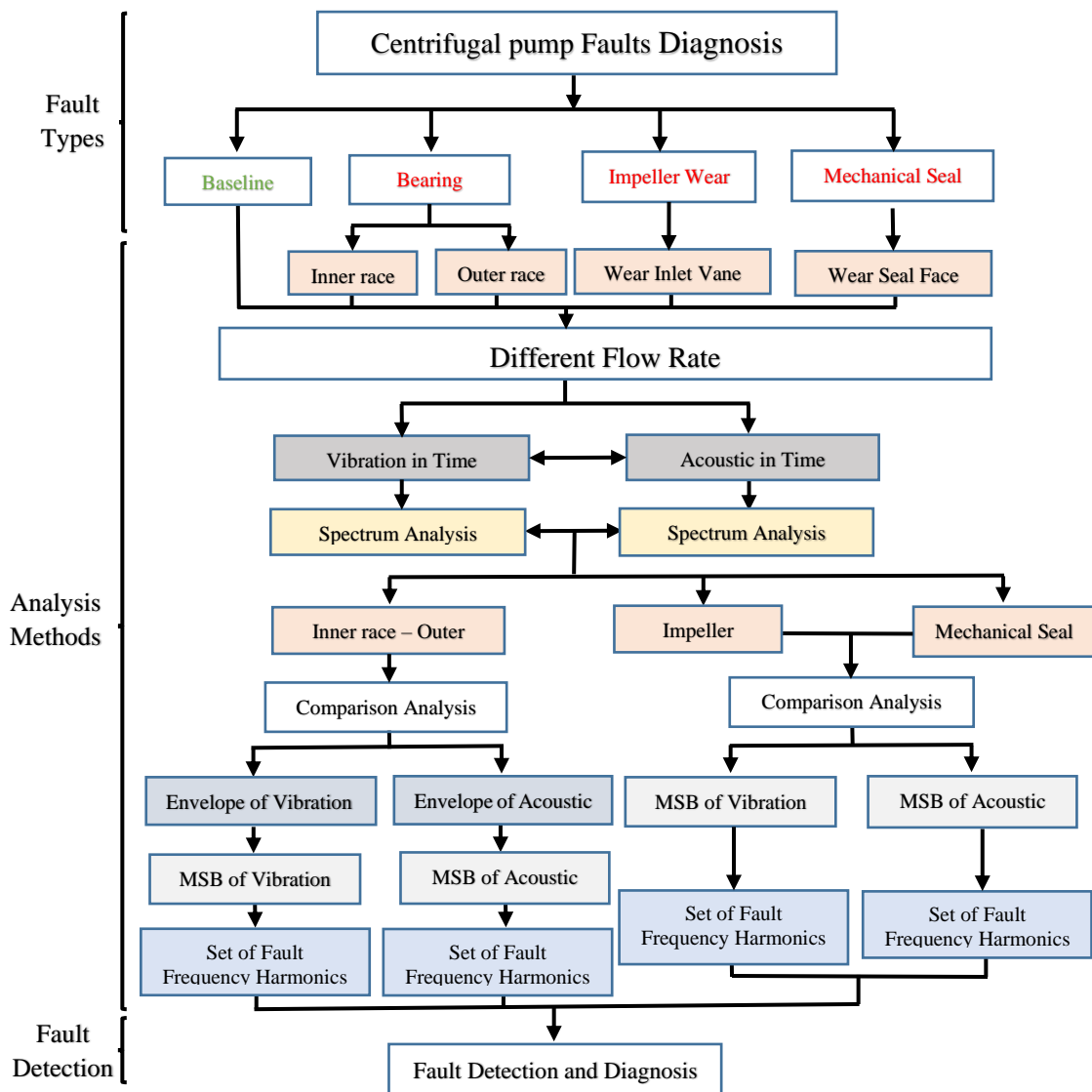


Figure 1-2 Flowchart of research work

CHAPTER 2:

Structure, Operation and Vibro-acoustic Sources in Centrifugal Pumps

This chapter summarises the fundamentals of the centrifugal pump, reviewing relevant literature to describe its structure and use in industry, providing an understanding for its various applications. Based on this, the pump characteristic curves, pump efficiency, and pump selection are all discussed. In particular, the mechanical configuration and the component parts of the pump, such as the impeller, bearings, mechanical seal, and stationary casing, are introduced. The chapter also describes hydraulic forces that degrade mechanical elements of the pump and generate vibro-acoustic signals.

2.1 Introduction

The most popular pump used in industry to raise and transport fluid through pipelines is the centrifugal pump. Typically, around 80–90% of petroleum facilities contain one or more centrifugal pumps because of their advantages in terms of rugged construction, and generally economic performance [86]. Failure to provide the ideal flow and head is one of the most widespread indications of pump deterioration. There are numerous conditions which are considered as the pump having failed; these include pump impeller and motor bearings defects, mechanical seal defects, leakages from pump casing, high noise and vibration levels, and motor faults. It is thus necessary to provide a maintenance programme to keep the pump in good operational condition. Typically, pump maintenance is responsible for a considerable proportion of the total maintenance cost [87, 88].

Often, the reason for a pump failure begins small and then grows gradually. Hence, detection of the first instance when the issue shows up can save the pump from permanent failure [87, 88]. The primary task in such circumstances is to detect the fault in the early stages, to determine if the pump has a mechanical fault or some deficiency in operation and provide accurate information on proper preventive measures to be taken.

To confidently prevent pumps from failure, any maintenance programme must show an understanding of the operation of the pump as well as its mechanics. Pump fault detection and diagnosis requires an ability to detect changes in performance over time, combined with the capability to thoroughly evaluate the condition of the pump and provide a reason for the loss of performance allowing remedial measures to be taken to resolve the problem and prevent its re-occurrence.

2.2 The Centrifugal Pump

The term 'centrifugal pump' includes many types of rotor-dynamic pumps, and Figure 2.1 illustrates the main classifications of such pumps [89]. Their relative simplicity of construction and capability of producing a high working pressure within a small space, means that they are popular tools in industry. A centrifugal pump's primary duty is to transfer liquid from lower levels to higher by adding kinetic energy to the liquid. A simple pump classification following [90] is presented in Figure 2-1 showing the pump of interest here a centrifugal pump with closed, radial impeller.

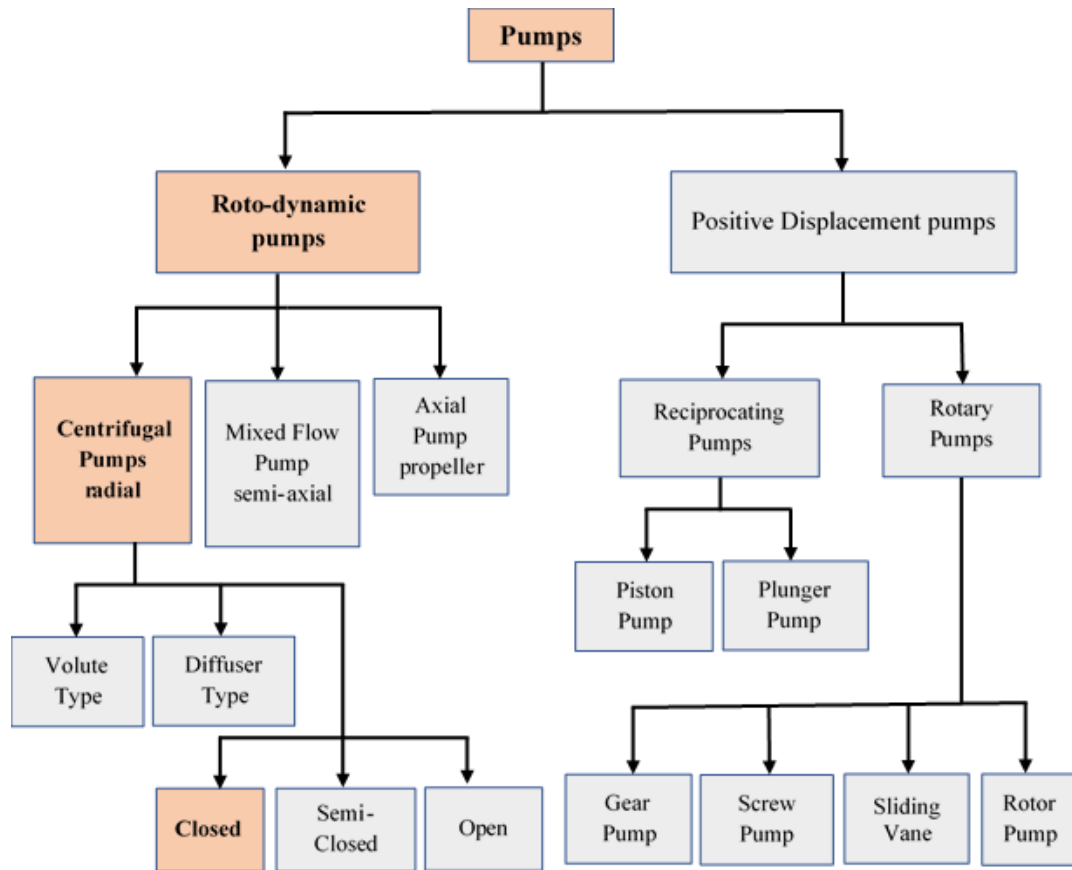


Figure 2-1 Pump classification [90]

The main task of a centrifugal pump is to transfer electrical energy from the motor into dynamic energy represented by the movement of the liquid being pumped. Two primary components of the hydraulic section of the centrifugal pump, the impeller and the diffuser, are responsible for the energy changes [91, 92]. In addition to industrial applications, centrifugal pumps have proved essential in a large number of service industries, such as water supply plants, electric power plants, food processing, jetting operations and hydraulic power services [93-95]. They are also commonly used for refrigeration, air-conditioning, paper mills, and textiles and pulp production. According to a report produced by Grand View Research the world's centrifugal pump market in 2019 was worth approximately US\$98bn [96].

2.3 The Centrifugal Pump in Industry

The primary purpose of pump machinery is to add mechanical energy to the working fluid via an impeller, and so move the liquid from one place to another. The energy increases the local pressure, which helps to transfer the fluid [97, 98]. Various end-use sectors, including chemicals, power, and oil and gas, are refurbishing plants, and pumping systems

in order to improve production efficiency. During the projection period, the water pumps market is expected to increase due to rising demand for retrofitting, improvements, and replacement of old assets and industrial systems in developed regions (2019-2029) as shown in Figure 2-2. By the end of this period, the worldwide water pumps market is expected to be worth US\$ 64 billion [99].

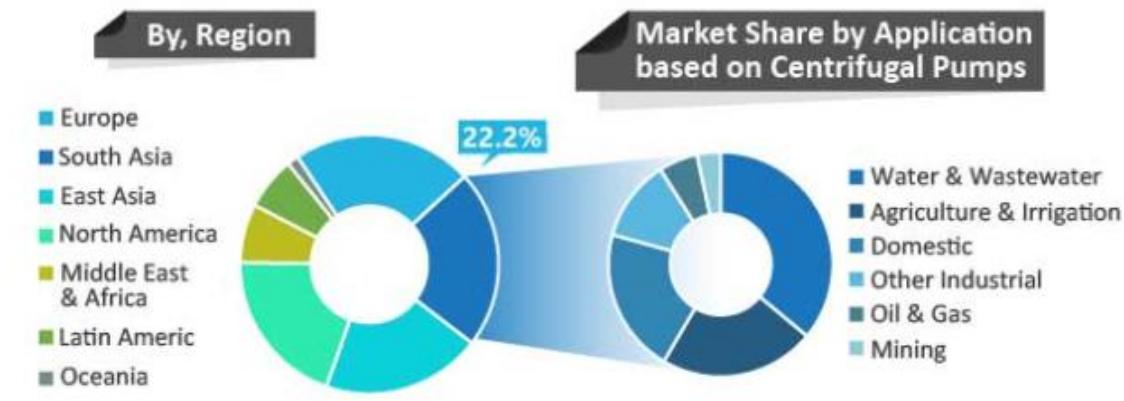


Figure 2-2 Investment in different pump applications[99]

Many forms and sizes of centrifugal pumps are available for different applications, and selection of the most appropriate pump for a given use is important. But it can prove hard to choose the “perfect” pump since the choice may be a compromise. For example, the experience of use, maintenance and repair of previous pumps, the strategy of the purchasing department, and collaboration between departments when pumps serve different needs.

2.4 Structure of a Centrifugal Pump

A centrifugal pump can be considered a rotary machine, in which the pressure and flow rate are generated dynamically. A vital feature of the pump is the impeller which transmits energy to the fluid by increasing its velocity; thus, the impeller speed will control the flow rate of the pump. The main parts of centrifugal pump are illustrated in Figure 2-3.

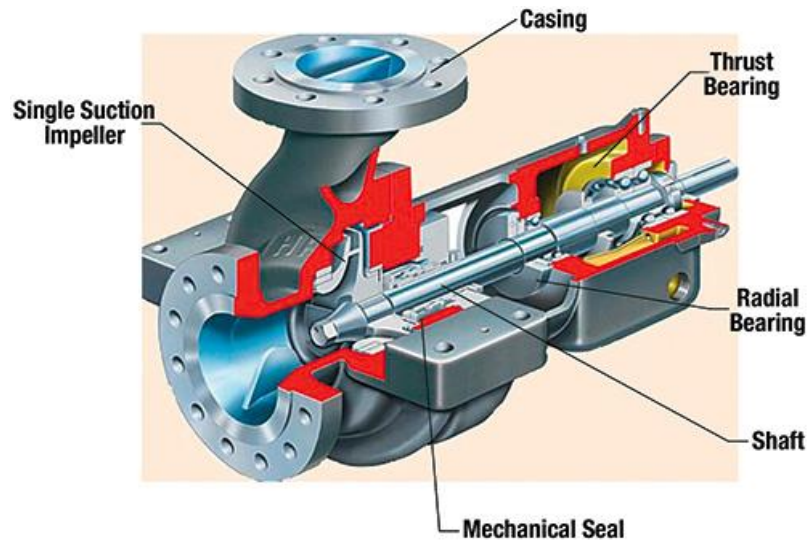


Figure 2-3 Centrifugal pump structure [100]

2.4.1 The Impeller

The impeller, which can be considered the core of the machine's rotating components, is responsible for accelerating the liquid after it enters the casing. It is the essential element of the pump liable for moving the fluid from one place to another [101]. To boost fluid velocity and pressure, mechanical energy is transferred from the rotating blades of the impeller to the fluid. Liquid enters the impeller via the so-called “suction eye” and the movement of the impeller pushes the liquid outwards through the channels shaped by the edges between the cover shroud and centre hub. The impeller types are determined by the requirements of the pressure, flow and application[102].

Following [102], impellers can be categorised as follows:

Open Impeller

An open impeller, see Figure 2-4, is one where the vanes are linked to the shaft axis and work as an uncovered part within the pump casing. While a closed impeller can be adversely affected by the accumulation of solid matter, which may cause a blockage of the flow, an open impeller's main feature is that it is used to drive unclean fluid that can include suspended material or large particles. However, frailty in vane structure is a drawback of this kind of impeller, particularly when the vanes are long. Open impellers are commonly made from rigid material to provide the necessary resistance not only to normal wear but also to resist the impact of solid particles [101, 103].



Figure 2-4 Open impeller [104]

Semi-Open Impeller

The vanes in this impeller are mounted on one face of the shroud; these impellers contain a limit number of vanes whose length is such as to avoid clogging during operation, as illustrated in Figure 2-5. This impeller is used to drive fluids which contain debris or suspended bodies, for instance, sewage water [101].



Figure 2-5 Semi-open impeller [105]

Closed Impeller

The third, and most prevalent, type of impeller employed in centrifugal pumps is the closed impeller, as shown in Figure 2-6. Because the suction eye can easily be impeded by solid debris, the main application of this kind of impeller is with clear liquids. The design of this impeller avoids the slippage of liquid that takes place with semi-open and open impellers [103].



Figure 2-6 Closed impeller

2.4.2 The Casing

The pump casing, which contains the impeller, provides several functions [95, 103]. Its main purpose is to “suck in” the working liquid through the suction eye and to discharge it at a higher velocity via the discharge. In addition, trapped gases in the liquid, that could affect the pumping system, can escape via a vent.

The casing of a centrifugal pump is categorised as a collector and its main purpose is to gather and trap liquid inside the housing, after which the impeller works to diffuse the fluid to a discharge pipeline. Figure 2-7 illustrates the pump casing [106].



Figure 2-7 Pump casing [106]

2.4.3 The Bearings and Bearing Housing

The bearing housing is illustrated in Figure 2-8 [107]. There are considerable demands on the bearings of a centrifugal pump due to both the load and speed of operation. Although maintenance costs are not high, the cost of replacement can be expensive in terms of side effects such as loss of production. A pump system operating continuously at high speed can lead to wear damage to the bearings. The most convenient type of bearing for a centrifugal pump is the rolling element, usually located between impeller and motor, with its main task, keeping the rotating shaft in balance. Bearing failure can be a serious source of pump degradation, including leakage. Unusual operating conditions can be another cause of pump failure [108, 109]. Bearing fault detection and early-stage diagnosis are dependent on many variables, including the specific defect and the bearing housing. Fault detection in the early stages has significant benefits, for example it allows appropriate preventive action to be taken to maintain performance operation and avoid breakdown. For exact analysis of a bearing fault, several strategies have been recommended over the last few decades. In particular, bearing defect features (bearing frequencies) identified from internal monitoring can be used [110].



Figure 2-8 Bearings of a centrifugal pump

2.4.4 Mechanical Seal

Mechanical seals, sometimes referred to as wear rings, prevent the leakage of working fluids and gases into the atmosphere. They are found in many rotating devices such as pumps and mixers to eliminate leaks. The advent of the industrial era at the beginning of the last century led to the invention of the steam turbine, the electric motor, and the

dynamo. Along with these was the necessity of developing a mechanical seal. A patent on a mechanical seal, published in 1919, exploited a spring action to compensate for axial motion of a shaft. An improved version, the balanced mechanical seal, was patented in 1933, this enhanced the capacity of the seal to withstand pressure and reduced heat generation between the seal's faces. With these developments, seals were used on propeller shafts in submarines, and to improve packing on the water pumps of moving vehicles and refrigeration compressors. With further development, oil refineries had accepted these as standard devices by the 1950s, which led to extensive research in the field of elastomer technology for more advanced seal materials.

Research led to mechanical seals with improved shelf-life, enhanced temperature and pressure threshold limits and better chemical resistance. The balanced O-ring-shaped mechanical seals are, to this day, the standard in industry. A mechanical seal usually comprises two main components, see Figure 2-9, one of which is stationary, while the other rotates against it, to achieve a seal. The factors that determine the design, placement and material of a seal are usually the working fluid, its temperature and pressure, and the speed of rotation. A wide variety of mechanical seals is available, ranging from a simple single spring to those with complex functions such as cartridge seal types [111, 112].

With present technology, nearly all liquids can be successfully sealed under most pumping conditions. Exploiting such efficient mechanical seals engineers have used centrifugal (multi-stage) pumps in extreme environmental conditions ranging from deep oceans to outer space [85]. Irrespective of seal manufacturer, these devices are heavily standardised and give similar performance: mechanical seals are designed to last several years with an approximate operating life of 40,000 hours [85, 112].

No matter how well the rings work when new, natural wear means leakage will occur in the end and a description of the relevant mechanisms is given in the next chapter. Pump performance can deteriorate rapidly with excessive wear, particularly for small pumps running at high speed, and replacement of the wear rings should take place whenever the pump goes to the shop for an overhaul [85, 112].



Figure 2-9 Mechanical seal [56]

Despite major improvements in shaft-sealing methods, shaft-sealing issues remain one of the most common primary sources of system failure. Mechanical seals' dependability is determined by the seal's configuration, suitability for the pump, and the purpose and conditions under which the pump is used, which might not be those for which it was designed [3]. Generally mechanical seals in a centrifugal pump control leakage of the working fluid by making a connection between two opposite recirculation faces. A fixed ring is attached to the casing, while a revolving ring is attached to the shaft. A loaded spring acts to provide a closing force, keeping the rotating and stationary faces close together, but the sealing pressure is low [113].

2.5 Operation of the Centrifugal Pump

In the centrifugal pump the circular motion of the impeller imparts kinetic energy to the working fluid. The stationary component is the diffuser or the volute, which transforms the kinetic energy of movement into pressure head. Equation 2.1 presents the velocity head, usually in meters of water produced by the kinetic energy transferred from pump to working fluid [3].

$$H = P / \rho \cdot g \quad \text{Equation 2.1}$$

Where;

H Velocity head (m)

P Pressure head produced by the pump (Pa)

ρ Density of working fluid ($\text{kg}\cdot\text{m}^{-3}$)

g 9.8 ms^{-2}

The most significant component in the centrifugal pump involved in pumping the working fluid is, of course, the impeller. The kinetic energy of the working liquid at any point

along the impeller is directly proportional to the square of the speed of the impeller at that point. So, the pressure head developed by the pump will be determined by the speed of the tip of the impeller. The diffuser /volute is a curved funnel of growing zone, see Figure 2-10, so that the speed of the fluid passing through it reduces, and the pressure increases. The shape of the volute acts to transform the kinetic energy of movement into pressure.

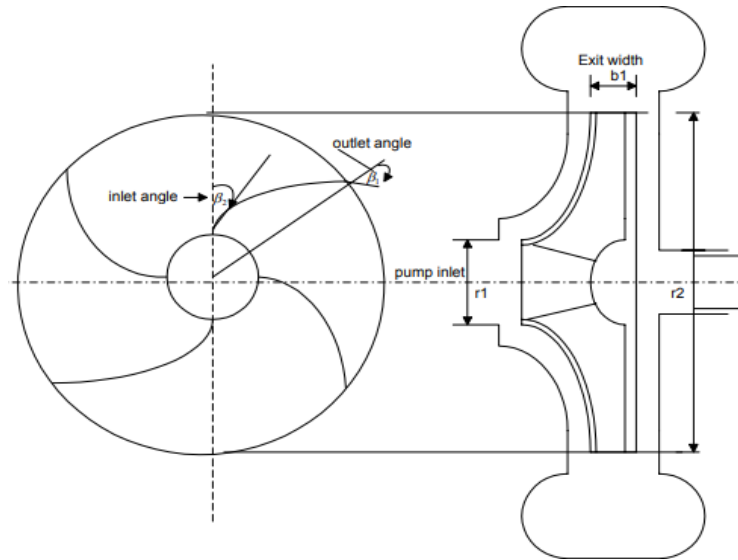


Figure 2-10 The cross-section of the impeller [3]

2.5.1 Pump Head, Theoretical

The shape of the volute blades strongly influences the pump's flow pattern and impeller effectiveness which are primary factors controlling the energy transmitted. By utilising the principle of conservation of angular momentum, it is possible to determine the hypothetical increase in pressure head, H_{th} , through the impeller.

Following the arguments presented by [92, 114], considering a volume of annular form contained by an inner radius r_1 and outer radius r_2 , the torque used to pump the liquid by the impeller and the angular momentum entering and leaving must be equivalent, see Figure 2-11.

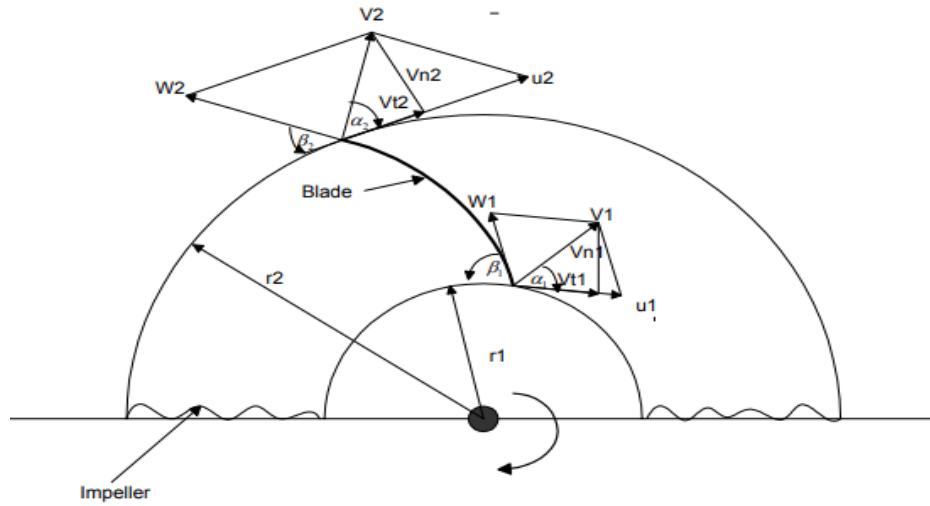


Figure 2-11 Diagram of inlet and exit velocities of the pump impeller [3]

$$T = Q\rho(r_2V_{t2} - r_1V_{t1}) \quad \text{Equation 2.2}$$

Where

T Torque acting on working fluid (N.m)

Q Volume flow rate of pump (m^3/s)

ρ Density of working fluid ($\text{kg}\cdot\text{m}^{-3}$)

r_1 Inner diameter of impeller (m)

r_2 Outlet diameter of impeller (m)

V_{t1} Absolute tangential velocity at inlet (m/s)

V_{t2} Absolute tangential velocity at exit (m/s)

The necessary power from prime mover (induction motor):

$$P_o = \omega T = \rho Q(\omega r_2 V_{t2} - \omega r_1 V_{t1}) \quad \text{Equation 2.3}$$

Where:

T Torque supplied to shaft (Nm)

ω Angular velocity of pump shaft (rad/s)

$$P_o = \rho Q(u_2 V_{t2} - u_1 V_{t1}) = \rho Q g H_{th} \quad \text{Equation 2.4}$$

Where:

H_{th} Pump head (m)

- g 9.8 m/s²
- u_1 The rotational velocity at the inlet (m/s)
- u_2 The rotational velocity at the outlet (m/s)
- ρ Density of working fluid (kg/m³)

Ideally, with is no losses, the power delivered (P_o) is equal to ρQgH_{th} . For a pump of efficiency, η , the shaft power required to drive the pump is:

$$BHP = \frac{P_o}{\eta} \quad \text{Equation 2.5}$$

Where

P_o Power supplied to the working fluid (kW)

BHP Motor power (kW)

Consequently, the theoretical pressure head across the pump will be:

$$H_{th} = \frac{\rho Q(u_2V_{t2} - u_1V_{t1})}{\rho Qg} \quad \text{Equation 2.6}$$

$$H_{th} = \frac{(u_2V_{t2} - u_1V_{t1})}{g} \quad \text{Equation 2.7}$$

2.5.2 Pump Capacity

The volume rate at which the fluid is conveyed by the pump is the capacity of the pump, measured in cubic meters per second [92]. When determining pump type, cost and size for any application, the pump's capacity is a significant parameter. When assessing pump capacity, various factors are taken into consideration. For example, when choosing the pump to distribute potable water, the choice should include not only the length of the water lines, but likely increase in populations over the next twenty to thirty years. However, a more precise estimate is possible of the capacity of a pump for, say, a factory operation which needs water [115]. The pump capacity, Q , could be calculated using Equation 2.8.

$$Q = 2\pi r_1 b_1 V_{n1} \quad \text{Equation 2.8}$$

Where:

r_1 Inner diameter of pump impeller (m)

b_1 Width of inlet blade (m)

V_{n1} Radial component of velocity (m/s).

2.6 Centrifugal Pump Characteristic and Performance Parameters

To specify a suitable centrifugal pump for a particular application: the pump must convey the desired capacity with the required head. The “pump performance characteristics” refer to the relationship between the net positive suction, the pump head, pump efficiency, power, and capacity. The interrelations are usually presented graphically by the pump manufacturer, as in the pump performance characteristics shown in Figure 2-12. Hence, to select and to operate a centrifugal pump one should consider the relevant pump performance characteristics. Pump selection for a particular purpose would assess its ability to deliver a specific flow rate during a process at a particular head: and would include consideration of pump efficiency, net positive suction head and power consumption [3, 92].

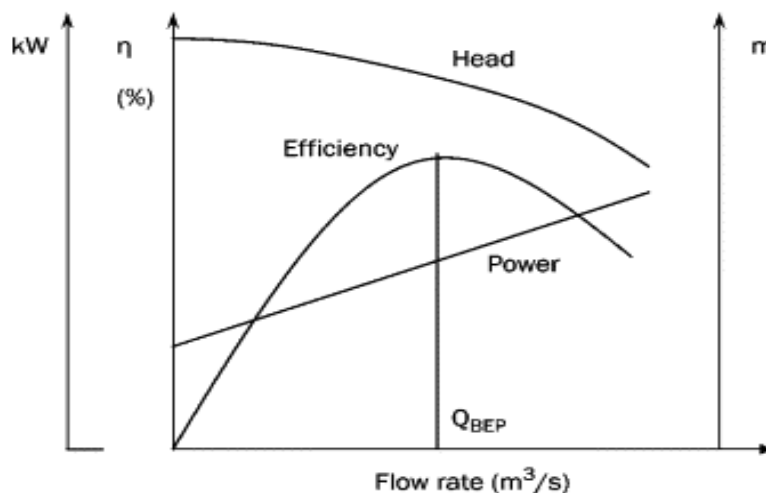


Figure 2-12 Pump performance and characteristics [116]

The pump's optimum operating point in Figure 2-12 is the BEP, where pump power and pump head combine to optimise pump efficiency. The best efficiency point is the point at the crossing between net positive section head available with head required. Away from the BEP, the pump can experience more wear and have a shorter working life.

One of the features of a centrifugal pump's performance is its ability to operate efficiently over a range of flow rates. Factors like pump size and suction conditions determine the speed of operation of the pump and its ability to deliver the pump capacity from zero to

the maximum rate. Pumping capacity will vary with power, efficiency, and the total pump head. One selects a reliable centrifugal pump for a particular propose by considering its characteristics: the head and capacity required to deliver a specific flow rate during a process [92, 117].

The laws of Specific Speed and Similarity are two of the laws that govern a pump's operation. These laws allow the researcher to predict pump behaviour, to determine how changes in working parameters, e.g., change in the running speed, will change the frequency of operation of component parts. It is possible to obtain the pump's operational features using these laws [92, 114]. The laws of affinity, also known as the pump laws, will become progressively significant with industrial pumps using variable-speed electric motors [3, 85].

2.7 Sources of Vibration In Hydraulic Systems

As a typical hydraulic machine transferring kinetic energy to the fluid by a rotating impeller, pumps are well placed to generate both mechanical and hydraulic vibration phenomena. Here we do not consider transfer of pump vibration externally to, for example, the piping system but only from the surface of the pump. The vibration generated will depend upon the type of pump, its working conditions (operating point), age, wear, and quality of maintenance. The sources of mechanical vibration are invariably mechanical imbalance of the rotating parts, or poor adjustment or imperfect assembly, distorted or defective impellers, material deposits on (or wear of) an impeller, and loose housing in the case of ball bearings. Thus the vibrations in a dynamic pump will generally be linked to the shaft rotation frequency, f_r [118, 119].

The shaft vibration frequency can match system torsional resonances, which are the system's characteristic natural frequencies, which can have large and damaging amplitudes. Other mechanical vibrations can occur at super synchronous (an integer multiple of the driving speed) frequencies or sub-synchronous (typically half the driving speed) [118, 119]. The sources of hydraulic vibrations will usually be due to pressure pulsations and turbulent fluid flow, these will include blade passing frequency, recirculation, stall and surge, uneven flow distributions generating hydraulic imbalance, misalignment causing unsteady flow (e.g., turbulence, vortex shedding), the pump

working away from the BEP which generates additional axial and radial hydraulic forces in the volute casing, and cavitation.

The vibrating surfaces couple with the ambient air and radiate outwards as sound. Likewise, the impeller vanes when the pump operates away from the BEP will generate pressure pulsations in the working fluid that will excite vibrations and airborne sound with specific frequencies determined by with numbers of impeller vanes and shaft speed. The non-stationary behaviour of the fluid flow, turbulence, and cavitation can also generate vibration and airborne sound, though this vibration and sound will exhibit largely random waveforms due to the complex interactions of localised flow fields.

The vibration and airborne signals demonstrate a clear association with the health of the pump, and analysis of the signals can establish the health of the pump [[120](#), [121](#)] and, in particular, to detect bearing, mechanical seal and impeller issues. However, the received signal will invariably contain wide-band noise from the excitations of hydraulic pressure sources, which in many cases do not represent different machine components [[69](#)]. The vibro-acoustic signatures of these mechanical parts permit the presence of defects to be detected.

2.7.1 Hydraulic Induced Vibration in Centrifugal Pump Systems

Hydraulic forces can cause considerable vibration in centrifugal pumps [[80](#)]. Excitations due to pulsations from liquid in contact with impeller vanes, flow turbulence, cavitation, and hydraulic instability are examples of hydraulic forces. Three types of non-stationary pump processes must be distinguished which can result in damaging pressure pulsations and even cavitation in the impeller's vane channels [[105](#)].

Fluctuations in the liquid inflow through the pump's suction eye result in corresponding changes in the hydraulic radial load and an unequal distribution of flow velocity around the impeller. Moreover, the pump casing design also affects the radial load, the regular distribution of pressure and velocity by the volute casing hypothetically results in the pump operating at the BEP. To predict the hydraulic radial thrust, accurate standard formula are used [[107](#), [122](#)]. It follows, for example, that use of a double volute with different diffuser shape, see Figure 2-13, the radial thrust could be reduced.

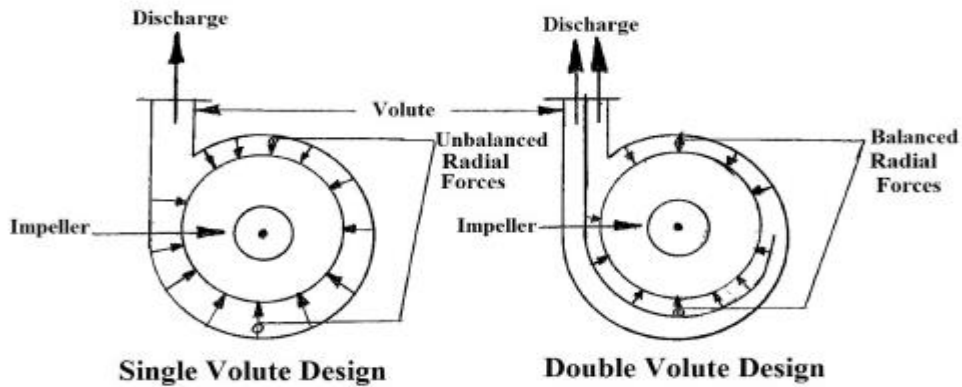


Figure 2-13 Double and single volute [107]

Asymmetry is the main reason for axial thrust (a net force) on the impeller of centrifugal pumps. Should the front shroud have a smaller surface area than the back shroud, there will be a net thrust (an unbalanced force) due to water pressure acting on the impeller in the opposite direction to the incoming flow as shown in Figure 2.14 [107]. These axial forces have been found to be of sufficient magnitude to seriously shorten bearing life and cause bearing failure [123].

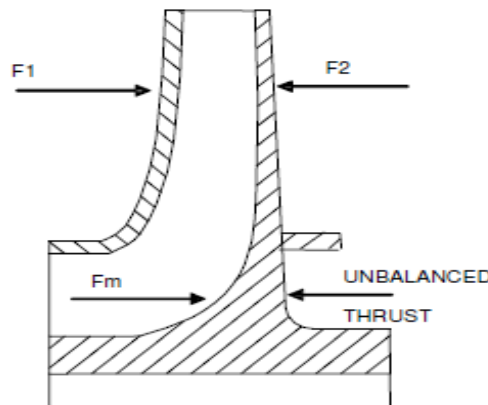


Figure 2-14 Components of axial thrust [107]

2.7.2 Cavitation

When the vibration generated by a centrifugal pump is clearly discernible over background noise, then cavitation is frequently found to be an issue [124]. Cavitation takes place when the pressure at a point in a liquid is lower than the local vapour pressure. It is considered a natural phenomenon that occurs when the local pressure drops due to external forces result in vapourisation of the fluid, after which the bubbles generated collapse sharply. The rapid collapse and uneven breakdown of these vapour bubbles leads to

surface damage due to the energy generated being highly focused [125]. This phenomenon must be guarded against when designing machines such as pumps, hydrofoils, and turbines [126].

Cavitation produces pressure-driven unsteadiness in centrifugal pumps and is considered one of the most important issues influencing pump efficiency, operability, and productivity [127, 128]. The high levels of noise and vibration associated with cavitation are obvious indications of its presence. To maintain pump operation strategically distant from cavitation, there needs to be an adequate minimum static pressure at the inlet channel, usually accomplished by having the NPSHa (Net Positive Suction Head Available) of at least 3% greater than the NPSHr (Net Positive Suction Head Required) [19]. Figure 2-15 shows the effect of cavitation on an impeller volute. When cavitation appears, the pump's execution and productivity will be unfavorably affected [3]. The vibration generated by cavitation is wideband and thus often excites resonances in the structure, particularly in the pipework, which can generate leaky joints and even fracture supply lines. Specifically, the presence of cavitation decreases pump productivity, and can also lead to erosion, vibration, hydraulic unbalance, and rapid deterioration in pump performance [129, 130].



Figure 2-15 Effects of cavitation on pump volute [131]

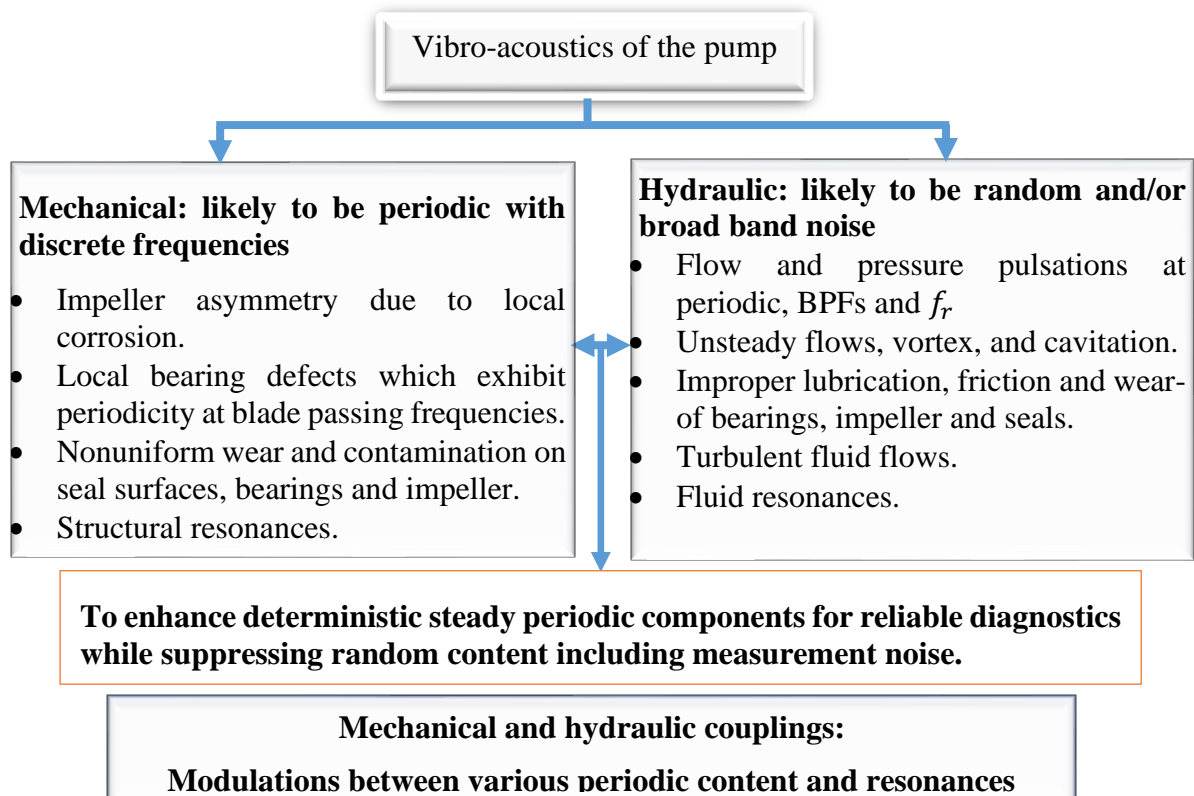
Pressure pulsations in a centrifugal pump are generated each time the tip of the rotating vane passes the volute tongue and thus it is often the tips of the impeller blades that suffer most wear. Factors such as pump design, total head produced, and the pump's operating point and its proximity to the BEP, as well as the inlet and outlet flow conditions, can be responsible for generating these large pressure pulsations. To evaluate the centrifugal pumps performance and condition, pressure pulsation should be monitored as a significant parameter [109, 122, 132].

2.8 Key Findings

Centrifugal pumps were introduced in this chapter, as well as their use in industrial applications. The pump function, pump characteristic curves, pump efficiency, pump applications, and pump selection are all summarised. In particular, the mechanical configuration and parts of the pump, such as the impeller, bearing, mechanical seal, and stationary casing, have been introduced. The chapter also described the hydraulic forces at work that degrade mechanical elements of the pump and generate vibro-acoustic signals.

The dynamic interactions between mechanical and hydraulic forces are the fundamental sources of the stationary modulation behaviour which can be observed in measured signals. Moreover, when faults occur on key components such as impellers, bearings, and seals due to mechanical wear and fluid erosion the modulation tends to become more significant. However, the modulation will be adversely influenced by random and background noises, making it difficult to define its characteristics.

Thus, data analytics will be developed to enhance the modulation components while suppressing random noise in the measured vibro-acoustic signals. To further clarify the measurement tasks, pump vibration and acoustic signals due to the interaction between mechanical and hydraulic forces are summarised in Figure 2-16.



CHAPTER 3:

Common Mechanical Faults in Centrifugal Pumps and Vibro-acoustic Measurement

This chapter presents a review of the faults in centrifugal pumps which occur in seals, bearings and impeller and can act as sources of vibration and sound. It is shown that these are the three most common mechanical faults. The mechanisms that generate such wear are described, as are the likely consequences. Faults to be seeded into the pump to demonstrate the early detection of such common faults are presented and discussed. Finally, the chapter introduces vibro-acoustic measurements in real, reverberant, environments.

3.1 Introduction to Centrifugal Pump Failures

Pump components can be divided into mechanical and electrical. Here we focus on mechanical faults related to pump components. Typical pump defects are usually in the seal, bearings or impeller, while the electrical motor faults that arise are often in the stator or rotor [3, 133]. Furthermore, although pumps vary in design and sophistication to meet different requirements, the most commonly occurring faults remain much the same. Fault occurrences are shown in Figure 3-1 [134]. In terms of the component parts of the pump Figure 3-1 shows the relative frequency of occurrence of faults and associated costs. Obviously, seal failure followed by bearing failure are the two most commonly identified causes of pumping system breakdown, with impeller faults a significant factor.

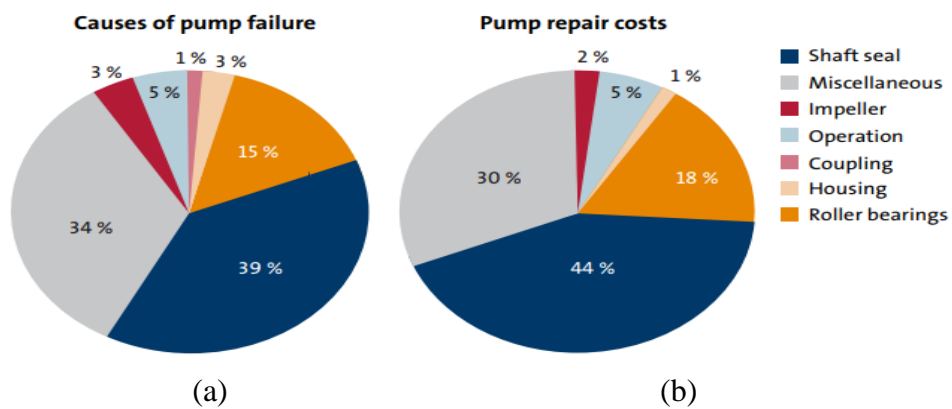


Figure 3-1 (a) Causes of pump failure (b) Pump repair costs [134].

3.2 Mechanical Seals

Figure 3-2 shows the most common failure of mechanical seals [134]. After one failure, to prevent similar failures, it is necessary to make an analysis of the damaged shaft seal. The necessary information would include detailed information on pump operation which, typically, would have been recorded in any incident report.

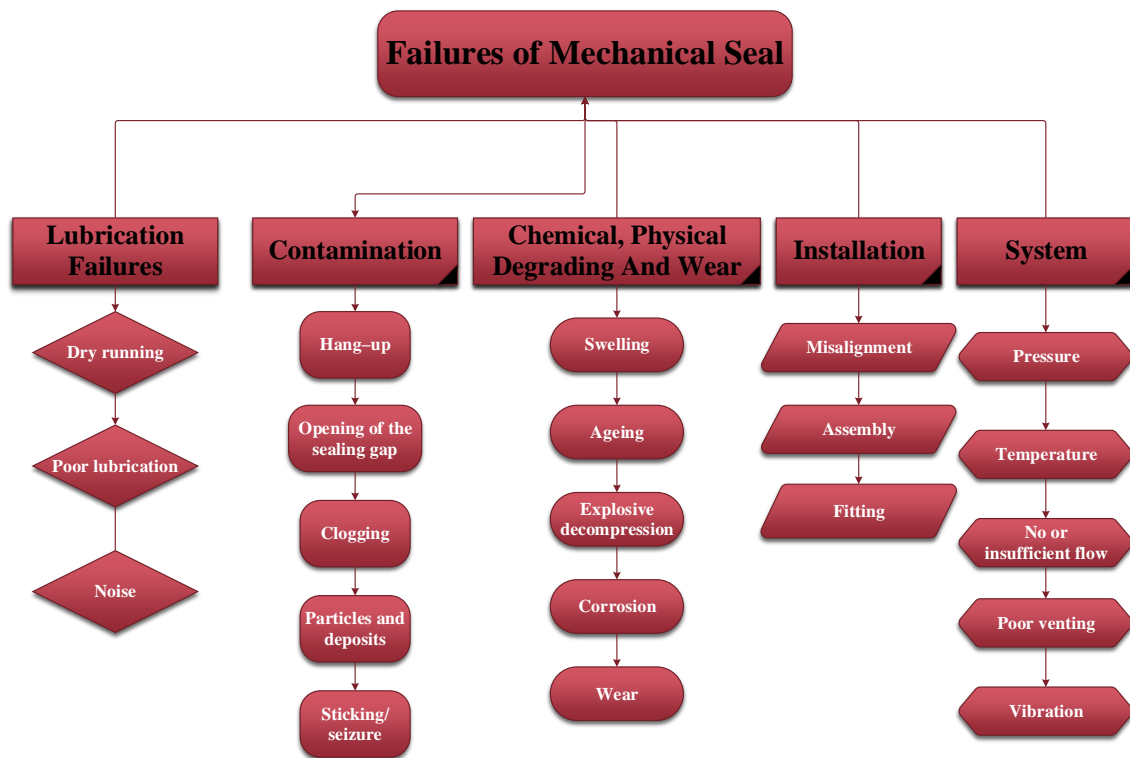


Figure 3-2 Common causes of failure in mechanical seals [134]

3.2.1 Basic Design and Sliding Contact

A mechanical seal is an essential requirement in any rotating device moving a liquid. Despite major improvements in shaft-sealing methods, shaft-sealing issues remain the most common primary source of system failure. A mechanical seals' dependability is determined by the seal's configuration, suitability for the pump, and how the pump is used [3]. The essential and most basic mechanism of a mechanical seal is the pairing of a rotating element with a stationary one. The stationary, fixed, ring is attached to the casing and pressed against it is the rotating part which is fixed on the shaft as seen in Figure 3-3, a schematic showing the position of the mechanical seal inside the pump and highlighting its constituent parts. The two faces each “ride” on a thin layer of lubricant typically 3×10^{-4} mm thick [134]. If the film is too thick the seal leaks, if the film is too thin the asperities on the two faces will come into contact generating noise and heat, the latter will, eventually, cause seal failure. A loaded spring provides the closing force, keeping the rotating and stationary faces close together, but the sealing pressure can be low [113]. Typical shaft seal failures are highly dependent on material matching and seal type, and mismatching can cause excessive wear on seal faces and seal hang-up. Again, mechanical shaft seals where both seals have hard face material pairings will often experience dry

running problems. Reliability of operation, low power consumption, and low leakage rates are all requirements for seals.

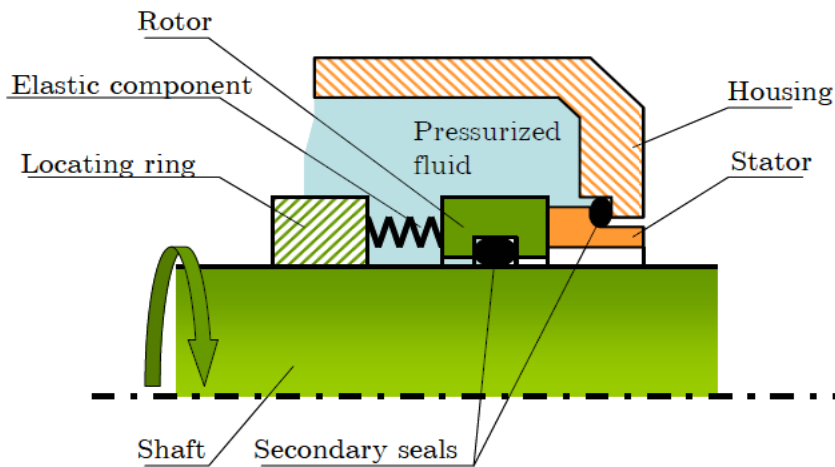


Figure 3-3 Mechanical seal component [135]

Given that a seal has been performing satisfactorily the most likely reason for leakage is wear of the seal faces due to poor or absent lubrication. Other possible causes of a seal fault include the development of a fault in the supporting bearings which generate shaft vibration [136], or the seal has been subjected to a change in operating conditions which become quite different from the conditions for which the seal had been designed [134].

Well-performing seals should not hamper performance for many years after installation and, provided the seal ring retains its axial flexibility, can perform efficiently even with heavily grooved seal faces and severe wear (up to 0.5–1.0 mm). The two most commonly observed features of wear, are grooves on the seal face towards the product medium side (suggesting hard particles suspended in the working medium have entered the sealing gap), and deep grooves towards the atmospheric side (suggesting that the pumped medium has created precipitates, where the lubricating film left voids after evaporating [134].

The vibration signal is produced by plastic deformation due to rubbing contact as one surface slides over the other, which generates vibration peaks at the rotation frequency and its harmonics, along with broad band content due to frictional effects but the signal will also be contaminated by background noise during the process. Unfortunately, the processes by which seal noise and vibration are generated are not well understood. A

recent review [137] has concluded that an acceptable model representing the phenomenon has not yet been established, and progress is still by empiric investigation and observation.

3.2.1.1 Sliding Contact of Mechanical Seal Faces

The sliding contact of a mechanical seal face can operate in one of three different kinds of lubrication (boundary, fluid, and mixed) conditions. In the case of the mechanical seal running with a full fluid film, the gap and leakage between faces will be high. If the lubrication is sliding contact, then hydrodynamic grooves will be formed in one, possibly both, of the mechanical seal faces, see Figure 3-4. In general, the mechanical seal face operates with a mixed lubrication film, which has an acceptable level of leakage and minimum wear of the faces. In boundary and mixed lubrication systems, the most important features are the materials of the mechanical face and coatings, including geometric properties such as surface waviness and surface roughness.

Furthermore, since the mechanical seals are not perfectly flat a partial hydrodynamic lubrication film will occur between the faces. If the sliding face temperature increases sufficiently, the lubricant will begin cavitating. This condition is unstable and could starve the contact area of lubricant, a condition which gives rise to high wear. The lubrication film will start to vaporise if the temperature gets any higher [138-141].

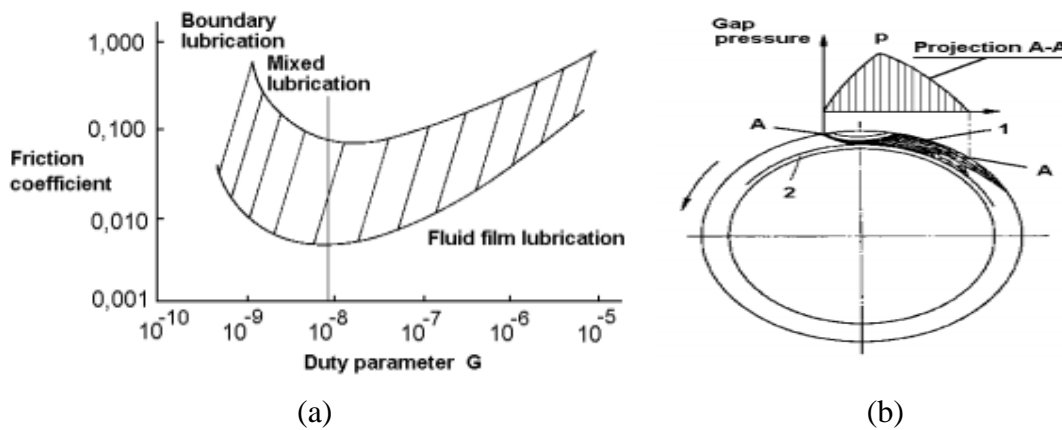


Figure 3-4 (a) Mechanical seal running with different lubrication films (b) Hydrodynamic groove in the surface of a sliding face [138]

Material deformation or fracture releases energy as elastic surface waves in the material, sometimes called stress wave emission while fluid leakage, friction, and impact can act as vibration sources [71, 142]. The mechanical seal is a vibration source where the vibration is generated via friction or collision between the active ring and stationary face.

The frictional forces active in mechanical seal and components vary with the surface roughness (frictional forces), geometry of the structure, characteristic of the medium and work conditions such as rotating speed, temperature, pressure, etc.

The friction condition between seal faces can be classified as follows:

- **Dry Friction**

The direct contact between seal faces takes place if a liquid (lubricant) film does not form, so that dynamic and stationary parts are in intimate contact. When the shaft speed and film pressure start by increasing slowly, direct connection between seal-end face components will produce serious levels of dry friction. However, the amplitude and frequency of the vibration signal will be high and there can be a small degree of leakage [71]. Dry friction is shown in Figure 3-5.

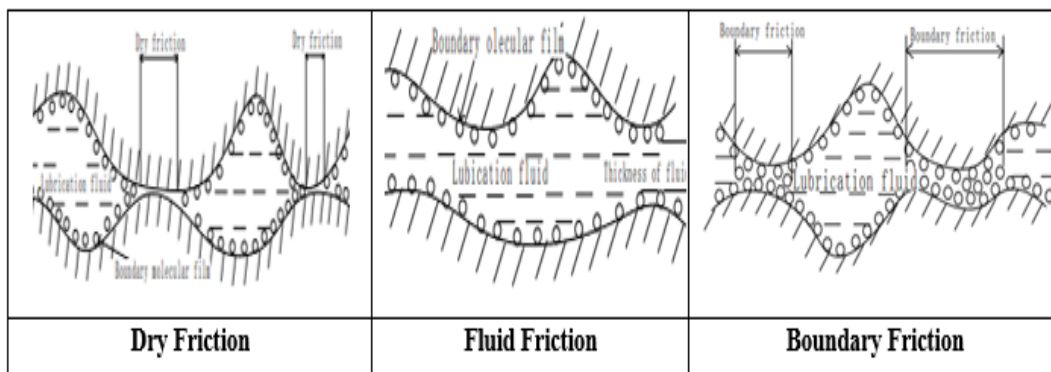


Figure 3-5 Friction conditions between seal faces [71]

- **Fluid Friction**

Fluid friction in a sliding bearing is when a thin film-like layer of lubricant forms between the mechanical faces of a seal. The very thin lubricated film separates the faces of the mechanical seal completely. In this case, the friction generated is due to viscous fluid shear. Power consumption, wear, and friction decline, which also reduces the heating effect. With fluid friction, the wear on the end-face is small, even with leakage. Also, fluid friction produces only weak vibration signals [71]. Fluid friction is shown in Figure 3-5.

- **Boundary Friction**

When the seal's end faces are in tight contact around the boundary of the mechanical seal, a thin liquid molecular layer is produced. This thin film can partially separate the faces of the mechanical seals. This kind of friction is termed boundary friction. Because the

lubrication film is thin it is a challenging task to measure the liquid pressure. In general, the molecular boundary membrane is only three or four molecular layers thick, around 20 nanometers [71, 143]. However, the contact is discontinuous, and parts of the mechanical faces come into direct contact, and the pressure is borne by the contacts made between the asperities on the surfaces. The characteristics of the resulting signal are between fluid friction and dry friction.

The viscosity of the lubricant film has some influence on friction characteristics. The performance of friction fundamentally depends on the lubricity of the liquid film, as does the material of the dynamic component and stationary face rings. In this process, the wear, as well as leakage, is relatively small. This is considered as an ideal mechanical seal friction condition [71].

- **Mixed Friction**

As the degree of the waviness of the seal faces decreases, so simultaneously, the gap between the seal faces is reduced, and the friction present will very alternate between the above three kinds. In general, mechanical seal end faces work in a mixed friction environment, though at high speeds and light loads, the mechanical seal faces are protected by a film of viscous fluid [71, 144].

3.2.2 General Failure Modes of Seals

Figure 3-1 shows that seal failure is the most common cause of pumping system breakdown. One possible reason is that the shaft seal has to endure a wide range of operating conditions, and there may occur situations when the operating conditions become quite different from the conditions for which the seal had been designed function [134]. Typical shaft seal failures are highly dependent on material matching and seal type, and mismatching can cause excessive wear on seal faces and seal hang-up. Again, mechanical shaft seals where both seals have hard face material pairings can experience dry running problems, which enhances seal wear and shortens seal life.

Bearings support the shaft to which the seals are attached, and these will, themselves, be subject to wear. As they wear the shaft will oscillate (vibrate) and as a consequence of this movement the rubbing of one seal face on the other will eventually cause the seal to leak.

When seal integrity becomes compromised, there is an egress of working fluid which evaporates leaving solid deposits. Experience shows these solid deposits can form on the sealing surfaces on the inside, on the working side and on any passage between. With time the solids build up and the leak grows [145].

No reports have been found which present a clear description of the frequencies associated with seal wear/faults. This is because so many factors and processes are involved. It is hoped that this research will provide some insight into this, but from the literature it appears that the amplitude of the acoustic and vibration signals associated with the shaft frequency may provide some help. In this project the seeded seal faults were agreed with the supervisor as a scratch in the surface of the seal similar to those introduced into the bearings (see below), to allow liquid to seep through. It was considered that this corresponded to erosion problems found in practice and the vibro-acoustic signals produced could be used to detect them at an early stage of development, see Chapter 5.

3.3 Bearings

Bearings play a vital role and are a critical component in centrifugal pumps and when selecting the most suitable bearing for a specific application, many factors have to be considered, such as temperature, flow, and pressure. Bearing failure is a common cause of failure in centrifugal pumps, see Figure 3-1, it can cause an unexpected breakdown, resulting not just in significantly reduced efficiency but also considerable production loss [108].

With centrifugal pump bearings there are many causes of failure, but the most common causes are; inadequate lubrication with excessive heat generated at the bearing, misalignment of the unit resulting in excessive radial load, and/or overloading the bearing element [146]. There are also various other reasons for failure in rolling-element bearings, such as contamination of the bearing oil by solid particles, water or corrosive materials which react chemically with the bearing's surface [109]. Manufacturing defects, careless handling and/or fitting resulting in inadequate internal bearing clearance, excessive axial thrust, and unbalanced rotating elements are other reasons for early failure in rolling-element bearings.

Lubrication is used to reduce the friction between moving components and helps to extend component life by decreasing wear. Non-contaminated oil at a temperature of 30 °C can remain useful for thirty years without requiring replacement [109]. Excessive heat generated by overloaded bearings will cause the temperature of the lubricant to rise and reduce its capacity to support the load [109, 147]. In such a case, bearing-overload can be detected by using infrared thermography to measure the temperature [148].

Increased reliability of rolling-element bearings has been the focus of extensive study in recent years. It is critical to recognize the primary reasons for these breakdown mechanisms and the analytical signatures to identify and treat them at an early stage [149, 150]. Early detection of these faults/flaws enables the problem to be corrected by having the bearing replaced in a timely manner.

Bearings can suffer various faults, such as scratches, grooves, excessive wear, or corrosion due to overload, speed, or length of operational life. Furthermore, foreign objects contained in infected lubricant may become stuck between the rolling elements and the raceway, causing the bearing to fail. Premature bearing failures are described as bearing failures that are not caused by material fatigue. Faulty mounting, poor lubrication, contamination, unsuitable handling, and improper maintenance cause the majority of premature bearing failures [151, 152]. Each of these premature failures may result in a different bearing failure with its own distinct damage, similar to the previously described failure mechanisms. Figure 3-6, summarises the various types of bearing damage [151, 153].

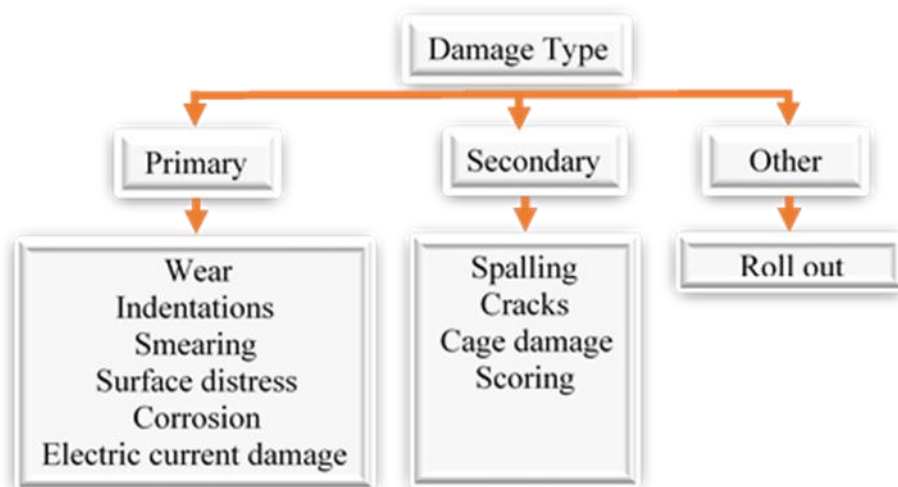


Figure 3-6 Damage type of bearing

3.3.1 Characteristic Bearing Fault Frequencies

All these above different factors can cause vibration of the bearings and increased noise levels. However, such issues are reflected by changes in the pump's operation, allowing defects to be detected and diagnosed via vibro-acoustic signals. The detection of faults in their early stages can provide timely information and enable preventive action to be taken before failure.

With the machine running, a defect generated in a bearing element will change its vibration patterns. The frequency of the signal that occurs due to the bearing defect is called a bearing defect frequency. The fault signature is due to a sequence of impulses occurring at a rate that will be a function of the structure of the faulty component, its geometric dimensions, and its rotational speed. Every bearing fault has a specific defect frequency, which shows as a peak in the frequency spectrum, as a result of increased vibration energy, see Table 3-1 [154]. Of course, harmonics of these frequencies will also be present, and in some cases where the harmonic matches a natural frequency of the structure their amplitudes can be larger than that of the first harmonic.

Table 3-1 Bearing fault frequencies

Location of Fault	Relevant Equation
Inner-Race	$f_i = \frac{nf_r}{2} \left(1 + \frac{Bd}{PD} \cos \Phi\right)$
Outer-Race	$f_o = \frac{nf_r}{2} \left(1 - \frac{Bd}{PD} \cos \Phi\right)$
Cage	$f_{cage} = \frac{f_r}{2} \left(1 - \frac{Bd}{PD} \cos \Phi\right)$
Rolling Element or Ball	$f_{ball} = \frac{PD}{Bd} f_r \left(1 - \left(\frac{Bd}{PD} \cos \Phi\right)^2\right)$

(Where f_{ball} , f_{cage} , f_i and f_o are the characteristic frequencies of the rolling element, the cage, and inner and outer races, respectively; f_r is the rotational speed in Hz, B_d is diameter of roller or ball, PD is pitch diameter, n is the number of rolling elements, and Φ is the contact angle.)

In this research project the seeded faults will be in the inner and outer races of a ball element and the predicted frequencies will be used to detect them at an early stage of development, see Chapter 6.

3.4 Impellers

The impeller is an essential component of centrifugal pump construction and an apparently minor defect on the impeller can easily interfere with pump performance and reduce its productivity [155]. The materials comprising centrifugal pump impellers are generally metal. Natural reactions between an unprotected impeller and the working fluid can corrode the impeller removing material, which is an irreversible process. Of course, the processes are accelerated if particulates are present in the working fluid due to physical abrasion. The higher the flow rate the faster the process, estimated as proportional to the cube of the flow velocity [156].

The processes of wearing of the interior pump components via particles and suspended solids in the working liquid are called erosion [156]. Small particles invisible to the eyes, such as dissolved minerals in hard water, or larger solid particles such as sand, rust, and boiler scale can all cause erosion [157]. The pump casing, shaft sleeves, mechanical seals, packing, and wear rings, all influential components in a centrifugal pump are adversely affected by erosion but the impeller suffers most. Unfortunately, common pumped liquids including industrial effluent, boiler feed water, well water, condensate water, raw water, etc., will all cause some degree of erosion [158].

The phenomena of electrochemical or chemical attack on a material's surface is called corrosion. Centrifugal pump housings are commonly cast iron so a working fluid with PH of 6 or more will cause corrosion. Corrosion generally increases with increase in temperature, or with the presence of oxygen in the liquid [159]. Corrosion is increased by high fluid velocity, and whenever skewed components produce a sudden change in flow rate, also loose-fitting bearings can be further and rapidly deteriorated by corrosion. Corrosion/erosion of the impeller occurs mainly at the junction of the hub and the trailing part of the blade pressure side, and the junction of the shroud and the rear part of the blade suction side [160], see Figure 3.7. This will be the type of impeller deterioration seeded into the pump to be investigated in this thesis.



Figure 3.7 Corrosion-erosion of a centrifugal pump impeller [159])

Both erosion and corrosion of cast iron structures can be reduced by a defensive covering on the outside of the metal. As long as the covering is undamaged the metal surface is protected. Such a protective layer can defend the surface from erosion and even metal to metal contact. To avoid these effects when greater concentrations of solids are present in the fluid being pumped, the interior of a pump can be composed of more resistant materials such as bronze, hardened stainless steel, carbon steel, and high chrome steel, or be coated in ultra-hard coatings such as tungsten alloy or ceramic [85, 157, 161]. However, such attempts to overcome erosion wear can be very expensive.

Fluid velocity is a significant factor in pump wear, for example, the Affinity Laws show that small impellers with high motor/impeller speeds can deliver the required pump pressure, but at the cost of the impeller wearing at a significantly faster rate. The high tip speed of the impeller would cause rapid wear. [85, 112] have shown that when greater than expected wear occurs in a pump, on 95% of occasions the responsibility is high-velocity liquid.

Should the velocity become turbulent it will often cause uneven and excessive wear to some parts, especially impellers [161]. Poor piping design or bad valve sizing could give rise to turbulence and irregular wear in pumps. Thus, whenever possible, the layout should use straight pipelines when building a pump system. Hence, for example, it is suggested not to place an elbow close to the pump as that would cause turbulent flow into the pump. In such situations, where elbows are unavoidable into the pump, it is advised to utilize long radius elbows along with flow straighteners. The use of short radius elbows will cause vibrations and pressure inequalities, and excessive wear of the pump. One

method of decreasing the liquid velocity and friction losses is by increasing the channel size, particularly in the discharge line [85, 161].

3.4.1 Blade Passing Frequency

Blade Passing Frequency (BPF) sometimes called “vane pass” refers to the pressure pulses produced as each impeller vane passes the cutwater (the end of the volute adjacent to the discharge). This phenomenon is common to all centrifugal pumps, and normally poses no problem and, under certain circumstances can be used as a diagnostic tool. However, under certain conditions the passing impeller vanes can initiate flow separation and, possibly, cavitation inside the pump casing.

The k th harmonic of the BPF, f_{bp} , is determined using Equation 3.1,

$$f_{bp} = kN_{bp} \times f_r \quad \text{Equation 3.1}$$

where f_r is the rotational frequency of the impeller in Hertz, and N_{bp} is the number of vanes on the impeller.

BPF is an important source of noise, followed by pressure fluctuations due to turbulence, flow separation, flow friction, as well as vortices in the axial and radial clearances, particularly between open or semi-open rotors and the fixed part of the casing. The frequency and the magnitude of the noise is different from one pump to another and even between two notionally identical pumps, depending on the pump head being produced and the distance the point of operation is from the BEP [118, 119]. The amplitude of the pressure pulsation is held to a minimum while the centrifugal pump operates at its (BEP).

3.5 Pump Vibration Overview

The vibration and resulting airborne sound generated by pumps can be ascribed for the most part to two sources: hydraulic and mechanical. Production flaws or mistakes in pump parts can generate unbalance, misalignment, and non-uniform surfaces (such as waviness of impeller surfaces), all of which generate intermittent or fluctuating forces that cause a vibration of pump components, including attached pipework. Pump surface vibrations couple with the ambient air and radiate outwards as sound. Likewise, the impeller vanes when the pump operates away from the BEP will generate pressure pulsations in the working fluid that will excite vibrations and airborne sound with specific frequencies determined by with numbers of impeller vanes and shaft speed. The non-

stationary behaviour of the fluid flow, turbulence, and cavitation can also generate vibration and airborne sound, though this vibration and sound will exhibit largely random waveforms due to the complex interactions of localised flow fields.

Two sorts of background noise, hydrodynamic and mechanical, are transmitted through the system via the working fluid and structure to the surrounding air as airborne noise. The pump is the leading player, hence, it is important to recognise the pump's contribution to the noise generated [118, 119]. The pressure pulsations produced in an operating pump cavity due to hydrodynamic phenomena are strongly related to its casing vibration levels and levels of radiated sound [162, 163]

Pump hysteresis and hydraulic pump leakage are both significant sources of vibration. The fluid's pressure pulsates primarily with the impeller because it interacts with the vanes of the impeller as well as stationary volute chambers. Thus, the vane number and pump rotational speed will be directly related to the rate of pulsation. If the pump operates too far from the BEP it will not only reduce pump efficiency but also generate high speed eddies or vortices that can cause unwanted vibrations with consequent stress and increased risk of failure. However minimum vibration/noise is generated not at the BEP but at about 10% below BEP [164]. When the liquid flow becomes unsteady and generates local eddies these can interact with the pump, valve body wall, pipeline, or other system elements. Similar interactions will occur when the flow is turbulent and/or vortices are present [162]. In fact, any pump operations which result in a difference between the angle of liquid velocity and the impeller's vane angle can produce vibration [163]. Appropriate features can be developed based on these characteristics to aid impeller fault diagnosis.

Surface vibration and airborne signals demonstrate a clear association with the health of the pump, and analysis of the signals can establish the health of the pump and permit the presence of defects such as leaking mechanical seals, defective bearings, and faulty impellers to be detected [121]. However, the received signal will invariably contain broadband noise from the excitation of hydraulic pressure sources, which in many cases do not represent machine components [69].

In the case of seals, bearings, and impeller, the fault generates vibration, and this is the initial mechanism by which the fault makes its presence felt. According to ISO 10816-8:2014, Evaluation of Machine Vibration, maximum acceptable levels of vibration of

small machines, medium machines and large machines are 2.80 mm/s, 4.50 mm/s, and 7.10 mm/s, respectively. For large machines with a “soft” base the limit is 11.2 mm/s. The vibration may be due to many factors such as unbalanced movement of components, the interaction of the working liquid with the pump or pipeline, and so on [103, 109]. Thus, the vibration levels from faults in the early stage of development will fall well within these limits which was a factor to be considered in selecting the accelerometer to be used here for measurement of the vibration of the pump casing. To investigate pump performance, different tests must be conducted to extract useful information, as the characteristic frequencies and their harmonics of the pump’s component parts will invariably be contaminated by background noise and the natural (resonant) frequencies associated with the pump.

3.6 Airborne Sound Radiation from Vibration Surface

The airborne sound power, P , radiated from the vibrating surface of the pump is, theoretically, given by:

$$P = \sigma \rho c S \bar{v}^2 \quad \text{Equation 3.2}$$

where σ is the radiation ratio of the surface (depends on size, shape and orientation), ρc is the acoustic impedance of the air (ρ , is the local density of air and c is the local speed of sound), S is the area of the vibrating surface and \bar{v}^2 is the mean square surface-averaged velocity of that surface [165].

Assuming σ is constant for the purpose of comparing the sound power emanating from similar surfaces, the sound power level in decibels from a source compared with a reference source, of area S_0 , and mean square surface-averaged velocity \bar{v}_0^2 is:

$$L_w = 10 \log \left(\frac{S}{S_0} \right) + 10 \log \left(\frac{\bar{v}^2}{\bar{v}_0^2} \right) \quad \text{Equation 3.3}$$

where S_0 , the reference surface zone is 1 m², and v_0 the reference mean square speed is 50 x 10⁻⁹ m/s, as indicated by ISO/TR 7849 [165].

3.6.1 Background of Airborne Acoustic: Propagation and Reverberation

Background noise will invariably be present in the measured signal, whether from the local environment or electrical noise generated within the measuring system. However, substantial advances have been made in the reduction of this interference. We are now a

long way from such simple procedures as turning off background noise sources in the vicinity of the test experiment. However, in most experiments the airborne acoustic signal will be produced by numerous sources, not just the primary sources. The task is to separate those signals carrying useful information from those that are not.

Removing undesirable signals requires knowing the range of frequencies of interest for a specific application. The rapid attenuation of high-frequency signals in the air means that signals arriving at the measurement point from significant distances will generally contain the sound of below 20 kHz. Typically, a reasonable frequency range for observation and investigation of airborne sound is 20 Hz to 20 kHz [166, 167]. Sensors with appropriate threshold values and built-in preamplifiers should be used to reduce electrical noise.

3.6.2 Sound Wave Propagation

Since the reverberant acoustic field can obstruct the function extraction, the performance of sound in volumes of air enclosed by boundary surface is important. To understand how the sound field in a closed room influences the essential acoustic features of a sound source, it is important to research the features of the sound field in a closed room.

The outdoor sound field characteristics are clear compared to those of the enclosed sound field since the sound wave from the source spreads out quickly without obstruction and only attenuates with distance. Owing to numerous reflections from the walls, ceiling, and floor, sound released in closed space produces a complex sound field [168, 169]. The sound field in the room becomes more problematic as the room shape becomes complicated; with various surface finishes, phenomenon such as echoes, and flutter echoes may become troublesome.

Assume that there is an omnidirectional source of sound in a closed space, as displayed in Figure 3-7. The acoustic waves are a series of waves propagating along various paths and each will be reflected several times at the wall surfaces; for example, the ray shown in the diagram is reflected first from wall A, then from B, C, and D. Correspondingly, each acoustic wave from the origin would be reflected several times in various ways inside the closed space, resulting in a complex sound field. When the sound energy emitted equals the sound energy absorbed at the wall's surfaces the reverberant field will stabilize [169].

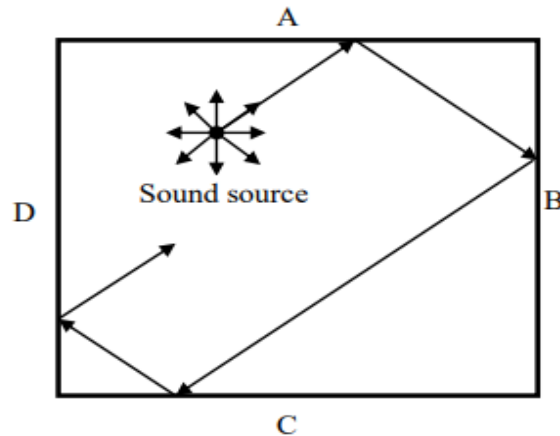


Figure 3-7 Diagrammatic representation of a reverberant sound field in a closed space [169]

3.6.3 Reverberation and Diffusion

In most environments, the sound is made up of direct sound coming straight directly from the source or sources, as well as indirect reflections from surfaces and other items. In room acoustics, for example, both direct sound and reflections from the sides of the wall, ceiling, and floor are important in determining the acoustic signal. When sound strikes a surface, it is transmitted, absorbed, and reflected; the relative amounts of energy used in transmission, absorption, or reflection are determined by the acoustic properties of the surface. Broad flat surfaces (specularly reflected) or a diffusing surface may either redirect or scatter reflected sound. A diffuse reflection happens when a large portion of the reflected sound is spatially and temporally scattered, and the surface involved is often referred to as a diffuse [170]. In a closed room reverberation is due to reflections and will dominate far from the source. The reverberant field is the name given to this reflection-dominated area [168].

The bending or spreading out of sound around obstacles in its path is referred to as diffraction. The size and shape of the barrier, as well as the frequency of the sound wave, interact in a complicated way. Diffraction happens when sound reaches a recess or a surface protrusion, and is more apparent at lower frequencies [171].

3.7 Key Findings

This chapter has examined vibration and consequent airborne sound originating from pump operations, including its behaviour in enclosed spaces. The dynamic interactions between mechanical and hydraulic forces are the fundamental sources, which exhibit stationary modulation behaviour in the measured signals. When faults occur in mechanical components due to wear and fluid erosion, the modulation is enhanced. However, the modulation will be adversely influenced by random noises generated by random flows, making it difficult to characterise the characteristics of the modulations. Thus, this study will take the direction of enhancing modulation components by suppressing random noise in the measured vibration and acoustic signals. To further clarify the research tasks, pump vibration and acoustics from the interaction between mechanical and hydraulic dynamics the reader is referred to Figure 2-16.

This chapter has described the three most commonly occurring mechanical faults in centrifugal pumps: in seals, bearings, and impeller. The mechanisms that generate such wear are described as are the likely consequences. These will determine the specific faults to be seeded into the pump to demonstrate the early detection of common faults. The characteristic frequencies, for bearings and impeller that can be used to detect the presence of bearing and impeller faults have also been presented. The best frequency to be used to detect seal faults will be investigated as part of this research.

CHAPTER 4:

Processing of Vibro-acoustic Signal from Centrifugal Pumps Techniques

This chapter presents an overview of signal processing techniques which are commonly used to analyse sets of dynamic data for detecting and diagnosing machine faults in their early stages. It starts with basic time-domain and frequency domain methods. Then it focuses on those methods that are more useful for demodulation analysis, in particular the Modulation Signal Bispectrum.

4.1 Introduction

Signals measured by sensors such as accelerometers and microphones are often contaminated by various noises including background interference. It is common practice to apply effective signal processing tools for cleaning the signals and extracting fault related information. Signal processing tools can be largely classified into three categories, as shown in Figure 4-1, which presents the most conventional methods utilised in data processing analysis [8, 172].

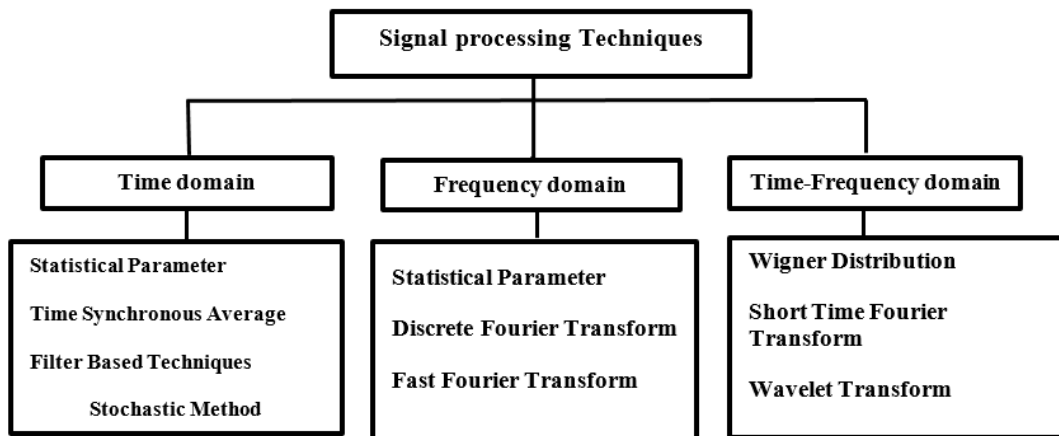


Figure 4-1 Data processing methods [106]

4.2 Time-Domain Analysis

Recording a system's reaction parameters against time, or analysing system data over a specific period, is known as time-domain analysis. Such analysis involves the specification of some measured parameter as a function of time and is an established method of observing a system. Time-domain analysis can provide valuable information regarding the broadband response of the system [173]. This type of analysis is generally connected to performance indices or statistical parameters, for instance, root mean square, crest factor and kurtosis. These statistical parameters are used as trend factors that can provide information about energy levels or signal shape. However, the effectiveness of such performance indexes depends on the mode and its operating environment and whether the faults affect only a narrow frequency band. If so, the amplitude in that frequency band may not be the largest overall component and may not affect the overall peak amplitude [174, 175]. Figure 4.2 shows an example of time domain signals.

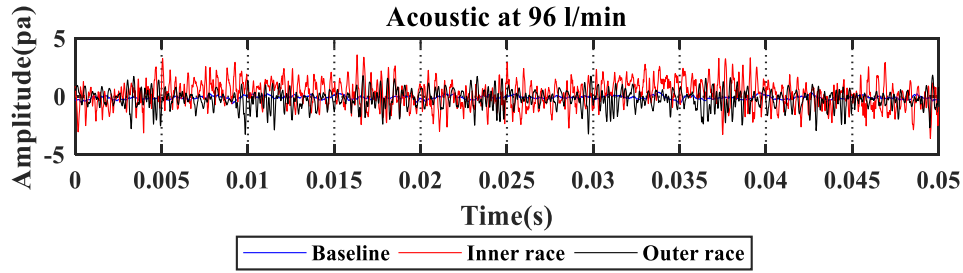


Figure 4-2 Specimen acoustic time domain signals of bearing inner race, bearing outer race and baseline, see Chapter 6.

4.2.1 Root Mean Square (RMS)

The most common statistical parameter, used very often to detect abnormality present in the system is the RMS, which is a measure of the energy content of a signal. This is the square root of the sum of individual samples' square values divided by the total number of samples in a signal, and is represented by Equation 4.1 [176].

$$RMS = \left(\frac{1}{N} \sum_{i=1}^N x_i^2 \right)^{1/2} \quad \text{Equation 4.1}$$

where N is the total number of samples and x_i is sampled time signal.

If the value of the RMS increases suddenly, exceeding a set value, it is assumed there is a fault in the system. However, the RMS is not sufficiently sensitive for detection of incipient faults.

4.2.2 Peak Value

This is the maximum value or amplitude of a signal. The peak to peak values can be positive or negative depending on the signal, see Equation 4.2 [177].

$$Peak = \frac{1}{2} \left(\max(x(t)) - \min(x(t)) \right) \quad \text{Equation 4.2}$$

where $x(t)$ is the signal of interest.

4.2.3 Crest Factor (CF)

The CF is the ratio of peak and RMS values of the signal, see Equation 4.3 [177].

$$CF = \frac{Peak\ Value}{RMS\ Value} \quad \text{Equation 4.3}$$

CF is taken to be an indication of how random the peaks are in the acquired signal.

4.2.4 Kurtosis

Kurtosis gives us shape information concerning the signal. Kurtosis measures the amount of probability in the tails, see Equation 4.4 [178].

$$Kur = \frac{\sum_{i=1}^N (x_i - \mu)^4}{N \cdot \sigma^4} \quad \text{Equation 4.4}$$

where the σ = standard deviation and μ = mean of the signal series $x_i (i = 1 - N)$.

From the literature survey, it is found that kurtosis has a low value for a pump operated in normal condition and a high value for a faulty condition due to the latter signal's abrupt nature. CF and Kurtosis are useful parameters for detection of incipient faults, although with complex or advanced failures they can sometimes fail to distinguish between healthy and faulty conditions of the machine [178].

4.3 Frequency Domain Analysis

As demonstrated by Baron Jean Baptiste Fourier many years ago, any waveform can be created by a combination of sine waves. Frequency domain analysis works by presenting, for example, vibration data in such a form by application of the Fast Fourier Transform (FFT) algorithm. This produces a frequency domain signal from the time domain. Irregularities in the time domain signal appear clearly as peaks in the frequency spectrum, which are usually much easier to detect than the original irregularities. Thus, if a fault generates specific characteristic frequency responses, detection and accurate diagnosis can be undertaken at a much earlier stage to avoid breakdown or deterioration of the system [23]. Frequency domain analysis is a popular means of detecting bearing faults [179]. In addition, the FFT is an efficient means of obtaining narrow band spectra in both low and high-frequency ranges for assessing defects in bearings. However, the drawbacks of frequency domain analysis are that a considerable quantity of data, such as transient or non-repetitive signal components, may be lost during the FFT conversion process as shown in Figure 4-3 [23].

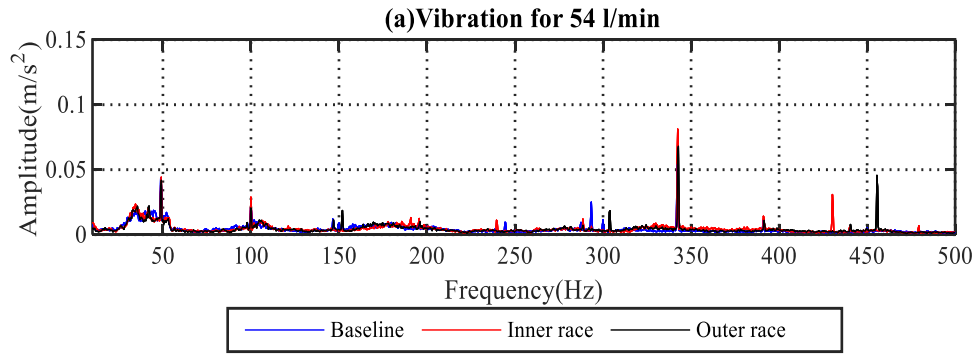


Figure 4-3 Specimen vibration frequency domain signals of bearing inner race, bearing outer race and baseline, see Chapter 6.

4.3.1 Envelope Analysis

In recent years, envelope analysis (EA) has become a common and useful technique for detecting and diagnosing different faults, in particular rolling element bearing faults [180]. A local fault will show itself as an impact frequency and harmonics of that frequency. The detected signal will be the raw signal as affected by the transmission path, so the frequency range in which the harmonics are likely to dominate is where structural resonances amplify the original harmonics [181]. EA examines the signal “obtained by amplitude demodulation” by analysing the frequency domain and utilising strong amplitude modulation phenomena to diagnose the presence of a fault rather than raw data [182, 183].

EA is commonly applied to vibration signals to diagnose incipient faults in machinery, especially when the defects are amplitude-modulating and hence affect the characteristic frequencies of the machine components [180, 184]. Ho and Randall [184] have used this approach very successfully to isolate the frequencies of the interplay between ball bearings and the raceway in a faulty bearing, demonstrating the ability of envelope analysis to present clear peaks, showing the presence of faults at certain harmonics within specific frequency bands. The spectrum provided rich information regarding both the repetition frequencies such as ball-pass frequency but also modulation, shown by the presence of sidebands, due to variation of the applied load [181].

In simple terms, EA is the FFT frequency spectrum of the modulating signal. EA is performed in five steps, see Figures 4.4 and 4.5, by eliminating unwanted noise and emphasising the low-frequency, and likely most useful, content when analysing the signals' frequencies.

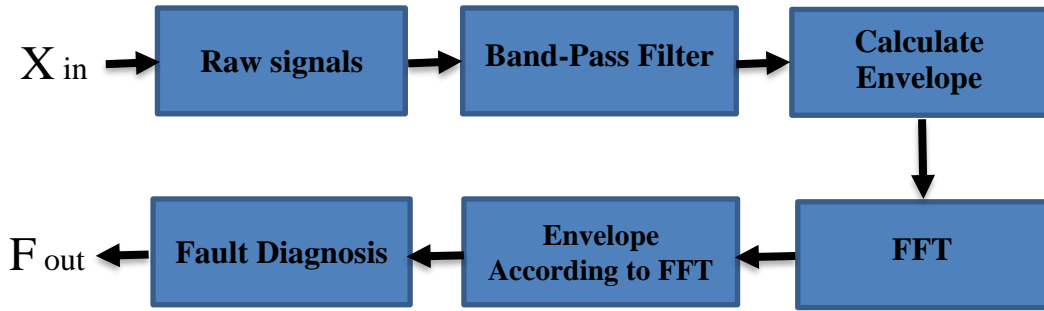


Figure 4-4 Steps in the process of envelope implementation

Referring to Figure 4-4, step one is composed of the first two blocks, the raw data is bandpass filtered to obtain the frequency range of interest and remove low frequency background noise levels, including that due to possible measurement system misalignment and imbalance. This process gives a good indication of signal-to-noise-ratio [180]. McFadden and Smith [185] showed that resonant frequencies of the structure should be considered when selecting the band-pass filter centre frequency, and that the filter bandwidth should be twice the highest fault frequency. That would ensure that the filter passes the carrier frequency and at least one pair of modulation sidebands.

Step two is calculation of the envelope which comprises full wave rectification of the signal from bipolar to unipolar, converting the bottom half of the waveform to the top, and vice versa. This stage is performed using a Hilbert Transform (HT) which returns a complex signal, the real part of which is the original signal and the imaginary part is the HT, which is the original signal subject to a 90° phase shift [186]. Then the carrier frequency is removed by applying peak-hold smoothing, smoothing /filtering the fast transitions in the signal. Finally in step two the high-frequency components are removed by low band pass filtering, and the remaining low-frequency components will include the fault frequencies.

In step three, the FFT is applied to the envelope signals to obtain the envelope spectrum which will reveal the amplitude peaks of the fault frequencies.

The procedure for computing the HT is shown in Equations (4.5), (4.6), and (4.7). The real part of the analytic signal x_a for x_{in} is the original data x_{in} and the imaginary part is HT of x_{in} . After that, Equation (4.8) for the envelope leads naturally to Equation (4.9) for the power spectrum.

$$X = fft(x_{in}) \quad \text{Equation 4.5}$$

$$X_a(n) = |x| = \begin{cases} -x, & x < 0 \\ x, & x \geq 0 \end{cases} \quad \text{Equation 4.6}$$

$$x_a = \text{ifft}(X_a) \quad \text{Equation 4.7}$$

$$x_{env} = \sqrt{x_a * \text{conj}(x_a)} \quad \text{Equation 4.8}$$

$$X_{env} = |\text{fft}(x_{env})| \quad \text{Equation 4.9}$$

Where x_{in} is the input signal; X is the FFT of x_{in} ; X_a is the FFT of analytic signal or complex time signal for x_{in} ; X_{env} is the envelope spectrum; x_a is the analytic signal for x_{in} ; and x_{env} is the analysed envelope signal.

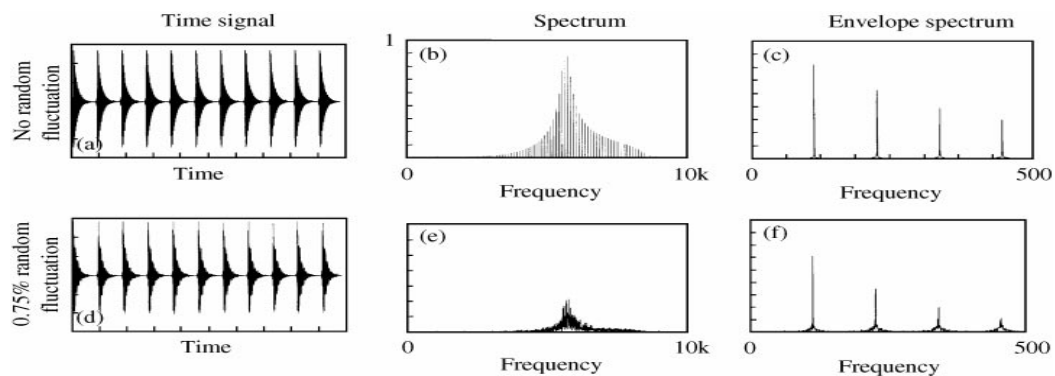


Figure 4-5 Example of envelope spectrums for two bearing faults. (a, b, c) Impulses at equal time intervals with no random noise. (d, e, f) original signal with 0.75% random fluctuations imposed [184]

4.4 Higher Order Spectra

In the early 1960's the general concept of higher-order spectra was introduced by Tukey and Brillinger [187]. Recently, higher-order spectra have been applied in numerous research projects [188]. First order and second-order statistics are commonly used in data analysis applications and considered as reasonable signal-processing tools such as mean, power spectrum, autocorrelation, and variance. Second-order statistics are convenient for describing linear and Gaussian processes, but in reality conditions exist that deviate from both linearity and Gaussianity and here second order statistics are no longer adequate [189].

4.4.1 Power Spectrum (PS)

The power spectrum of the time domain of an acoustic signal presents the acoustic power in the signal in terms of the signal's frequency components. It is a second-order calculation of the harmonic power, which is a true, positive number. The $P(f)$ is a second-order

frequency domain measure of the time-varying series $X(n)$ and is calculated according to [190] [191]:

$$p(f) = E(X(f)X^*(f)) \quad \text{Equation 4.10}$$

Where $X(f)$ is the Fourier transform of the sequence $x(t)$, $X^*(f)$ is the complex conjugate of $X(f)$ at frequency (f) for the time signal, $E(.)$ is a mathematical operators representing the statistical expectation [192].

The definition of the Discrete Fourier Transform, $X(f)$, used to calculate the power spectrum of the discrete-time signal $x(t)$ [193] is presented in Equation (4.11):

$$X(f) = DFT[x(t)] = \sum_{t=-\infty}^{\infty} x(t)e^{-j2\pi ft} \quad \text{Equation 4.11}$$

Where DFT is the Discrete Fourier Transform

It is generally found that the amplitude of the power spectrum increases when the fault severity increases [194]. The power levels contained in different frequency ranges within the spectrum can be distinguished and this can be used for fault detection; however, the accuracy of the results for fault diagnosis can also be affected by the noise contained in the spectrum.

4.4.2 Traditional Bispectrum

In 1980s, a large number of researchers started using conventional bi-spectrum analysis, which is a high order spectral analysis [195]. The advantages and properties of the traditional bi-spectrum analysis were extensively compared with the power spectrum for nonlinear system identification and proved able to substantially reduce Gaussian noise while retaining phase information. The bi-spectrum analysis also proved an effective approach for detecting quadratic phase coupling (QPC) which occurs due to the nonlinear interactions between two signals producing a third whose frequency and phase are equal to the sum or difference of the previous two signals [196].

The traditional bi-spectrum $B(f_1, f_2)$ can be illustrated in the frequency domain as follows:

$$B(f_1, f_2) = E[X(f_1)X(f_2)X^*(f_1 + f_2)] \quad \text{Equation 4.12}$$

Where $E[.]$ and $X^*(f)$ are defined above. f_1, f_2 and $f_1 + f_2$ indicate the three individual frequency components achieved from the Fourier series integral.

Third order spectra differ from the second-order spectra in that they contain both the phase information and magnitude of the original time signal. The frequency components f_1 , f_2 and $f_1 + f_2$ are independent of each other and each frequency can be characterised by statistically independent random phases that are distributed over $(-\pi, \mu)$:

$$\varphi(f_1) + \varphi(f_2) = \varphi(f_1 + f_2) \quad \text{Equation 4.13}$$

Peaks that appear in the bi-spectrum at the bi-frequency $B(f_1, f_2)$ are due to nonlinear coupling. The normalised form of the bi-spectrum, or bicoherence is adopted as a measure of the degree of coupling between the various frequencies, and is expressed as in Equations (14):

$$b^2(f_1, f_2) = \frac{|B(f_1, f_2)|^2}{E[|X(f_1)X(f_2)|^2]E[|X(f_1+f_2)|^2]} \quad \text{Equation 4.14}$$

4.4.3 Modulation Signal Bispectrum

In order to improve the performance of the bi-spectrum for characterising faults, particularly in rotary machinery, the modulation signal bispectrum (MSB) has been developed to include the possibility of the occurrence of an interaction at $f_1 - f_2$, see Equation (16)[197]:

$$B_{MS}(f_1, f_2) = E[X(f_2 + f_1)X(f_2 - f_1) X^*(f_2)X^*(f_2)] \quad \text{Equation 4.16}$$

The total phase of the MSB is:

$$\varphi_{MS}(f_1, f_2) = \varphi(f_2 + f_1) + \varphi(f_2 - f_1) - \varphi(f_2) - \varphi(f_2) \quad \text{Equation 4.17}$$

When two components f_1 and f_2 are coupled together, their phases can be obtained as:

$$\varphi(f_2 + f_1) = \varphi(f_2) + \varphi(f_1) \quad \text{Equation 4.18}$$

$$\varphi(f_2 - f_1) = \varphi(f_2) - \varphi(f_1) \quad \text{Equation 4.19}$$

From Equations (4-18, 4-19) it can be seen that combining the equations, the total phase of MSB in Equation (4-17) will be zero. The MSB amplitude is the product of four magnitudes. The bi-spectral peak appears at (f_1, f_2) . If $(f_1 + f_2)$, $(f_1 - f_2)$ are both produced due to nonlinear effect between f_1 and f_2 the bi-spectral peak will appear at bi-frequency $B_{MS}(f_1, f_2)$. In this way, sideband characteristics of a modulation signal are effectively represented by the MSB. MSB magnitude would be almost zero if these components have a random distribution but are not coupled. Wide-band noise in vibration signals can be effectively suppressed in this way, allowing for accurate detection of

discrete components. The rate of coupling among three components can be measured using a modulation bicoherence signal. Equation (4-20) is used to calculate the degree of coupling between three components [196, 197].

$$b_{MS}^2(f_1, f_2) = \frac{|B_{MS}(f_1, f_2)|^2}{E[|X(f_2)X(f_2)X^*(f_2)X^*(f_2)|^2]E[|X(f_2+f_1)X(f_2-f_1)|^2]} \quad \text{Equation 4.20}$$

4.4.4 The Performance of Bispectrum

The bispectrum approach has various positive properties compared with the conventional power spectrum; as stated in the previous section, non-linear system recognition, Gaussian noise elimination, phase information preservation and recognition of the QPC that can emerge when two signals interface non-linearly with one another and produce a third with a frequency and phase equivalent to the sum or difference between the initial two signals. This could apply, for example, to a signal generated by a non-linear interaction between just two segments: the shaft speed and bearing, or shaft speed and seal. So it is suggested that the bispectrum can give a more exact diagnostic analysis of signals from mechanical elements under fault conditions [196].

4.5 Key Findings

This chapter has overviewed the background of different signal processing techniques often used for vibro-acoustic measurements. Amongst a large family of signal processing tools, it is identified in theory that two potential tools: envelope analysis and MSB are potentially useful to characterise the modulated vibration and airborne acoustic signals.

Especially, the demodulation analysis by MSB has the merits of suppressing random noises generated by vortex flows, friction excitations and measurement noise and promises to give reliable and robust results for detection and diagnosis. Comparatively, envelope analysis can be implemented with less computing cost but has very limited noise reduction capability.

CHAPTER 5:

Experimental Test Rig Facility and Fault Simulation

This chapter presents a comprehensive description and justification of the devices and equipment used in the pump test-rig and explains the choice of the sensors and acquisition hardware used for appropriate and precise measurements of the vibro-acoustic parameters describing the performance of the centrifugal pump and used for fault detection. It also explains how the different faults were chosen and manually seeded into the test pump.

5.1 Introduction

The focus of this investigation is on developing a new and potentially useful method for detecting and diagnosing deficiencies in the performance of a centrifugal pump. This will involve experimentally checking the condition of a pump using vibro-acoustic measurements to investigate and detect faults/flaws. To accomplish this aim, the test-rig available in the University of Huddersfield's Centre for Efficiency and Performance Engineering (CEPE) was used but with capability enhancement carried out by introducing the centrifugal test pump, renewing and replacing pump parts to simulate different faults and adding data acquisition sensors suitable for the required vibro-acoustic measurements. The developed fault simulations were bearing inner race and outer race faults, wear on the impeller inlet vane, and a faulty mechanical seal. It was also necessary to update and upgrade the software so that it could provide the higher order analysis (MSB). This was a reasonable and cost-effective way to provide a test rig that met the essential requirements of the proposed project.

5.2 Test-Rig Facility and Description

Figure 5-1 presents the test-rig, the core of which is the Pedrollo centrifugal pump, model F32/200A. The pump is a closed type of single-stage driven by a three-phase electric pump motor at 9.5 A and 380-400 V, with a rated rotation speed of 2900 rpm. The pump can deliver 450 l/min with a head of 0.55 bar, it is integral to a closed loop recirculatory system containing water at a maximum pressure of 10 bar. The piping is steel connected to plastic water tanks.

Figure 5-2 is a schematic of the system, showing the pump and transducers, which were located appropriately and positioned precisely. The specifications of the transducers are listed in Table 5-1 and Table 5-2 and were used to measure the multiple operating parameters commonly used in experimental hydrodynamics, such as flow rate, flow pressures at the different flow rates, as well as surface vibration and airborne sound.

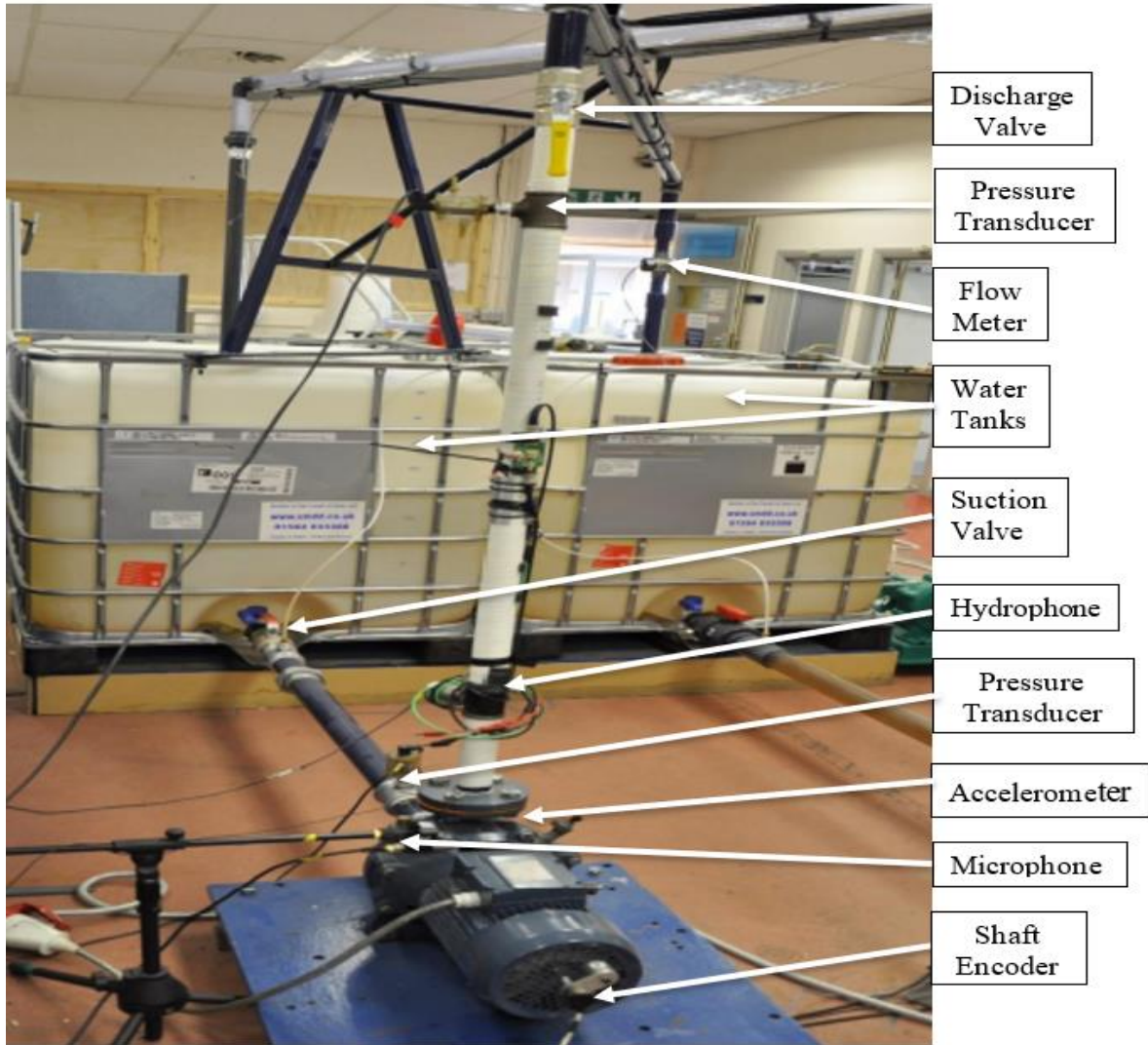


Figure 5-1 The Test-Rig, showing Pedrollo pump and transducers

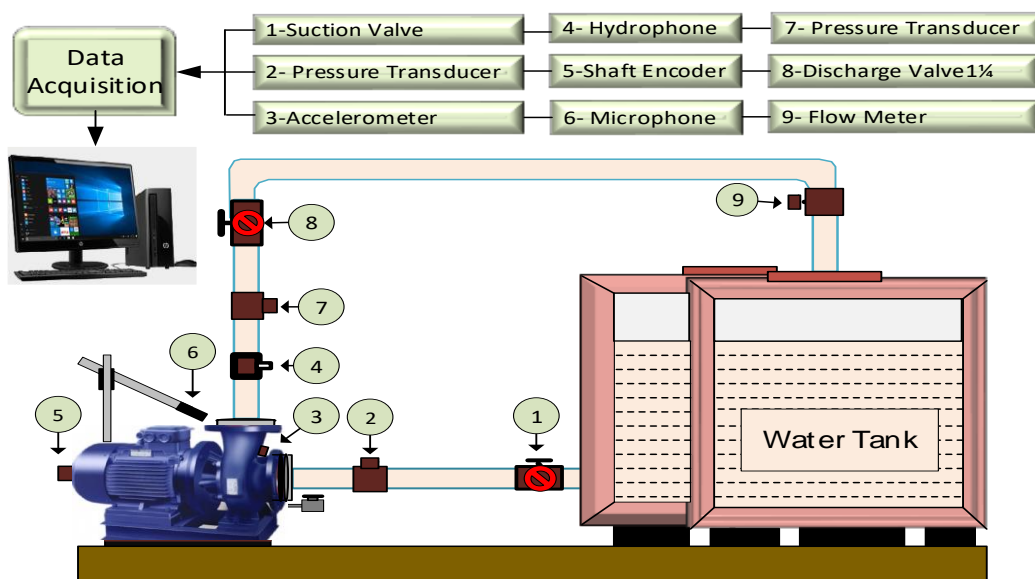


Figure 5-2 Test rig schematic.

Table 5-1 Test-rig components

Components	Type	No	Remarks
Centrifugal pump	Pedrollo F32/200AH	1	Main operator part
Water flow rate Transducer	Gems Rotor flow RFO	1	In the discharge line
High-pressure transducer	Sinocera CY-YB-025-1 MPa	1	Discharge line 0-10 bar
Low-pressure transducer	Sinocera CY-YB-025-0.5MPa	1	In suction line 0-5bar
Accelerometers	Sinocera YD3 8180	1	Inlet and outlet of pump
Shaft encoder	Hengstler R1 32	1	On the pump shaft
Microphone	Sinocera type 4130	1	Close to pump casing
Hydrophone	Sinocera precision hydrophone	1	In the discharge line
Speed controller	Omron 3G3MV	1	In the discharge line
Spectrum analyser	Type R4131D	1	Connected with power
Data acquisition	Sinocera, YE6230B	1	Connected with sensors

Table 5-2 Piping system components.

System Item	Specification	No	Remark
Water tank (plastic)	Volume = 0.911m ³ Dimensions 870*1080*970 mm	2	
Steel valve 1½" BSP		1	Suction line
Steel reducing bush 2" to 1½" BSP		1	Suction line
Steel valve 2" BSP		1	Suction line
Steel pipe 2" BSP	ID = 50.8mm; OD = 60mm Length between the tank and pump 1690mm	1	Suction line
Equal tee 2" BSP		3	Suction line
Steel coupling 2" BSP		1	Suction line
Steel socket 2" BSP		1	Suction line
Steel reducing screwed socket 1½" -1¼" BSP		1	Suction line
Steel pipe 1¼" BSP	ID = 31.75mm OD = 42mm Height 1970mm ; Length 1770mm Drop = 1070mm	1	Discharge line
Equal tee 1¼" BSP		2	Discharge line
Steel valve 1¼" BSP		1	Discharge line
Steel elbow 1¼" BSP		2	Discharge line
Steel coupling 1¼" BSP		1	Discharge line
Steel reducing coupling 1¼" to 1" BSP		2	Discharge line

5.3 Measurement System

The test-rig was originally constructed for the purpose of monitoring and evaluating the pump system's performance, and this was enhanced to include the necessary sensors and measurements to determine the effects of seeding simulated faults/flaws into the pump. This required selection of the vibro-acoustic sensors to be used and where they were to be positioned. A condenser microphone situated 50 mm from the body of the pump to

measure the airborne sound generated by the pump. The nearfield in which the direct sound radiated from the pump will dominate over its reverberant extends to about one wavelength from the pump surface [198]. Thus, a distance of 50 mm puts an upper limit on the nearfield of about 6 kHz which is well above the frequency of the sounds of interest. The vibration generated will be measured by a piezoelectric accelerometer mounted vertically on the pump body. Already positioned on the test rig were a high-pressure transducer in the discharge line and a low-pressure transducer in the suction line. The flow rate in the discharge line was measured using an electronic sensor. Rotational speed of the pump was determined using an encoder mounted on the end of the motor shaft. A hydrophone was fixed on the discharge line.

The datasets representing the experimental results were gathered for the healthy pump and pump with seeded faults/flaws. It was decided that the pump should be tested with nine different flow rates from zero to around 450 l/min in steps of 50 l/min.

The existing seven-channel data acquisition system (DAS) sampled at a rate of 96 kHz. The duration of each sampling period was 40 seconds, giving 3.84×10^6 data points.

5.3.1 The Speed Controller

Typically a centrifugal pump requires a speed controller interface to enable motor speed to react to the requirements of the system. In other words, pump speed must be integrated with the system's demands in terms of pumping power. Here the decision was made to have a range of fixed flow rates but with a constant pump speed of 2900 rpm. The Omron 3G3MV inverter-type speed controller was already present on the test-rig, see Figure 5-3, and this was used to advantage here because it allowed the use of a lower-cost pump with a single impeller. This was important because it enabled a more direct investigation of the effects of the seeded faults/flaws.

The principles of operation of the speed controller are based on converting the AC supply to DC, then reverting to AC in order to meet the pump's demands and match the frequencies required for operation. This method can save energy while controlling the pump speed [199]. The controller is capable of providing high-torque control at low speeds. The 3G3MV was a three-phase model appropriate for the power supply available. For a pump with a maximum speed of 2900 rpm, the controller can decrease this speed at regular intervals to zero. However, there are limitations to this approach, if the impeller

is designed with a particular running speed for a given flow rate, any changes in speed may reduce the pumping efficiency significantly [200].



Figure 5-3 Omron 3G3MV inverter-type speed controller

Table 5-3 Characteristics of the Omron 3G3MV inverter-type speed controller

Speed controller specification	Omron
Model	3G3MV
Allowable frequency fluctuation	± 5%
Heat radiation	20.1 W
Frequency control range	0.1 to 400 Hz
Allowable voltage fluctuation	±15% to 10%
Output frequency resolution	0.01 Hz
Control method	Sine wave PWM
Max output frequency	400 Hz
Ambient temperatures	Operating ± 10 to 600C
Location	indoor
Power supply	380 to 460 V AC at 50/60 Hz

5.3.2 Vibration Sensor-Accelerometer

The most widely used transducer for system CM and detection of faults is the piezoelectric accelerometer. Here a Sinocera type YD38180 piezoelectric accelerometer was selected as having an appropriate frequency range, a suitable sensitivity, was relatively small so that it could be fitted easily to the pump surface, of small enough mass that it didn't affect the movement of the surface, adequately robust to withstand the likely environmental conditions, easy to attach to the required surface, and relatively inexpensive. Table 5-4 presents its specifications. The accelerometer was attached to the discharge casing at the outlet of the pump. This was chosen as the point at which the flow

was likely to generate most vibration. Figure 5-4 shows the accelerometer fixed on the pump outlet.

Table 5-4 Characteristics of the vibration sensor

Maker	Sinocera
Model	YD38180
Type	piezoelectric
Sensitive	1.56mv/m. s⁻²
Temperature range	To 250 °C
Range acceleration	<2000ms⁻²
Frequency range	10Hz – 10kHz



Figure 5-4 Accelerometer and location of accelerometer

Advice in the literature from professionals concerned with monitoring pumps is that a single accelerometer is sufficient for smaller pumps, of which the Pedrollo is one. The accelerometer should be rigidly attached to the metal comprising the pump housing with the sensor mounted so that it is in normal (90°) to the face of the bearings [201]. To ensure the accelerometer was rigidly attached to the pump a brass stud was screwed into the casing and the accelerometer attached to the stud using superglue. The output was fed to a Sinocera YD3 131 charge amplifier, then to the DAS and finally to the PC. All recorded information was sent to the PC hard drive preparatory to analysis.

5.3.3 Acoustic Microphone

Acoustic techniques are regarded as a non-destructive form of testing and are becoming increasingly familiar as a sensor in CM systems for the measurement and analysis of the noise waveforms generated by machinery in operation [202]. Airborne sound techniques focus on the analysis of the waveforms of the noise signals picked up from microphones.

The major advantage of most microphones is their wide frequency response and relatively ease of mounting. Figure 5-5 shows the position of the microphone, 50 mm from the pump casing, this was a compromise between the sound radiated from the pump and the background noise that would be likely to be present in an industrial environment.

The further away from the source the relatively stronger the background noise, the closer to the pump the more likely the measured sound would be dominated by the area of pump surface closest to the microphone. The decision on where to position of the microphone was a balance, and it is not suggested that the chosen microphone position would be the ideal position in other circumstances.

The microphone specifications are given in position close to the pump

Table 5-5. The microphone output was linked to a pre-amplifier after that to the DAS and from there to the PC.



Figure 5-5 Acoustic microphone and position close to the pump

Table 5-5 Acoustic microphone characteristics

Manufacturer	Sinocera
Microphone	Electret condenser microphone
Sensitivity	40mv/Pa
Microphone preamplifier	YG201
Sensitivity	50 mV/Pa
Dimensions	Ø 12.7 mm x 70 mm (including connector)
Max output voltage	5.0 Vrms
Linear frequency range	20Hz – 100 KHz ±0.2dB
Operating temperature range	-40 °C to +80 °C
Linear frequency range	20 Hz – 20kHz (free field)

5.3.4 Flow Rate Transducers

The flow rate transducer used on the test-rig was Rotor Flow RFO comprising six vanes and a cylindrical rotor, see Figure 5-6. The fluid (water) flowing through the pipe causes the rotor to rotate, and the flow rate was determined by measuring the number of rotor revolutions per unit time. The meter was situated on the outlet at the end of the discharge line, see item 9 in Figure 5.2. The accuracy of the device is high, at around 1 per cent with a frequency range from about 25 to 225 Hz, for the given pipe diameter that represents a range from 50 to around 450 l/min. Further specifications are provided in Table 5-6.

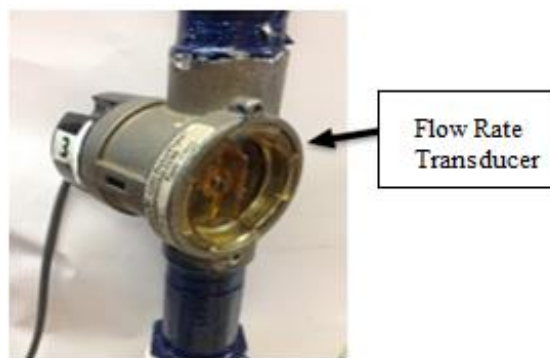


Figure 5-6 Rotor Flow Meter

Table 5-6 Flow meter characteristics

Flow Meter Manufacturer	Gems
Type	Rotor flow RFO
Operating pressure, maximum Polypropylene body	6.7 bar at 21 °C, 2.8 bar max at 80 °C
Max. operating temperature	80 °C
Current consumption	8mA, no load
Electronics (both bodies)	65 °C Ambient
RFO type	0-10VDC Analogy signal @1mA max.
Max. viscosity	45 cSt
Input power	4.5 to 24 Vdc, (24Vdc regulated supply)
Output signal	4.5 to 24 Vdc pulse. Pulse rate dependent on flow rate, port size and range
RFO type	25mA max.
Frequency output range	15 Hz (low flow) to 225 Hz (high flow)
Max. current source output	70 mA

5.3.5 Shaft Encoder

The encoder used in this test-rig was a Hengstler Model-RI 32, as shown in Figure 5-7. This was fixed on the end of the pump shaft to gather data on instantaneous angular speed. The specifications are shown in Table 5.7. The encoder consists of a glass disc with opaque and clear areas. It determines the position of the shaft at different times by using a light source and an optical detector array which reads an optical pattern. The control device reads this code via a microprocessor and that defines the angle and speed of the shaft. As with the other transducers the encoder was connected to the PC through the DAS which was capable of recording the output pulses for every revolution of the shaft and this enabled the shaft speed to be determined.

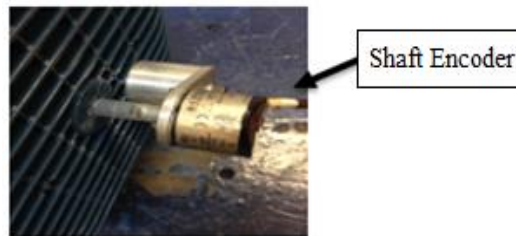


Figure 5-7 Hengstler Model-RI 32 shaft encoder

Table 5-7 Characteristics of Hengstler Model-RI 32 shaft encoder

Manufacturer of encoder	Hengstler
Type	RI 32
Maximum speed	6,000 RPM
Out put	High 2.5V, low 0.5V
Pulse shape	Rectangular
Power supply	5 V d.c
Mounting round	Flange
Shaft diameter	5 mm,6 mm
Max pulses per revolution	360
Torque	$\leq 0,05$ Ncm
Protection class housing/ball bearing	IP 50/40
Vibration performance	(IEC 68-2-6) 100 m/s ² (10 ... 2000 Hz)
Connection	cable axial/radial
Bearing life	In excess of 10 ⁷ revolutions
Material	flange: aluminium, cover: plastics
Weight	50 g approx.
Shock resistance	(IEC 68-2-27) 1000 m/s ² (6 ms)
Operating temperature	-10 ... +60 °C

5.3.6 Data Acquisition System

The data acquisition system (DAS) utilised in this system was a 16 channel, 16-bit resolution Sinocera YE6232B, as shown in Figure 5-8. This system can collect and record data from analogue devices such as chart recorders, physically plotting the signal on a paper sheet, while displaying it on an oscilloscope. The system can acquire the values of eight different variables simultaneously, see Table 5-8. Each input was sampled at 96 kHz. All sensors attached to the test-rig were connected to the DAS.

The sensor outputs were conditioned (e.g., amplified as needed) to convert the signal to a common voltage range, $\pm 5V$. In order for the data to be displayed and stored on the PC, the voltage signals were controlled by the microprocessor system before being input to the multiplexer. The multiplexer processed the signals by using A/D conversion via a sampling and holding unit to an A/D converter and so produces a parallel input to the PC where it can be processed before being displayed and stored. The PC therefore had both an A/D converter and a multiplexer mounted in one of the expansion slots. The specifications of the Sinocera YE6232B are shown in Table 5-9.



Figure 5-8 Data Acquisition system Sinocera YE6232B
Table 5-8 Connection Order for Channels

Chanel No	Variable
CH 1	Speed
CH 2	The pressure transducer of section
CH 3	The static pressure transducer of discharge
CH 4	Vibration
CH 5	Acoustic microphone
CH 6	Hydrophone
CH 7	Flow rate

Table 5-9 Characteristics of Sinocera data acquisition system

DAQ system manufacturer	Sinocera Type YE6232B
Company: Sinocera	YE6232B
Number of channels	16 channels selectable voltage/IPE input, multiplexing is Used to sample each channel in turn.
A/D conversion resolution	16 bit
Sampling rate (maximum)	100kHz per channel parallel sampling
Input range	±5V
Gain	Selectable, either 1, 10 or 100
Filter	Anti-aliasing filter
Interface	USB 2.0
Software	YE6232B analysis software

5.3.7 Intel Pressure Transducer and Discharge Sensors

The pressure transducer used in the suction line was the Sinocera CY-YB-0-5, used for general industrial purposes with an upper gauge parameter of around 10 bar, see Figure 5-9 for its positioning in the suction line. Its specifications are shown in Table 5-10. The essential operation of this kind of transducer is to function as a strain gauge for pressure sensors bonded onto a diaphragm, which flexes in accordance with the applied pressure. The movement of the strain gauge is proportional to that of the diaphragm and directly reflects the pressure in the system. The strain gauge was incorporated into a Wheatstone bridge circuit in order to regulate the readable electrical signal. Although the changes in resistance would normally be too small to be appropriate for monitoring analysis and recording, a condition transmitter/signal was used to convert the voltage signals produced by the two pressure sensors applied to the rig.

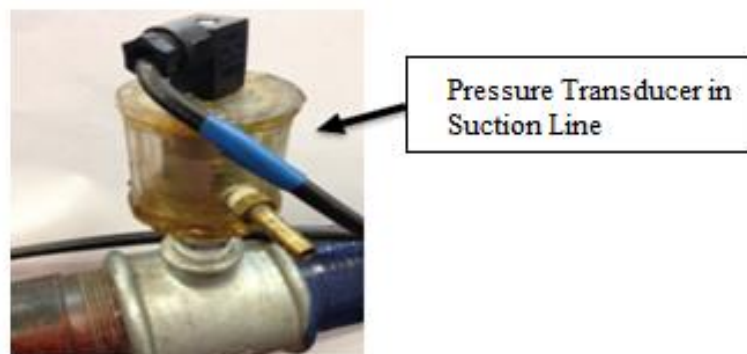


Figure 5-9 Pressure transducer Sinocera CY-YB-0-5 in suction line

Table 5-10 Characteristics of transducer in inlet line

Pressure Transducer Parameter	Sinocera
Product	Strain gauge pressure transducer
Type	Y084602
Measurement range	6 bar G
Operating voltage	12 VDC
Output mode	0-5 ± 0.2 Vdc
Static precision	< 0.3% FS
Screw joint	1/4- NPT external
Operating temperature range	-20 °C to +125 °C

The transducer used in the outlet line, Sinocera Y084602, is shown in Figure 5-10, and Table 5-11 provides its specifications. Typically, the pressure of water in a test-rig for a pump system should range from 0 to 5 bars, subject to the guidelines provided by the manufacturer. Here, the pressure maximum measured in the discharge line was 10 bar, and the pressure maximum in the suction inlet line was 5 bar. The power supply for both transducers was a Farnell Instruments Ltd. L30/2.

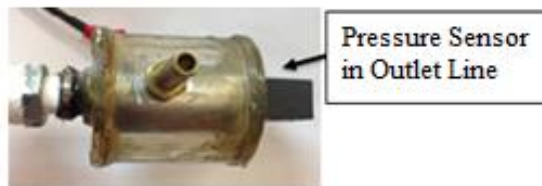


Figure 5-10 Sinocera Y084602 pressure sensor in outlet line

Table 5-11 Characteristics of Sinocera Y084602 pressure transducer in outlet line

Pressure Transducer Parameter	Sinocera
Product	Strain gauge pressure transducer
Type	Y084602
Measurement range	6 bar G
Operating voltage	12 VDC
Output mode	0-5 ± 0.2 Vdc
Static precision	< 0.3% FS
Screw joint	1/4- NPT external
Operating temperature range	-20 °C to +125 °C

5.4 The Centrifugal Pump

The pump selected for use in this study was a Pedrollo F32/200AH, which is categorised as a horizontal entrance, single-stage, machine with a closed impeller, see Figure 5-11. This kind of pump is intended for general use with clean water in agriculture, civil, and several industrial processes. It is of relatively simple construction and very suitable for the insertion of the given simulated faults/flaws: inner and outer race bearing faults, wear of the impeller and a faulty mechanical seal. Further specifications are given in Table 5-12.



Figure 5-11 Centrifugal pump Pedrollo F32/200AH

Table 5-12 Characteristics of the centrifugal pump Bedrollo F32/200AH.

Centrifugal Pump Parameter	Specification Pedrollo
Type	Centrifugal pump F32 / 200AH
Capacity	10 – 30 (m ³ /h)
Head	46 – 57 (m)
Maximum pressure	10 (bar)
Speed	2900 (rpm)
Impeller type	Closed, brass
Number of stages	Single
Power	4 kW
Frequency	50 Hz
HP	5.5
Rated current	8.9 A
Rated voltage	400 V
Connection	Closed

5.4.1 The Relation Between Pump Flow Rate and Pump Head

The curve showing the pump flow rate as a function of pump head is presented in Figure 5.12. This graph represents the healthy baseline (BL) case which will be used for comparison with flow rates obtained after the faults/flaws are introduced. Figure 5-12 shows that that an increase in pump flow rate is accompanied by a reduction of the pump head. However, decreasing the flow resistance at flows over 300 l/min produces little increase in the flow.

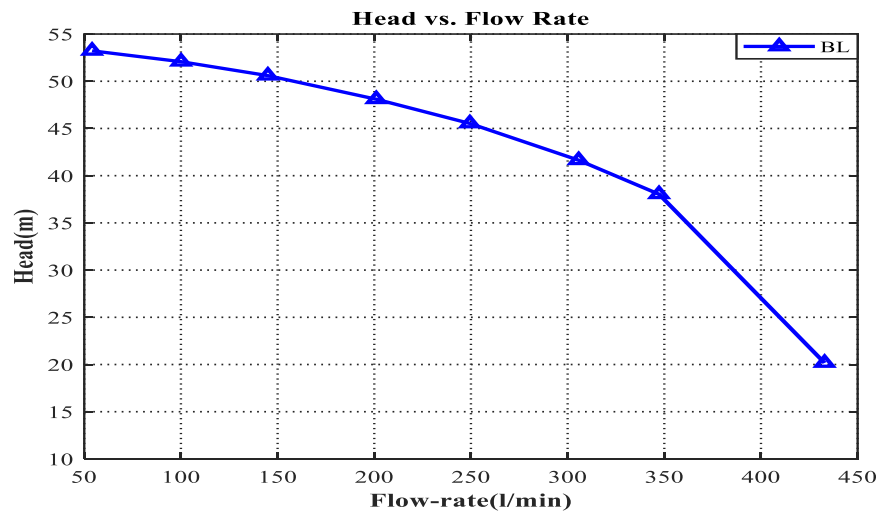


Figure 5-12 The baseline curve of pump flow rate against pump head

5.5 Fault Simulation

These experiments will investigate the detection and diagnosis of seeded localised mechanical faults/flaws. Two strategies could be utilised. The first method is run-to-failure. The machine runs until failure occurs after a fault grows gradually, this method is time-consuming and costly and is rarely used. The other process is deliberately creating an imperfection in the system and to then analyse the impact of the defect by comparing healthy and faulty cases. The latter approach is much quicker and cheaper to implement and was adopted in this experimental study.

5.5.1 Bearing Faults

This study's experiments have examined a common type of deep groove in the ball race of type FAG 6307 bearings, see Figure 5-13, which were attached to the pump shaft. Bearing specifications are presented in Table 5-13. The study was divided into three separate cases; the first case was the healthy bearing as a baseline, the second was a

bearing with a seeded inner race fault, and the third was a seeded fault in the outer race, both faults were designed to simulate abrasive wear.

Abrasive wear can be the result of varying loads, or contamination with micro debris, or lack of lubricant. All these can lead to sliding contact between the balls and the raceway surfaces which ultimately produce this type of bearing fault. Care was taken to ensure the size and shape of the simulated faults agree with the type of abrasive wear of bearings that occurs in industry. This included taking advice from production engineers at HB Bearing Ltd, the company which supplied the bearings. The fault to be seeded also had to be capable of being easily produced in the research centre. Combining these requirements, the final bearing defects were small scratches, see Figure 5-13. The fault measurements were 0.5 mm wide by 0.2 mm deep and 7 mm long, extending across the surfaces of the bearing's inner and outer races.



Figure 5-13 Bearings faults (a) Inner-race, and (b) Outer-race

Table 5-13 The bearing characteristics

Parameters	Measurement
Number of balls	n=8
Ball diameter	Bd=13.49 mm
Pitch diameter	PD=58.42 mm
Contact angle	$\Phi=0$

5.5.2 Mechanical Seal Fault Simulation

Some working fluids contain suspensions that can cause scattered deposits to appear on the faces of mechanical seals, and which then build up. If the deposits cover only a proportion of the face, there will be gaps in the seal around the deposits. The result is a leaky seal. Unfortunately, while the leakage may be small initially, typically it grows at an accelerated pace and more and more of the working fluid escapes. The simulated seal fault introduced here has not, to the author's knowledge, been reported previously. The seeded

fault was a scratch introduced onto the seal surface, as shown in Figure 5-14, that allowed a small leakage.



Figure 5-14 Seal fault simulation

5.5.3 Impeller Wear Inlet Vane Fault Simulation

Erosion due to solid-fluid contact is the primary cause for impeller failures due to wear of the surface of the material. Pump impellers can be subject to severe wear damage, significantly reducing pump efficiency and, eventually, its working life. The impeller needs protection against such wear.

Here wear faults were simulated using closed impeller type 166GRF3228H with two levels of impeller inlet vane fault. The seeded wear faults can be seen in Figure 5-15, simulating erosion-corrosion wear. For the “small” fault a length of 1 mm was removed from one inlet vane, see Figure 5-15, and for the “large” fault 2 mm was removed. Comparisons of the vibro-acoustic signals and flow rates were made between the healthy and faulty cases of impeller wear under constant motor speed and different flow rates.

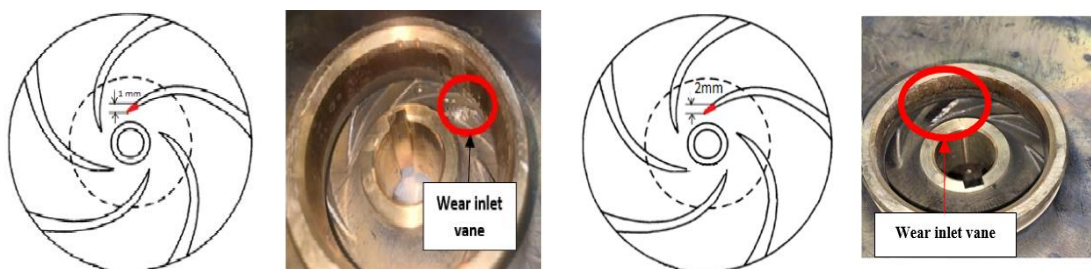


Figure 5-15 Wear fault in inlet vane of impeller

5.6 Test Procedures

The experimental datasets were collected from:

- (i) The test bearings for three different cases: baseline, inner-race, and outer-race faults.
- (ii) The mechanical seal: healthy and faulty.

(iii) The inlet vane of the impeller: with small, large and without wear fault.

The experimental study was carried out under steady-state conditions. The test equipment was started up and left to run a half hour before any data was collected. The DAS collected the measured data on seven of its channels for 40 seconds as described in Section 5.3. Also as described above the pump speed was 2900 rpm and the water flow rates were 0 (blockage) 50, 100, 150, 200, 250, 300, 350, and full flow rate around 450 l/min. The flow rates were controlled manually using the throttling valve in the discharge line. The flow in each case was maintained constant, but the accuracy was around ± 5 l/min.

The pressure sensors in the suction and discharge lines, the accelerometer, the microphone, the flow sensor in the discharge line, the encoder was all set up as described above.

To evaluate the impact of the various faults on pump performance, the sensor signals were measured for the given flow rates. The reliability of the data obtained was confirmed by repeating every test five times under the same conditions. After that, the acquired data were prepared and analysed through a MATLAB program.

5.7 Key Findings

The centrifugal pump CM investigation was carried out using the described pump test rig. The test rig components, including the required measuring equipment and sensors, as well as the data acquisition system used to collect data from the test rig, are described in this chapter. Each test rig cable, DAS channel, and fault form was given its own mark so that the conditions of each record could be easily identified. Different faults were seeded into the centrifugal pump in a realistic industrial scenario to analyse centrifugal pump output under various operating conditions. Before running the test, rig and collecting data, a safety check was performed, which included inspecting all cables and covering any moving parts with a safety grid. The centrifugal pump was then worked under each fault state, and data was collected for that condition. The data was organised, including a test number, date, and condition, and stored in a MATLAB environment for further study. The results revealed that the test rig was well-built and can be used to evaluate various fault cases under wide pump operating conditions.

CHAPTER 6:

Detection and Diagnosis of Bearing Faults Using Envelope Analysis of Vibro-acoustic Signals

This chapter evaluates envelope analysis for detection of seeded bearing faults based on vibro-acoustic signals. After applying time domain and frequency domain analysis, more advanced signal processing, envelope analysis, was used to find the fault signatures corresponding to the inner and outer race faults. The chapter consolidates the main merits of using acoustics signals for monitoring compared to using vibration signals.

6.1 Introduction

In recent years airborne acoustics has been increasingly used for CM of rotating machinery [169]. The acoustic signals are obtained by relatively cheap microphones, that can be easily installed, can be analysed using convenient signal processing software to obtain useful information on the condition of the system. Such airborne sound techniques are non-intrusive, and so is regarded as an ideal option for, e.g., bearing CM, and can give a direct indication of the presence of changes in the noise produced by a machine [43]. Here the acoustic and vibration signals from the bearings were obtained from the microphone installed 50 mm from the pump housing and the accelerometer mounted on the pump casing, see Section 5.3 and Figures 5.1 and 5.2.

6.2 Generation of Surface Vibration and Sounds

Vibration and acoustic noise generated by the pump can be traced to two key sources – hydraulic and mechanical forces, the relative magnitude depending on the build and operation of the pump. The generation of periodic forces acting on the pump housing result in periodic vibration of the surface. These forces, as stated previously, can be due to manufacturing imperfections or errors in rotating components such as imbalances, or non-uniform impellers, or assembly errors such as misalignment. Likewise, pressure pulsations of the fluid induced by the impeller vanes, especially when the pump operates far from its BEP, can also generate small movements in the housing. The vibration of the housing generates sound waves which are radiated into the surrounding air, resulting in the generation of airborne sound. The vibration can have a unique periodicity that correlates with the source, such as number of vanes or rollers in the bearings. Additionally, turbulent flow, especially cavitation, will generate vibration and sound that can exhibit large random waveforms as a consequence of the complex interaction of local flow fields.

These vibration and sound signatures have been shown to bear a close relation to the operation of the pump and its health, and can provide the basis for fault detection [121, 203] as described in Section 3.1. Particularly interesting is the study by Hamomd, et al., [69] which shows the possibility of using such methods to detect bearing faults despite the signal containing a high noise content from other sources, e.g., hydraulic excitations that are normally absent in other machines such as engines and gearboxes. In this case the

characteristics of a faulty bearing were sufficiently different from the random nature of the hydraulic sources to make the presence of a fault detectable. This is a good indication that the sound signal produced by the vibration of the pump casing has the potential to be useful in the detection of bearing faults/flaws.

6.3 Bearing Fault Frequency Calculations

The bearing element to be investigated is a popular type of deep groove ball bearing and is shown in Figure 6-1. The theoretical characteristic faults frequencies were calculated using equations (1), (2), (3), and (4). Table 6-1 shows expected fault/flaw frequencies for the inner and outer races, the rollers and the cage predicted in accordance with the bearing dimensions and operating speed [154]. This type of bearings transmits both axial thrust and radial forces produced by the action of the impeller on the working fluid to be transmitted. The main specifications are shown in Table 6-2.

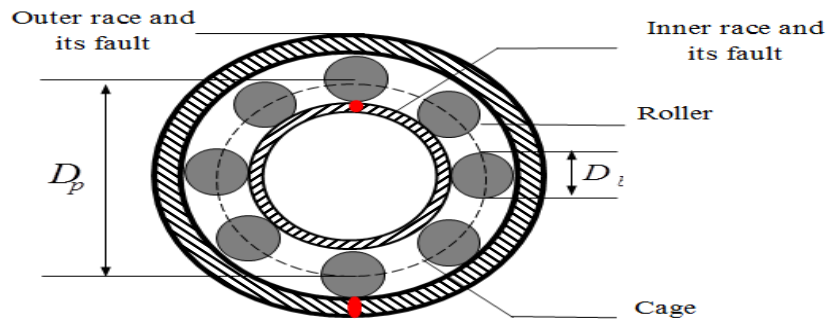


Figure 6-1 Bearing structure

Table 6-1 Bearing fault frequencies

Location of Fault	Relevant Equation	Fault Frequency (Hz)	Equation No
Inner-Race	$f_i = \frac{nf_r}{2} \left(1 + \frac{Bd}{PD} \cos \Phi \right)$	241.5 Hz	(1)
Outer-Race	$f_o = \frac{nf_r}{2} \left(1 - \frac{Bd}{PD} \cos \Phi \right)$	150.9 Hz	(2)
Cage	$f_{cage} = \frac{f_r}{2} \left(1 - \frac{Bd}{PD} \cos \Phi \right)$	18.7 Hz	(3)
Rolling Element or Ball	$f_{ball} = \frac{PD}{Bd} f_r \left(1 - \left(\frac{Bd}{PD} \cos \Phi \right)^2 \right)$	100.5 Hz	(4)

Table 6-2 Specification of FAG TYPE 6307 ball bearing

Parameters	Measurement
Number of balls	n=8
Ball diameter	Bd=13.49 mm
Pitch diameter	PD=58.42 mm
Contact angle	$\Phi=0$

With rolling element bearings the predominant fault is minute spalling indentations generated on the surfaces of rolling elements and races [154]. Such surface fatigue phenomenon is frequently enhanced during running and installation by overloading or shock loading. The fault/ flaw usually begins as a below-the-surface crack which gradually migrates to the surface of the component causing a small piece of the surface metal to break away and leave a corresponding pit. The change in surface geometry immediately impacts on the surfaces with which it comes into contact, there are corresponding changes in the contact pattern with the production of short, sharp contact stresses. There will be a sequence of impulses with a duration and periodicity determined by the dimensions and motion of the bearing. A major reference for identifying and diagnosing of bearing faults is the characteristic frequency at which these occur.

Time and frequency domain signals are used to detect and diagnose the fault. The latter tend to be more useful as they contain the given characteristic components which show as peaks in the spectrum. These can indicate both the presence of a fault/ flaw and indicate what the fault is likely to be.

6.4 Impact of Bearing Defects on Pump Performance Curve

Figure 6-2 presents the performance curve for the baseline and the two defective bearings. We see that at low flow rates there is no significant difference in flow rates due to the presence of either fault. However, at higher flow rates, above about 350 l/min, there does appear to be a slight increase when an outer race fault bearing fault is introduced.

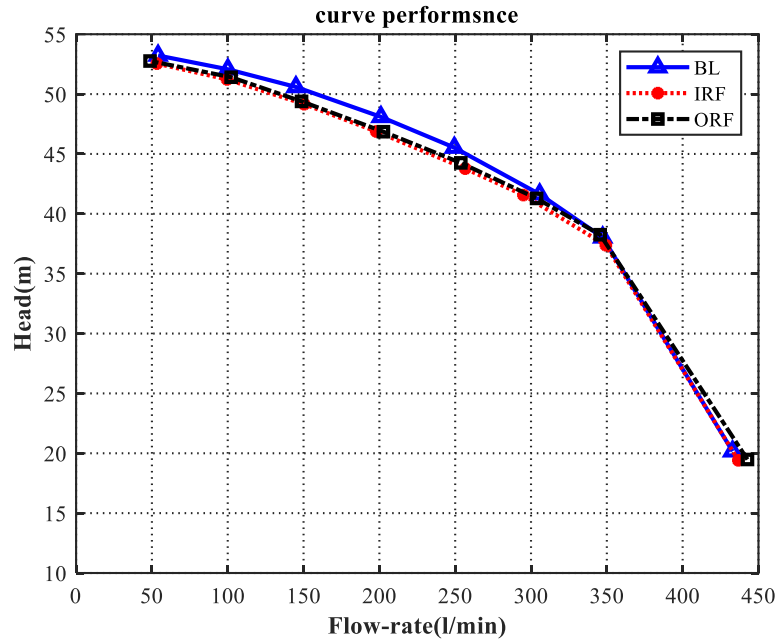


Figure 6-2 Impact of bearing defect on the performance curve

6.5 Time Domain of Acoustic Signals

Figure 6-3 presents the time domain signals for baseline, inner and outer race defects for three flow rates. The measurement run was 40 seconds for all cases. We see that the presence of either bearing defect increases the RMS amplitude of the signal, see Figure 6-4, which is indicative of the presence of a fault. In fact, RMS is the most common statistical parameter, used very often to detect abnormality present in a system. The RMS is a measure of the energy content of a signal, and is represented by Equation 6.1 [176].

$$RMS = \left(\frac{1}{N} \sum_{i=1}^N x_i^2 \right)^{1/2} \quad \text{Equation 6.1}$$

where N is the total number of samples and x_i is sampled time signal.

If the value of the RMS increases suddenly, exceeding a set value, it is assumed there is a fault in the system. However, the RMS has two serious constraints, it is not sufficiently sensitive for detection of incipient faults, and it is a summative measure making identification of the source difficult, if not impossible when it is contained in random noise of much the same magnitude as the fault frequency peak.

The RMS value of the acoustic waveforms demonstrated a clear distinction between the healthy state and defective cases. It also established an apparent difference between the healthy operation and faulty inner and outer bearing races. Except for the highest flow

rate, it was able to separate not only between healthy and faulty conditions but also between the inner and outer race faults. Though, of course, the separation of the faults will depend on their relative magnitudes.

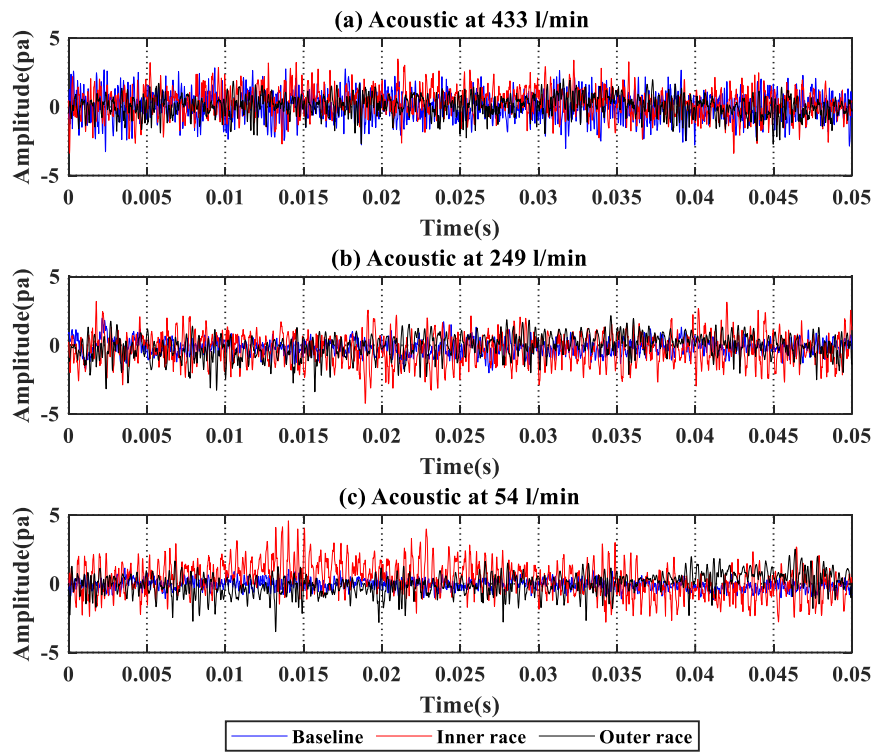


Figure 6-3 Samples of time-domain acoustic signal for baseline, inner and outer races

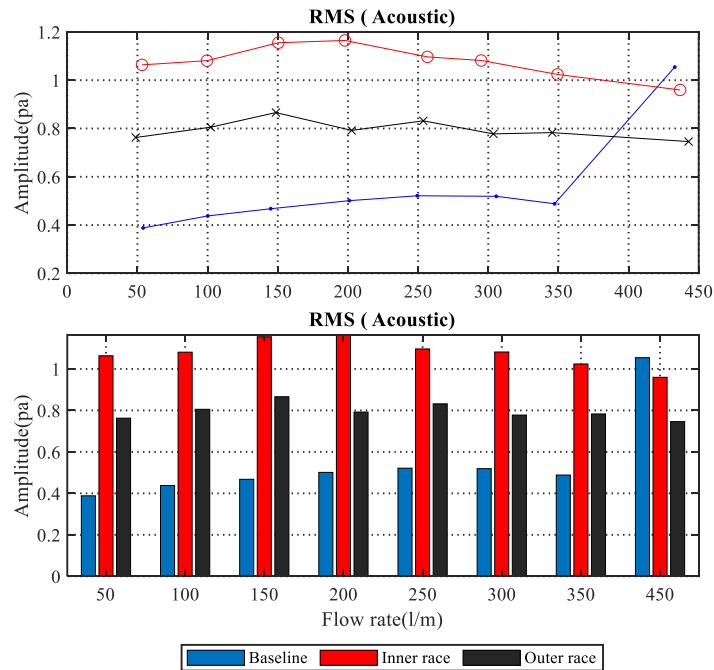


Figure 6-4 RMS of time domain acoustic signals for baseline, inner and outer races

6.6 Spectrum Analysis of Vibro-Acoustic Signals

Figures 6-5 and 6-6 presents the acoustic and vibration spectrums up to 500 Hz, for three flow rates, for the BL condition and both bearing faults. An upper limit of 500 Hz was considered adequate as it encompassed the first and second harmonics of both inner and outer characteristic fault frequencies. It is evident, from these figures that spectrum analysis provides more useful information on the presence of faults than the time domain signal.

Peaks at 150.9 Hz and 241.5 Hz, corresponding to the outer and inner race signature frequencies respectively, can be clearly identified in the spectrums. This is a good demonstration of the inclusion of fault information in both acoustic and vibration signals. We also see peaks at harmonics of the motor's rotational frequency (48.3 Hz), and at 144.9 Hz and 193.2 Hz. Moreover, in on-site operation there can be large variations in low frequency noise making it difficult to reliably estimate the peak values for fault identification. Additionally, due to the non-linearity of impact sounds, it is hard to precisely estimate the peak values present in the spectrum to assess the severity of the fault. Figure 6.6 presents the vibration spectrums for the healthy and bearings with seeded faults for the given flow rates. It is seen that the spectrum peak at 241.5 Hz indicates an inner race defect, while the peak at 150 Hz indicates the outer-race defect, again for all three flow rates. However, on-site both sets of spectrum results for bearing fault detection and diagnosis could be influenced by background noise which would directly affect bearing fault detection and diagnosis.

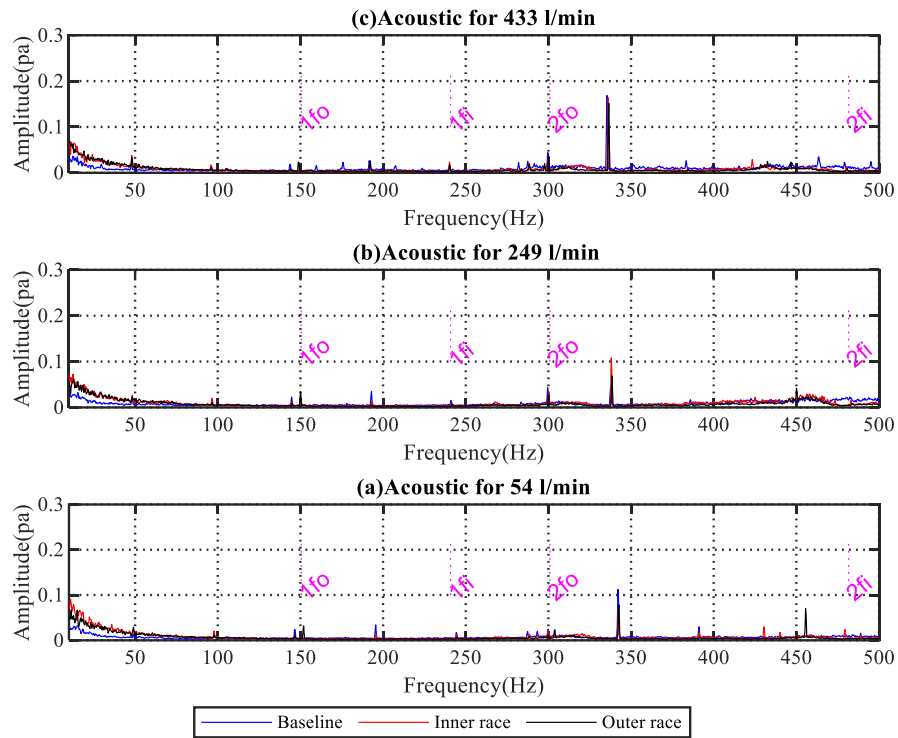


Figure 6-5 Acoustic spectrum for three flow rates Acoustic spectrum for bearings with and without faults for three flow rates (f_i and f_o are inner and outer race characteristic frequencies, respectively)

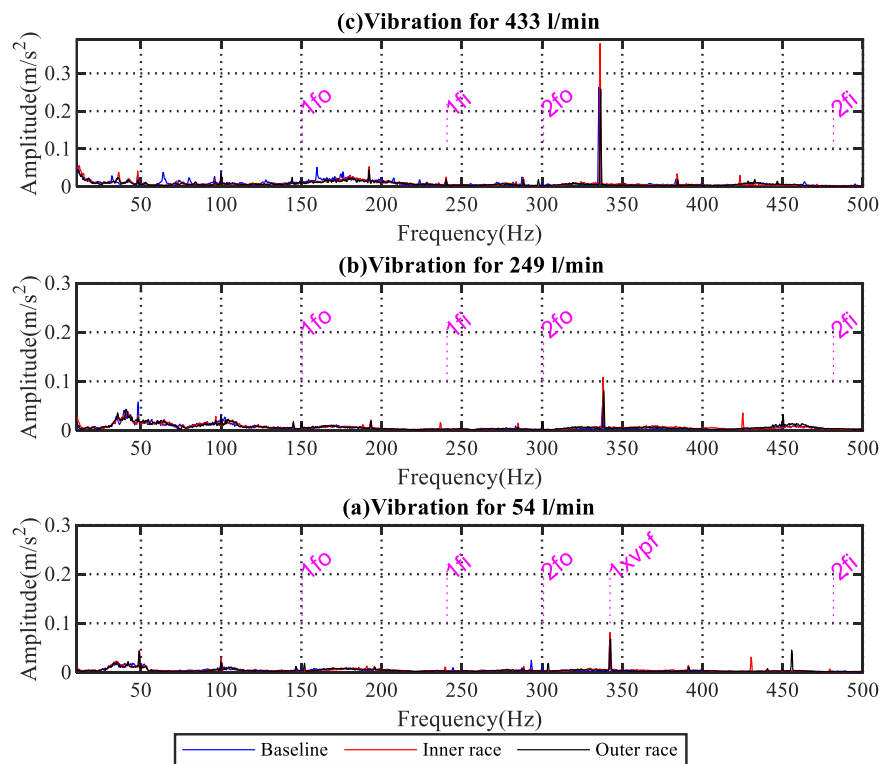


Figure 6-6 Vibration spectrum for bearings with and without faults for three flow rates (f_i and f_o are inner and outer race characteristic frequencies, respectively, and vpf is vane passing frequency)

6.7 Envelope Spectrum of Vibro-acoustic Signals

Envelope analysis is one way to enhance the characteristic fault frequencies effectively and efficiently. Figure 6-7 displays the envelope spectrum for baseline and inner and outer race faults for airborne sound signals for the maximum flow rate of 431 l/min. It can be seen that the inner and outer race characteristic frequencies, f_i and f_o respectively, on the figure, are clearly observable, much more so than in the BL acoustic spectrum. We also note that the harmonics, $2f_i$, $2f_o$ and $3f_o$ are clearly visible.

Figure 6-8 displays the envelope spectrum for baseline and inner and outer race faults for vibration signals for the highest flow rate of 431 l/min. The characteristic frequency for the inner race fault is predicted to be 241.5 Hz, and this can be discerned in the spectra of the vibration signal, Figure 6-8, as can its second harmonic. However, comparison of these peaks with the corresponding peaks in the acoustic spectrum show that they are not so clearly identifiable. This result was somewhat surprising but was confirmed by re-taking the measurements a total of five times.

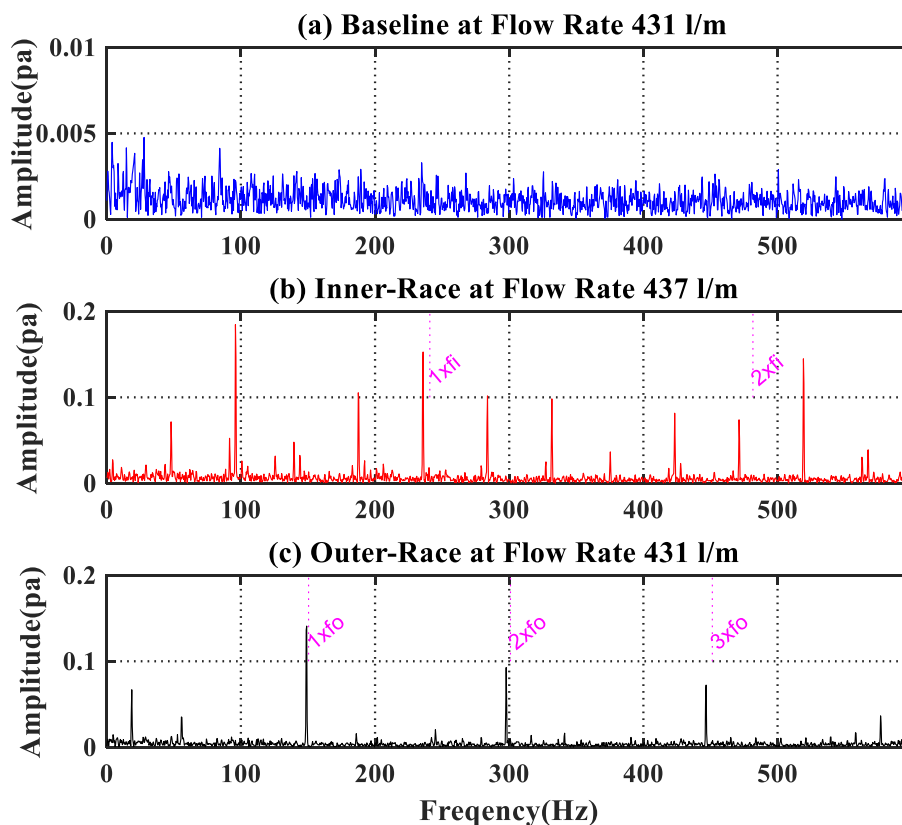


Figure 6-7 Envelope spectra of acoustic signals for maximum flow rate 431 l/min (f_i and f_o are inner and outer race characteristic frequencies, respectively)

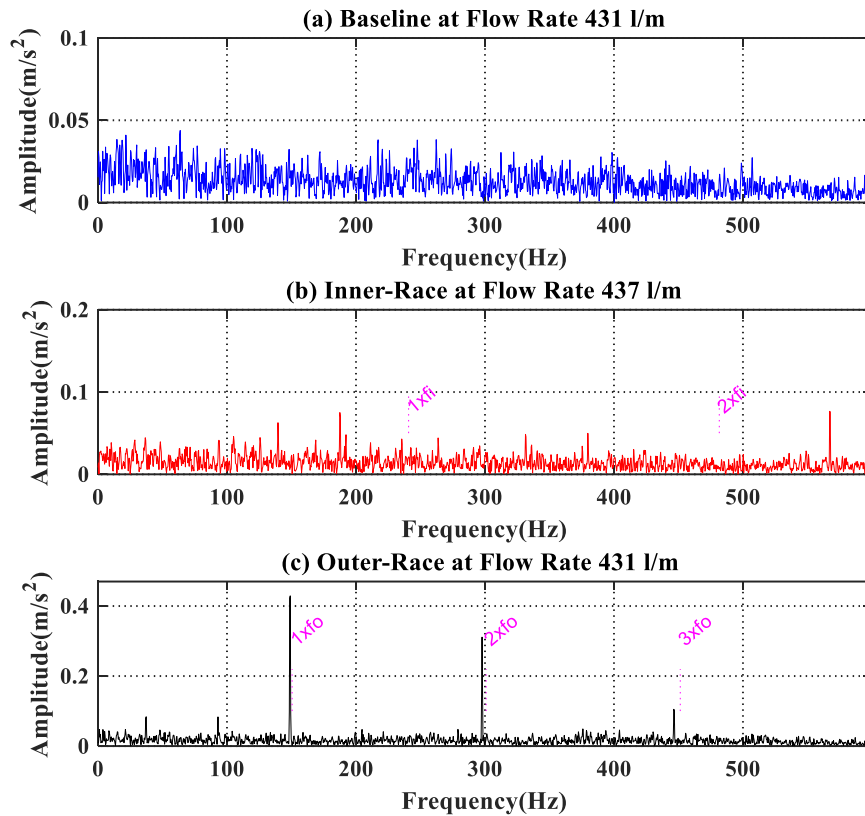


Figure 6-8 Envelope spectra of vibration signals for maximum flow rate 431 l/min (f_i and f_o are inner and outer race characteristic frequencies, respectively)

The envelope spectrum of vibration signals at maximum flow clearly identifies the outer-race fault frequency at 150.9 Hz, together with its second and third harmonics.

Knowing the shaft speed, its harmonics should be easily recognized, and in this plot we see the appearance of harmonics of the shaft frequency (48.3Hz), at 96.6, 144.9 and 193.2 Hz.

Clearly, envelope spectra effectively identified two common bearing faults and distinguished between them using characteristic fault frequencies. It can be seen that the outer race characteristic frequency f_o and its harmonics $2f_o$ and $3f_o$ are obvious in both the acoustic and vibration spectrums. However, the peaks associated with the inner race fault and its harmonics are not so clearly identified on the vibration plots as on the acoustic.

6.8 Comparison of Fault Diagnoses

6.8.1 Envelope Spectrums at Different Flow Rates

Figure 6-9 and Figure 6-10 present the envelope spectrums obtained for both acoustic and vibration signals for the baseline, and inner and outer race faults for three flow rates, the maximum flow is included for comparison purposes. In the plots for both the acoustic and vibration signals, the peaks representing the frequency of the outer-race fault (150.9 Hz) and its harmonics are very clear, and it is almost exactly the frequency predicted, and appears to be independent of flow rate.

The predicted value of the characteristic frequency of the inner-race fault was 241.5 Hz. In the spectrum of the acoustic signal there is a clearly discernible peak close to this frequency, with another peak at the second harmonic for the two lower flow rates. However, while there is no clearly defined peak associated with the inner race fault in the vibration signal spectrum at full flow, there are small peaks at this frequency for the two lower flow rates. It is seen that the envelope spectrum analysis can detect inner and outer-race defects, and the data gathered will be useful for the diagnosis of such faults.

It has been noted that peaks occur in the acoustic spectrum at 50 Hz and 100 Hz that do not occur in the vibration spectrum. On cross-checking with other plots, they are seen only for this set of readings. The peaks represent a one-off incident. 50 Hz and 100 Hz peaks such as these tend to be associated with electrical machinery and referred to as mains hum. The most likely cause of the peaks is that some electrical machinery in the vicinity was active when the contaminated readings were taken but not noticed at the time. Later checks have been unable to identify the machine responsible.

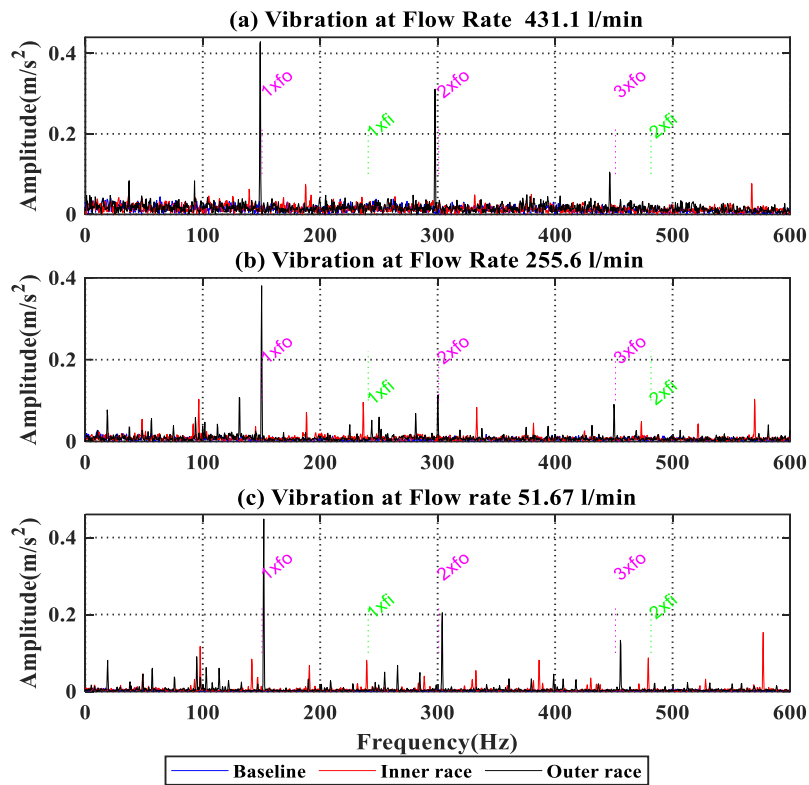


Figure 6-9 Envelope spectrum of vibration signals (f_i and f_o are inner and outer race characteristic frequencies, respectively)

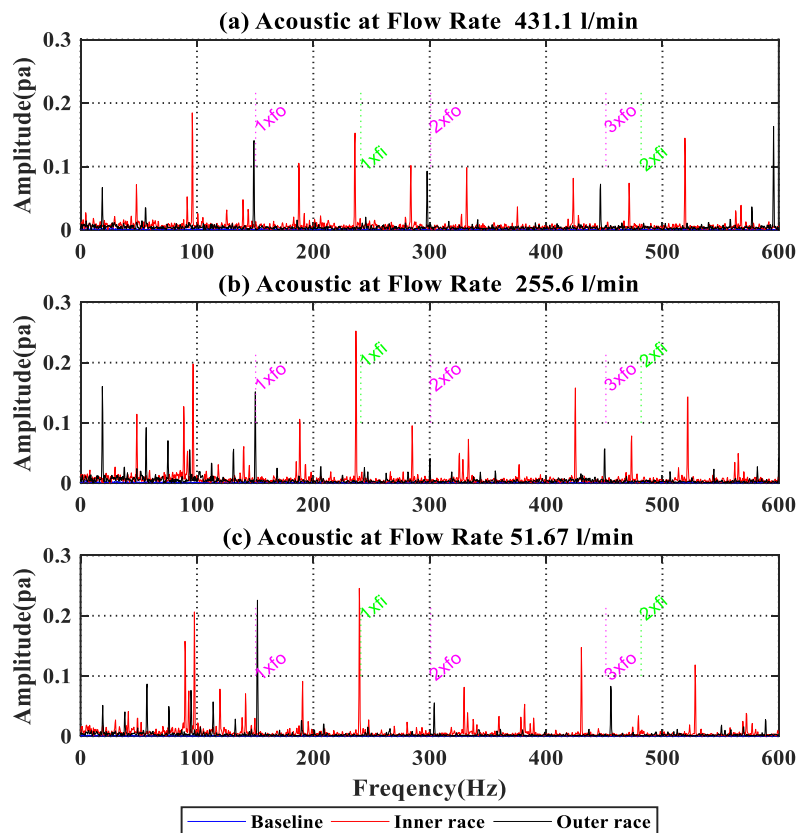


Figure 6-10 Envelope spectra of acoustic signals (f_i and f_o are inner and outer race characteristic frequencies, respectively)

6.8.2 Statistical Parameters for Envelope Signals

Figure 6-11 and Figure 6-12 present the RMS values of statistical measures obtained from the envelope signals obtained for both acoustic and vibration signals for the baseline case and inner and outer race faults. It can be seen that the vibration measures can distinguish between the baseline case and between the two-seeded faults.

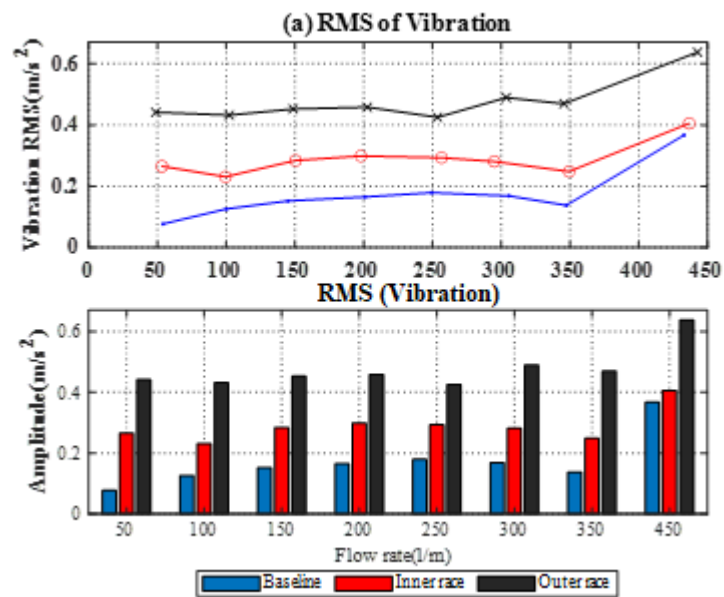


Figure 6-11 Envelope signal RMS of vibration signals for baseline, inner and outer race faults

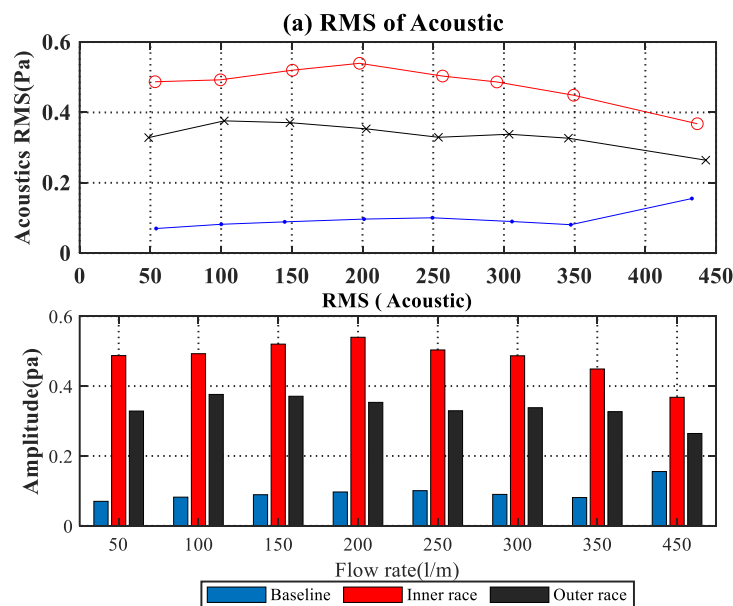


Figure 6-12 Envelope RMS values of acoustic signals for baseline, inner and outer race faults

However, RMS is invariably a measure of the energy contained across the spectrum, and so can indicate the presence of a fault but cannot diagnose a particular fault. The separation between the three cases is generally consistent across the flow rates used, except that at the highest flow rate, the magnitude relating to the baseline increases relative to the others. Also, as seen in the envelope spectrum, the outer race fault is more prominent in the plots than the inner race fault.

Similarly, we see that the RMS for the acoustic spectrum can distinguish between the baseline case and between the two-seeded faults. It confirms the differences between the three plots, including a clearer separation of fault plots from the baseline than occurred for the vibration signal. Once again, however, because the RMS is a measure of the energy contained across the spectrum it is not able to diagnose a particular fault.

6.9 Key Findings

These results confirm that acoustic signals acquired remotely and analysed using envelope analysis are an effective approach for detecting and tracking pump bearing faults. The method produces a more detailed analysis that can provide ample diagnostic information to differentiate between the healthy state of a centrifugal pump with inner and outer race faults/flaws. The signal envelope effectively eliminates unwanted background noise, as well as fluid-induced noise found in the acoustic signal range. Furthermore, the airborne sound RMS values was superior to the vibration signal, in providing a clear indicator of the existence of the inner race fault and the complete distinction between safe and defective conditions. This is because that sound signals perceived by a remote microphone is more compressive in terms of that it is resulted from larger area of vibrations of the pump and thus more sensitively and reliable reflect changes in pump dynamics. In contrast, the vibration signal is only from the dynamic responses of a local point where the vibration response sometimes is less significant due to antinode effect of structural resonances.

CHAPTER 7:

Acoustic and Vibration Signal Based Detections of Bearing Faults using Modulation Signal Bispectrum Analysis

This chapter examines the enhancement of detection of bearing faults seeded into the inner and outer races of the bearings of a centrifugal pump using the Modulation Signal Bispectrum (MSB). It begins by presenting the attempts to find the fault via time and frequency domain analyses. Because of its capability to substantially reduce random noise and detect nonlinear components, the MSB was used for fault detection using vibro-acoustic measurements. Finally, a comparison was made of the fault detection process using the data acquired from the acoustic and vibration signals.

7.1 Introduction

Bearings are an integral component of nearly all rotating devices. The primary function of the rolling element in any rotating object is to hold rotating parts in proper alignment when radial and axial loads are applied. Early identification of bearing faults allows proper action to be taken to sustain and/or increase performance while lowering lifetime costs. One aim of this research is to improve bearing condition monitoring in centrifugal pumps. In contrast to surface vibration measurement, the airborne sound signature and its remote measurement and analysis eliminates the need for sensors attached to the pump.

High levels of background noise, especially with airborne sound signals, makes conventional approaches to detecting and diagnosing machine faults difficult. As a result, advanced signal processing such as the MSB is used to greatly minimise unwanted noise, detect nonlinear components and, when applied to airborne sound and vibration signatures, improve the identification and diagnosis of inner and outer race bearing faults for a range of operating conditions.

The identification and diagnosis of internal and external race bearing defects provide data for comparing the effectiveness of measured vibration and airborne sound signals. The results show that the diagnostic features obtained by applying the MSB to the acoustic signal revealed a greater distinction between safe and defective cases than those obtained when using the vibration signal for detecting inner race defects.

The characteristic frequencies of rolling element bearing faults will depend on operating speed and dimensions. For the given race, FAG Type 6307, see Figure 5-13 and Table 5-13, these are listed in Table 6-1: inner-race, outer-race, cage and rolling element fault frequencies for a motor speed of 2900 rpm (48.3 Hz) are, respectively: 241.5 Hz, 150.9 Hz, 18.7 Hz, and 100.5 Hz.

7.2 The Flow Chart for Bearing Fault Detection

This study was divided into three separate cases; the first was the healthy bearing as a baseline, the second was the seeded fault on the inner race, and the third was the seeded fault on the outer race. The seeded bearing defects are described in Section 5.5.1

The outline of the plan for detection and diagnosis of the seeded bearing faults based on the airborne sound signals and surface vibration is shown in Figure 7-1. Time and frequency domain analyses provide the initial means for finding the fault, see Chapter 6, then, advanced signals processing is applied in the form of MSB analysis for both the airborne sound and vibration signals. Finally, the MSB results obtained for airborne sound and surface vibration for detecting and diagnosing the two bearing faults are compared.

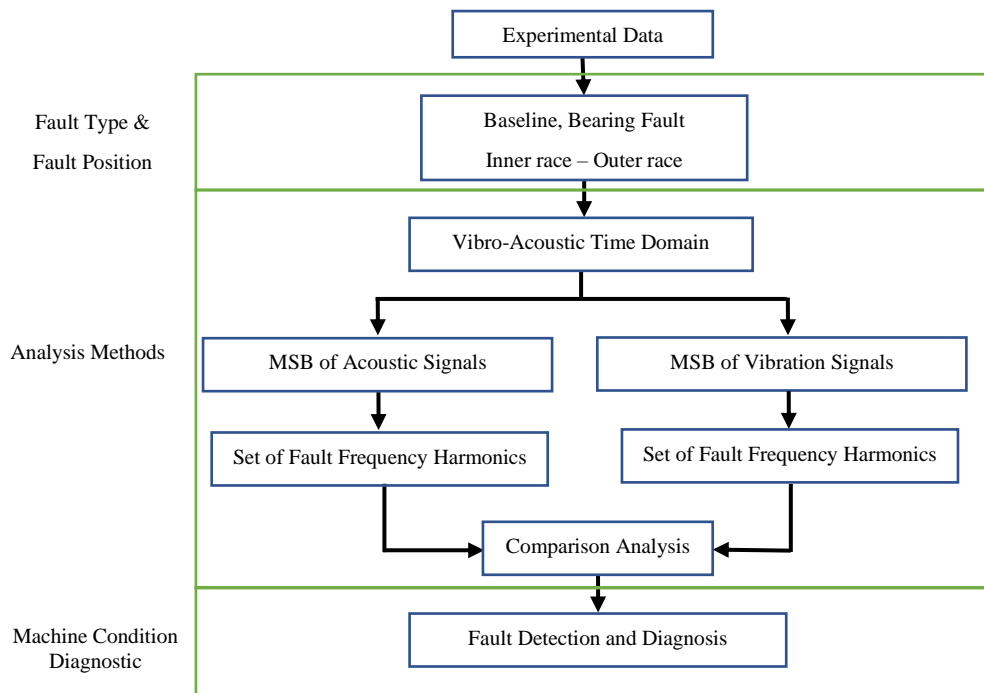


Figure 7-1 Framework of the process for bearing fault detection and diagnosis.

7.3 Test Rig and Experimental Procedure

Three bearing faults examined in this study were in three separate bearings identical save only for the presence of the seeded fault. Each time a bearing was replaced, it was ensured there was no leakage nor any change in operating conditions. Vibration and acoustic datasets were collected for all three bearings for the same range of flow rates, from fully open at 450 l/m the flow was decreased gradually in steps of 50 l/m, 450, 400, 350, 300, 250, 200, 150, 100, and 50 l/m, and then zero flow with the valve fully closed. Control of the flow rate was by a manual valve; Pump motor speed was held constant at 2900 rpm, and the flow rate set to 250 l/min for a pressure head of 10-bar. The pump operated under various flow rates and heads, allowing the pump features to be analysed under a full range of operating conditions.

In this research, MSB analyses based on airborne sound signals and surface vibration signals were conducted in parallel and the results compared to assess the more efficient method of determining the signature frequencies and magnitudes of the spectral peaks. This allowed the differences between the two approaches (vibration and acoustic signal analysis) to fault detection and diagnosis to be evaluated.

7.4 Bearing Fault Detection and Diagnosis Using MSB Analysis

Figure 7-2 displays magnitudes of the MSB peaks and coherence values for the acoustic signal; baseline and seeded bearing faults. We see that the magnitudes are substantially different for the three signals, lowest for the baseline, noticeably higher for the outer race and higher again for the inner race. As expected, the seeded faults in the pump bearing are detectable by the increased magnitudes of specific peaks. When contrasting the baseline with the spectrum levels for the inner and outer races, these peaks are clearly discernible. We also see in Figure 7-3 the presence of nonlinear coupling indicated by the MSB coherence.

Figure 7-4 and Figure 7-5 present the same information for the vibration signals. Once again, we see the magnitudes of the MSB peaks vary between the three tests giving a strong indication of the presence of faults. It can be seen again observe nonlinear coupling. The two findings each suggest clear differences between the baseline signals and those generated by the faulty bearings due to the mechanical driving forces generated by the defects.

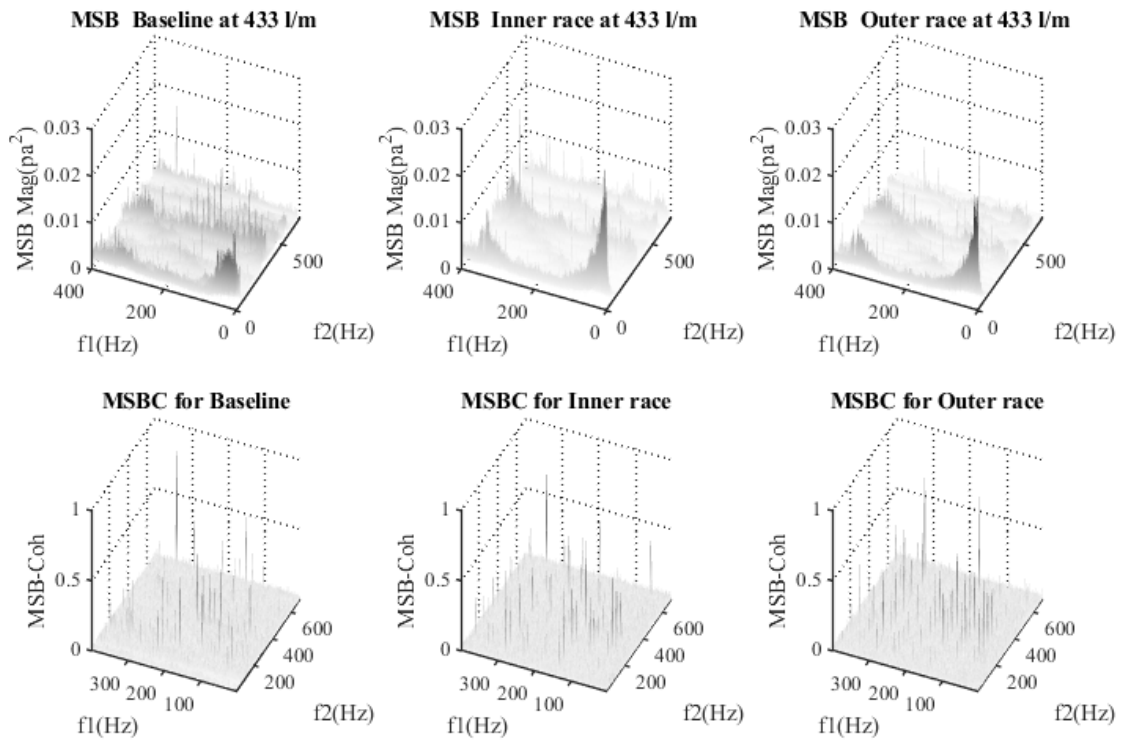


Figure 7-2 MSB magnitudes and coherences for the acoustic signal for flow rate around 450l/m for bearings with and without seeded faults

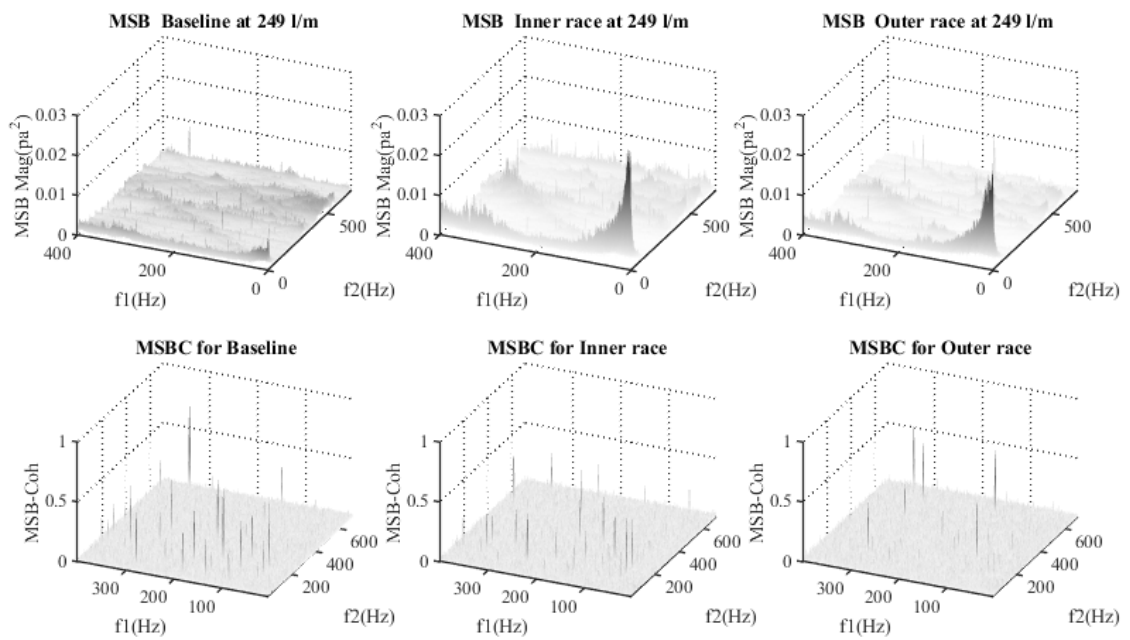


Figure 7-3 MSB magnitudes and coherences for the acoustic signal for flow rate around 250 l/m for bearings with and without seeded faults

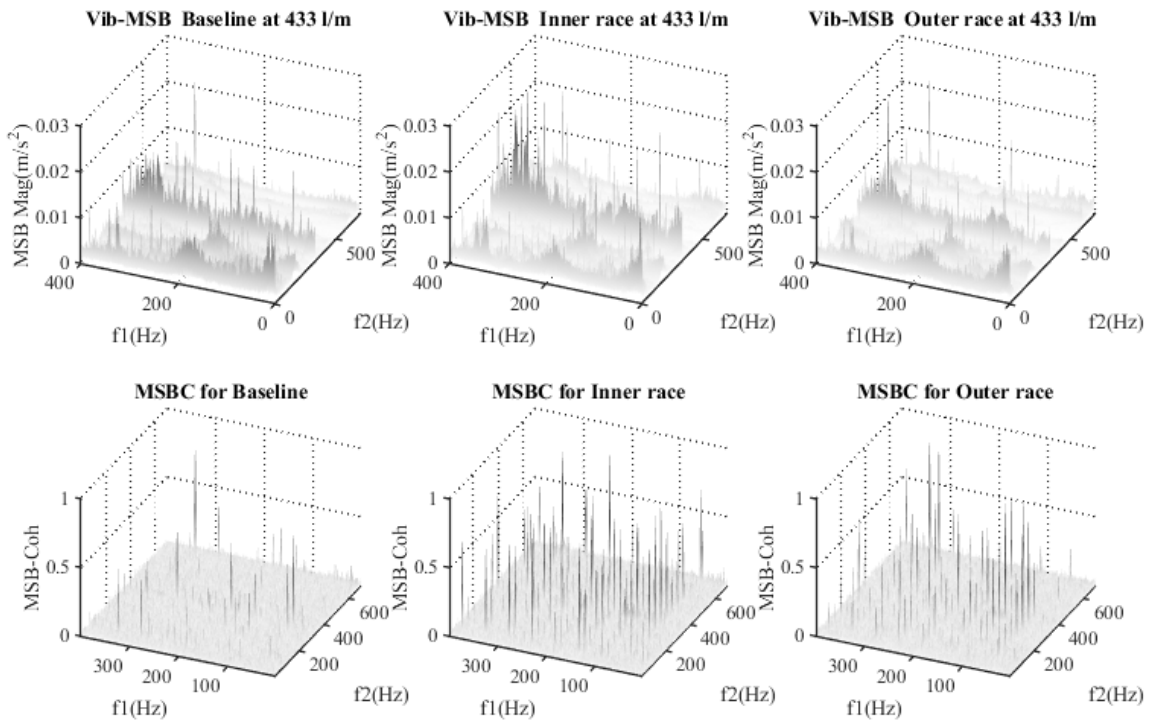


Figure 7-4 MSB magnitudes and coherences of vibration signal for flow rate around 450 l/m for bearings with and without seeded faults

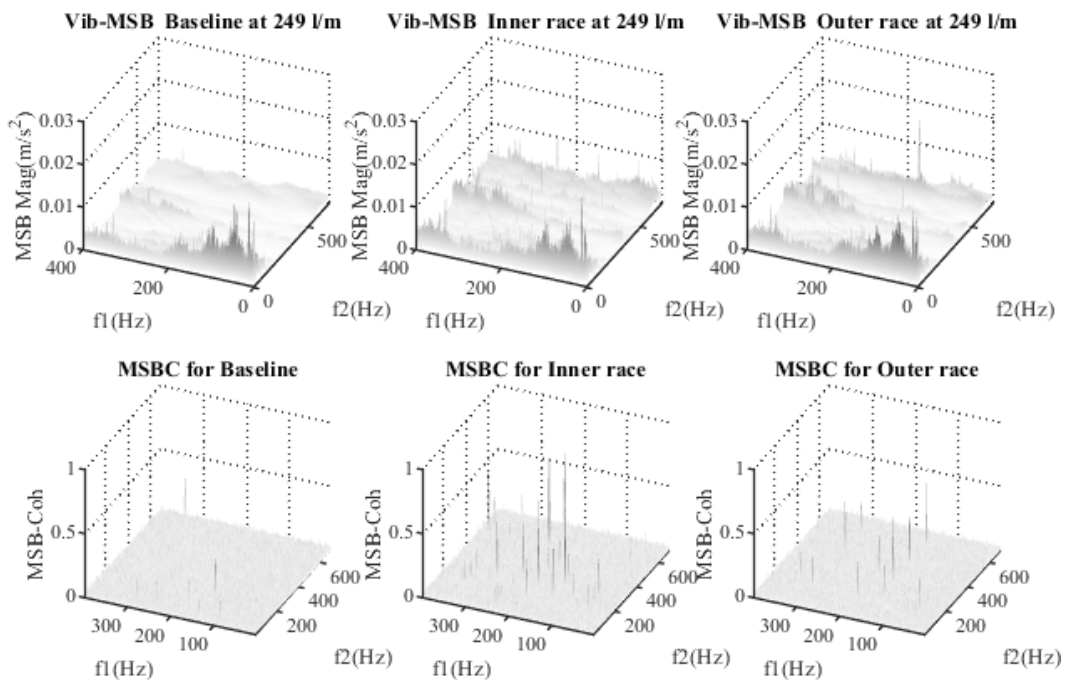


Figure 7-5 MSB magnitudes and coherences of vibration signal for flow rate around 250 l/m for bearings with and without seeded faults

7.5 Comparison of detection results based on MSB peaks

The results obtained using the MSB technique for both vibration and airborne sound signals are discussed and compared in this section to investigate their relative merits in detecting the seeded bearing faults.

Figure 7-6 presents the amplitude of the first and the second harmonic of the MSB peaks for the outer race fault and the baseline, at 150.9 Hz and 301.8 Hz as a function of flow rate. Figure 7-6 (a) shows the results for the vibration signal, we see that for the vibration signals the first harmonic provides little differentiation between cases except for the highest flow rate. For the second harmonics of the outer race, it gives a much clearer separation compared with the first harmonic. Figure 7-6 (b) shows the averaged values of the first and second harmonic peaks of the acoustic signals, there is a clear separation between cases except for the highest flow rate with the second harmonic. Figure 7-6 demonstrates a better separation of the defective case from the BL using the acoustic signal than using the vibration.

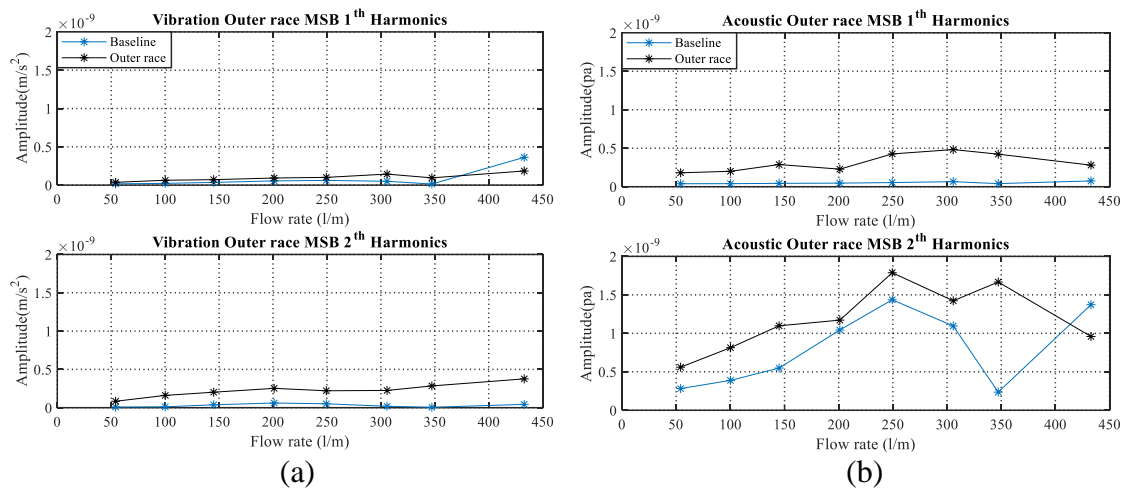


Figure 7-6 Averaged MSB peaks for 1st and 2nd harmonics of outer race fault and baseline for (a) Vibration signals, and (b) Acoustic signals

Figure 7-7 (a) and (b) presents combined average of the MSB peaks for 1st and 2nd harmonics of outer race fault for the vibration signals and acoustic signals respectively. The plots confirm that the average MSB peaks of the 1st and 2nd harmonics for both vibration and acoustic signals can clearly distinguish between the baseline and seeded fault in the outer race, except possibly for the MSB analysis of the acoustic signal at the highest flow rate.

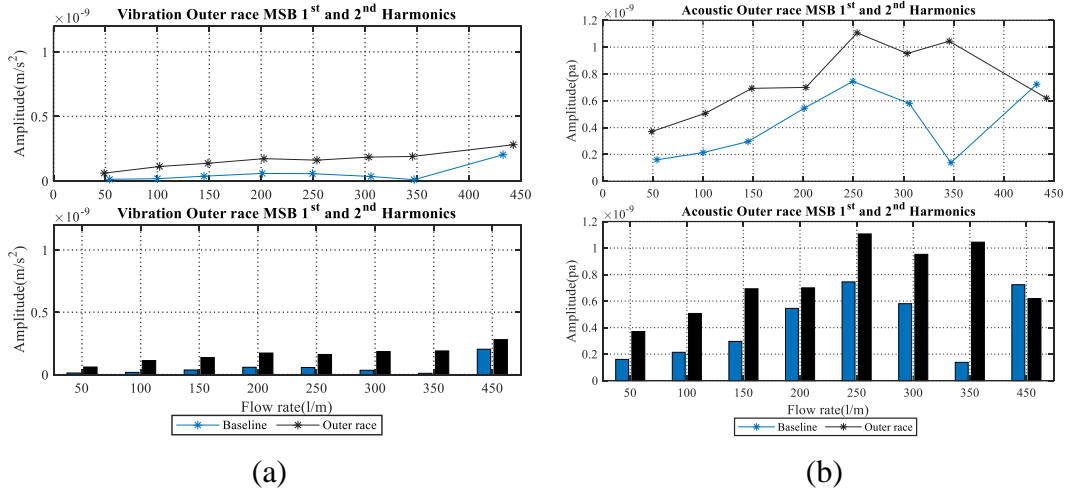


Figure 7-7 Combined averaged of MSB peaks for 1st and 2nd harmonics of outer race fault and baseline (a) Vibration signals and (b) Acoustic signals

Figure 7-8 (a) and (b) presents the average MSB peaks for 1st and 2nd harmonics of inner race fault for the vibration and acoustic signals respectively, as a function of flow rate. For the vibration plots, Figure 7-8 (a), there is significantly less separation between baseline and averaged MSB peaks for 1st and 2nd harmonics of outer race fault than for the acoustic signal. The MSB vibration plots show only slight separation, with the exception of low flow 50 l/m. The acoustic signal, Figure 7-8 (b), shows a clear and significant difference between MSB signals for the baseline and 2nd harmonic for the inner race fault. The peaks for the first harmonic, however, fluctuated and did not differentiate consistently between BL and inner race fault condition.

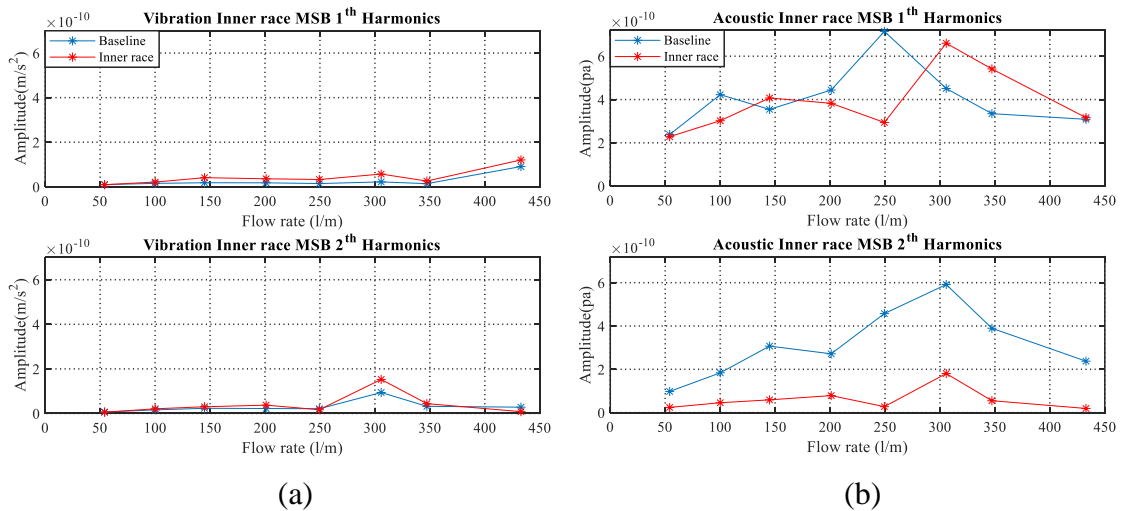


Figure 7-8 Average MSB peaks of 1st and 2nd harmonics of inner race fault (a) Vibration signals, and (b) Acoustic signals.

Figure 7-9 (a) and (b) presents the combined average of the MSB peaks for 1st and 2nd harmonics of the inner race fault for the vibration and acoustic signals, respectively, as a

function of flow rate. The vibration peaks showed no significant difference between this combined average over the range of flow rates and did not provide a strong and clear distinction between the two plots. On the other hand, the peaks in the acoustic spectrum related to the average of the combined 1st and 2nd harmonics showed a significantly larger peak in the presence of faults, demonstrating that the acoustic signal with MSB analysis outperforms vibration analysis for the given test arrangement. Despite a noisy atmosphere that impacted the signals, it was better able to extract modulation characteristics from the bearing faults.

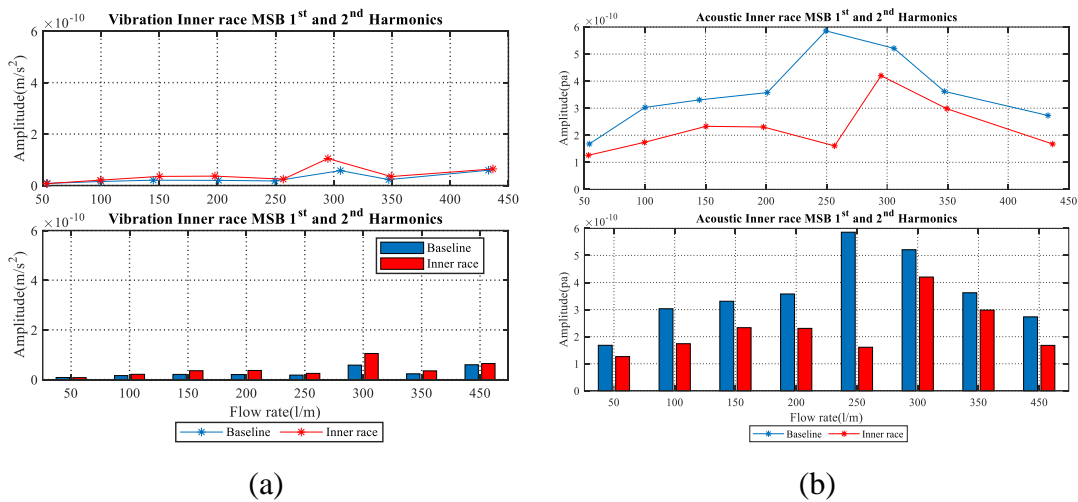


Figure 7-9 Combined average of MSB peaks at 1st and 2nd harmonics of inner race fault (a) Vibration signals, and (b) Acoustic signals

7.6 Key Findings

This study has shown that both the acoustic and vibration signals from a centrifugal pump can be effective in the detection of the given seeded bearing faults. It has been demonstrated that the MSB is able to suppress random noise and enhance detection of the modulation components in both the airborne sound and vibration signals.

The outcome was the successful separation of the averaged magnitudes of the first and the second harmonic peaks of outer and inner race bearing fault compared with the baseline condition, for both surface vibration and airborne sound signals. The results demonstrate that for inner race fault detection acoustic analysis can show a better separation between healthy and faulty signals than the vibration signal. But for the outer race fault the acoustic signal gives greater separation of baseline and fault condition.

CHAPTER 8:

Detection of Fault Modes of Mechanical Seals of a Centrifugal Pump Using Vibro-Acoustic Measurements

This chapter evaluates vibro-acoustic measurements for detecting a mechanical seal fault seeded into a centrifugal pump. Firstly, time and frequency domain analyses were implemented to detect the fault signatures corresponding to the seal fault. Then, advanced signals analysis using MSB was applied. Finally, the chapter summarises and compares the results of the analyses, presenting the main merits of using the airborne acoustic signal for fault detection compared to the vibration signal.

8.1 Introduction

One of the most important components in fluid machines for preventing leaks is the mechanical seal. The seal performance degrades due to improper operations, scratching, impulsive forces, wear, and overheating, resulting in low-performance activity and pollution of the environment. In this chapter the mechanical seal faces, and friction conditions are monitored using vibration and airborne sound signals. Seal failures often produce additional vibration and sound due to the direct interaction of two sliding surfaces, according to their operating mechanisms with surface asperity colliding as a series of random impulses. The resulting vibro-acoustic signals are likely to have a broadband characteristic. The materials used in the structure of the pump and its seals will affect not only the degree to which the elements wear, but also the amplitude of the vibration signal [204]. The amplitude of the vibration signal will increase with increased number and size of wear elements.

An aim of this research is to establish a potentially useful method for the detection and diagnosis of failing mechanical seals in a centrifugal pump using pump surface vibration and airbourne acoustic signals. The broadband sound emitted due to the rotating components will experience low frequency modulation at the shaft drive frequency (48.3 Hz). Based on this information, it is possible to derive fault signatures from noisy sound signals using the MSB, which has the ability to demodulate the signal while also reducing noise. Experiments show that sound signals combined with MSB analysis can detect mechanical seal faults remotely in the early stages, outperforming spectrum analysis. Moreover, the findings presented here demonstrate the efficacy of remote acoustic-based monitoring and provide a clear indication of complete fault separation under various pump operating conditions.

8.2 Flow Chart for Mechanical Seal Fault Detection

The general method is the same as that described in Chapter 7 for detection of bearing faults. However, whereas with the bearing faults we were looking for pre-defined fault frequencies here we are looking for a set of fault frequencies not known in advance that will define the presence of a fault in the seal, see Figure 7-1 and Figure 8-1. Given the mechanism by which the vibration is generated it is expected that the spectrum will contain, as a fundamental frequency that of the shaft

The fault detection is in three stages, beginning with fault form and location, which is the simulated fault, and wear of the mechanical seal face. Next is the analysis of the vibroacoustic signals based on the standard power spectrum and MSB analysis. The last step is detection of the presence of the mechanical seal fault.

Some suspensions and solutions create a build-up of dispersed deposits on the mechanical seal faces. A gap in the seal opens as a result of deposits covering only a fraction of the seal faces. As liquid flows through the gap, the leakage, which is slight at first, accelerates, causing settlement to accelerate, see Chapter Five, Figure 5-14. Of course, mechanical seal defects can also be induced by friction between the two seal faces.

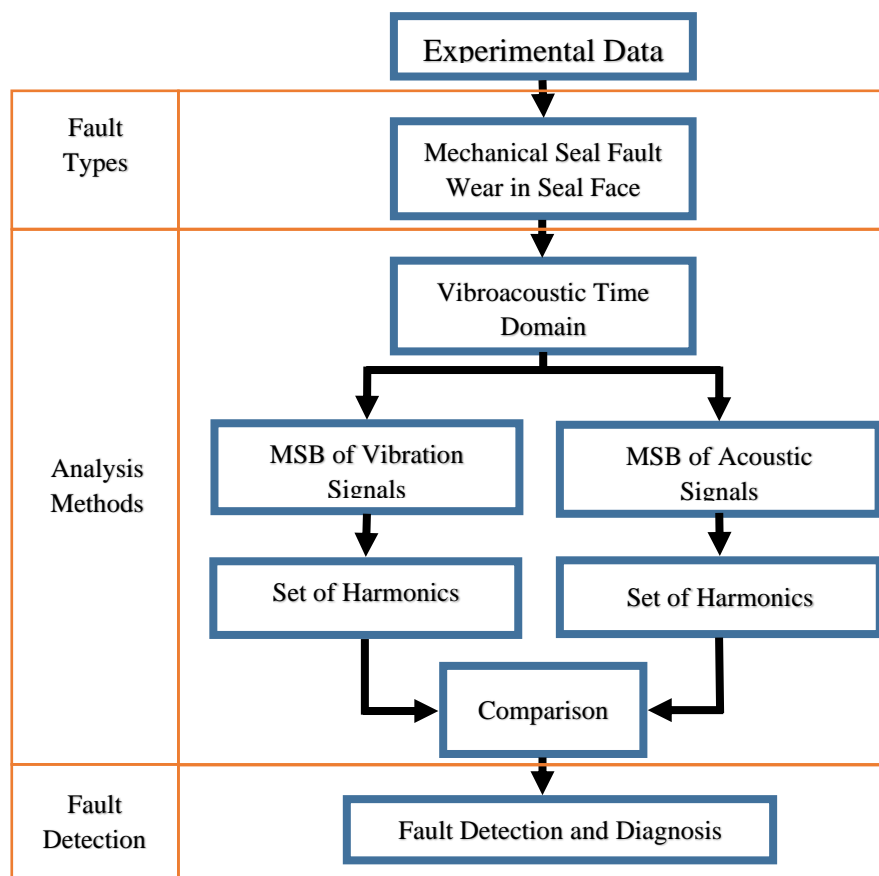


Figure 8-1 Framework of the process for pump mechanical seal fault detection and diagnosis

8.3 Performance Curve of Pump with Defective Seal

Figure 8-2 presents the performance curve for the baseline and with the faulty seal. We see that at low flow rates, below 350 l/min, the flow rate in the presence of the fault is significantly less than for the healthy case, this is because the flow rate depends directly on pump efficiency, and this will be decreased by the presence of the faulty seal. The

consequential and substantial reduction in flow rate due to the seal wear fault may, of course, be used as an additional means of confirming the presence of the fault and its identification.

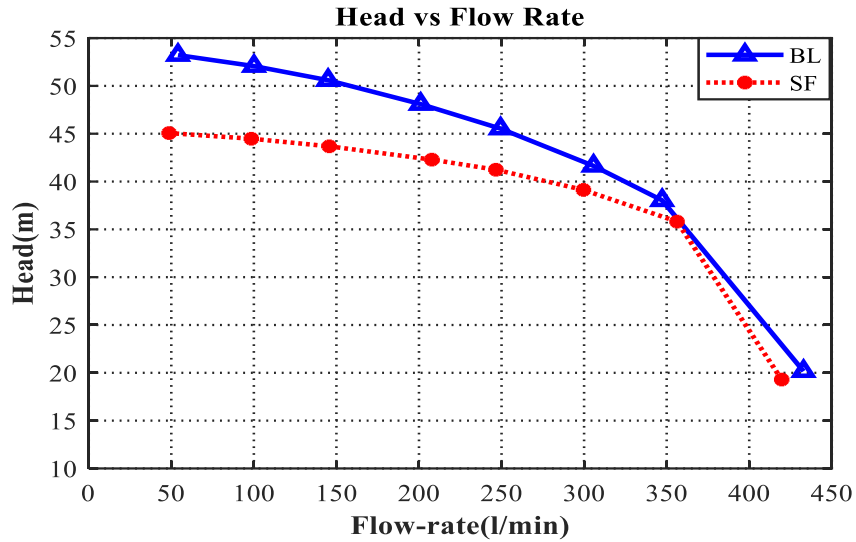


Figure 8-2 Impact of seal fault on performance curve

8.4 Time and Frequency Domains of the Vibration Signal

Figure 8-3 shows the time domain of the vibration signals for the BL and faulty mechanical seal for three flow rates. We see significant differences between the BL and faulty case with the increase in amplitude at all three flow rates indicating a defective condition.

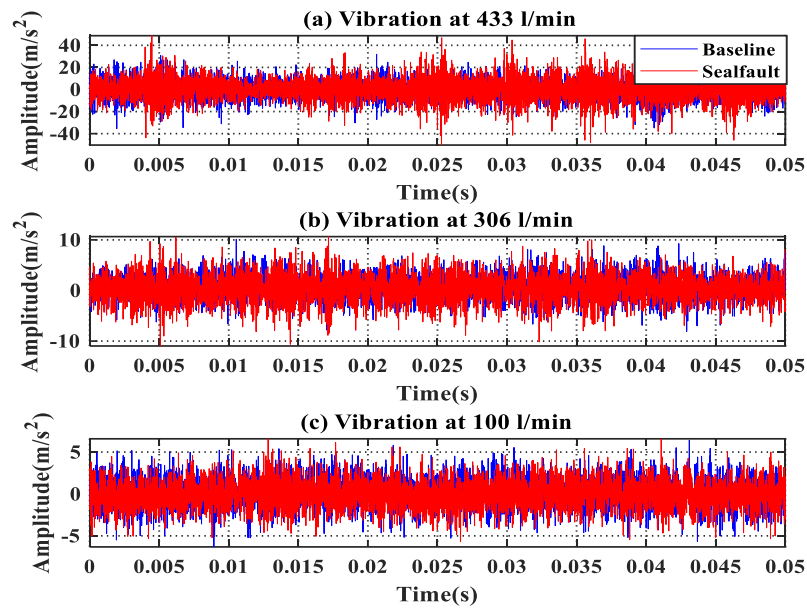


Figure 8-3 Vibration signal in the time domain with and without faulty seal for three flow rates

Figure 8-4 shows the frequency domain analysis of the vibration signals for BL and faulty seal conditions for three flow rates. We see peaks at characteristic frequencies and their harmonics which relate to the defective case. Besides, the peaks at characteristic frequencies and their harmonics contribute to the defective such as the shaft frequency of 48.3 Hz and the vane-pass frequency of 338.3 Hz. A very distinct difference in the magnitude of the signals can be seen at low frequencies. The vibration spectrum indicates the presence of the mechanical seal defect.

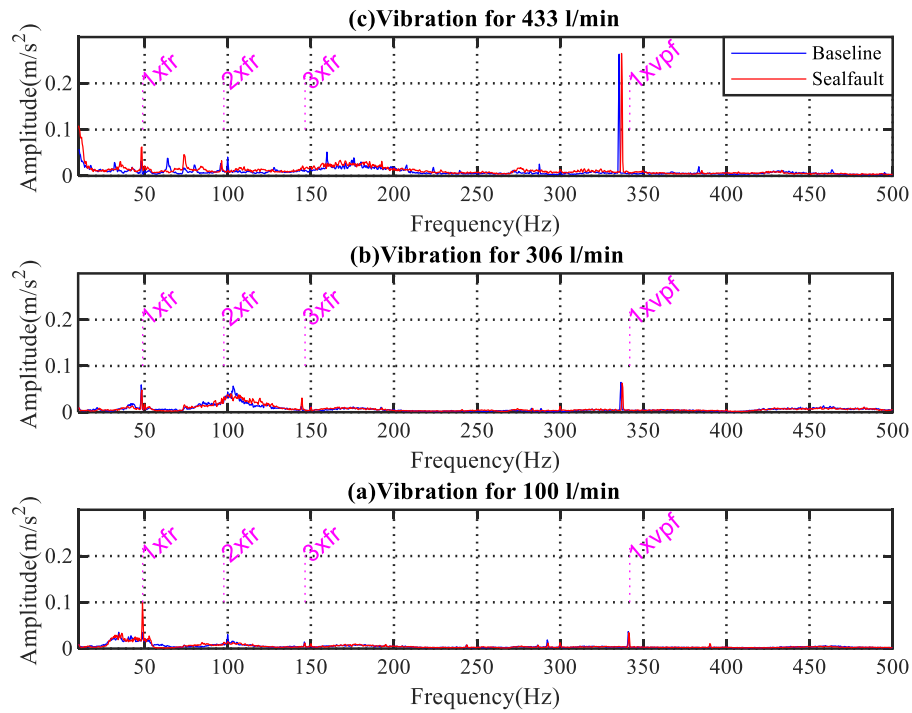


Figure 8-4 Frequency domain of vibration signal with and without faulty seal

8.5 Time and Frequency Domains of the Acoustic Signals

Figure 8-5 shows the time domain of the acoustic signals for BL and faulty mechanical seal for three flow rates. A significant difference between the amplitude of the BL and faulty case can be seen at all three flow rates indicating a defective condition. An indicator of a system fault may be the difference between the amplitude of the BL signal and signal generated by the faulty condition, but the degree of randomness in the signals makes the cause of any abnormality challenging to classify.

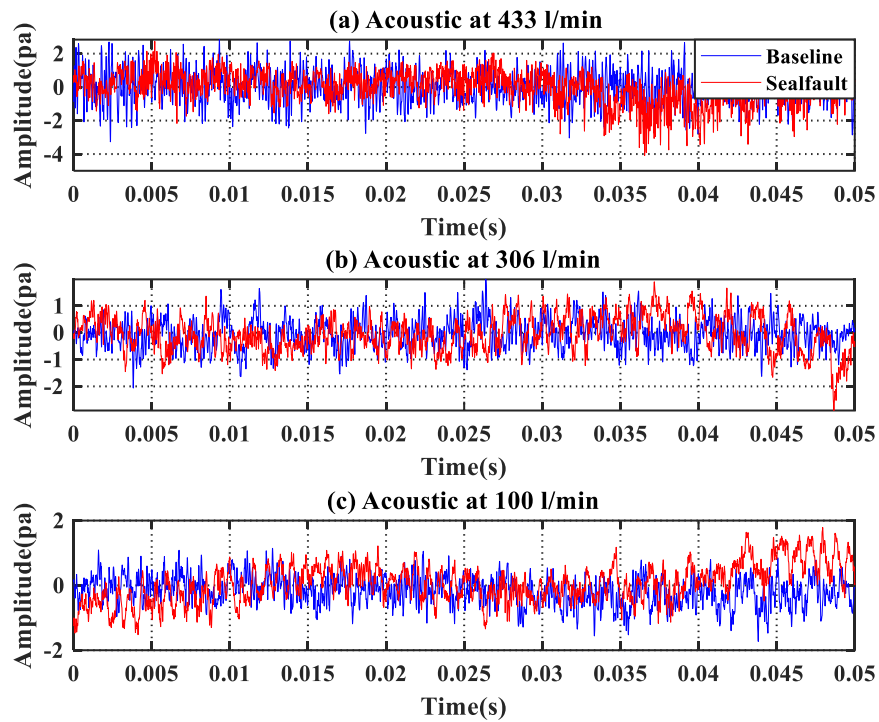


Figure 8-5 Acoustic signal in the time domain with and without faulty seal for three flow rates

Figure 8-6 shows the frequency domain analysis of the acoustic signals for BL and faulty seal conditions, for three flow rates. A very definite difference in magnitudes of the signals can be seen at low frequencies suggestive of stick-slip instabilities which can excite low frequency wideband noise [205]. In addition, peaks at characteristic frequencies particular the shaft frequency of 48.3 Hz and its harmonics which would be expected to relate to faulty seal. The acoustic spectrum confirms the presence of a fault in the mechanical seal.

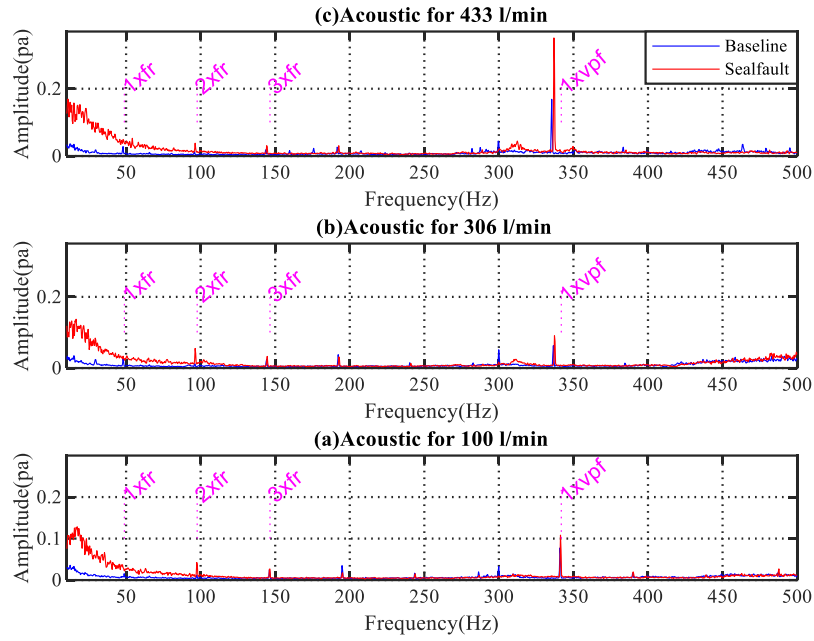


Figure 8-6 Spectrum of the acoustic signal with and without faulty seal

8.6 Comparison of Statistical Parameters: Acoustic and Vibration Signals

Figure 8-7 shows the relationship between the vibration RMS values and flow rates for the healthy condition and case of the mechanical seal faults. It can be seen that the RMS values of the faulty and healthy states are not well separated. However, at the maximum flow rate there is the suggestion that the faulty condition exhibits a significantly greater level of vibration than the BL.

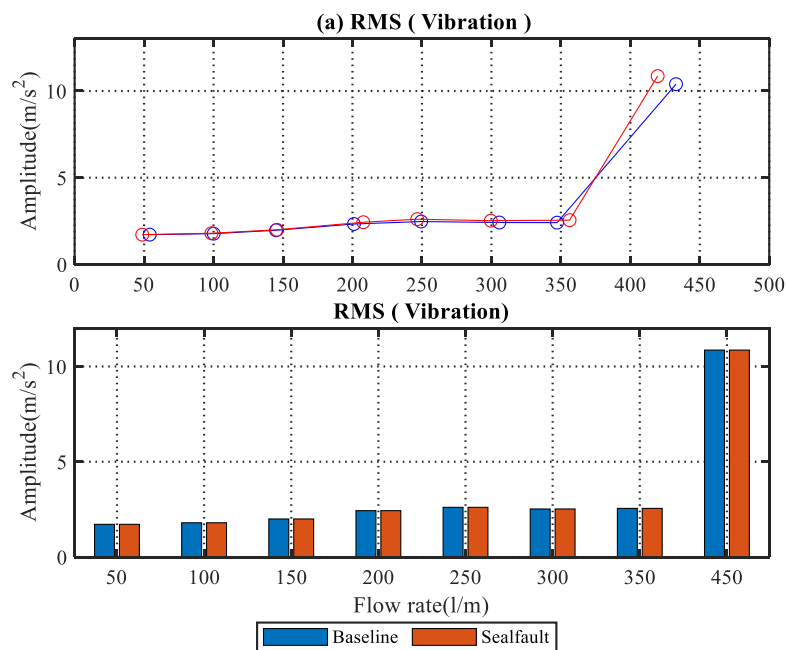


Figure 8-7 RMS of vibration signals in the time domain

Figure 8-8 shows the RMS values of the time-domain acoustic signals for the healthy and faulty states of the mechanical seal. It can be seen that the RMS values for the fault are consistently higher than for the faulty seal compared to the BL.

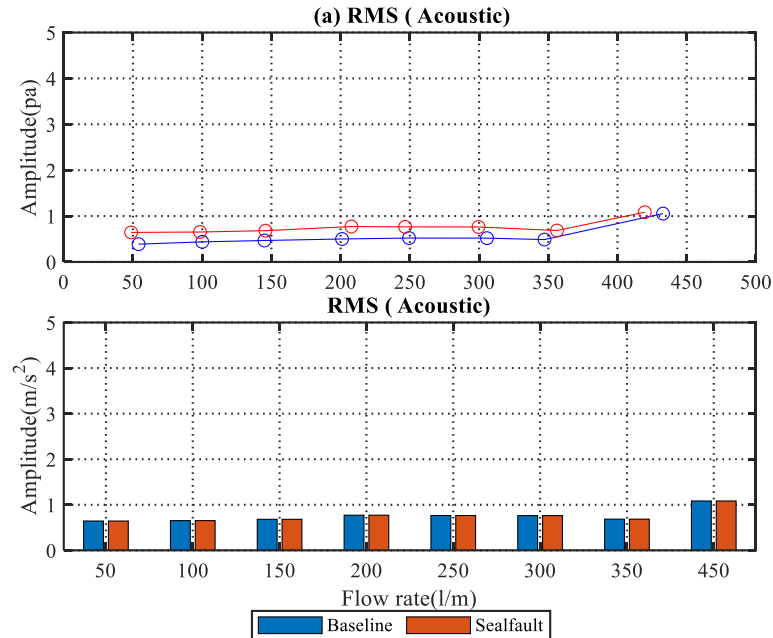


Figure 8-8 RMS of acoustic Signals in the time domain

8.7 Fault Detection by MSB Analysis

8.7.1 MSB Analysis of the vibration signals

Figure 8-9 presents the MSB results for both magnitude and coherence for the vibration signal for the BL condition and with a faulty mechanical seal for a flow rate of around 430 l/min. We see that the magnitude of the pulses is substantially greater with the faulty seal than the BL case. This is due to the MSB's superior ability to suppress random wideband noise. Also, see the coherence plots, which enhance discrete components. In Figure 8-10, flow rate around 300 l/min, the MSB peaks in the low-frequency range show the presence of noise due to the leaking seal. Figure 8-11, flow rate around 100 l/min also shows the presence of additional peaks due to the presence of a leaky seal though they are more obvious in the coherence plots.

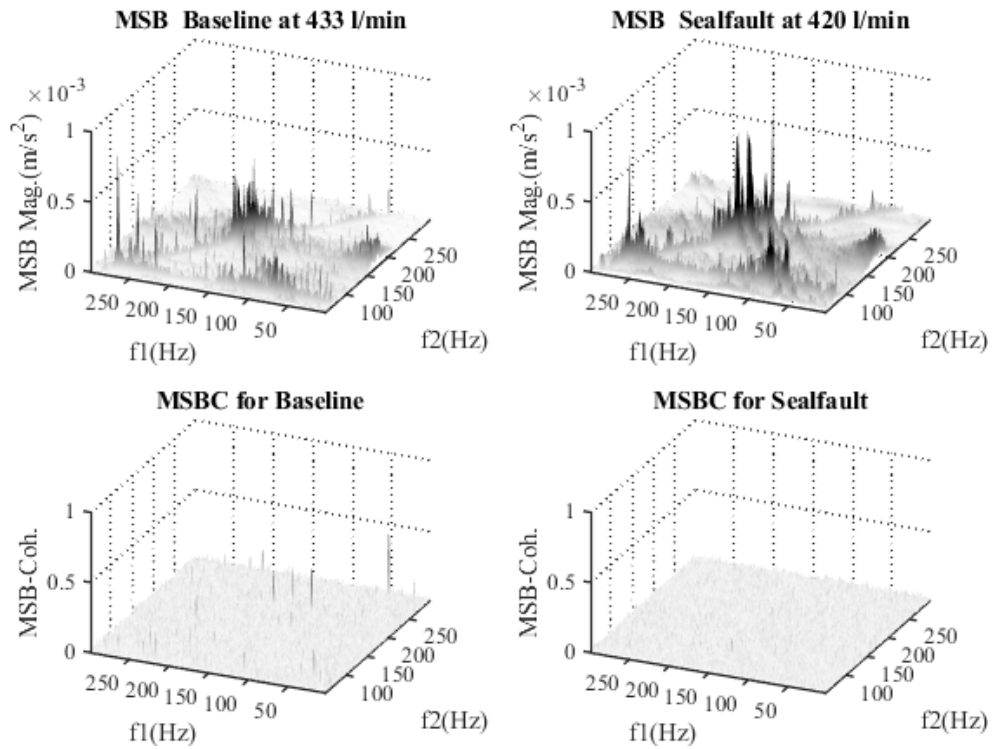


Figure 8-9 The MSB magnitude and coherence of vibration signal at around 430 l/m with and without faulty seal

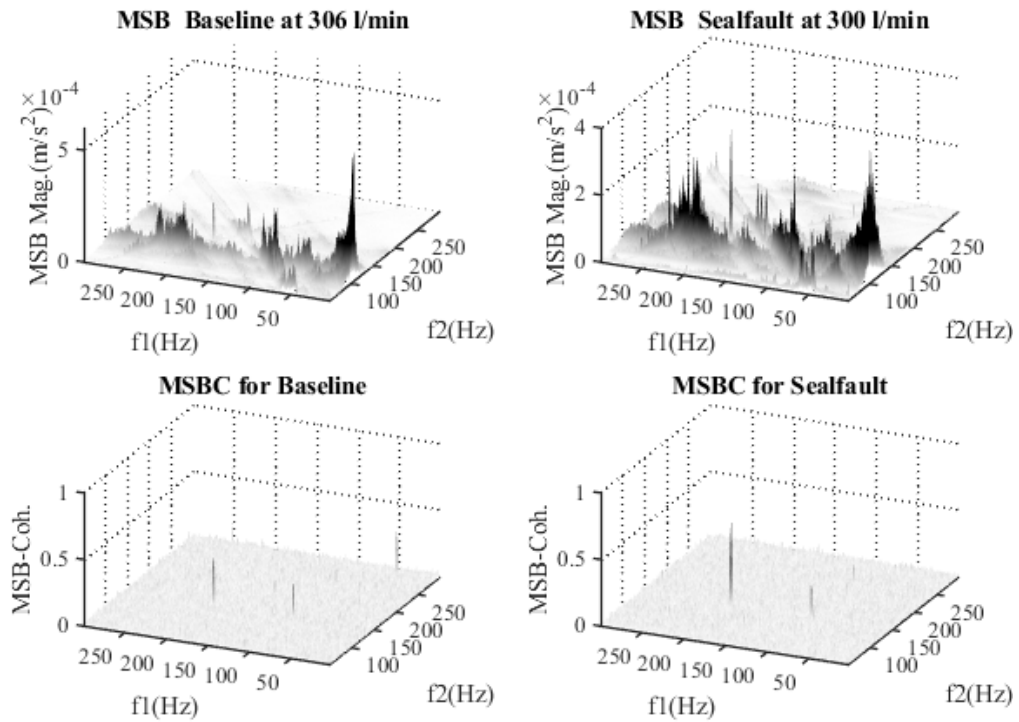


Figure 8-10 The MSB magnitude and coherence of vibration signal at around 300 l/m with and without faulty seal

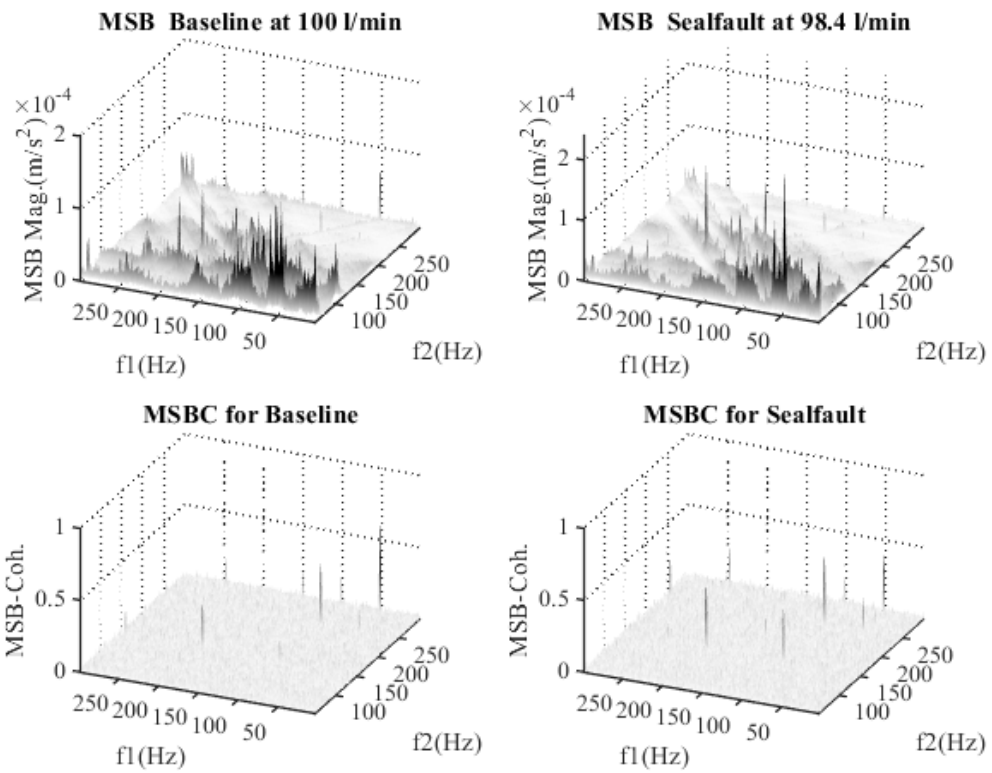


Figure 8-11 The MSB magnitude and coherence of vibration signal at around 100 l/m with and without faulty seal

Figure 8-12 shows the average magnitude of the peak at the shaft rotational frequency (48.3 Hz) and its first five harmonics in the power spectrum of the vibration signal, for the baseline case and faulty seal, as a function of flow rate. The magnitudes of the peaks follow the same general trend, and no clear pattern is discerned for the difference between the cases.

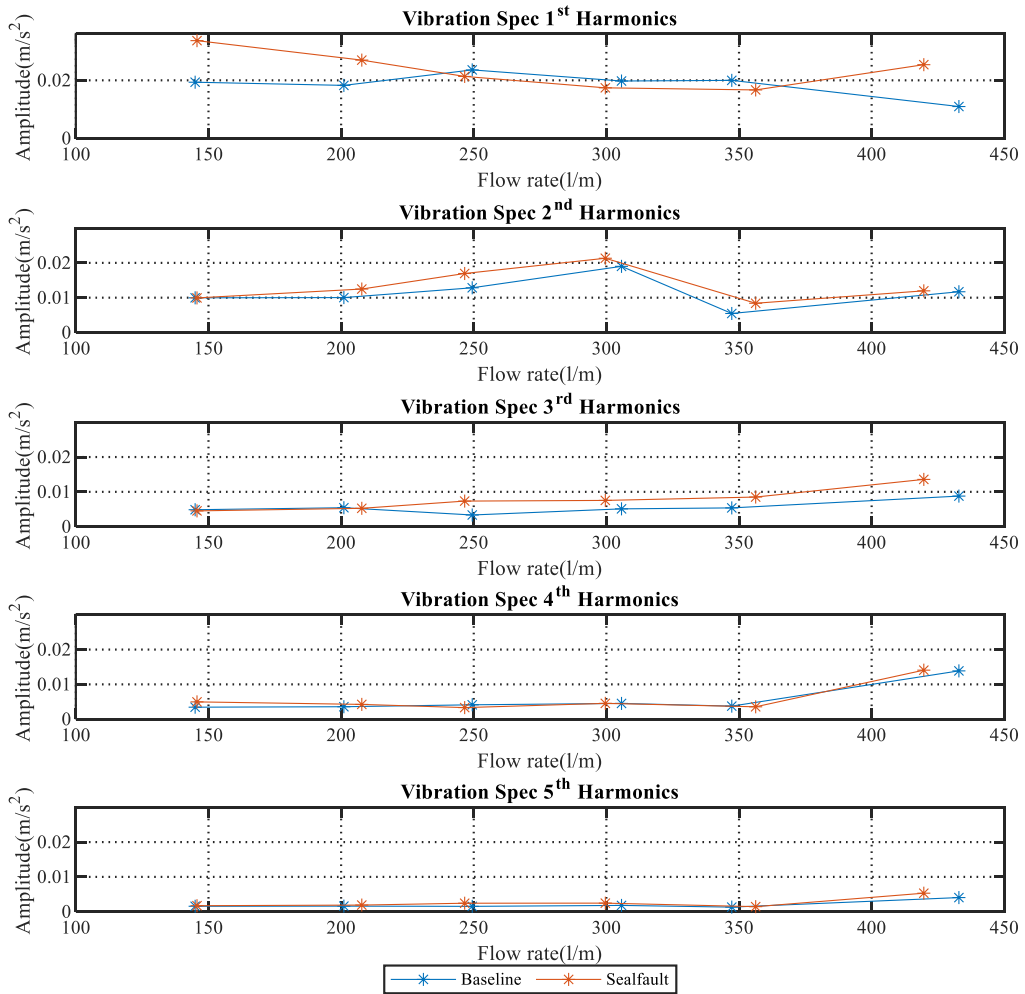


Figure 8-12 Magnitude of vibration peaks at the first five harmonics of shaft drive frequency (48.3 Hz), with and without faulty seal

Figure 8-13 shows the averaged MSB peaks for the vibration signal, at the shaft rotational frequency (48.3 Hz) and its first five harmonics with and without faulty seal as a function of flow rate. We see very little differentiation between the baseline and faulty case except at the highest flow rate where the magnitude of the fault signal increases.

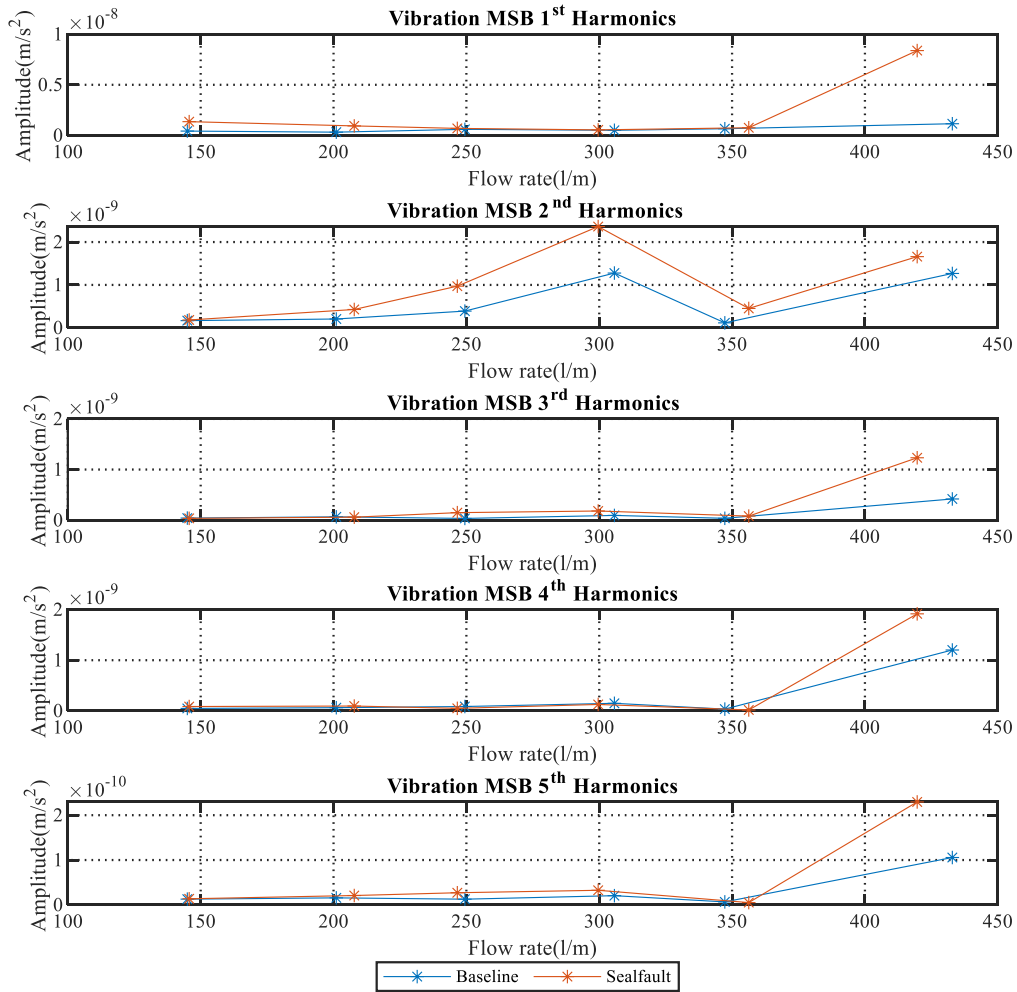


Figure 8-13 Averaged MSB peak for vibration signal, first five harmonics of shaft drive frequency (48.3 Hz) with and without faulty seal

8.7.2 MSB Analysis of the Acoustic Signal

Figure 8-14 presents the MSB results for both magnitude and coherence for the acoustic signal for the BL condition and with a faulty mechanical seal, for two flow rates. We see that for the flow rate of 420 l/min the magnitude of the peaks is substantially greater with the faulty seal than the BL case. We note that pulses of higher magnitudes can have an effect on the seals due to mechanical and hydraulic impact. Figures 8-15 and 8-16 presents similar figures for flow rates of 300, and 100 l/min.

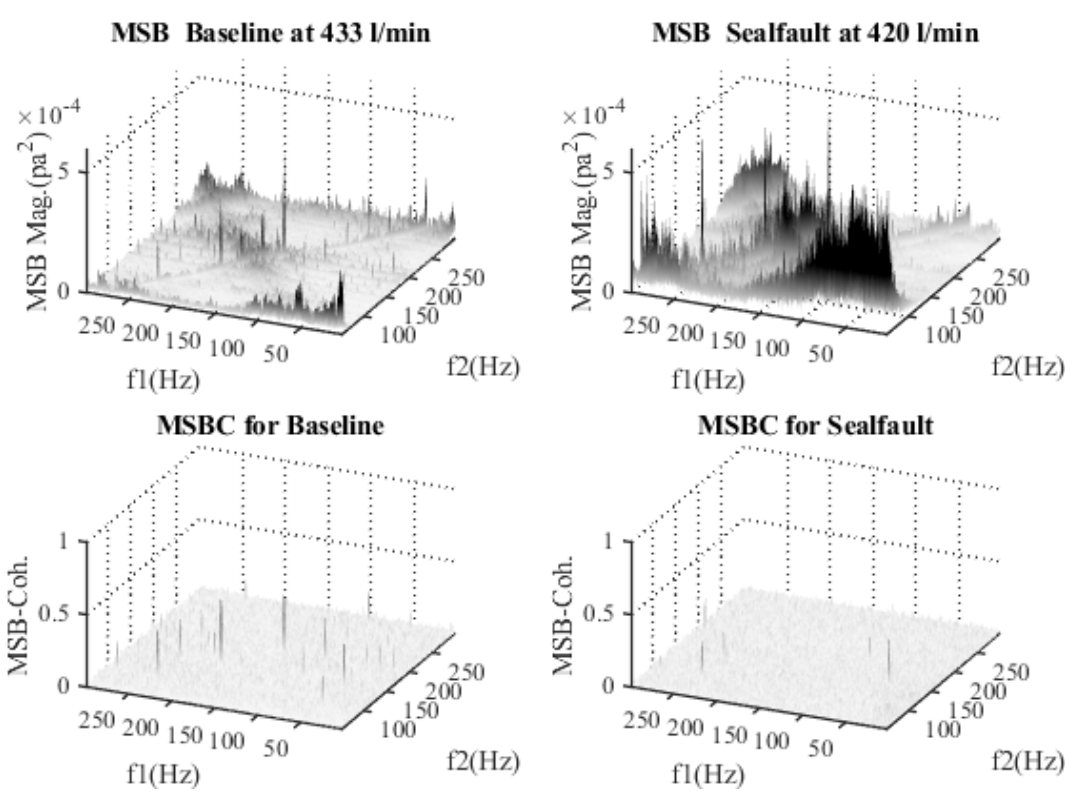


Figure 8-14 The MSB magnitude and coherences of acoustic signal at around 430 l/m flow rate with and without faulty seal

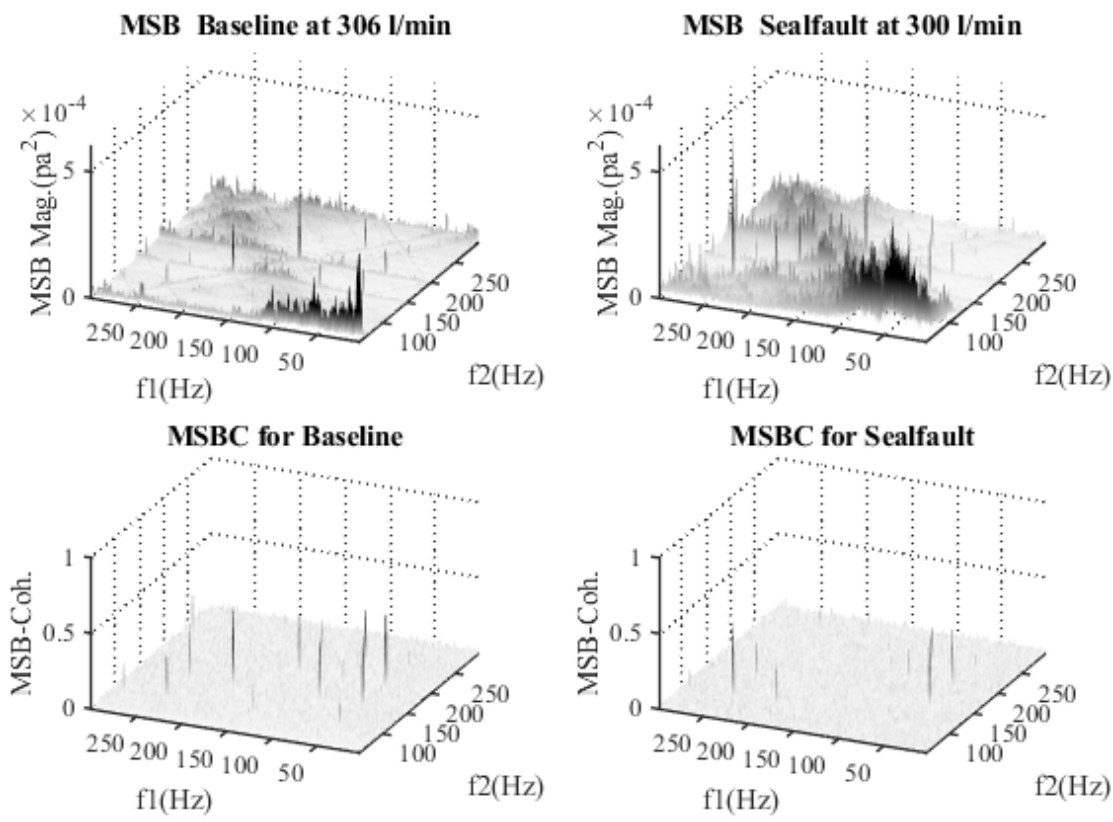


Figure 8-15 The MSB magnitude and coherences of acoustic signal at around 300 l/m flow rate with and without faulty seal

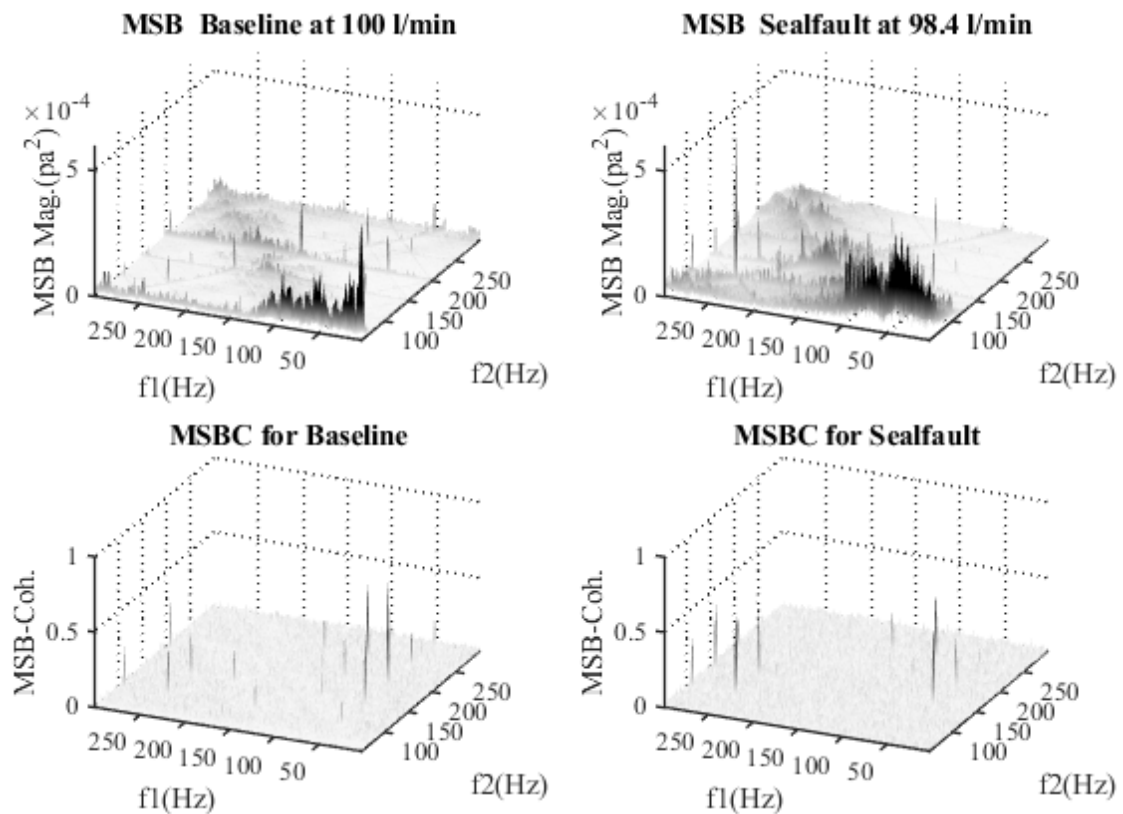


Figure 8-16 The MSB magnitude and coherences of acoustic signal at around 100 l/m flow rate with and without faulty seal

Figure 8-17 shows the average value of the peaks in the acoustic power spectrum, at shaft drive frequency (48.3 Hz) and its first five harmonics, for base line and faulty seal, as a function of flow rate. The plots of the amplitudes of the first and second harmonics show good separation between baseline and faulty conditions. However, the other harmonics, show little or no difference between baseline and defective condition.

Figure 8-18 shows that MSB of the acoustic signal can provide a more consistent difference between baseline and faulty seal condition over the range of spectral harmonics of shaft drive frequency (48.3 Hz). The MSB analysis is capable of excluding background noise interference and extracting the modulation characteristics in the sensor signal indicating the degradation of the mechanical seal.

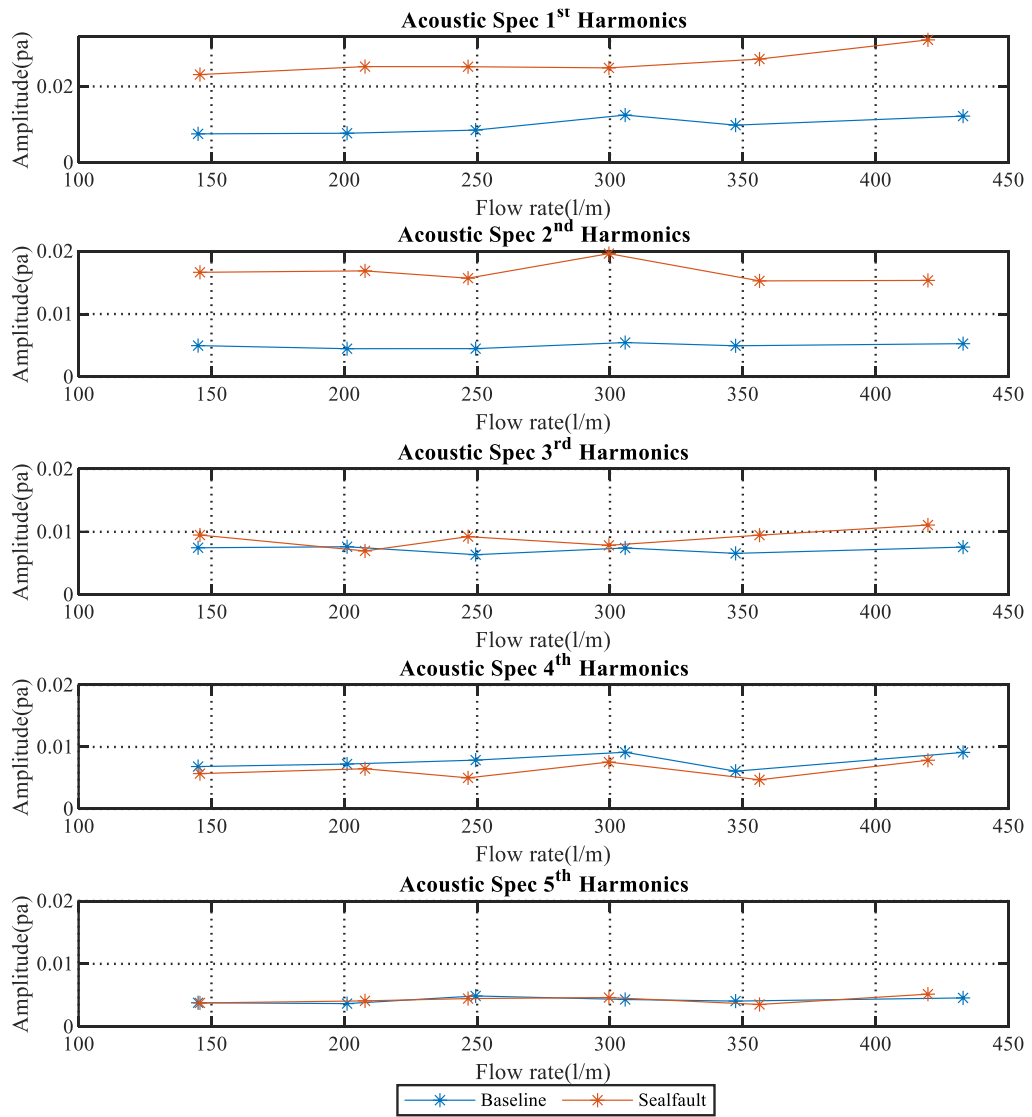


Figure 8-17 Magnitude of MSB acoustic spectral harmonics for shaft drive frequency (48.3 Hz), with and without faulty seal

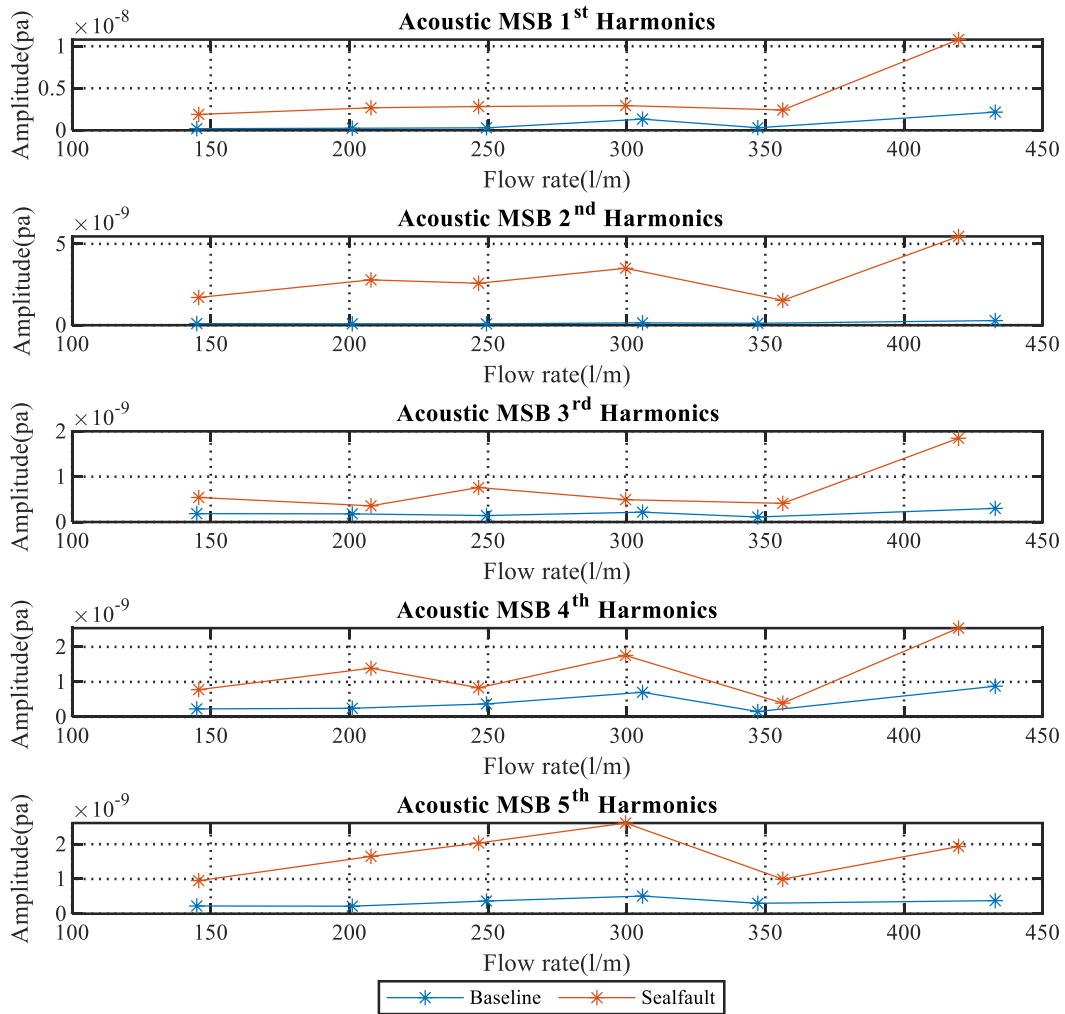


Figure 8-18 Amplitude of first five harmonics of shaft drive frequency (48.3 Hz) in the acoustic power spectrum with and without faulty seal

Comparing Figure 8-17 and 8-18, we see that for the flow rate of 420 l/min the MSB analysis consistently shows the magnitude of the signal is substantially greater with the faulty seal than the BL case. This figure shows that for the acoustic signal the faulty mechanical seal is more clearly discernible using MSB analysis than the power spectrum.

8.8 Key Finding

This experimental investigation used the airborne sound and vibration signals produced to detect the presence of a fault seeded into a mechanical seal. Power spectrum and MSB analysis-based approaches were used separately for fault identification. The outcomes show that the harmonics of the shaft drive frequency (48.3 Hz) contained in the MSB analysis of the acoustic signal enabled fault identification more readily than the power spectrums of either the acoustic or vibration signals or MSB analysis of the vibration signal. MSB provides a strong separation between baseline and fault harmonics across a range of flow rates, which could be useful for effective online monitoring, allowing the mechanical seal fault to be successfully detected and diagnosed.

CHAPTER 9:

Detection of Impeller Wear in Centrifugal Pumps Using Modulation Signal Bispectrum Analysis of Vibro-acoustic Signals

This chapter presents the use of the Modulation Signal Bispectrum for detection of an impeller wear fault seeded into a centrifugal pump. Included are time and frequency domain analyses to help determine the fault signatures corresponding to the impeller wear defects. Finally, the chapter presents the MSB analysis of both vibration and acoustic signals and compares their performance in detecting the impeller fault with that of the power spectrum of the signals. The chapter emphasises the advantages of using the acoustic signal for fault detection rather than the vibration signal.

9.1 Introduction

Here we focus on the CM of a pump with the aim of detecting impeller wear using vibro-acoustic signals. An enclosed impeller as described in Section 2.4.1 and shown in Figure 2-6 was used. The pump impeller requires attention because mechanical wear can cause serious harm, reducing the pump's lifetime and performance. Impeller wear was studied in this chapter using vibro-acoustic signals obtained at various flow speeds. Fluid flow and the presence of particulates cause a small amount of wear in the region of the impeller inlet vane, this wear grows with time. The uniform corrosive wear area is defined as the area where the impact velocity is less than the critical value, and it grows as the impeller velocity increases. In reality, wear mechanisms vary from one region to the next; it is larger when the tangential portion of the impact velocity is heavy, and this is what eventually causes the impeller to fail. MSB analysis was carried out to extract incipient fault signatures, due to its advantages as described previously. The experimental results show that the MSB's diagnostic features can detect impeller wear at an early stage.

The MSB approach was then compared to a conventional method, the power spectrum. As described in previous chapters, the vibration and airborne sound signals were collected for different operating conditions, the signals were then analysed to discover the presence, or not, of the seeded fault. This MSB study of vibro-acoustic signals and their spectrums offers a clear distinction between healthy and defective impeller wear conditions at various flow rates.

9.2 Fault Simulation

Two typical centrifugal pump impeller defects were simulated experimentally and seeded into the experiment rig. Corrosion/erosion faults on the impeller vanes were simulated by removing a short length of material from the vane tip close to the hub: 1mm to represent a small degree of wear, and 2 mm a large degree of wear, see Figure 9-1 and Section 5.5.3. As previously the vibro-acoustic signals corresponding to each fault were analysed.

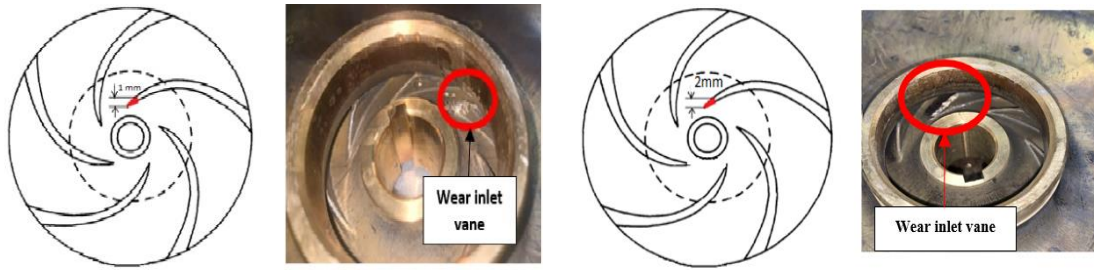


Figure 9-1 Initial fault simulation of impeller wear

9.3 Framework of Impeller Fault Detection

In this section, the test process followed closely those described in Chapters 7 and 8 for bearing fault detection and mechanical seal faults, respectively, and is shown again in Figure 9-2. The initial step is the simulation of the impeller fault, i.e., inlet vane wear. The following step is the gathering of relevant acoustic and vibration data and its analysis using both the power spectrum and MSB. The final stage is detection of the seeded fault. The two sets of results were compared, to assess their relative performance.

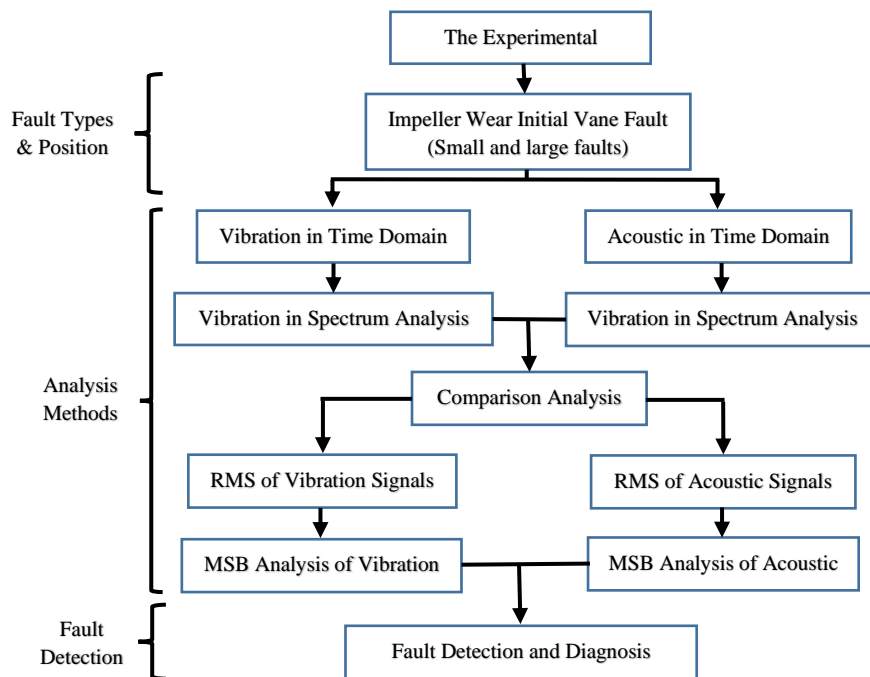


Figure 9-2 Framework of impeller wear fault analysis

9.4 Impact of Impeller Wear on Pump Performance Curves

Figure 9-3 shows the performance curves for the centrifugal pump healthy and with the seeded impeller faults. As expected, impeller wear reduces the pressure head relative to

the healthy case across the range of flow rates tested. Significantly, there was no discernible difference between flow rates with the smaller and larger faults present save at the highest flow rate.

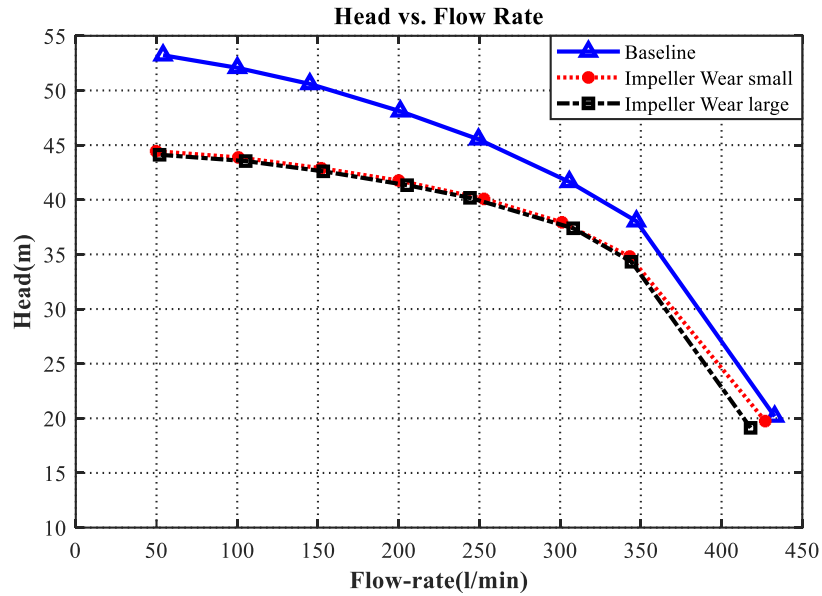


Figure 9-3 Performance curve of centrifugal pump with and without impeller wear faults

9.5 Time Domain Analysis of Vibration and Acoustic Signals

Figure 9-4 shows the airborne sound and vibration signals in the time domain for three flow rates for baseline and defective impeller conditions. It can be seen that at different flow speeds the defective cases have greater amplitude than the baseline, which could be an indication of the presence of a fault. However, the signal appears highly random, making it challenging to confidently claim the presence of a fault let alone identify it.

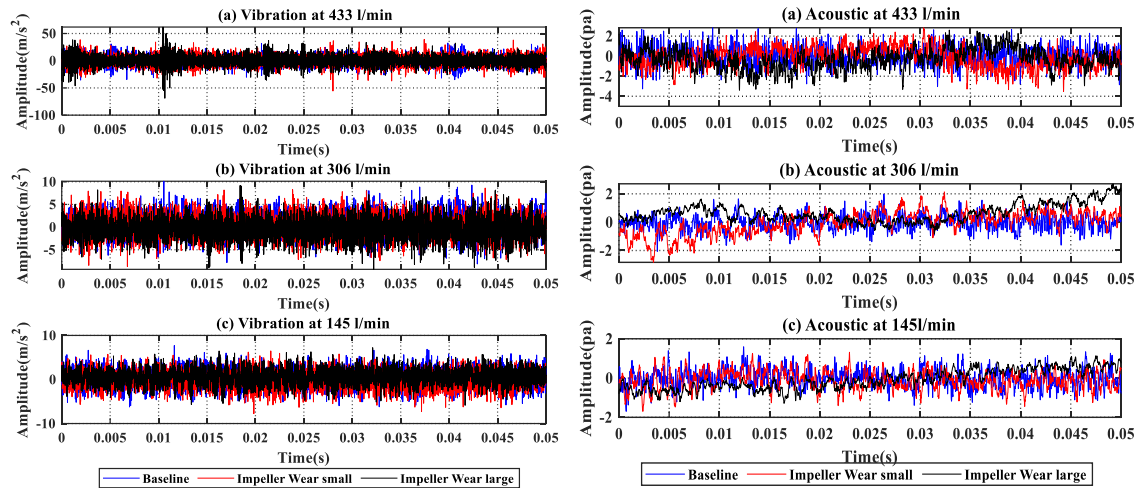


Figure 9-4 Acoustic and vibration signals in the time domain for healthy impeller and impeller with “small” and “large” faults

9.6 Statistical Parameter Comparison of Acoustic and Vibration Signals

Figure 9-5 shows four statistical parameters (RMS, peak, peak factor and kurtosis) of the vibration and acoustic signals derived from the time domain. It is clear from Figure 9-5 that the vibration data cannot generally clearly distinguish between the baseline case and when an impeller fault is present. However, we see that for the peak, peak factor and kurtosis the acoustic signals can differentiate between the baseline and fault case certainly at lower flow rates.

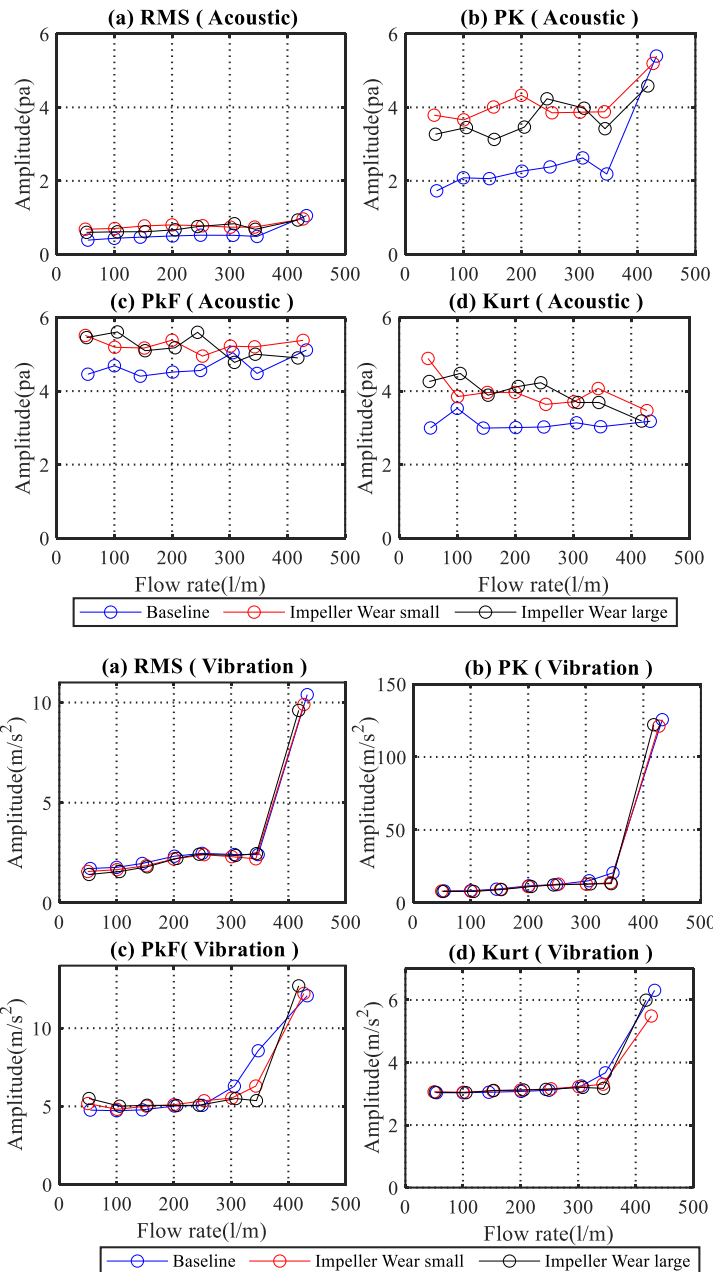


Figure 9-5 Statistical parameters (RMS, Peak, Peak Factor and Kurtosis) for vibration and acoustic signals in the time domain with and without impeller faults

The difference in the RMS values is much smaller than for the other measures, and since RMS is an aggregate measure, it will seldom be able to diagnose a particular fault. With peak factor and kurtosis, while the general trend is for a clear difference in signal level between the two cases, the individual baseline values fluctuate to a degree that would undermine confidence in wear fault detection using this measure.

9.7 Impeller Fault Vibration and Acoustic Signal Spectrum Analysis

Figure 9-6 shows the spectrum of the vibration signal for a healthy impeller and impeller with wear faults for three flow rates, 433, 306 and 150 l/min. Because the impeller is driven by the motor we expect, and do see, peaks characteristic of the drive frequency, ($f_r = 48.3$ Hz), and its harmonics clearly visible in the spectrum. We also see a peak corresponding to the vane passing frequency vpf (338.3 Hz). These peaks are clearly visible for all three flow rates and the spectrum of the vibration signal tends to confirm the presence of the impeller wear faults. However, these frequency peaks could be contaminated by noise generated either by fluid flow or other system components. But the effects of fluid flow on vibration characteristics that occur in the low-frequency range are difficult to remove by conventional approaches such as FFT during the signal processing.

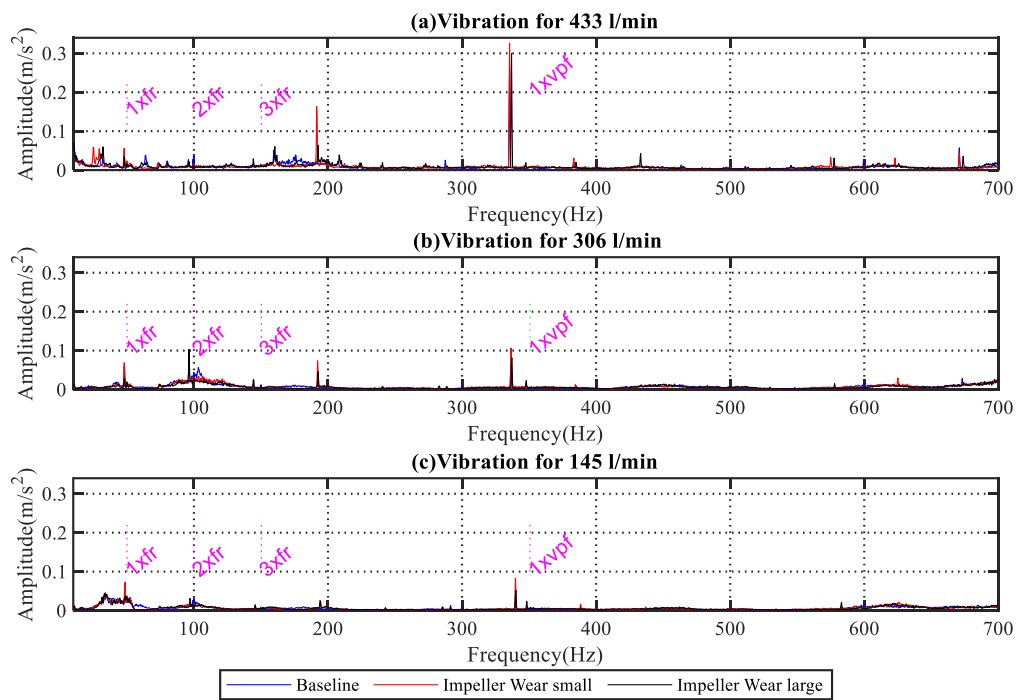


Figure 9-6 Spectrum analysis of vibration signal with and without impeller faults for three flow rates

Figure 9-7 displays the acoustic signal frequency domain for the three given flow rates for baseline and defective conditions. Again, the characteristic fault frequencies, f_r (48.3 Hz) and vpf (338.3 Hz) and their related harmonics are clearly noticeable and significantly higher than the baseline levels. Thus, the spectrum of the acoustic signal demonstrates the presence of the impeller wear fault. As with the vibration signal, these frequency peaks

could be contaminated by noise generated either by fluid flow or other system components.

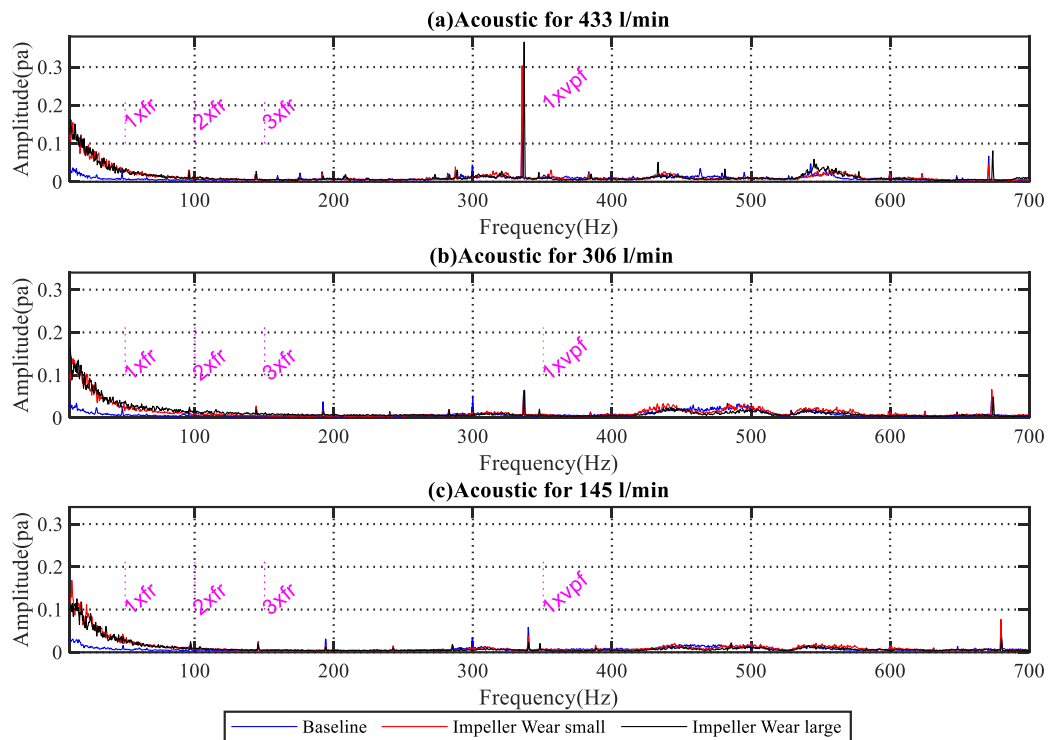


Figure 9-7 Spectrum analysis of acoustic signal with and without impeller faults for three flow rates

9.8 MSB Analysis Based Detection

This section aims to investigate the detection of impeller wear faults using the MSB and to compare the results obtained with those from the power spectrum for both vibration and acoustic signals.

9.8.1 Impeller Wear Fault Detection by MSB of Vibration Signals

Detection of the seeded wear fault by MSB analysis via the magnitude and coherence of the signals is presented in Figure 9-8 for the vibration signal obtained from the centrifugal pump without and with impeller faults. In the tests the flow rate for the baseline case was 430 l/m, however seeding an impeller fault, but maintaining the remainder of the system constant reduced the flow rate. It was decided that it was better to work with a reduced flow rate rather than introduce additional changes to the test rig. The corresponding flow rate for the small seeded fault (1 mm) was 427 l/min and for the large seeded fault (2 mm) was 418 l/min.

Again, the merit of the MSB is it suppresses random wideband noise and so improves detection of impeller wear faults. The MSB magnitude results in the low-frequency range in Figure 9-8 ($f_1 < 300$ Hz and $f_2 < 500$ Hz) show less noise smear of impeller faults than baseline case. To detect the presence of the wear faults, confirmed by distinct corresponding coherence peaks of the fundamental frequency (48.3 Hz) and vane passing frequency (338.3 Hz). The MSB coherence is the result of coupling between two frequency components and the MSB plots show distinct peaks at fault frequencies of 48.3 Hz and 338.3 Hz that are clearly different from the baseline plot. The largest pulses due to mechanical and hydraulic effects are shown in Figure 9-10. The tallest peaks are due to high levels of hydraulic asymmetry and mechanical vibrations and indicate the presence of the impeller wear fault.

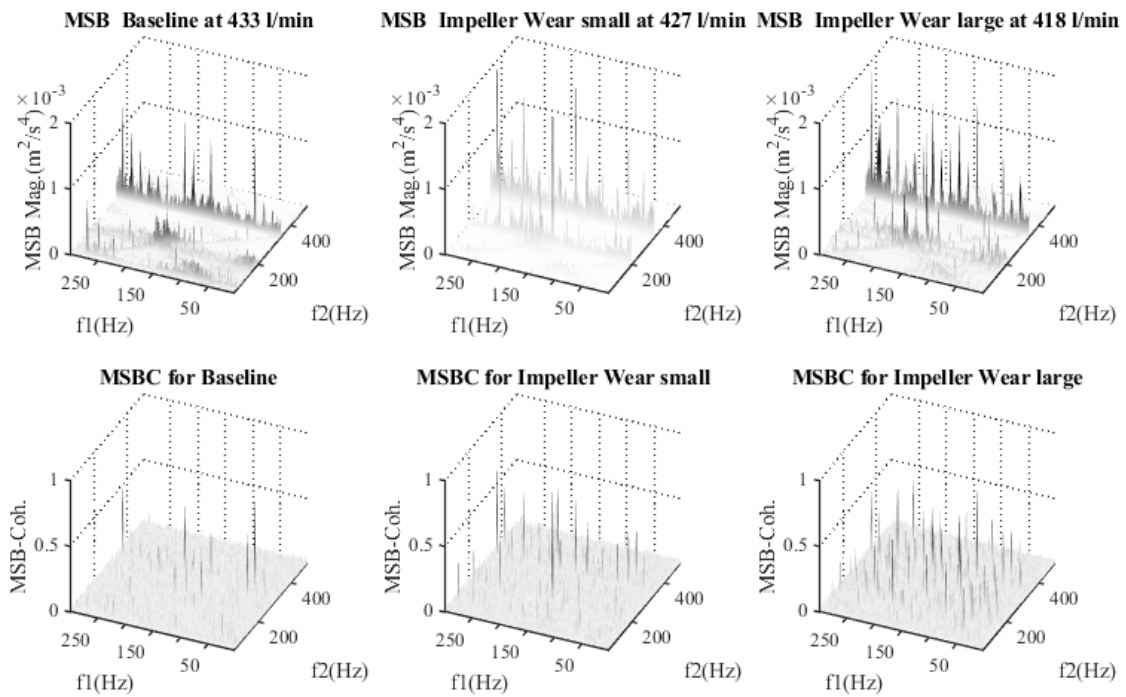


Figure 9-8 MSB Magnitude and coherence of vibration signals for impeller with and without faults at flow around 430 l/min

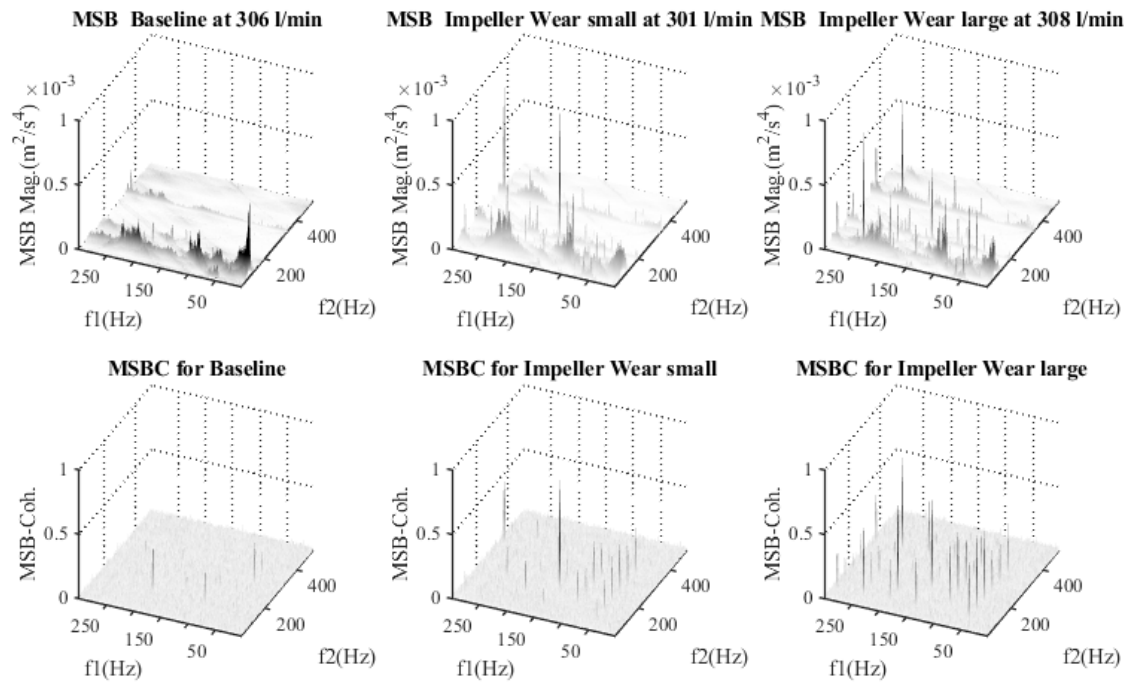


Figure 9-9 MSB Magnitude and coherence of vibration signals for impeller with and without faults at flow around 300 l/min

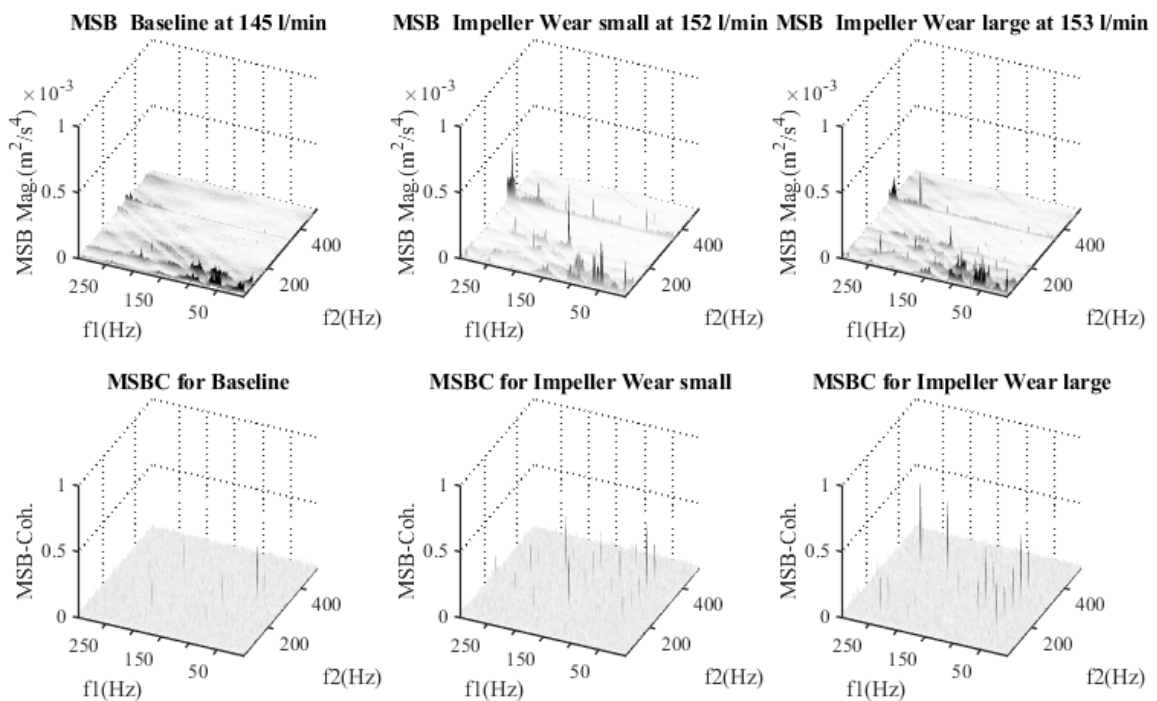


Figure 9-10 MSB Magnitude and coherence of vibration signals for impeller with and without faults at flow around 150 l/min

9.8.2 Comparison of Detection of Impeller Wear Faults Based on the Power Spectrum and MSB Analysis of the Vibration Signals

Figure 9-11 presents the averaged magnitude of the first 5 harmonics in the power spectrum for f_r (48.3 Hz) for the baseline case and the two-seeded wear faults as a function of flow rate. The figure shows that none of the plots provides consistent or significant differences between healthy and either wear fault.

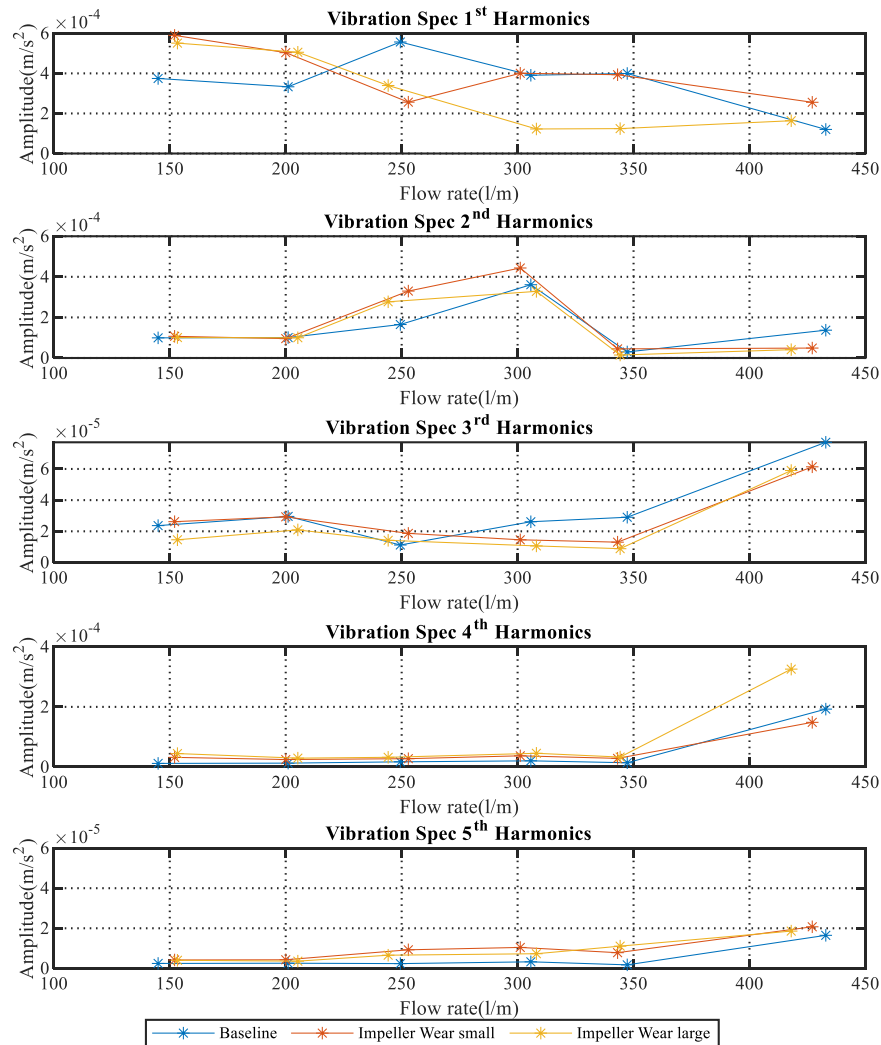


Figure 9-11 Magnitude of the vibration power spectrum plots of the first five harmonics of 48.3 Hz with flow rate.

Figure 9-12 shows the magnitudes of the first five harmonics of the shaft rotation ($f_r = 48.3$ Hz) for baseline and both wear faults as obtained using MSB analysis of the vibration signal. The MSB improved discrimination between the results by removing noise and aperiodic low-frequency impact impulses but did not significantly separate the baseline

and two fault cases for all harmonics. However, the first harmonic gives a useful separation at the highest flow rates, but the other harmonics generally do not provide a significant or consistent separation between the baseline and faulty cases.

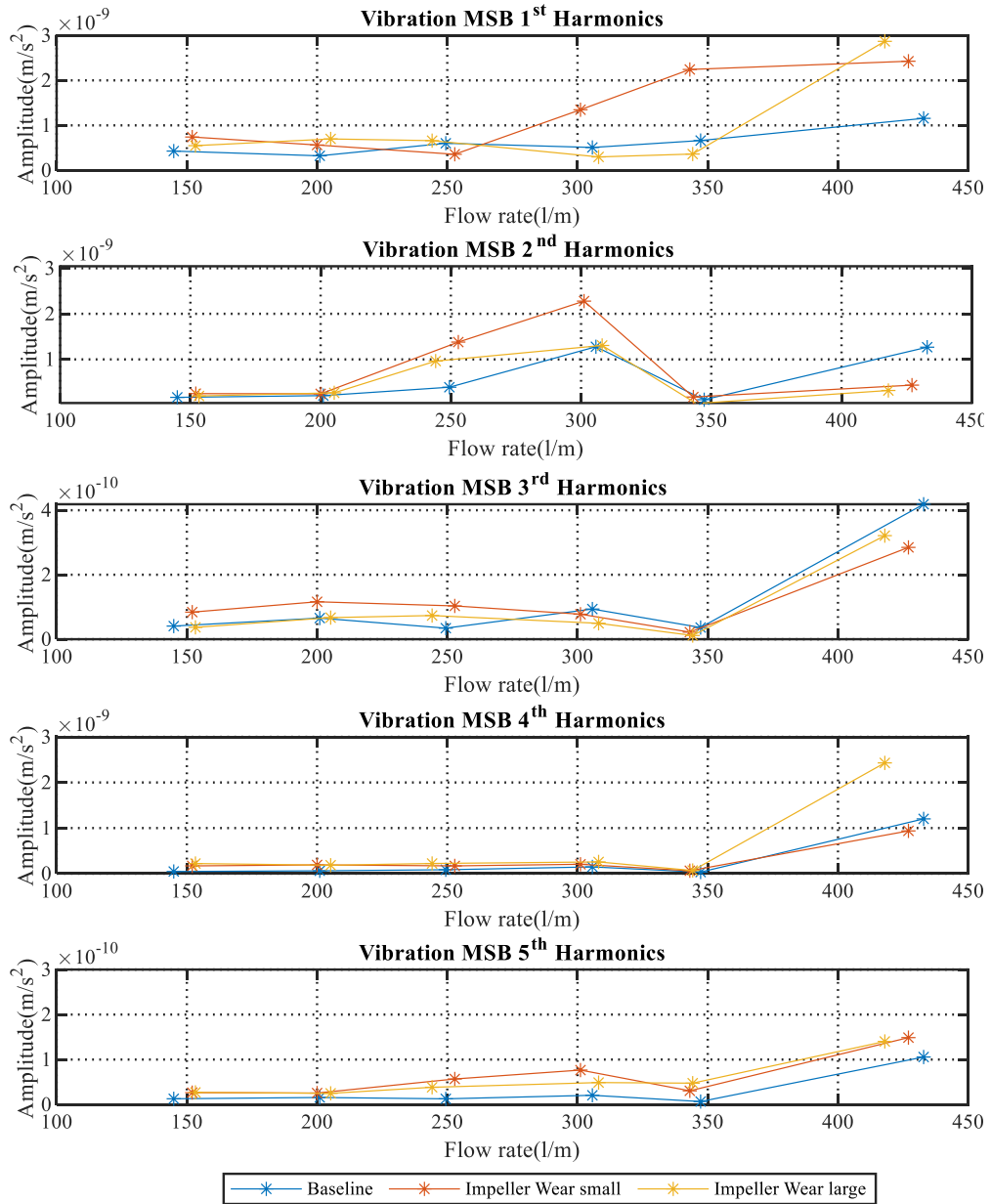


Figure 9-12 Magnitude of the MSB vibration plots of the first five harmonics of 48.3 Hz with flow rate.

Figure 9-13 shows a comparison of results obtained by the vibration power spectrum and MSB analysis for the magnitude of the peak obtained at the vane passing frequency (338.3 Hz) for the baseline and both seeded impeller faults. For both power spectrum and MSB plots, there is a clear separation of the vibration peak magnitudes between baseline and small and large wear faults, but the magnitude of the separation varies with flow rate.

Additionally, in Figure 9-13(a) we see a separation between the small and large wear faults for all flow rates except 300 l/m. On the other hand, Figure 9-13 (b), while consistently showing a separation of baseline and fault signals, there is an overlap of the two wear fault signals. Thus, while the increase in peak level at the blade passing frequency could be an indication of an impeller wear fault at all flow rates, the magnitude of that difference could not be taken as a measure of the degree of the fault.

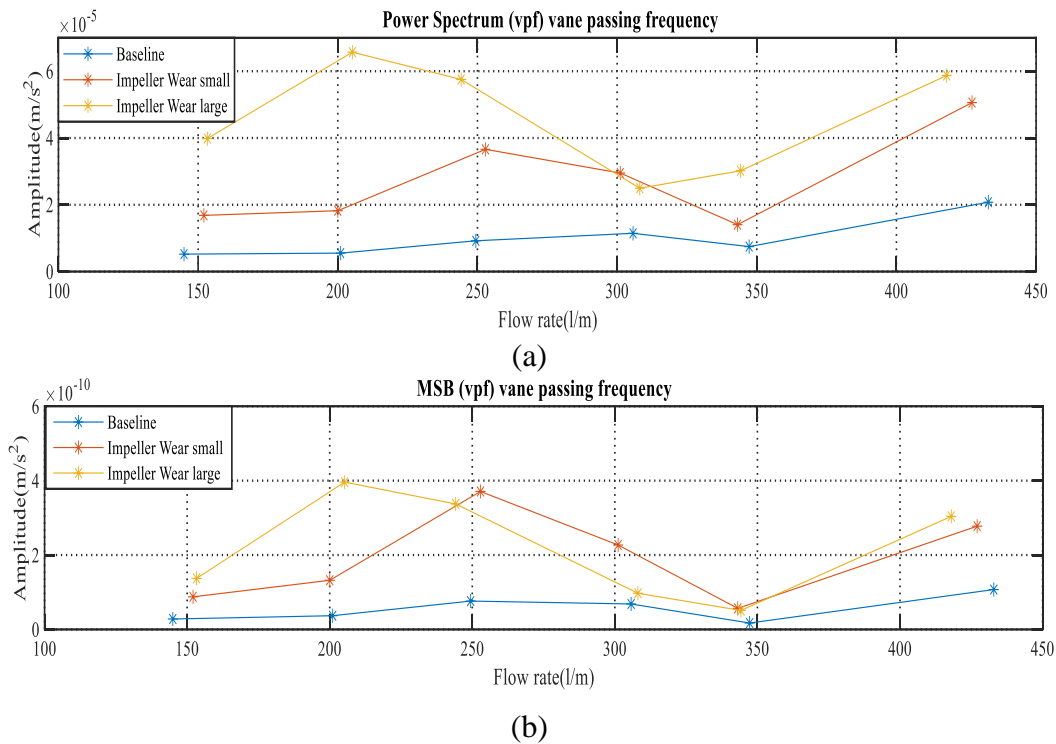


Figure 9-13 Comparison of (a) power spectrum plots and (b) plots obtained using MSB for the vane passing frequency (338.3 Hz) of the vibration signal.

9.8.3 Impeller Wear Fault Detection by MSB of Acoustic Signal

Figure 9-14 presents the magnitude and coherence obtained from the MSB analysis of the acoustic signals for a flow rate of 450 l/m for baseline and both seeded faults. The baseline plot has lower peak magnitudes than those for the wear faults, suggesting a defect in both cases. The MSB plots in the low frequency range shown in Figure 9-15 and Figure 9-16 show less noise smear, and that can also be recognized in the corresponding MSB coherences, especially with the distinctive peaks corresponding to the shaft rotational frequency of 48.3 Hz and its harmonics, and the vane passing frequency, of 338.3 Hz.

The findings show that the seeded wear faults tend to appear as simple peaks related to the fault frequency, while in the case of baseline, the peaks are minimal. The MSB magnitude and coherence plots indicate distinct differences between baseline and faulty

cases with the higher magnitude peaks triggered by the mechanical pulses due to hydraulic asymmetry suggesting the presence of an impeller wear fault.

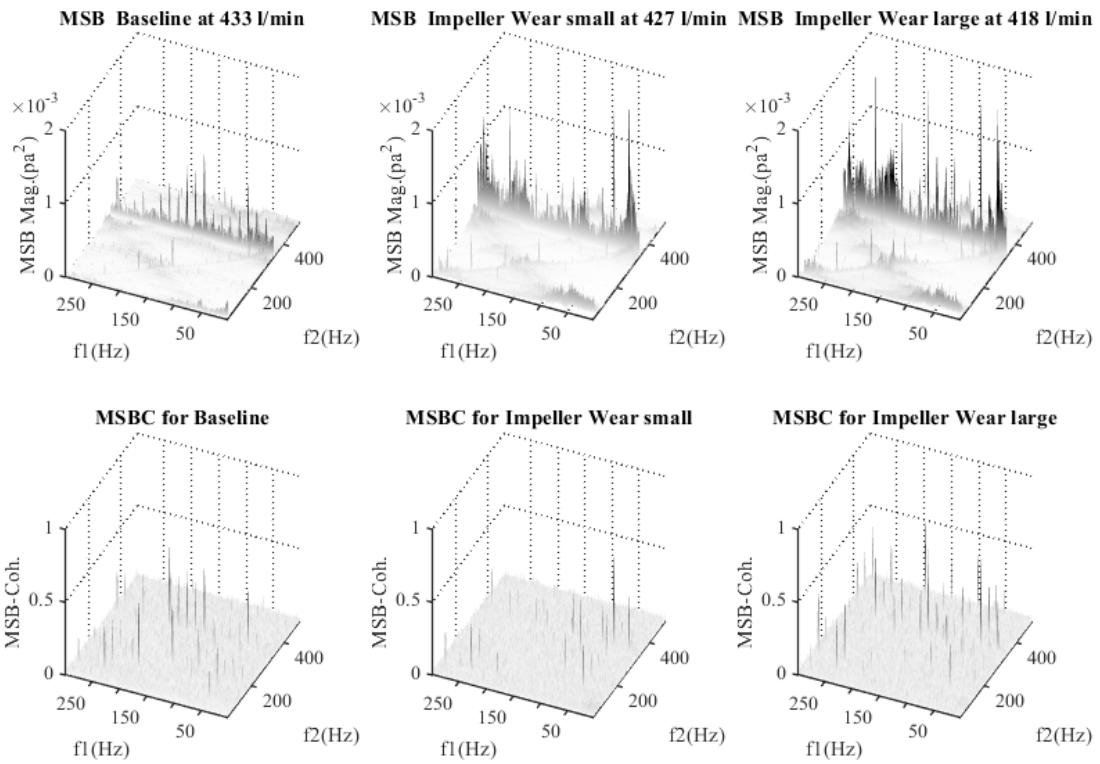


Figure 9-14 MSB Magnitude and coherence of acoustic signals for impeller with and without faults at flow around 430 l/min

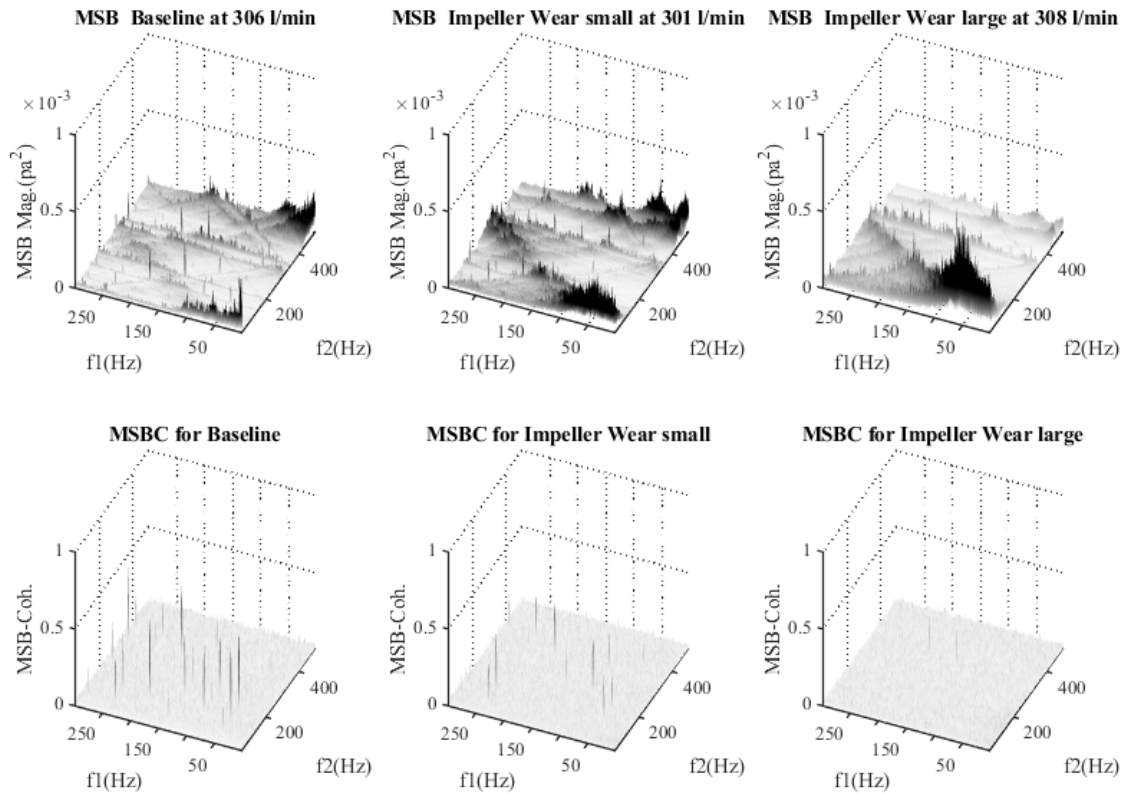


Figure 9-15 MSB Magnitude and coherence of acoustic signals for impeller with and without at flow around 300 l/min

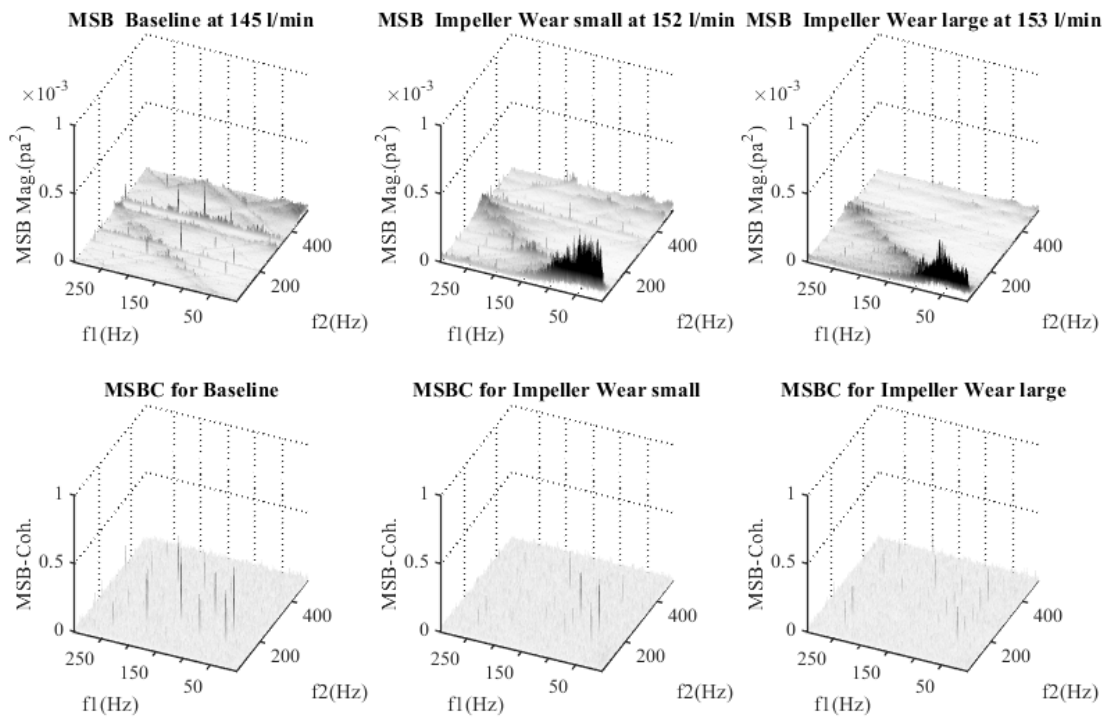


Figure 9-16 MSB Magnitude and coherence of acoustic signals for impeller with and without at flow around 150 l/min

9.8.4 Comparison of Detection of Impeller Wear Faults Based on the Power Spectrum and MSB Analysis of the Acoustic Signals

Figure 9-17 shows the magnitudes of the peaks of the first five harmonics of the drive shaft's rotational frequency of 48.3 Hz that appear in the power spectrum, for baseline and the two seeded faults as a function of flow rate. The first harmonic shows a consistent and significant separation between the baseline and the faulty conditions, but does not effectively separate the two fault conditions. The second harmonic also shows a consistent separation between baseline and defective conditions, but the separation is of much lower magnitude than for the first harmonic. The second harmonic also fails to clearly distinguish between the two fault conditions. The 3rd, 4th and 5th harmonics, however, show a different pattern, the baseline signal produces a higher amplitude peak than either fault condition.

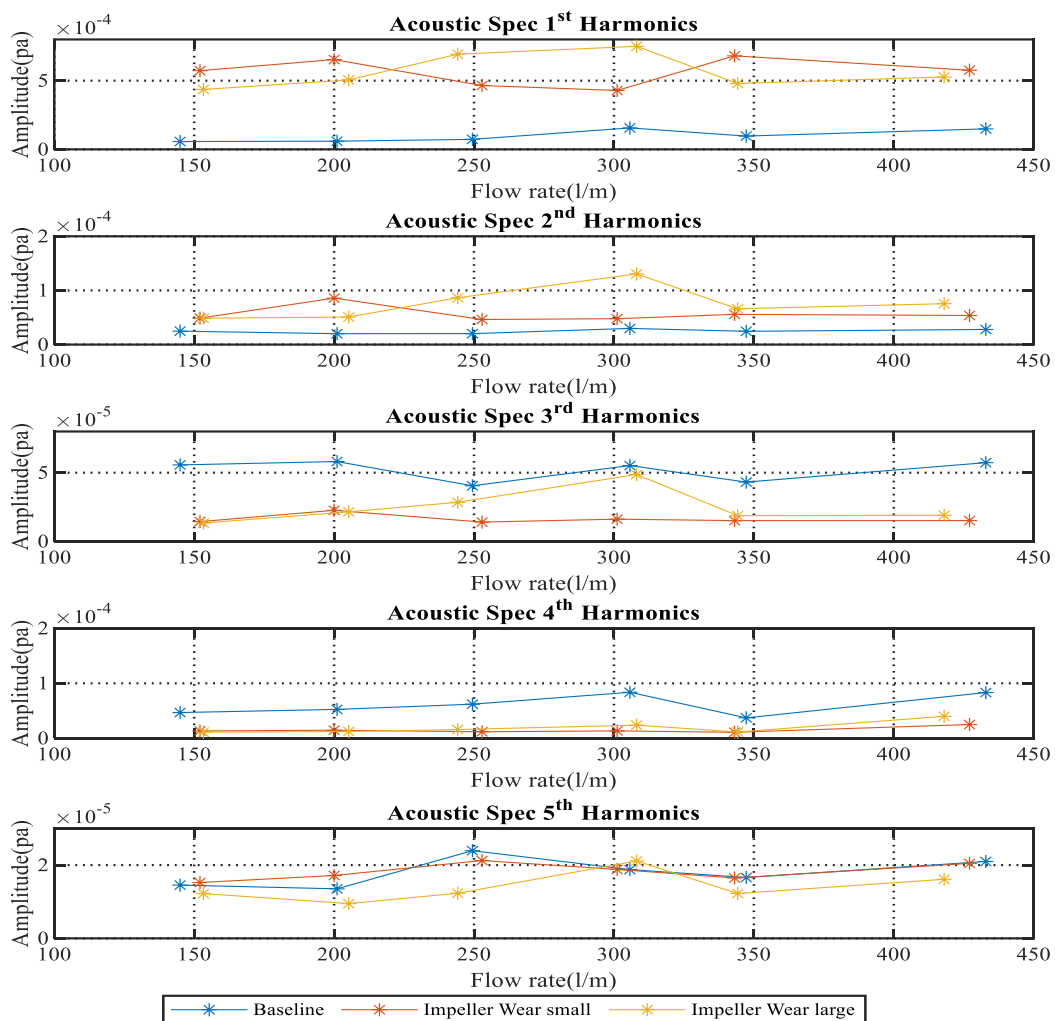


Figure 9-17 Magnitude of the acoustic power spectrum plots for the first five harmonics of 48.3 Hz with flow rate

Figure 9-18 shows the magnitudes of the MSB peaks for the first five harmonics of the shaft drive frequency (48.3 Hz) obtained from the acoustic signals for the baseline and two seeded faults.

The MSB results for impeller wear offer useful data and a stronger pattern for the separation of the harmonics for the healthy and impeller fault cases compared to the power spectrum analysis. For the first and, especially, the fifth harmonics there is a clear separation between baseline and fault conditions (except at a flow rate of 350 l/min with the first harmonic) though there is no consistent separation of the two faults. The 2nd, 3rd and 4th harmonics show no significant separation of the small fault and baseline and only separate the baseline and large fault at a flow rate of 350 l/min.

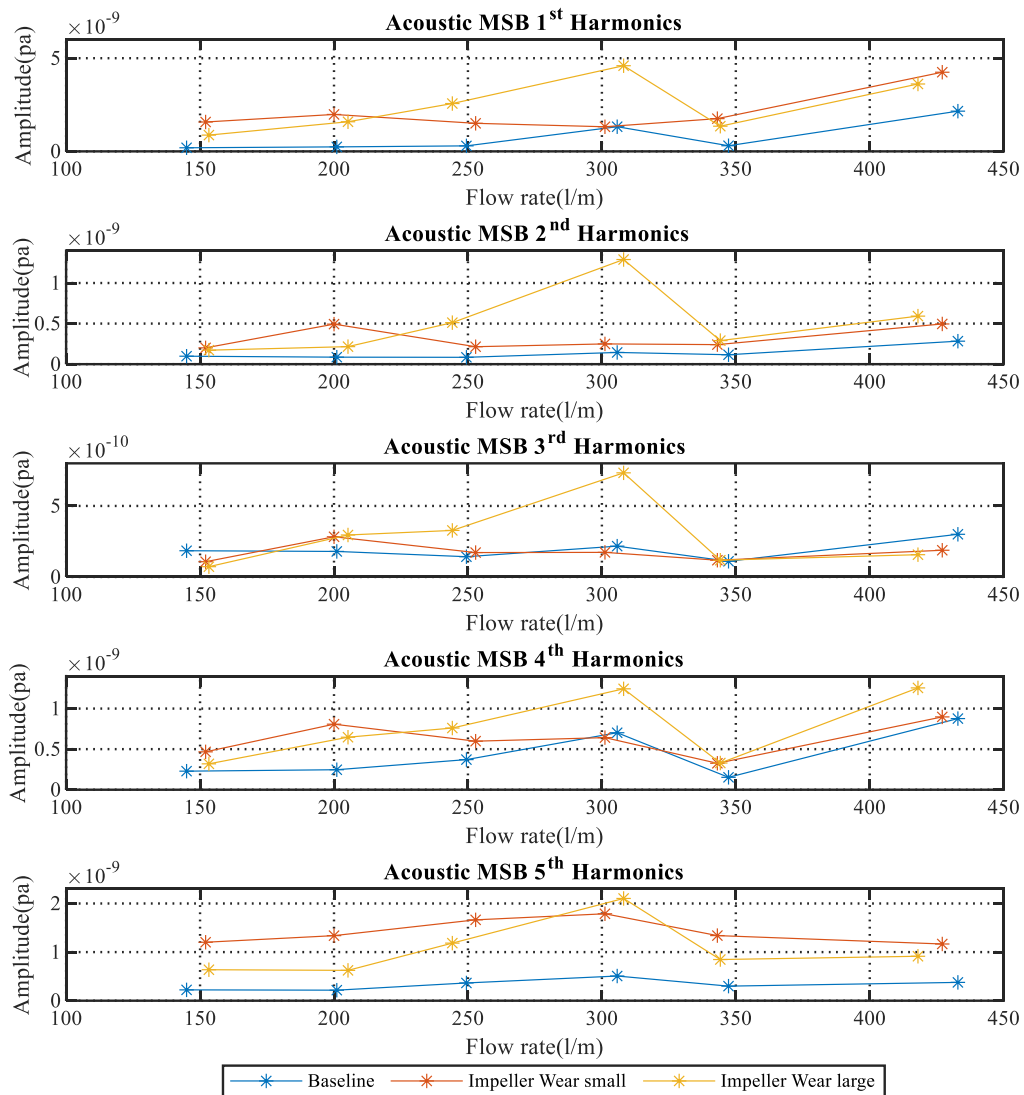


Figure 9-18 Magnitude of the MSB plots for the first five harmonics of 48.3 Hz in the acoustic signals with flow rate

Because of its capacity to reduce wideband, low-frequency noise, the MSB shows stronger results at low-frequencies for all flow rates. The vibration amplitude for the broad impulses of the impeller wear fault of the pump gets higher as the flow pressure gets lower. Thus, it shows that MSB analysis is able to extract characteristic modulations representative of degradation due to wear of the impeller by largely eliminating noise effects on signals.

Figure 9-19 shows comparable results for the peaks obtained at the vane passing frequency (338.3 Hz) for the power spectrum and MSB analysis of the acoustic signals for the baseline and two seeded wear faults. There is a consistent separation between baseline and both wear faults for both the power spectrum and MSB plots. In Figure 9-19 (b) the results provide a more comprehensive separation and strong and clear distinction between the healthy and both impeller fault plots. The MSB results show good separation between the baseline and faults for all flow rates, but not between the two-seeded defects. Despite background noise that influenced the acoustic signals, it shows the ability to extract modulation characteristics of impeller wear faults. The experimental results show that the acoustic signal, whether analysed using MSB analysis or the power spectrum, outperforms vibration analysis.

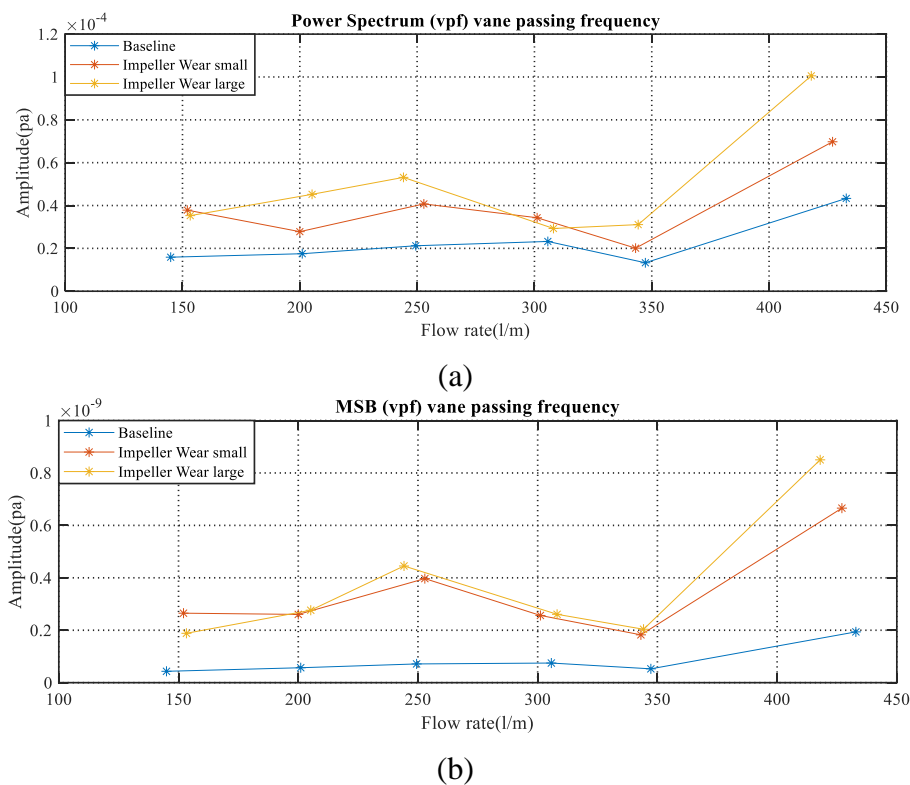


Figure 9-19 Comparison of (a) Power spectrum plot and (b) Plot obtained using MSB for the vane passing frequency (338.3 Hz) of the acoustic signal

9.9 Key Findings

In this research, analysis of the experimentally measured vibration and airborne sound signals generated was able to identify impeller wear. Fault detection was carried out separately using power spectrum and MSB analyses. The harmonics of the shaft frequency in the acoustic signals as obtained using MSB showed better results than the power spectrum. It also provided a strong separation between all harmonics at various flow rates, which can be used effectively for online monitoring. It is concluded that harmonics obtained using MSB analysis detected the seeded impeller wear faults successfully. This high level of diagnosis is achieved because MSB has the ability to minimize noise and demodulate nonlinearities.

The results show MSB analysis, and the power spectrum of the acoustic signal displayed good separation of faulty and healthy condition at the vane pass frequency. Also, the vibration power spectrum shows a little clearer separation of baseline and the faults than for the acoustic. For the MSB of the acoustic signal does offer a slightly better differentiation between the plots than a vibration. This should enable strong differentiation of impeller wear defects by averaging MSB peaks in the low-frequency range. In addition, the presence of either wear fault in the impeller caused a significant drop in the flow rate strongly indicating the presence of a fault.

CHAPTER 10:

Conclusions and Proposals for Future Work

This chapter presents the conclusions drawn from this research and its main achievements. It describes how the aim and objectives stated in Chapter One were achieved. After that, a summary of the contributions to knowledge made by this research is presented. Finally, recommendations for future studies on this topic are made.

10.1 Aim, Objectives and Achievements

This research has successfully achieved the stated aims of improving condition monitoring performance by developing the effective analytics of surface vibration and airborne acoustics signals for detection of faults seeded into a centrifugal pump by applying advanced signal processing techniques. It has also carried out a systematic comparison of results obtained from analysis of the measured acoustic and vibration signals regarding identification of the faults seeded into the pump. This work proposes means for the detection, at an early stage of development and before breakdown, of three common pump defects: bearing faults, mechanical seal defect, and wear of the impeller.

Each objective and how it was achieved are now listed.

Objective 1. To describe operational functionalities of condition monitoring systems and identify the mechanical components of centrifugal pumps.

Achievement 1. A general evaluation of the most popular CM approaches used for detecting and diagnosing faults in rotary machines is presented in Section 1.2, with the focus on the reliability of vibro-acoustic measurements to detect pump faults. This provided support for the research aim and its associated objectives, and provided motivation inspired by the research gaps identified. Fundamentals of centrifugal pumps were addressed in Section 2.2, while the main mechanical components and centrifugal pump applications were presented in Section 2.4.

Objective 2. To clarify the pump test rig test requirements and facilities to be used to perform the experiments, seeding different faults, and gaining experimental data. To study advanced methods, including data analytics of pumps, monitoring and detecting defects using multiple data sources (surface vibration and airborne sound) and identifying the main research gaps. The latter are presented in Sections 1.2.5, 1.2.6 and 1.3.

Achievement 2. The test rig used to perform the experiments is detailed in Chapter 5, including a description of the simulated faults and the experimental procedure. Sections 5.2, 5.3 and 5.4 describe the test rig used to conduct investigations, explaining its constituent parts, while Section 5.5 explains the role played by the

author in deciding what faults to simulate, how to seed them into the test rig, selecting the vibro-acoustic sensors, and their positioning.

Objective 3. To simulate different mechanical faults: inner and outer race bearing faults, mechanical seal, and impeller wear, and to investigate how these faults influence pump performance under different flow rates.

Achievement 3. The mechanical faults seeded into the centrifugal pump are reviewed in Section 2.8. It is shown in Chapter 3 that mechanical faults adversely affect pump performance and generate increased pump vibration and noise emitted and degrade system performance. With a consequent decrease in the efficiency of the centrifugal pump and shortening of the pump's working life. The details of how the particular faults were decided upon and introduced into the system is given in Section 5.5 and 5.6. The vibro-acoustic measurements with seeded faults were compared with those made for the baseline condition at a fixed motor speed of 2900 rpm. Several system parameters were varied during the tests to determine the pump's condition at different flow rates.

Objective 4. To explore the dynamic interactions between mechanical and hydraulic sources of centrifugal pump and the critical behaviours of these sources when faults occur.

Achievement 4. The noise and vibration generated by pump operations were addressed in chapter 3. The fundamental sources that display stationary modulation behaviour in measured signals are dynamic interactions between mechanical and hydraulic sources. Furthermore, when mechanical wear and fluid erosion cause failures on essential components such as impellers, bearings, and seals, the modulation becomes more substantial. Furthermore, random noises from random flows will have a negative impact on modulation, which making it harder to characterise modulation behaviour.

Objective 5. To examine the traditional methods (e.g., time and frequency domain analysis) for pump CM and detection of mechanical defects. To improve detection of the modulation components in both the vibration and acoustic signals and enhance them by implementing advanced signal processing techniques such as the

modulation signal bispectrum and envelope analysis, and then compare these results with conventional methods to ascertain how to obtain a more accurate identification and quantification of the faults.

Achievement 5. Detection and diagnosis of the seeded faults using time and frequency domain analyses were implemented on the collected data, see Sections 4.2, and 4.3. Separate evaluations of pump fault detection were carried out based on the vibration and acoustic signals separately. Then, advanced signal processing techniques were used to improve fault detection: envelope and MSB analyses, as described in Section 4.4. Comparison with results obtained by conventional methods is presented in Chapters 6, 7, 8 and 9. These chapters contain details of the detection of wear defects in the seals, bearings, and impeller. The descriptions given include details of the advanced signal processing techniques used (envelope and MSB analyses).

Objective 6. To examine vibration and acoustic measurements and compare these techniques for healthy and faulty cases.

Achievement 6. The tests were carried out with the accelerometer attached to the pump casing, and the acoustic sensor positioned 50 mm away from the pump casing. Data were recorded at a sampling rate of 96 kHz. Each fault was installed in the pump in turn, and for each defect nine flow rates were tested: 0 (blockage), 50, 100, 150, 200, 250, 300, 350, and 450 (l/min). The pump's flow curve was found to show significant variations in the presence of the faults, see Sections 6.4, 8.2, and 9.4. The vibro-acoustic signals for the seeded mechanical pump faults were obtained and used to show the presence of the faults at the different flow rates and compare these techniques for healthy and faulty cases are presented in Chapters 6, 7, 8 and 9.

Objective 7. To examine the capacity of vibro-acoustic signals to extract weak and noise-contaminated fault signals from the centrifugal pump for detection and diagnosis of pump faults with a high degree of accuracy.

Achievement 7. Sections 4.3 and 4.4 present the principles of envelope analysis, the power spectrum and MSB analysis used for diagnosing the presence of faults seeded into the centrifugal pump. Chapter 6 presents and compares the outcomes obtained using envelope analysis and the power spectrum to analyse the airborne sound

emitted from the pump when the bearing faults were seeded into it. It was shown that the envelope analysis was an efficient mechanism for detecting and tracking pump bearing faults when using the acoustic signal. Chapter 7 presents the results of MSB analysis and shows that use of MSB enables the accurate extraction of the modulation features. It also shows that the acoustic signal is better than the vibration signal for detecting the seeded bearing defects. The outcome was the successful separation of baseline and fault signals for the averages of the first and the second harmonic peaks of an outer race bearing fault for both vibration and acoustic signals.

Chapter 8 presents the results when detecting the mechanical seal defect using MSB analysis and the power spectrums of both the vibration and acoustic signals. It shows that MSB analysis of the acoustic signal provided the most sensitive assessment of the presence of the fault, compared to the vibration signal and the power spectrum. The first five harmonics of the shaft rotational frequency (48.3 Hz) obtained using MSB analysis gave good separation between baseline condition and the seal defect.

Chapter 9 presents the results obtained when detecting impeller wear faults using the power spectrum and MSB analysis of the vibration and airborne sound signals. The acoustic signal analysed using MSB gave better separation of baseline and fault signals than either the vibration signal or the power spectrum when using harmonics of the shaft frequency. The seeded impeller wear faults were successfully detected using harmonics obtained through MSB analysis.

Objective 8. To provide recommendations and guidelines for future research in pump condition monitoring

Achievement 8. Section 10.4 makes numerous proposals for possible future research into condition monitoring of centrifugal pumps.

10.2 Conclusions

The principal conclusions of the study can be summarized as:

1. The efficient detection of mechanical defects (bearings, impeller, and seal) seeded into a centrifugal pump using vibro-acoustic signals has been successfully achieved.

2. The seeded defects were detected by comparing signals obtained with a fault present with those obtained for the baseline (healthy) condition. This was achieved for a range of flow rates from blockage (zero flow) to the maximum, 450 l/min but at constant motor speed, 2900 rpm.
3. Comparison of the effectiveness of the vibration and acoustic signals revealed that the airborne acoustic signal was at least as informative as the vibration signal and, in some cases, as presented in Chapters 6, 7, 8 and 9, could provide more information on the presence of a fault.
4. The detection of the simulated bearing faults was achieved using both envelope analysis and MSB signal processing techniques for both vibration and acoustic signals. This tested the relative efficacy of envelope and MSB analysis of surface vibration and acoustic sound signals for detecting the presence of bearing faults. Both envelope analysis and MSB were effective in eliminating random background noise present in the signal, improving the identification of modulation components in both vibration and acoustic signals, and able to distinguish between the healthy state and with inner- and outer-race faults. It was found that the acoustic signals offered a clearer distinction between baseline and defective signals. In addition, the RMS of the acoustic signal was superior to that of the vibration in giving good separation between the healthy and defective conditions.
5. The detection of the simulated seal faults was achieved using MSB signal processing for both vibration and acoustic signals. It was found that averaging the MSB peaks for the first and lower harmonics of the drive shaft frequency present in the acoustic signal provided a strong separation between baseline and fault harmonics across a range of flow rates enabling the mechanical seal fault to be successfully detected. This part of the investigation showed the airborne sound signal gave better results than the vibration for the detection of the seeded seal fault. Reduction of background noise using MSB also enabled the RMS of the acoustic signals to give full separation between faulty and healthy cases over a wide range of pump operations.
6. The results show that MSB provided a more consistent and clear difference between baseline and faulty seal condition over the range of harmonics associated with the shaft frequency (48.3 Hz) at different flow rates. Furthermore, the

mechanical seal defect provides a significant reduction in the flow rate curve which would be an additional marker of the presence of a seal fault. The power spectrum was also used to detect the presence of the mechanical seal fault with both vibration and acoustic signals. Results showed that MSB analysis separated the mechanical seal fault from the healthy case with greater certainty than was achieved using the power spectrum.

7. Power spectrum and MSB both detected the simulated impeller wear faults with both vibration and airborne sound signals. The seeded impeller wear faults were identified using harmonics of the vane passing frequency present in the acoustic signal obtained through MSB analysis, but the power spectrum of the acoustic signals gave a clearer indication of the presence of wear faults. Nevertheless, the experimental results showed that both the MSB and power spectrum of the acoustic signals showed good separation of baseline and fault condition at the vpf, implying that averaging MSB peaks in the low-frequency range should allow strong differentiation of impeller wear defects.

10.3 Contributions to Knowledge

The research accomplishments have resulted in a number of contributions to knowledge in the field of centrifugal pump CM, which can be summarised as:

First Contribution: As a typical hydraulic machine the vibration and acoustic responses of a centrifugal pump are deemed modulations due to the interaction of steady and deterministic components, including high frequency structural fluid resonances. This important finding clarifies the direction of selecting and developing effective data analytic tools including envelope and MSB analysis.

Second Contribution: The detection and diagnosis of bearing (inner race, outer race) faults in centrifugal pumps using envelope analysis of the vibro-acoustic measurement is entirely novel when using remote acoustic measurements. No other work has been found describing this method in any detail. This is a novel application for detecting a particular fault taking advantage of the ability of envelope analysis to suppress noise and interference.

Third Contribution: Applying the MSB to the vibration and acoustic signals obtained with rolling element bearing faults in a centrifugal pump is a new approach to noise and

interference suppression. This novel application has never been done before. Such advanced monitoring means faults such as those seeded into the pump can now be detected and diagnosed more precisely.

Fourth Contribution: No study has been found which used MSB analysis based on vibro-acoustic signals for fault detection and diagnosis of mechanical seals in centrifugal pumps. It is believed that this is a unique application of MSB analysis.

Fifth Contribution: This work fully confirms that remote airborne acoustic measurement can achieve excellent detection and diagnosis performance for pump monitoring, which is comparable to the localised vibration measurements. For the first time, this is backed by experimental evidence. No one has reported this point before although many works did foresee that acoustic signal could be used for pump fault detection and diagnosis.

10.4 Recommendations for Future Work

A number of suggestions for future work are made based on this study that could develop CM and fault detection and diagnosis of centrifugal pumps:

Recommendation One: Applying different AI signal processing methods to vibro-acoustic measurements.

Recommendation Two: To establish a theoretical background of the experimental behaviour via developing a mathematical model of pump behaviour to study the vibro-acoustic signals for different fault conditions.

Recommendation Three: Further simulation of wear of the impeller vanes, by including simulated faults on every vane with different severity levels, again using vibro-acoustic measurements.

Recommendation Four: To investigate an integrated approach, the merging of the vibration and airborne acoustic signals into a single measure for fault detection, Such an approach would aim to combine the best of both methods.

Recommendation Five: To extend the work to the development of a novel, low-cost system for condition monitoring the different faults based on vibro-acoustic measurements and MSB techniques.

References:

1. Ilott, P. and A. Griffiths. *Development of a pumping system decision support tool based on artificial intelligence*. in *Tools with Artificial Intelligence, 1996., Proceedings Eighth IEEE International Conference on*. 1996. IEEE.
2. Choi, J.-S., D.K. McLaughlin, and D.E. Thompson, *Experiments on the unsteady flow field and noise generation in a centrifugal pump impeller*. *Journal of sound and vibration*, 2003. **263**(3): p. 493-514.
3. Al-Hashmi, S.A. and A. Ball, *Detection and Diagnosis of cavitation in Centrifugal Pumps*. 2005: University of Manchester.
4. Ciocoiu, L., E.-M. Hubbard, and C.E. Siemieniuch, *Implementation of remote condition monitoring system for predictive maintenance: An organisational challenge*. 2015.
5. Spellman, F.R., *Water and Wastewater Conveyance: Pumping, Hydraulics, Piping, and Valves*. 2016: CRC Press.
6. Juneja, B., *Fundamentals of metal cutting and machine tools*. 2003: New Age International.
7. Davies, A., *Handbook of condition monitoring: techniques and methodology*. 2012: Springer Science & Business Media.
8. Al Thobiani, F., F. Gu, and A. Ball, *The monitoring of cavitation in centrifugal pumps based on the analysis of vibro-acoustic measurements*. 2010.
9. Nasiri, M., M. Mahjoob, and H. Vahid-Alizadeh. *Vibration signature analysis for detecting cavitation in centrifugal pumps using neural networks*. in *Mechatronics (ICM), 2011 IEEE International Conference on*. 2011. IEEE.
10. Yunlong, Z. and Z. Peng, *Vibration fault diagnosis method of centrifugal pump based on emd complexity feature and least square support vector machine*. *Energy Procedia*, 2012. **17**: p. 939-945.
11. Rao, S.S. and F.F. Yap, *Mechanical vibrations*. Vol. 4. 2011: Prentice Hall Upper Saddle River.
12. Batchelor, B. and A.V.I. Hodgson, *IFS (Publications) Ltd*. Kempston, Bedford, UK, 1985.
13. Beebe, R.S. and R.S. Beebe, *Predictive maintenance of pumps using condition monitoring*. 2004: Elsevier.
14. Huang, K., T.J.J.o.S. Liu, and vibration, *Dynamic analysis of a spur gear by the dynamic stiffness method*. 2000. **234**(2): p. 311-329.
15. Smith, C.J., *Investigation of transient interactions in centrifugal pumps*. 2017.
16. Gu, F., et al., *The condition monitoring of diesel engines using acoustic measurements part 1: acoustic characteristics of the engine and representation of the acoustic signals*. 2000, SAE Technical Paper.
17. Mousmoulis, G., et al., *Experimental analysis of cavitation in a centrifugal pump using acoustic emission, vibration measurements and flow visualization*. 2019. **75**: p. 300-311.
18. Sachse, W., K. Yamaguchi, and J. Roget. *Acoustic emission: current practice and future directions*. 1991. ASTM.
19. Alfayez, L., et al., *The application of acoustic emission for detecting incipient cavitation and the best efficiency point of a 60 kW centrifugal pump: case study*. 2005. **38**(5): p. 354-358.

20. Al-Ghamd, A.M., D.J.M.s. Mba, and s. processing, *A comparative experimental study on the use of acoustic emission and vibration analysis for bearing defect identification and estimation of defect size*. 2006. **20**(7): p. 1537-1571.
21. Tandon, N. and B.J.J.o.a.e. Nakra, *Defect detection in rolling element bearings by acoustic emission method*. 1990. **9**(1): p. 25-28.
22. Sharma, R.B. and A.J.A.A. Parey, *Modelling of acoustic emission generated in rolling element bearing*. 2019. **144**: p. 96-112.
23. Jayaswal, P., A. Wadhvani, and K. Mulchandani, *Machine fault signature analysis*. International Journal of Rotating Machinery, 2008. **2008**.
24. Zhou, Z.-D., et al., *Actualities and development of heavy-duty CNC machine tool thermal error monitoring technology*. 2017. **30**(5): p. 1262-1281.
25. Kia, S.H., H. Henao, and G.-A. Capolino, *A high-resolution frequency estimation method for three-phase induction machine fault detection*. IEEE Transactions on Industrial Electronics, 2007. **54**(4): p. 2305-2314.
26. Bravo-Imaz, I., et al. *Motor current signature analysis for gearbox health monitoring: Experiment, signal analysis and classification*. in *Second European Conference of the Prognostics and Health Management Society (PHM 2014)*. 2014.
27. Mohanty, A.R., et al., *Fault detection in a centrifugal pump using vibration and motor current signature analysis*. 2012. **6**(3-4): p. 261-276.
28. Irfan, M. and A.J.A.S. Glowacz, *Design of a novel electric diagnostic technique for fault analysis of centrifugal pumps*. 2019. **9**(23): p. 5093.
29. Sakthivel, N., V. Sugumaran, and S.J.E.S.w.A. Babudevasenapati, *Vibration based fault diagnosis of monoblock centrifugal pump using decision tree*. 2010. **37**(6): p. 4040-4049.
30. Kamiel, B., et al., *Impeller fault detection for a centrifugal pump using principal component analysis of time domain vibration features*. 2005.
31. Peck, J.P. and J. Burrows, *On-line condition monitoring of rotating equipment using neural networks*. ISA Transactions, 1994. **33**(2): p. 159-164.
32. Randall, R.B., *Vibration-based condition monitoring: industrial, aerospace and automotive applications*. 2011: John Wiley & Sons.
33. Troyer, D.D. and M. Williamson. *Effective integration of vibration analysis and oil analysis*. in *Proceedings of the International Conference on Condition Monitoring, University College of Swansea, Swansea, UK*. 1999.
34. Gu, F. and A. Ball. *Vibration based fault diagnosis in diesel fuel injection system*. in *IMEchE Seminar on Diesel Fuel Injection Systems, London*. 1995.
35. Nandi, A.J.C.M. and C.I. Diagnostic Engineering Management, *Vibration based fault detection-features, classifiers and novelty detection*. 2002.
36. Edwards, D.J., G.D. Holt, and F.J.J.o.Q.i.M.E. Harris, *Predictive maintenance techniques and their relevance to construction plant*. 1998.
37. Goldman, S., *Vibration spectrum analysis: a practical approach*. 1999: Industrial Press Inc.
38. Rgeai, M.N., *Helical gearbox fault detection using motor current signature analysis*. 2007: The University of Manchester (United Kingdom).
39. Swansson, N. *Application of Vibration Signal Analysis Techniques to Condition Monitoring*. in *Conference on Lubrication, Friction and Wear in Engineering 1980, Melbourne: Preprints of Papers*. 1980. Institution of Engineers, Australia.
40. Rehab, I., et al., *A study of the diagnostic amplitude of rolling bearing under increasing radial clearance using modulation signal bispectrum*. 2016.

41. Delvecchio, S., et al., *Vibro-acoustic condition monitoring of Internal Combustion Engines: A critical review of existing techniques*. 2018. **99**: p. 661-683.
42. Jiang, J., *Acoustic condition monitoring in industrial environments*. 2011, Saarbrücken (Germany): LAP Lambert: LAP LAMBERT Academic Publishing. 212.
43. Ramroop, G., et al. *Airborne Acoustic Condition Monitoring of a Gearbox System*. in *2001 5th Annual Maintenance and Reliability Conference (MARCON 2001)*. 2001.
44. Lee, Y.-T., C. Hah, and J. Loellbach. *Unsteady flow interaction inside a high-Reynolds-number, axial-flow pump stage*. in *36th AIAA Aerospace Sciences Meeting and Exhibit*. 1998.
45. Ahmaida, A., et al., *Gear wear process monitoring using acoustic signals*. 2014.
46. Benesty, J., J. Chen, and Y. Huang, *Microphone array signal processing*. Vol. 1. 2008: Springer Science & Business Media.
47. Al-Hashmi, S.A.J.I.J.o.E.T. and A. Engineering, *Statistical Analysis of Acoustic Signal for Cavitation Detection*. 2013. **3**(4): p. 55-66.
48. Baydar, N., *The vibro-acoustic monitoring of gearboxes*. 2000: University of Manchester.
49. Rapur, J.S., R.J.J.o.D.S. Tiwari, Measurement,, and Control, *Multifault diagnosis of combined hydraulic and mechanical centrifugal pump faults using continuous wavelet transform and support vector machines*. 2019. **141**(11).
50. Ooijevaar, T., et al., *A Comparison of Vibration based Bearing Fault Diagnostic Methods*. 2019.
51. Cococcioni, M., B. Lazzerini, and S.L.J.I.T.o.I.I. Volpi, *Robust diagnosis of rolling element bearings based on classification techniques*. 2012. **9**(4): p. 2256-2263.
52. Henriquez, P., et al., *Review of automatic fault diagnosis systems using audio and vibration signals*. 2013. **44**(5): p. 642-652.
53. Sait, A.S. and Y.I. Sharaf-Eldeen, *A review of gearbox condition monitoring based on vibration analysis techniques diagnostics and prognostics*, in *Rotating Machinery, Structural Health Monitoring, Shock and Vibration, Volume 5*. 2011, Springer. p. 307-324.
54. Bettahar, T., et al., *New method for gear fault diagnosis using empirical wavelet transform, Hilbert transform, and cosine similarity metric*. 2020. **12**(6): p. 1687814020927208.
55. Kumar, A., et al., *Fault diagnosis of rolling element bearing based on symmetric cross entropy of neutrosophic sets*. 2020. **152**: p. 107318.
56. Admin, M.B. *How A Mechanical Seal Prevents Pump leakage*. 2016 Created Aug 31 2016]; Available from: <https://www.pumpproducts.com/blog/importance-mechanical-seals/>.
57. Lara, R., et al., *Influence of constructive parameters and power signals on sound quality and airborne noise radiated by inverter-fed induction motors*. 2015. **73**: p. 503-514.
58. Jena, D. and S.J.A.A. Panigrahi, *Automatic gear and bearing fault localization using vibration and acoustic signals*. 2015. **98**: p. 20-33.
59. Glowacz, A.J.M.S.R., *Recognition of acoustic signals of synchronous motors with the use of MoFS and selected classifiers*. 2015. **15**(4): p. 167-175.

60. Hemmati, F., W. Orfali, and M.S.J.A.A. Gadala, *Roller bearing acoustic signature extraction by wavelet packet transform, applications in fault detection and size estimation*. 2016. **104**: p. 101-118.
61. He, M., et al., *A new signal processing and feature extraction approach for bearing fault diagnosis using AE sensors*. 2016. **16**(5): p. 821-827.
62. Scheffer, C. and P. Girdhar, *Practical machinery vibration analysis and predictive maintenance*. 2004: Elsevier.
63. Mendel, E., et al. *Automatic bearing fault pattern recognition using vibration signal analysis*. in *2008 IEEE International Symposium on Industrial Electronics*. 2008. IEEE.
64. Kumar, A., R.J.N.C. Kumar, and Applications, *Adaptive artificial intelligence for automatic identification of defect in the angular contact bearing*. 2018. **29**(8): p. 277-287.
65. Wang, D., et al., *Sparsity guided empirical wavelet transform for fault diagnosis of rolling element bearings*. 2018. **101**: p. 292-308.
66. Bandt, C. and B.J.P.r.l. Pompe, *Permutation entropy: a natural complexity measure for time series*. 2002. **88**(17): p. 174102.
67. Tian, Y., et al., *Self-adaptive bearing fault diagnosis based on permutation entropy and manifold-based dynamic time warping*. 2019. **114**: p. 658-673.
68. Glowacz, A., W.J.S. Glowacz, and Vibration, *Vibration-based fault diagnosis of commutator motor*. 2018. **2018**.
69. Hamomd, O., et al. *Vibration based centrifugal pump fault diagnosis based on modulation signal bispectrum analysis*. in *Automation and Computing (ICAC), 2017 23rd International Conference on*. 2017. IEEE.
70. Mondal, D., et al. *Airborne Acoustic Signature Analysis for Fault Diagnosis of Reciprocating Compressors Using Modulation Signal Bi-spectrum*. in *2019 25th International Conference on Automation and Computing (ICAC)*. 2019. IEEE.
71. Zhang, E., et al., *Mechanical seal opening condition monitoring based on acoustic emission technology*. *Sensors & Transducers*, 2014. **172**(6): p. 139.
72. Towsyfyhan, H., et al., *Tribological behaviour diagnostic and fault detection of mechanical seals based on acoustic emission measurements*. 2019. **7**(6): p. 572-586.
73. Olmos, F. *Evolution Of A Mechanical Seal Condition Monitoring System*. in *Proceedings of the 7th International Pump Users Symposium*. 1990. Turbomachinery Laboratories, Department of Mechanical Engineering, Texas A&M University.
74. Bloch, H.P. and F.K. Geitner, *Repair and Maintenance of Rotating Equipment Components, Machinery Component Maintenance and Repair, 4th Ed.* 2019: Elsevier.
75. Gupta, L.A. and D. Peroulis, *Wireless temperature sensor for condition monitoring of bearings operating through thick metal plates*. *IEEE Sensors Journal*, 2013. **13**(6): p. 2292-2298.
76. Li, X., et al., *The contact state monitoring for seal end faces based on acoustic emission detection*. *Shock and Vibration*, 2016. **2016**.
77. Jianjun, S., et al., *Numerical analysis on a new pump-out hydrodynamic mechanical seal*. *Tribology International*, 2017. **106**: p. 62-70.
78. Zhang, E., et al., *Study on AE in mechanical seal lift-off recognition of mechanical main shaft*. *Sensors & Transducers*, 2014. **173**(6): p. 158.

79. Fan, Y.B., F.S. Gu, and A. Ball. *Acoustic emission monitoring of mechanical seals using MUSIC algorithm based on higher order statistics*. in *Key Engineering Materials*. 2009. Trans Tech Publ.
80. Birajdar, R., R. Patil, and K. Khanzode. *Vibration and noise in centrifugal pumps-Sources and diagnosis methods*. in *3rd International conference on Integrity, Reliability and Failure*. 2009.
81. Lu, J., et al., *Investigation on the vibration and flow instabilities induced by cavitation in a centrifugal pump*. 2017. **9**(4): p. 1687814017696225.
82. Al-Obaidi, A.R.J.E.T., *Detection of cavitation phenomenon within a centrifugal pump based on vibration analysis technique in both time and frequency domains*. 2020. **44**(3): p. 329-347.
83. Liao, Z., et al., *Multi-scale hybrid HMM for tool wear condition monitoring*. 2016. **84**(9-12): p. 2437-2448.
84. Thanikachalam, V.J.I.J.o.A.i.E.R., *The Corrosion and Erosion of Centrifugal Pumps in a Marine Environment: Causes, Effects and Mitigation*. 2017. **13**(6): p. 34-52.
85. Bachus, L. and A. Custodio, *Know and understand centrifugal pumps*. 2003: Elsevier.
86. Girdhar, P. and O. Moniz, *Practical centrifugal pumps*. 2011: Elsevier.
87. Marscher, W.D. *Avoiding Failures in Centrifugal Pumps*. in *Proceedings of the 19th International Pump Users Symposium*. 2002. Texas A&M University. Turbomachinery Laboratories.
88. Hashim, N., A. Hassan, and M.F.A. Hamid. *Predictive maintenance model for centrifugal pumps under improper maintenance conditions*. in *AIP Conference Proceedings*. 2020. AIP Publishing LLC.
89. Cooper, P.a.G.T., *Performance of Centrifugal Pumps*. Pumping station design, 2006.
90. Bloch, H.P. and A.R. Budris, *Pump user's handbook: life extension/by Heinz P. Bloch & Allan R. Budris*. 2010, Lilburn, GA: The Fairmont Press: CRC Press; Boca Raton, FL: Distributed by
91. Tuzson, J., *Centrifugal pump design*. 2000: John Wiley & Sons.
92. Wilson, K.C., et al., *Slurry transport using centrifugal pumps*. 2006: Springer Science & Business Media.
93. Karassik, I. and J.T. McGuire, *Centrifugal pumps*. 2012: Springer Science & Business Media.
94. Kutbi, I., *Evaluation of centrifugal pump performance in nuclear power plants*. *Annals of Nuclear Energy*, 1991. **18**(11): p. 629-654.
95. A, y.M., *Profitable Condition Monitoring*. 1996, Harrogate, UK: in BHR Group
96. Limited, E.I.F.E.I.F., *The World Pump Market 2014-2019*. 2014. **Volume I**: p. III 8.
97. Nelik, L., *Centrifugal & Rotary Pumps: Fundamentals With Applications*. 1999: CRC Press.
98. Karassik, I.J., et al., *Pump handbook*. Vol. 3. 1986: McGraw-Hill New York.
99. Persistencemr, *Global Water Pump Market To Record Robust Compound Annual Growth Rate Post-Covid-19*, In *Inter Press Service News Agency - Business*. 2020: Persistence Market Research.
100. Nelik, L. *PUMPS&SYSTEMS*. Simplify Pump Design 2013 10/22/2013 [cited 2013 10/22/2013]; Available from: <https://www.pumpsandsystems.com/>.
101. Sahu, G., *Pumps: rotodynamic and positive displacement types: theory, design and applications*. 2000: New Age International.

102. Jacobsen, C.B., *The Centrifugal Pump*. RESEARCH AND TECHNOLOGY, ed. D. book. GRUNDFOS.
103. Karassik, I.J., et al., *Pump handbook*. Vol. Vol 3. 2001: McGraw-Hill New York.
104. Elsey, J. *10 Ways to Improve Your Impeller*. Common Pumping Mistakes 2017 04/10/2017]; Available from: <https://www.pumpsandsystems.com/10-ways-improve-your-impeller>.
105. Hamomd, O.H., *Compound Fault Diagnosis of Centrifugal Pumps Using Vibration Analysis Techniques*. 2018, University of Huddersfield.
106. Al Thobiani, F., *The non-intrusive detection of incipient cavitation in centrifugal pumps*. 2011, University of Huddersfield.
107. Godbole, V., R. Patil, and S. Gavade. *Axial thrust in centrifugal pumps—experimental analysis*. in *15th International Conference on Experimental Mechanics, Porto/Portugal*. 2012.
108. Janjarasjitt, S., H. Ocak, and K. Loparo, *Bearing condition diagnosis and prognosis using applied nonlinear dynamical analysis of machine vibration signal*. *Journal of Sound and Vibration*, 2008. **317**(1-2): p. 112-126.
109. McKee, K., et al. *A review of major centrifugal pump failure modes with application to the water supply and sewerage industries*. in *ICOMS Asset Management Conference Proceedings*. 2011. Asset Management Council.
110. Antoni, J., *Cyclic spectral analysis in practice*. *Mechanical Systems and Signal Processing*, 2007. **21**(2): p. 597-630.
111. Lebeck, A.O., *Principles and design of mechanical face seals*. 1991: John Wiley & Sons.
112. DaqiqShirazi, M., et al., *The effect of wear ring clearance on flow field in the impeller sidewall gap and efficiency of a low specific speed centrifugal pump*. 2018. **232**(17): p. 3062-3073.
113. Mammadov, V.A., A. Yusifov, and K.P. Tacon. *Upstream Pumping Technology In Centrifugal Pump Mechanical Sealing Applications—Field Experience With High Duty Seawater Injection Pumps*. in *Proceedings of the 26th International Pump Users Symposium*. 2010. Turbomachinery Laboratory, Texas A&M University.
114. Zhang, Q., et al., *Hydraulics and Blading of Centrifugal Pump Impellers: A Systematic Review and Application*. 2019: p. 1-12.
115. Appadoo, R., et al. *Performance Monitoring and Fault Diagnosis of Vacuum Pumps based on Airborne Sounds*. in *2018 24th International Conference on Automation and Computing (ICAC)*. 2018. IEEE.
116. Yu, J., T. Zhang, and J. Qian, *Electrical Motor Products: International Energy-Efficiency Standards and Testing Methods*. 2011: Elsevier.
117. Yedidiah, S.J.L.C. and Hall, *Centrifugal pump user's guidebook*. 1996.
118. Čudina, M.J.H.o.N. and V. Control, *Pumps and pumping system noise and vibration prediction and control*. 2007: p. 897-909.
119. Gülich, J.F., *Centrifugal pumps*. Vol. 2. 2008: Springer.
120. Yu, Y., C.J.J.o.s. Junsheng, and vibration, *A roller bearing fault diagnosis method based on EMD energy entropy and ANN*. 2006. **294**(1-2): p. 269-277.
121. Qiu, H., et al., *Wavelet filter-based weak signature detection method and its application on rolling element bearing prognostics*. *Journal of sound and vibration*, 2006. **289**(4-5): p. 1066-1090.
122. Shingai, K., et al., *Long-period pressure pulsation estimated in numerical simulations for excessive flow rate condition of francis turbine*. 2014. **136**(7).

123. Henshaw, T. *Centrifugal Pump Axial Thrust, Pumps and Systems*. 2012
Accessed 03/Jan/2020.].
124. Fraser, W. *Centrifugal Pump Hydraulic Performance and Diagnostics*. in *Pump Handbook, New York, New York: McGraw-Hill. Negative Flows,* " Eleventh International Conference of the British Pump Manufacturers' Association New Challenges-Where Next. 1985.
125. Evans, J., *Cavitation—A largely Misunderstood Phenomenon*. 2005, August.
126. Schiavello, B. and F.C. Visser. *Pump Cavitation: various NPSHR criteria, NPSHA margins, impeller life expectancy*. in *Proceedings of the 25th international pump users symposium*. 2009. Texas A&M University. Turbomachinery Laboratories.
127. Al-Braik, A., et al., *Diagnosis of Impeller Faults in a Centrifugal Pump Using Vibration Signals*. 2014.
128. Younes, M. *Investigation of hydraulic problems in pumping station; case study*. in *Twelfth International Water Technology Conference, IWTC12*. 2008. Citeseer.
129. Grist, E., *Cavitation and the centrifugal pump: a guide for pump users*. 1998: CRC press.
130. Thai, Q., C.J.J.o.M.S. Lee, and Technology, *The cavitation behavior with short length blades in centrifugal pump*. 2010. **24**(10): p. 2007-2016.
131. Ramirez, C. *Why Is My Pool Pump So Loud*. 2015 January 15, 2015]; Available from: <http://www.inyopools.com/blog/pool-pump-loud/>.
132. Tucker, P.G., *Unsteady computational fluid dynamics in aeronautics*. Vol. 104. 2013: Springer Science & Business Media.
133. Wolfram, A., et al. *Component-based multi-model approach for fault detection and diagnosis of a centrifugal pump*. in *American Control Conference, 2001. Proceedings of the 2001*. 2001. IEEE.
134. a/s, g.m., *Mechanicalshaft seals for pumps Failure of mechanical shaft seals* 2009.
135. *Constitution and phenomenolgy of mechanical seals*. Tribology, lubrication and mechanical seals 2011 [cited 2011 10 June 2011]; Available from: <http://blogs.univ-poitiers.fr/noelbrunetiere/2011/06/10/constitution-and-phenomenolgy-of-mechanical-seals/>.
136. Sutton, I., *Plant design and operations*. 2017: Gulf Professional Publishing.
137. Lontin, K. and M.J.F. Khan, *Interdependence of friction, wear, and noise: A review*. 2021: p. 1-27.
138. Miettinen, J. and V. Siekkinen, *Acoustic emission in monitoring sliding contact behaviour*. International Journal of Multiphase Flow, 1996. **22**: p. 153-153.
139. Summers-Smith, J.D., *Mechanical seal practice for improved performance*. 2nd rev. ed 1992: Published by Mechanical Engineering Publications for The Institution of Mechanical Engineers
140. Williams, M. and N. Barnes. *The use of acoustic emissions for monitoring mechanical seals*. in *13th BPMA Pump Technical Conference*. 1993.
141. Zeus, D., *Cavitation—A little noticed Factor in the Operation of Mechanical Seals*. Industrial Lubrication and Tribology, 1993. **45**(2): p. 3-6.
142. Mathews, R., *Acoustic Emission*. 1983.
143. Yongquan, G., *The Fluid Dynamic Seal*, in *University of Petroleum Press*. 1990.
144. Long, W., G. Boqing, and S. Jianjun, *Review of mechanical seal faces friction condition*. Lubrication Engineering, 2003(5): p. 30-33.

145. Flexachem. *Mechanical Seal* 2010 [cited retrieved January 2020; Available from: www.flexachem.com.
146. Williams, T., et al., *Rolling element bearing diagnostics in run-to-failure lifetime testing*. Mechanical systems and signal processing, 2001. **15**(5): p. 979-993.
147. Mc Nally, W., *Troubleshooting the ball bearings in a centrifugal pump*. World pumps, 2004. **2004**(454): p. 28-29.
148. Epperly, R.A., G.E. Heberlein, and L.G. Eads. *A tool for reliability and safety: predict and prevent equipment failures with thermography*. in *Petroleum and Chemical Industry Conference, 1997. Record of Conference Papers. The Institute of Electrical and Electronics Engineers Incorporated Industry Applications Society 44th Annual*. 1997. IEEE.
149. Harris, T.A. and M.N. Kotzalas, *Rolling Bearing Analysis: Advanced Concepts of Bearing Technology*. 2007: CRC.
150. Goddard, K.N. and B.D.J.L.e. MacIsaac, *The use of oil borne debris as a failure criterion of rolling element bearings*. 1995. **51**(6): p. 481-487.
151. Rehab, I.A., *The Optimization of Vibration Data Analysis for the Detection and Diagnosis of Incipient Faults in Roller Bearings*. 2016, University of Huddersfield.
152. AG, F.K.J.P.N.W., *Rolling Bearing Damage Recognition of damage and bearing inspection*. 2003. **82**(102): p. 2.
153. Miller, J.L. and D. Kitaljevich. *In-line oil debris monitor for aircraft engine condition assessment*. in *2000 IEEE Aerospace Conference. Proceedings (Cat. No. 00TH8484)*. 2000. IEEE.
154. Patidar, S., P.K.J.I.J.o.E.T. Soni, and Technology, *An overview on vibration analysis techniques for the diagnosis of rolling element bearing faults*. 2013. **4**(5): p. 1804-1809.
155. Shiels, S., *Troubleshooting centrifugal pumps: rolling element bearing failures*. World pumps, 2001. **2001**(423): p. 28-30.
156. GÜNER, M. and M.M.J.Y.Y.Ü.T.B.D. ÖZBAYER, *Wear and its Effects in Centrifugal Pumps*. 2019. **29**(3): p. 569-582.
157. Noon, A.A. and M.-H.J.W. Kim, *Erosion wear on centrifugal pump casing due to slurry flow*. 2016. **364**: p. 103-111.
158. Oluk, O., & Öztürk, D., *Erosion and Corrosion*. (2011).
159. Sulzer Pumps, S. and L. Gebrüder Sulzer Aktiengesellschaft. *Sulzer Pumps, Centrifugal pump handbook*. 3rd ed. 2010, Amsterdam: Elsevier.
160. Huang, S., et al., *Study on wear properties of the flow parts in a centrifugal pump based on EDEM–Fluent coupling*. 2019. **7**(7): p. 431.
161. Gülich, J.F., *Centrifugal Pumps*. 2010, Springer Berlin Berlin, Heidelberg.
162. Ning, C. and X. Zhang. *Study on Vibration and Noise For the Hydraulic System of Hydraulic hoist*. in *Proceedings of the 1st International Conference on Mechanical Engineering and Material Science*. 2012. Atlantis Press.
163. Timouchev, S. and J. Turret. *Numerical simulation of BPF pressure pulsation field in centrifugal pumps*. in *Proceedings of the 19th International Pump Users Symposium*. 2002. Texas A&M University. Turbomachinery Laboratories.
164. Anon. *Impact of off-BEP Pump Operation*. Chemical Engineering 2015 [cited retrieved January 2010; Available from: <https://www.chemengonline.com/impact-bep-pump-operation/>].
165. Yantek, D.S., *Estimated sound power radiated by surfaces on a continuous miner tail section using vibration measurements*. 2003.

166. Tan, C.K., et al., *A comparative experimental study on the diagnostic and prognostic capabilities of acoustics emission, vibration and spectrometric oil analysis for spur gears*. 2007. **21**(1): p. 208-233.
167. Miller, R.K. and P. McIntire, *Acoustic emission testing*. 1987, American Society for Nondestructive Testing.
168. Jacobsen, F., et al., *Fundamentals of acoustics and noise control*. 2011, Note.
169. Ahmaida, A.M., *Condition Monitoring and Fault Diagnosis of a Multi-Stage Gear Transmission Using Vibro-acoustic Signals*. 2018, University of Huddersfield.
170. Cox, T. and P. D'Antonio, *Absorbers and Diffusers in Rooms and Geometric Room Acoustic Models*. 2017, CRC Press. p. 497-514.
171. KANG, J., *Acoustics of Long Spaces: Theory Design and Practice; London 2002*. 2002, Telford Publishing Ltd.
172. Norton, M.P. and D.G. Karczub, *Fundamentals of noise and vibration analysis for engineers*. 2003: Cambridge university press.
173. Note, A., *The Fundamentals of Signal Analysis*. Hewlett Packard: p. 98-107.
174. Randall, R., *Computer-aided Vibration Spectrum Trend Analysis for Condition Monitoring*. Maintenance Management International, 1985. **5**(3): p. 161-167.
175. Sun, Q. and Y. Tang, *Singularity analysis using continuous wavelet transform for bearing fault diagnosis*. Mechanical systems and signal processing, 2002. **16**(6): p. 1025-1041.
176. Shao, Y., et al., *A new fault diagnosis algorithm for helical gears rotating at low speed using an optical encoder*. Measurement, 2016. **93**: p. 449-459.
177. Aye, S.A. and P.S. Heyns, *Effect of Speed and Torque on Statistical Parameters in Tapered Bearing Fault Detection*. World Academy of Science, Engineering and Technology, International Journal of Mechanical, Aerospace, Industrial, Mechatronic and Manufacturing Engineering, 2011. **5**(6): p. 1122-1124.
178. Wang, H. and P. Chen, *Fault diagnosis method based on kurtosis wave and information divergence for rolling element bearings*. WSEAS Transactions on System, 2009. **8**(10): p. 1155-1165.
179. Gupta, P. and M.J.M.T.P. Pradhan, *Fault detection analysis in rolling element bearing: A review*. 2017. **4**(2): p. 2085-2094.
180. Feng, G., et al. *The real-time implementation of envelope analysis for bearing fault diagnosis based on wireless sensor network*. in *Automation and Computing (ICAC), 2013 19th International Conference on*. 2013. IEEE.
181. Randall, R.B., J.J.M.s. Antoni, and s. processing, *Rolling element bearing diagnostics—A tutorial*. 2011. **25**(2): p. 485-520.
182. Pan, Y., J. Chen, and L. Guo, *Robust bearing performance degradation assessment method based on improved wavelet packet–support vector data description*. Mechanical Systems and Signal Processing, 2009. **23**(3): p. 669-681.
183. Randall, R.B., J. Antoni, and S. Chobsaard, *The relationship between spectral correlation and envelope analysis in the diagnostics of bearing faults and other cyclostationary machine signals*. Mechanical systems and signal processing, 2001. **15**(5): p. 945-962.
184. Ho, D. and R. Randall, *Optimisation of bearing diagnostic techniques using simulated and actual bearing fault signals*. Mechanical systems and signal processing, 2000. **14**(5): p. 763-788.
185. McFadden, P., J.J.J.o.s. Smith, and vibration, *Model for the vibration produced by a single point defect in a rolling element bearing*. 1984. **96**(1): p. 69-82.

186. McInerny, S.A. and Y.J.I.T.o.e. Dai, *Basic vibration signal processing for bearing fault detection*. 2003. **46**(1): p. 149-156.
187. Davis, R.J.S.W.o.M.R., *By David R. Brillinger*. 2011: p. 11.
188. Saidi, L., J.B. Ali, and F.J.I.t. Fnaiech, *Application of higher order spectral features and support vector machines for bearing faults classification*. 2015. **54**: p. 193-206.
189. Collis, W., et al., *Higher-order spectra: the bispectrum and trispectrum*. 1998. **12**(3): p. 375-394.
190. Haba, U.A., *Information Extraction Based on the Analysis of Motor Supply and Structural Vibration for Machinery Condition Monitoring*. 2019, University of Huddersfield.
191. Ahmed, M., et al. *Fault diagnosis of reciprocating compressors using relevance vector machines with a genetic algorithm based on vibration data*. in *2014 20th International Conference on Automation and Computing*. 2014. IEEE.
192. Alwodai, A., et al., *A study of motor bearing fault diagnosis using modulation signal bispectrum analysis of motor current signals*. 2013. **4**(03): p. 72.
193. Li, X., et al. *Feature Extraction of Underwater Signals Based on Bispectrum Estimation*. in *2011 7th International Conference on Wireless Communications, Networking and Mobile Computing*. 2011. IEEE.
194. Naid, A., et al. *Bispectrum analysis of motor current signals for fault diagnosis of reciprocating compressors*. in *Key Engineering Materials*. 2009. Trans Tech Publ.
195. Zhang, G., et al., *Bispectral analysis for on-line monitoring of stamping operation*. 2002. **15**(1): p. 97-104.
196. Gu, F., et al., *Electrical motor current signal analysis using a modified bispectrum for fault diagnosis of downstream mechanical equipment*. 2011. **25**(1): p. 360-372.
197. Gu, F., et al., *A new method of accurate broken rotor bar diagnosis based on modulation signal bispectrum analysis of motor current signals*. 2015. **50**: p. 400-413.
198. Anon. *Sound Fields: Free versus Diffuse Field, Near versus Far Field*. 2020; Available from: <https://youtu.be/PcwFjB6z17A>.
199. Chapman, S.J., *Electric machinery and power system fundamentals*. 2002: McGraw-Hill.
200. Stavale, A.E., J. Lorenc, and E. Sabini. *Development of a Smart Pumping System*. in *PROCEEDINGS OF THE INTERNATIONAL PUMP USERS SYMPOSIUM*. 2001.
201. Engineering, P. *Vibration Monitoring for Centrifugal Pumps*. 2020 [cited retrieved January 2020; Available from: <https://www.pch-engineering.dk/467/vibration-monitoring-for-centrifugal-pumps>. .
202. Beattie, A.G.J.A. and Livermore, *Acoustic emission non-destructive testing of structures using source location techniques*. 2013.
203. Ao, H., et al., *A roller bearing fault diagnosis method based on LCD energy entropy and ACROA-SVM*. 2014. **2014**.
204. Hase, A. and H. Mishina, *Wear elements generated in the elementary process of wear*. *Tribology International*, 2009. **42**(11-12): p. 1684-1690.
205. Akay, A.J.T.J.o.t.A.S.o.A., *Acoustics of friction*. 2002. **111**(4): p. 1525-1548.

Appendix A

The specification of Centrifugal Pump

F

50 Hz n= 2900 min⁻¹

Standardised "EN 733" centrifugal pumps

-  Clean water
-  Industrial use



PERFORMANCE RANGE

- Flow rate up to **6000 l/min** (360 m³/h)
- Head up to **98 m**

APPLICATION LIMITS

- Manometric suction lift up to **7 m**
- Liquid temperature between **-10 °C** and **+90 °C**
- Ambient temperature between **-10 °C** and **+40 °C**
- Max. pressure in pump body **10 bar** (PN10)
- Continuous service **S1**

CONSTRUCTION AND SAFETY STANDARDS

EN 60335-1
IEC 60335-1
CEI 61-150

EN 60034-1
IEC 60034-1
CEI 2-3



Pump body dimensions in compliance with **EN 733**

EU REGULATION N. 547/2012

INSTALLATION AND USE

- Water supply
- Pressure boosting
- Irrigation
- Water circulation in air-conditioning units
- Cleaning sets
- Firefighting sets
- Industrial applications
- Agricultural applications

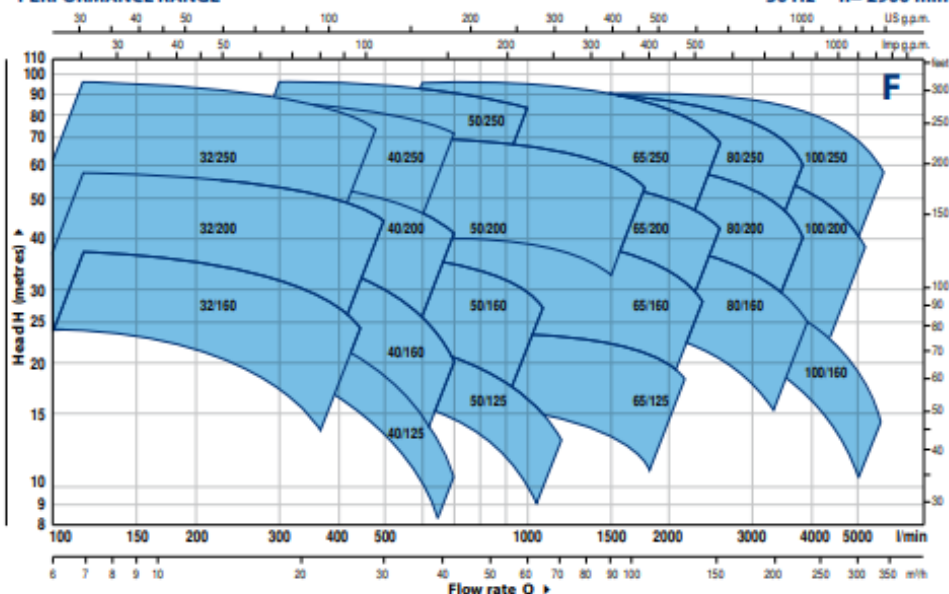
Installation needs to be undertaken in well ventilated closed areas or anyway protected from bad weather.

OPTIONS AVAILABLE ON REQUEST

- Counter flange KIT complete with bolts, nuts and washers
- Special mechanical seal
- Other voltages or 60 Hz frequency
- Compatibility with hotter or colder liquids
- Compatibility with hotter or colder environments

PERFORMANCE RANGE

50 Hz n= 2900 min⁻¹



PERFORMANCE DATA

50 Hz n= 2900 min⁻¹

MODEL	POWER (P ₂)		▲	PERFORMANCE	
	kW	HP		Q l/min	H metres
F 32/160C	1.5	2	IE3	100-350	24-14
F 32/160B	2.2	3		100-400	30-17
F 32/160A	3	4		100-450	37-24
F 32/200C	4	5.5		100-450	44-31.5
F 32/200B	5.5	7.5		100-500	51-36
F 32/200A	7.5	10		100-500	57-44
F 32/200BH	3	4		100-300	45-37
F 32/200AH	4	5.5		100-320	55-44
F 32/250C	9.2	12.5		100-450	75-60
F 32/250B	11	15		100-500	87-70
F 32/250A	15	20		100-500	97-80
F 40/125C	1.1	1.5		IE3	100-550
F 40/125B	1.5	2	100-600		20.5-9
F 40/125A	2.2	3	100-700		26-10
F 40/160C	2.2	3	100-600		27-14
F 40/160B	3	4	100-600		32-20
F 40/160A	4	5.5	100-700		38-20
F 40/200B	5.5	7.5	100-700		47-28
F 40/200A	7.5	10	100-700		55-41
F 40/250C	9.2	12.5	100-700		64-47
F 40/250B	11	15	100-700		71-55
F 40/250A	15	20	100-700		88-72
F 50/125C	2.2	3	IE3		300-1200
F 50/125B	3	4		300-1200	20.7-9
F 50/125A	4	5.5		300-1200	23.5-13
F 50/160C	4	5.5		300-1000	27-16
F 50/160B	5.5	7.5		300-1100	32-21
F 50/160A	7.5	10		300-1100	37-27
F 50/200C	11	15		400-1700	44-30
F 50/200B	15	20		400-1700	52-38
F 50/200A	18.5	25		400-1800	61-45
F 50/200AR	22	30		400-1800	69-53
F 50/250D	9.2	12.5		300-900	51-32
F 50/250C	11	15		300-900	59-42
F 50/250B	15	20	300-1000	72-59	
F 50/250A	18.5	25	300-1000	85-73	
F 50/250AR	22	30	300-1000	95-83	

MODEL	POWER (P ₂)		▲	PERFORMANCE		
	kW	HP		Q l/min	H metres	
F 65/125C	4	5.5	IE3	600-1800	16-11	
F 65/125B	5.5	7.5		600-2000	18-13	
F 65/125A	7.5	10		600-2200	23-18	
F 65/160C	9.2	12.5		600-2200	32-22	
F 65/160B	11	15		600-2400	36.5-23	
F 65/160A	15	20		600-2400	40.5-28	
F 65/200B	15	20		200-2400	44-30.5	
F 65/200A	18.5	25		200-2500	50-36.5	
F 65/200AR	22	30		200-2600	57-42	
F 65/250C	30	40		400-2350	76-53	
F 65/250B	37	50		400-2500	87-62	
F 65/250A	45	60		400-2600	95-68	
F 80/160D	11	15	IE3	500-4000	25-10	
F 80/160C	15	20		500-4000	30-15	
F 80/160B	18.5	25		500-4000	35-20	
F 80/160A	22	30		500-4000	40-25	
F 80/200B	30	40		500-3650	56-34.5	
F 80/200A	37	50		500-3900	62-40	
F 80/250B	45	60		600-3600	77-54	
F 80/250A	55	75		600-3900	88.5-60	
F 100/160C	15	20		IE3	1000-5000	30-12
F 100/160B	18.5	25			1000-5200	34-14.5
F 100/160A	22	30			1000-5500	38-17.5
F 100/200C	30	40			833-4650	51-28
F 100/200B	37	50	833-4900		57-33	
F 100/200A	45	60	833-5250		63-38	
F 100/250B	55	75	800-5150		75-48	
F 100/250A	75	100	800-5750		89-58	

Q = Flow rate

H = Total manometric head

Tolerance of characteristic curves in compliance with EN ISO 9906 Grade 3B.

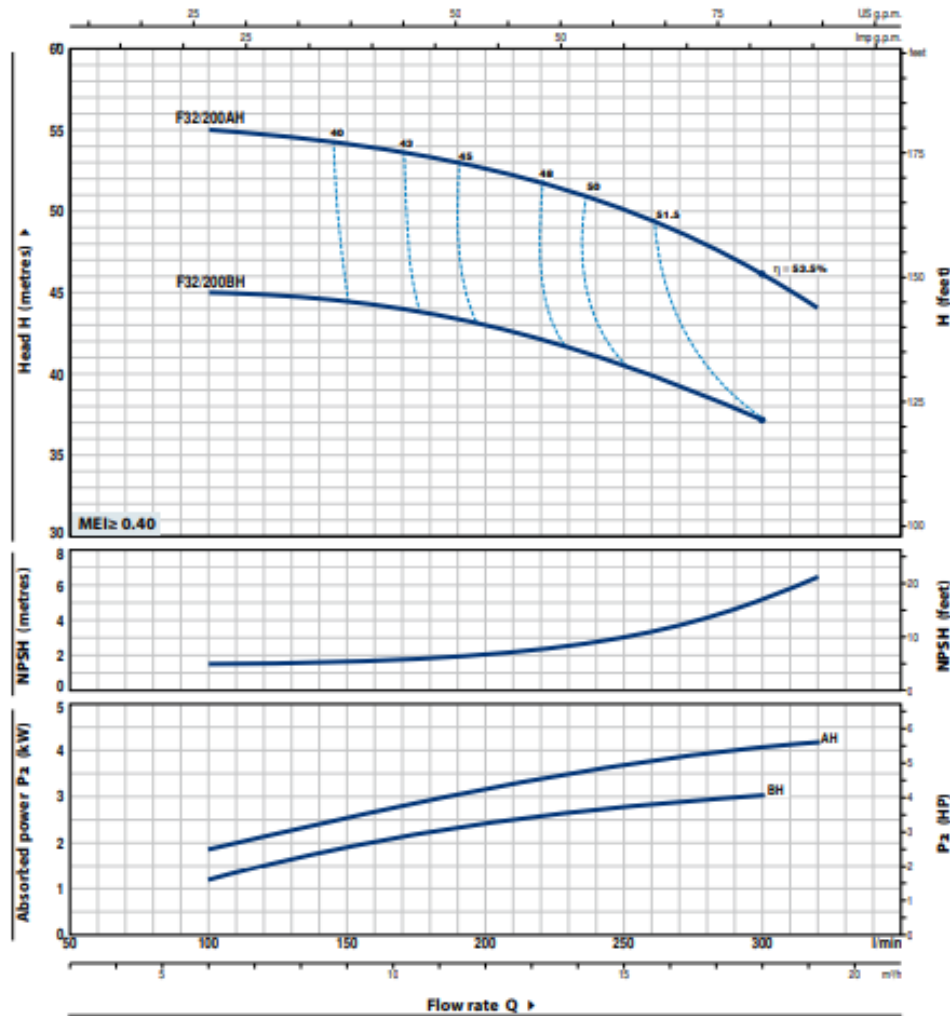
▲ Three-phase motor efficiency class (IEC 60034-30-1)

F | 50 Hz

F32/200H

CHARACTERISTIC CURVES AND PERFORMANCE DATA

50 Hz n= 2900 min⁻¹ HS= 0 m



MODEL	POWER (P ₂)		Q	0	6	9	12	15	18	19.2
	kW	HP		0	100	150	200	250	300	320
F 32/200BH	3	4	H metres	47	45	44.5	43	40.5	37	
F 32/200AH	4	5.5	H metres	57	55	54	52.5	50	46	44

Q = Flow rate H = Total manometric head HS = Suction height

Tolerance of characteristic curves in compliance with EN ISO 9906 Grade B8.